

Development of a Rate-Based Model for Multi-Component Distillation in a Rotating Packed Bed based on Mass Transfer Experiments

vorgelegt von
Matthias Hilpert, M.Sc.
ORCID: 0000-0003-0498-9517

von der Fakultät III – Prozesswissenschaften
der Technischen Universität Berlin
zur Erlangung des akademischen Grades

Doktor der Ingenieurwissenschaften
- Dr.-Ing. -

genehmigte Dissertation

Promotionsausschuss:

Vorsitzender:	Prof. Dr.-Ing. Harald Kruggel-Emden
1. Gutachter:	Prof. Dr.-Ing. habil. Jens-Uwe Repke
2. Gutachter:	Prof. Dr. Michel Meyer

Tag der wissenschaftlichen Aussprache: 17. Mai 2022

Berlin, 2022

To my family

Affidavit

Hiermit erkläre ich an Eides statt, dass ich die vorliegende Arbeit selbstständig und eigenhändig sowie ausschließlich unter Verwendung der aufgeführten Quellen und Hilfsmittel angefertigt habe.

Matthias Hilpert
Berlin, 4. Juli 2022

I hereby confirm that I prepared this thesis independently and by exclusive reliance on literature or tools indicated herein.

Matthias Hilpert
Berlin, July 4, 2022

Acknowledgements

With gratitude I look back on my past years at dbta, during which I was given the opportunity to learn much, both on a professional and on a personal level. At this point, I would like to especially thank my advisor Prof. Dr.-Ing. Jens-Uwe Repke, who gave me the opportunity to complete a Ph.D. at his department. His advice, encouragement and guidance were invaluable. Furthermore, I would like to thank Prof. Dr. Michel Meyer for accepting to examine this thesis.

Next, I thank my colleagues for their support, whether in many discussions, the preparation for conferences or the HAZOPs. It was great being a part of the team at dbta. I would like to expressly thank my colleagues Alexander Ressemann for his support, valuable insights and discussions on RPBs and Tim Karsten for his cheerfulness and his help with the DCS. But no experimental thesis is possible without the great staff of the workshops and laboratories. So a very special thanks goes to Dietmar with his great ideas, Martin with his knowledgeable planning and Marita, Uta, Abdullah and Andreas for their continued support.

Another important contribution to this thesis was made by many students, who took part in the design, construction, start-up and operation of the test stand and development of the model: Tobias Vlaminck, Niclas Krink, Fabian Ebert, Karim Kayed, Lukas Gottheil, John Paul Gerakis, Stephan Herrmann and Gerson Uriel Calvillo Aranda. I hope you learned as much from me as I learned from you!

Furthermore, I would like to thank our colleagues from Prof. Górak's chair at TU Dortmund, especially Konrad Gładyszewski, for the advice in designing the RPB, and Michał Pawłowski from Proceler, for the construction.

Finally, I thank my parents and especially my partner Martina for their support, patience, encouragement and love, that so very much helped me complete this work.

Kurzreferat

Rektifikation ist eine der am häufigsten eingesetzten Trennoperationen der Verfahrenstechnik und hat erheblichen Anteil am Energieverbrauch der chemischen Industrie. In der Regel werden zur Rektifikation große Boden- oder Packungskolonnen genutzt, die viel Raum und Material verbrauchen. In bestimmten Anwendungen, wie Retrofits oder offshore, sind Platz und zulässiges Gewicht jedoch begrenzt.

Ein Ansatz zur Intensivierung von Rektifikationsprozessen und damit u.a. zur signifikanten Verringerung des Platzbedarfes ist die Nutzung der Fliehkraft anstelle der Schwerkraft, um die Flüssigkeit durch die Packung strömen zu lassen. Eine Art der Stofftransportmaschinen, die dieses Prinzip nutzt, sind s.g. Rotating Packed Beds (RPBs). Obwohl erste erfolgreiche Versuche zur Rektifikation in RPBs bereits in den 1970er Jahren durchgeführt wurden, existieren insgesamt nur wenige Veröffentlichungen zu diesem Thema. Insbesondere wurden in der englischsprachigen Literatur bisher keine Daten zur Trennung von Mehrstoffgemischen publiziert. Daher existiert keine Datenbasis, die zur Validierung von Modellen der Trennung von Mehrstoffgemischen durch Rektifikation in RPBs genutzt werden könnte. Gemische aus mehreren Stoffen sind jedoch die Regel in industriellen Anwendungen. Das Fehlen einer Datengrundlage ist eines der Hindernisse zum industriellen Einsatz von RPBs für Rektifikationsanwendungen.

Die vorliegende Arbeit zielt darauf ab, diese Lücke zu verkleinern, indem eine Datenbasis geschaffen und ein Modell zur Mehrkomponentendestillation in RPBs entwickelt sowie validiert wird. Um den Einfluss der RPB-Geometrie und der Betriebsparameter abzubilden, wird ein stofftransportbasierter Modellierungsansatz gewählt. Dieser basiert auf Korrelationen für dampf- und flüssigseitige volumetrische Stofftransportkoeffizienten $k^V a_e$ und $k^L a_e$. Verfügbare Literaturdaten enthalten in der Regel nur abgeleitete Größen (z.B. HETP-Werte anstelle von Konzentrationen) und es fehlen häufig relevante Angaben zur RPB-Geometrie, was die Entwicklung neuer Korrelationen behindert. Außerdem sind vorhandene Korrelationen zwischen unterschiedlichen RPB-Maschinen nur begrenzt übertragbar, da nicht alle Einflussgrößen in den Korrelationen

enthalten sind. Aus diesem Grund wird ein RPB-Versuchsstand für Stofftransportuntersuchungen in dieser Arbeit entworfen und daran gemessene Daten genutzt, um die benötigten Stofftransportkorrelationen zu entwickeln.

$k^L a_e$ wird anhand der Sauerstoffdesorption aus Wasser in einen Stickstoffstrom gemessen. $k^V a_e$ wird aus gemessenen volumetrischen gasseitigen Stoffdurchgangskoeffizienten $K^V a_e$ unter Zuhilfenahme der zuvor entwickelten Korrelation für $k^L a_e$ berechnet. Die Messung der $K^V a_e$-Werte erfolgt durch Rektifikation eines Ethanol/n-Propanol-Gemisches bei unendlichem Rücklauf. Die entwickelten Korrelationen sind im Gegensatz zu verfügbaren Literaturkorrelationen in der Lage, das bekannte Maximum der Trennleistung bei mittleren Drehzahlen von RPBs abzubilden. Das Model wird anhand von Daten aus der Rektifikation eines Ethanol/Wasser- und eines Ethanol/n-Propanol/Wasser-Gemisches bei unendlichem Rücklauf validiert. Das entwickelte Modell ist in der Lage, den Großteil der Messdaten mit einer Genauigkeit von ±30 % abzubilden, was typisch ist für empirische Korrelationen, wie sie zur Modellierung konventioneller Destillationskolonnen eingesetzt werden. Bestimmte Einflussfaktoren, wie das Design der Packungshalter, Flüssigverteiler oder besondere hydrodynamische Zustände, sind nicht in den entwickelten Korrelationen enthalten, können aber einen Einfluss auf den Stofftransport haben. Daher sind auftretende Abweichungen größer, wenn das entwickelte Modell zur Simulation der beschränkten verfügbaren Literaturdaten zur Rektifikation in RPBs angewendet wird. Nichtsdestotrotz illustriert die vorliegende Arbeit eine Methodik zur Entwicklung eines Stofftransportmodells der Rektifikation in RPBs, die ohne die separate Messung von $k^V a_e$ durch zusätzliche Testsysteme auskommt. Aufgrund der begrenzten verfügbaren Daten zur Rektifikation in RPBs und den Beschränkungen vorhandener Korrelationen werden solche experimentellen Untersuchungen auch in absehbarer Zukunft ein wichtiger Schritt in der Prozessentwicklung sein.

Schlüsselwörter: *Rotating Packed Bed (RPB); HIGEE; Ternäre Distillation; Wasserdeoxygenierung; Stofftransportmodellierung; Stofftransportkorrelationen*

Abstract

Distillation is one of the most used separation processes in chemical engineering and accounts for a significant portion of the industry's energy consumption. Typically, distillation is performed in large columns with packings or trays, requiring substantial amounts of space and material. In certain applications, such as retrofits or off-shore, however, available space or weight are limited.

A solution to intensify distillation processes and thus, inter alia, significantly reduce equipment size is to use centrifugal force instead of gravity to drive the liquid through the packing material. One type of mass transfer machines using this principle is the Rotating Packed Bed (RPB). Though first successful tests of distillation in RPBs were conducted in the 1970s, overall only few publications on the subject exist. Especially, no data on distillation of multicomponent mixtures has been published in English language literature. Hence, there is no basis for validation of models for multicomponent distillation in RPBs. Mixtures with more than two components are, however, typical for industrial applications. This lack is one of the obstacles to industrial application of RPBs for distillation tasks.

The present work aims to narrow this gap by creating a data basis, developing and validating a model for multicomponent distillation in RPBs. To account for geometrical and operational variables, a rate-based modeling approach is chosen. This requires correlations for vapor and liquid side volumetric mass transfer coefficients $k^V a_e$ and $k^L a_e$. Available literature data is usually reported in a processed fashion (e.g. HETP instead of concentrations) and often lacking relevant details on RPB geometry, hindering the development of new correlations. Furthermore, transferability of existing correlations between different RPBs is limited since not all influences are captured in the correlations. Therefore, an RPB test stand for mass transfer measurements is designed in this thesis and used to develop required mass transfer correlations.

$k^L a_e$ is measured by oxygen desorption from water into a nitrogen gas stream. $k^V a_e$ is back-calculated from overall vapor side mass transfer coefficients $K^V a_e$, measured

using distillation of an ethanol/n-propanol mixture at infinite reflux, along with the previously obtained $k^L a_e$ correlation. The developed correlations are capable of describing the known maximum in separation efficiency of RPBs at intermediate rotational speeds, as opposed to available literature correlations. The model is validated using data from infinite reflux distillation of an ethanol/water mixture and of the ternary mixture of ethanol/n-propanol/water. The developed model is capable of representing most of the data within ±30 %, which is typical for empirical correlations as used in modeling of conventional distillation columns. Certain influences, such as the design of packing supports, liquid distributors or special hydrodynamic conditions, are not contained in the developed correlations, but can influence mass transfer. Therefore, when applied to the limited literature data available for distillation in RPBs, deviations are more significant. Nonetheless, the present thesis demonstrates a methodology to develop a rate-based mass transfer model for distillation in RPBs that does not require separate measurement of $k^V a_e$ by dedicated test systems. Due to the limited amount of data available on distillation in RPBs at the time and the limitations of existing correlations, such experiments will remain an important part in process development for the near future.

Keywords: *Rotating Packed Bed (RPB); HIGEE; Ternary Distillation; Water Deoxygenation; Rate-based Modeling; Mass Transfer Correlations*

Publications

This thesis is partially based on already published contributions. In the following, these are divided into journal articles, oral presentations and posters without papers, and a list of all supervised theses.

Journal Articles

- M. Hilpert and J.-U. Repke (2021): Experimental Investigation and Correlation of Liquid-Side Mass Transfer in Pilot-Scale Rotating Packed Beds. *Industrial & Engineering Chemistry Research* 60 (14), 5251–5263. ISSN: 0888-5885. DOI: 10.1021/acs.iecr.1c00440
  The full text is available via the ACS articles on request direct link below:
  https://pubs.acs.org/articlesonrequest/AOR-JT9TUDCMEAFPFCUUTKQW

- M. Hilpert, G. U. Calvillo Aranda, and J.-U. Repke (2022): Experimental analysis and rate-based stage modeling of multicomponent distillation in a Rotating Packed Bed. *Chemical Engineering and Processing: Process Intensification* 171, 108651. ISSN: 0255-2701. DOI: 10.1016/j.cep.2021.108651

Oral Presentations and Posters Without Proceedings

- M. Hilpert and J.-U. Repke (2015b): Neue hybride Systematik zum Retrofit komplexer destillativer Trennprozesse (Presentation). *Jahrestreffen der Fachgemeinschaft Fluiddynamik und Trenntechnik*. Sept. 9-11, Bamberg (Germany)

- M. Hilpert and J.-U. Repke (2015a): Coupling CHEMCAD and Matlab through an OPC interface (Presentation). *CHEMCAD User Meeting*. Sept. 18, Berlin (Germany)

– M. Hilpert and J.-U. Repke (2019c): Systematische Untersuchungen des Stofftransportes in Rotating Packed Beds – Konzeption und erste Ergebnisse (Presentation). *Jahrestreffen der ProcessNet-Fachgruppen Fluidverfahrenstechnik und Membrantechnik*. March 27-29, Potsdam (Germany)

– M. Hilpert and J.-U. Repke (2019b): Investigation of the liquid-side mass transfer in an RPB (Presentation). *High Gravity Colloquium*. June 25, Dortmund (Germany)

– M. Hilpert and J.-U. Repke (2019a): Experimental Investigation of Mass Transfer in a Miniplant Scale Rotating Packed Bed (Poster). *12th European Congress of Chemical Engineering (ECCE)*. Sept. 16-19, Florence (Italy)

– M. Hilpert and J.-U. Repke (2020): Systematische Untersuchungen des Stofftransportes zur Modellierung der Rektifikation in Rotating Packed Beds (Presentation). *Jahrestreffen der ProcessNet-Fachgruppen Fluidverfahrenstechnik, Adsorption und Extraktion*. Feb. 26-28, Berchtesgaden (Germany)

Supervised Theses related to this Work

– S. Herrmann (2019): Stationäre Nicht-Gleichgewichtsmodellierung, Konvergenzanalyse und Simulation einer Rektifikationskolonne. *Master Thesis*. Berlin: Technische Universität Berlin

– T. Vlaminck (2019): Planung und Aufbau eines Rotating-Packed-Bed-Versuchsstandes zur Destillation bei erhöhter Schwerkraft. *Master Thesis*. Berlin: Technische Universität Berlin

– N. Krink (2019): Implementierung des Prozessleitsystems und Inbetriebnahme eines Rotating-Packed-Bed-Versuchsstandes. *Master Thesis*. Berlin: Technische Universität Berlin

– F. Ebert (2019): Experimentelle Untersuchung des flüssigkeitsseitigen Stoffüberganges in einer rotierenden Packungskolonne (RPB). *Research Internship Report*. Berlin: Technische Universität Berlin

– K. Kayed (2019): Untersuchung des flüssigseitigen Stoffübergangs in einem Rotating Packed Bed-Versuchsstand. *Bachelor Thesis*. Berlin: Technische Universität Berlin

– G. U. Calvillo Aranda (2020): Steady State Rate-Based Modeling of Distillation in a Rotating Packed Bed. *Master Thesis*. Berlin: Technische Universität Berlin

– L. Gottheil (2021): Experimentelle Untersuchung der Destillation in einer rotierenden Packungskolonne (RPB). *Research Internship Report*. Berlin: Technische Universität Berlin

– J. P. Gerakis (2021): Experimental Investigation and Model Validation of Multi-Component Distillation in a Rotating Packed Bed Test Stand. *Bachelor Thesis*. Berlin: Technische Universität Berlin

Supervised Theses not related to this Work

– N. Knobbe (2016): Entwicklung eines stationären Modells in CHEMCAD zur Auslegung einer Reaktivdestillationskolonne. *Master Thesis*. Freiberg: TU Bergakademie Freiberg

– A. Reitze (2017): Industrie 4.0 in der Chemischen Industrie – Untersuchung von Anwendungsmöglichkeiten auf reale Destillationsprozesse. *Master Thesis*. Berlin: Technische Universität Berlin

– B. Li (2021): Investigation of Cyclic Operation of Distillation Processes. *Master Thesis*. Berlin: Technische Universität Berlin

Contents

List of Figures i

List of Tables v

List of Symbols vii

List of Abbreviations xv

1 Introduction 1

2 State-of-the-art 5
2.1 Fundamentals of mass transfer in gas-liquid systems 5
2.1.1 Mass transfer modeling 5
2.1.2 Mass transfer experiments 9
2.2 Hydrodynamics and mass transfer in RPBs 14
2.2.1 Hydrodynamics 14
2.2.2 Mass transfer 20
2.2.3 RPB design modifications 25
2.3 CFD modeling of RPBs 27
2.4 Modeling of mass transfer in RPBs 29
2.4.1 Modeling of mass transfer coefficients in RPBs 30
2.4.2 Comparison of the modeling of ab- or desorption and distillation in RPBs 34
2.5 Experimental and modeling studies of distillation in RPBs 35
2.6 Characteristics and exemplary industrial applications of HIGEEs . . . 43

3 Research gap, objective and approach 47
3.1 Analysis of the research gap 47
3.2 Objective and approach 49

4 Generation of an experimental data basis for modeling of mass transfer in RPBs 53
4.1 Selection of suitable component test systems 53
4.1.1 Distillation test systems 54
4.1.2 Test system for determination of $k^L a_e$ 58
4.2 Design of the test stand 59
4.2.1 Design of the RPB 60

4.2.2 Development of the process flow diagrams 62
4.2.3 Operating range of the RPB test stand 67
4.3 Experimental procedure 71
4.3.1 Experimental procedure for desorption experiments 71
4.3.2 Experimental procedure for distillation experiments 72

5 Rate-based mass transfer model of the RPB 75
5.1 MERSHQ-equations 77
5.2 Calculation of mass transfer coefficients 80
5.3 Estimation of volumetric heat transfer coefficients 82

6 Investigation of liquid-side mass transfer 83
6.1 Evaluation of the experiments 83
6.1.1 Influence of pre-saturation of nitrogen with water vapor 85
6.1.2 Investigation of spraying nozzle type and the influence of packing material 86
6.1.3 Influence of gas flow rate 88
6.1.4 Influence of cocurrent operating mode 91
6.2 Modeling and simulation of $k^L a_e$ 91
6.2.1 Evaluation of literature correlations 92
6.2.2 Suggestion of a correlation for $k^L a_e$ capable of producing a maximum in separation efficiency 94
6.2.3 Parameters for the suggested $k^L a_e$ correlation based on full jet nozzles 95
6.2.4 Parameters for the suggested $k^L a_e$ correlation based on flat fan nozzles 96
6.3 Conclusion for the investigation of liquid-side mass transfer 99

7 Investigation of distillation 101
7.1 Evaluation of the experiments 101
7.1.1 Influence of initial liquid jet velocity 103
7.1.2 Distillation of binary mixtures 104
7.1.3 Distillation of ternary mixtures 108
7.1.4 Investigation of outer end effects 110
7.2 Simulation using literature correlations 112
7.2.1 Discretization of the RPB rotor in the rate-based model 113
7.2.2 Evaluation of the predictive capabilities of selected literature correlations 114
7.3 Suggestion of a correlation for $k^V a_e$ capable of producing a maximum in separation efficiency 116
7.4 Model validation 120
7.4.1 Simulation of the distillation experiments with ethanol/water 121
7.4.2 Simulation of the distillation experiments with ethanol/n-propanol/water 123
7.5 Sources of deviations of model predictions 124
7.6 Transferability of the developed model to different RPB machines . . . 126

7.7 Conclusion for the investigation of distillation 129

8 Conclusion and Outlook **131**

A Measurement uncertainty calculation **135**

B Experimental data of water deoxygenation experiments **139**

C Transport property methods for calculation of $k^L a_e$ for water deoxygenation **145**

D Literature overview of experimental investigations of $k^L a_e$ in RPBs using water deoxygenation **147**

E Assessment of the predictive capabilities of literature correlations for $k^L a_e$ data measured in this study **151**

F Experimental data of distillation experiments **157**

G Overview of MOSAICmodeling elements of the developed rate-based RPB model **177**

H Simulation of distillation data from literature using the developed model **179**

List of References **183**

List of Figures

1.1 Countercurrent gas-liquid flow paths in an RPB 3

2.1 Concentration profiles for mass transfer across a phase interface . . . 6
2.2 Precipitates observed on rotor plates of RPBs 15
2.3 Hydrodynamic operating window of an RPB 21
2.4 Sketch of end effect zones in an RPB 22
2.5 Sketch of some HIGEE design modifications 25

3.1 Schematic representation of the strategy applied to obtain mass transfer coefficients 50

4.1 Change of various variables along the radius of an RPB 54
4.2 Potential component test systems for distillation 56
4.3 NCX1116 metal foam packing 61
4.4 Spraying characteristics of nozzles employed in this study 62
4.5 Photograph of the RPB test stand 63
4.6 PFD for distillation at infinite reflux 65
4.7 Analogy between distillation column and RPB 66
4.8 PFD for distillation in rectifying and stripping mode 67
4.9 PFD for countercurrent water deoxygenation 68

5.1 Schematic representation of a non-equilibrium stage 77

6.1 Comparison of $k^L a_e$ values with and without pre-saturation of the nitrogen gas stream with water vapor 86
6.2 Comparison of $k^L a_e$ values of flat fan and full jet nozzles 87
6.3 Comparison of $k^L a_e$ values at two gas flow rates in the packed and empty rotor 89
6.4 NTU_{OL} in dependence of rotational speed of the RPB for countercurrent desorption 91
6.5 $k^L a_e$ in dependence of rotational speed of RPB for cocurrent desorption in the packed rotor 92
6.6 Performance of literature correlations for $k^L a_e$ in comparison to the experimental data 94
6.7 Comparison of experimental and calculated data using the developed $k^L a_e$ correlation for the empty rotor with jet nozzles 97

6.8 Comparison of experimental and calculated data using the developed $k^L a_e$ correlation for the packed rotor with full jet nozzles 97
6.9 Comparison of experimental and calculated data using the developed $k^L a_e$ correlation for the empty rotor with flat fan nozzles 98
6.10 Comparison of experimental and calculated data using the developed $k^L a_e$ correlation for the packed rotor with flat fan nozzles 98
6.11 Performance of the developed correlation for $k^L a_e$ with flat fan nozzles at different packing geometries 99

7.1 Comparison of the behavior of $K^V a_e$ values of 0.7 mm and 1.0 mm jet nozzles using ethanol/n-propanol 104
7.2 Experimental $K^V a_e$ values for distillation of ethanol/n-propanol and ethanol/water 105
7.3 Pressure drop across the packing for distillation of ethanol/water using 0.7 mm jet nozzles at different rotational speeds 106
7.4 Experimental NTU_{og} values for distillation of ethanol/n-propanol and ethanol/water 107
7.5 Residue curve map of ethanol/n-propanol/water system with experimental balance lines 109
7.6 Experimental $N_{th,ethanol}$ from distillation of ethanol/n-propanol/water 110
7.7 $K^V a_e$ of ethanol/n-propanol and ethanol/water system calculated based on different sampling locations to assess outer end effects 111
7.8 Discretization approaches (left: equidistant; right: equiareal discretization) 113
7.9 Results of the RPB distillation model discretization study 114
7.10 Experimental vs. simulated $K^V a_e$ of ethanol/n-propanol system using correlations from literature 117
7.11 Experimental vs. simulated $K^V a_e$ for distillation of ethanol/n-propanol using the developed correlations 120
7.12 Experimental vs. simulated $K^V a_e$ for distillation of ethanol/water using correlations from this study and Reddy et al. (2006) 122
7.13 Comparison of radial temperature and concentration profiles simulated with correlation from this study and Reddy et al. (2006) 122
7.14 Experimental vs. simulated $N_{th,ethanol}$ for distillation of ethanol/n-propanol/water using correlations from this study and Reddy et al. (2006) 123
7.15 Experimental vs. simulated $N_{th,ethanol}$ for distillation of ethanol/n-propanol/water using correlations from this study with different models for liquid diffusivity at finite dilution 126
7.16 Examples of various inner and outer RPB packing supports from literature 127
7.17 Experimental vs. simulated HETP for distillation of methanol/ethanol using correlations from this study for data of Lin et al. (2002) 128

E.1 Application of literature correlations for $k^L a_e$ to countercurrent desorption data of this study 155

E.2 Application of literature correlations for $k^L a_e$ to countercurrent desorption data of this study (contd.) 156

H.1 Separation performance vs. throughput for RPB at ICI 180
H.2 Comparison of experimental data of Kelleher and Fair (1996), Qammar et al. (2019), and Nascimento et al. (2009) for distillation at infinite reflux with simulations using correlations from this study 181

List of Tables

2.1 Publications quantifying outer end effects in RPBs 23
2.2 Overview of experimental investigations of distillation in RPBs 39

4.1 Recommended distillation test systems 55
4.2 Properties of the chosen components for design of the RPB test stand 58
4.3 Summary of the component systems for experimental mass transfer investigations in the RPB test stand 59
4.4 RPB geometry, packing and liquid distributor specifications 63
4.5 Overview of employed measurement devices 64
4.6 Selected F-factors for investigations of distillation in RPBs from literature 69
4.7 Summary of design operating ranges of the RPB test stand 71

6.1 Literature correlations for the estimation of $k^L a_e$ 93

7.1 Some published ranges of HETP values for distillation in RPBs 106
7.2 Employed literature correlations for mass transfer coefficients 112
7.3 Input variables and results for simulations in this work 115
7.4 Comparison of dimensions of RPBs used in studies for derivation of the tested mass transfer correlations from literature 116
7.5 Comparison of liquid mixture viscosity data for ethanol/n-propanol/water with different viscosity models 125

B.1 $k^L a_e$ data measured in the empty rotor with full jet nozzles in countercurrent operation 139
B.2 $k^L a_e$ data measured in the packed rotor with full jet nozzles in countercurrent operation 140
B.3 $k^L a_e$ data measured in the packed rotor with full jet nozzles in cocurrent operation 141
B.4 $k^L a_e$ data measured in the packed rotor with full jet nozzles in countercurrent operation, with pre-saturation of the N2 gas stream 141
B.5 $k^L a_e$ data measured in the empty rotor with flat fan nozzles in countercurrent operation 142
B.6 $k^L a_e$ data measured in the packed rotor with flat fan nozzles in countercurrent operation 143
B.7 $k^L a_e$ data measured in the packed rotor with an outer radius of 95 mm instead of 225 mm with flat fan nozzles in countercurrent operation . 144

B.8 $k^L a_e$ data measured in the packed rotor with a packing height of 20 mm instead of 10 mm with flat fan nozzles in countercurrent operation . . 144

C.1 Coefficients for calculation of transport properties of water (VDI-Wärmeatlas 2013, Ch. D3.1) 146

D.1 Overview of experimental investigations of $k^L a_e$ in RPBs using water deoxygenation 148

E.1 Overview of semi-empirical correlations for volumetric liquid-side mass transfer coefficients in RPBs obtained from desorption of oxygen or Volatile Organic Compounds (VOCs) from water 152

G.1 MOSAICmodeling IDs of the RPB mass transfer models employing literature correlations for the component system ethanol / n-propanol, discretized using 101 elements 177

G.2 MOSAICmodeling IDs of the developed RPB mass transfer models for distillation, discretized using 101 elements 177

List of Symbols

Constants

Symbol	Description	Unit
π	Mathematical constant = 3.141 59...	1
R	Universal gas constant = 8.314 46	$\mathrm{J\,mol^{-1}\,K^{-1}}$

Dimensionless Numbers

Symbol	Definition
Eu^{L}	$\left(P(2\pi r h_p)^2\ \rho_{Mix}^{L,mass}\right) / \left((LM_{Mix}^{L})^2\right)$
Eu^{V}	$\left(P(2\pi r h_p)^2\ \rho_{Mix}^{V,mass}\right) / \left((VM_{Mix}^{V})^2\right)$
Fr^{L}	$(LM_{Mix}^{L})^2 / \left((2\pi r h_p)^2\ a_p\ r\omega^2\ \rho_{Mix}^{L,mass}\ d_p\right)$
Fr'^{L}	$(LM_{Mix}^{L})^2 / \left((2\pi r h_p)^2\ a_p\ r\omega^2\ \rho_{Mix}^{L,mass}\ r_i\right)$
Ga^{L}	$\left((\rho_{Mix}^{L,mass})^2\ r\omega^2\right) / \left((\eta_{Mix}^{L})^2\ (a_p)^3\right)$
Ga^{V}	$\left((\rho_{Mix}^{V,mass})^2\ r\omega^2\right) / \left((\eta_{Mix}^{V})^2\ (a_p)^3\right)$
Ga''^{L}	$\left((\rho_{Mix}^{L,mass})^2\ d_p^3\ r\omega^2\right) / (\eta_{Mix}^{L})^2$
Ga''^{V}	$\left((\rho_{Mix}^{V,mass})^2\ d_p^3\ r\omega^2\right) / (\eta_{Mix}^{V})^2$
Ga'^{L}	$\left((\rho_{Mix}^{L,mass})^2\ (d'_p)^3\ r\omega^2\right) / (\eta_{Mix}^{L})^2$
Ga'^{V}	$\left((\rho_{Mix}^{V,mass})^2\ (d'_p)^3\ r\omega^2\right) / (\eta_{Mix}^{V})^2$
Ga_{empty}^{L}	$\left((\rho_{Mix}^{L,mass})^2\ (r_o - r_i)^3\ r\omega^2\right) / (\eta_{Mix}^{L})^2$
Ga_{empty}^{V}	$\left((\rho_{Mix}^{V,mass})^2\ (r_o - r_i)^3\ r\omega^2\right) / (\eta_{Mix}^{V})^2$
Pr	$\left(c_{p,Mix}^{Mass}\ \eta_{Mix}\right) / \lambda_{Mix}$
Re^{L}	$\left(LM_{Mix}^{L}\right) / \left(2\pi r h_p\ a_p\ \eta_{Mix}^{L}\right)$
Re_{empty}^{L}	$\left(LM_{Mix}^{L}\ (r_o - r_i)\right) / \left(2\pi r h_p\ \eta_{Mix}^{L}\right)$
Re^{V}	$\left(VM_{Mix}^{V}\right) / \left(2\pi r h_p\ a_p\ \eta_{Mix}^{V}\right)$

Re^{V}_{empty}	$\left(VM^{V}_{Mix}\ (r_o - r_i)\right)\ /\ \left(2\pi r h_p\ \eta^{V}_{Mix}\right)$
Re'^{L}	$\left(LM^{L}_{Mix}\ d_p\right)\ /\ \left(2\pi r h_p\ \eta^{L}_{Mix}\right)$
Re'^{V}	$\left(VM^{V}_{Mix}\ r_i\right)\ /\ \left(2\pi r h_p\ \eta^{V}_{Mix}\right)$
Re''^{L}	$\left(LM^{L}_{Mix}\ r_i\right)\ /\ \left(2\pi r h_p\ \eta^{L}_{Mix}\right)$
Sc^{L}	$\eta^{L}_{Mix} / \left(\rho^{L,mass}_{Mix}\ D^{L}\right)$
Sc^{V}	$\eta^{V}_{Mix} / \left(\rho^{V,mass}_{Mix}\ D^{V}\right)$
Sh	$(kl)\ /D$
St	$\overline{k}/\overline{u}$
St_{α}	$\alpha / \left(\rho^{mass}_{Mix}\ c^{Mass}_{p,Mix}\ \overline{u}\right)$
We^{L}	$(LM^{L}_{Mix})^2 / \left((2\pi r h_p)^2\ a_p\ \rho^{L,mass}_{Mix}\ \sigma^{L}_{Mix}\right)$
We'^{L}	$\left((LM^{L}_{Mix})^2\ d_p\right)\ /\ \left((2\pi r h_p)^2\ \rho^{L,mass}_{Mix}\ \sigma^{L}_{Mix}\right)$
We''^{L}	$\left((LM^{L}_{Mix})^2\ r_i\right)\ /\ \left((2\pi r h_p)^2\ \rho^{L,mass}_{Mix}\ \sigma^{L}_{Mix}\right)$
We^{V}	$\left((VM^{V}_{Mix})^2\ r_i\right)\ /\ \left((2\pi r h_p)^2\ \rho^{V,mass}_{Mix}\ \sigma^{L}_{Mix}\right)$

Latin Symbols

Symbol	Description	Unit
$\dot{E}_{kin}$	Rate of kinetic energy	$\mathrm{J\,s^{-1}}$
$\dot{m}$	Mass flow rate	$\mathrm{kg\,s^{-1}}$
$\dot{v}^{L,avg}$	Average liquid volume flux	$\mathrm{m^3\,m^{-2}\,s^{-1}}$
$\dot{V}_G$	Volumetric gas flow rate	$\mathrm{m^3\,s^{-1}}$
$\dot{V}_L$	Volumetric liquid flow rate	$\mathrm{m^3\,s^{-1}}$
$\overline{F}^{V}_{int}$	Average value of the integrated gas capacity factor	$\mathrm{Pa^{0.5}}$
$\overline{h}$	Partial molar enthalpy	$\mathrm{J\,mol^{-1}}$
$\overline{Re}^{V}_{int}$	Average value of the integrated vapor Reynolds number	-
$\overline{x}_i$	Average of steady state values of i^{th} input variable	various
$\overline{y}$	Weighted mean of repeat experiments for output y	various
A_c	Cross sectional area	$\mathrm{m^2}$
a_p	Specific surface area of packing	$\mathrm{m^2\,m^{-3}}$
a_b	Specific surface area of a 2 mm diameter reference bead	$3000\,\mathrm{m^2\,m^{-3}}$
A_{CH}	RPB configuration dependent parameter to calculate the centrifugal head	-
A_{eye}	Cross sectional area of the packing at the eye of the RPB	$\mathrm{m^2}$
A_e	Effective interfacial area	$\mathrm{m^2}$
a_e	Specific effective interfacial area	$\mathrm{m^2\,m^{-3}}$
A_{jets}	Cross sectional area of the liquid distributor jets	$\mathrm{m^2}$

ATU_{og}	Area of an overall transfer unit based on the gas phase	m^2
ATU_{OL}	Area of an overall transfer unit based on the liquid phase	m^2
c	Concentration	$mol\,m^{-3}$
c	Square mesh opening size of structured wire mesh	m
c_G	Oxygen concentration in the gas phase	$mol\,m^{-3}$
c_L	Oxygen concentration in the liquid phase	$mol\,m^{-3}$
$c_{1,..,7}$	Correlation coefficients	various
c_p	Specific heat capacity at constant pressure	$J\,kg^{-1}\,K^{-1}$ or $J\,mol^{-1}\,K^{-1}$
D	Binary diffusion coefficient	$m^2\,s^{-1}$
d	Diameter	m
d	Fiber thickness of structured wire mesh	m
d_p	$6 \cdot (1-\epsilon)/a_p$, Spherical equivalent diameter of packing	m
d'_p	$6 \cdot (1-\epsilon)/a_p \cdot \psi^{Sphere}$, Spherical equivalent diameter of packing	m
E	Energy transfer flow rate	$J\,s^{-1}$
F	Gas capacity factor (F-Factor)	$Pa^{0.5}$
f_{obj}	Objective function	-
h	Specific enthalpy	$J\,mol^{-1}$
h_p	Axial height of packing	m
He	Henry coefficient	$Pa\,m^3\,mol^{-1}$
j	Molar diffusional flux	$mol\,m^{-2}\,s^{-1}$
K	Overall mass transfer coefficient	$m\,s^{-1}$
k	Mass transfer coefficient	$m\,s^{-1}$
$K^y a_e$	Overall gas-side volumetric mass transfer coefficient	$mol\,m^{-3}\,s^{-1}$
Ka_e	Overall volumetric mass transfer coefficient	s^{-1}
ka_e	Volumetric mass transfer coefficient	s^{-1}
L	Liquid flow rate	$mol\,s^{-1}$
l	Characteristic length	m
LL	Liquid load	$m^3\,m^{-2}\,h^{-1}$
M	Model for calculation of output	-
M	Molar mass	$kg\,mol^{-1}$
m	Local slope of the equilibrium curve	-
N	Mass transfer flow rate	$mol\,s^{-1}$
N_i	Number of input variables for uncertainty calculation	-
N_k	Number of measurements for one steady state of i^{th} measured variable for uncertainty calculation	-
N_r	Number of repeat experiments of one steady state for uncertainty calculation	-
N_{net}	Net mass transfer flow rate	$mol\,s^{-1}$
n_{Rot}	Rotational speed	revolutions/min

N_{th}	Number of theoretical stages	-
NC	Number of components	-
NE	Number of experiments	-
NJ	Number of discrete elements	-
NTU_{og}	Number of overall transfer units based on the gas phase	-
NTU_{OL}	Number of overall transfer units based on the liquid phase	-
P	Pressure	Pa
P^{LV}	Vapor pressure	Pa
R	Inverted volumetric mass transfer coefficient	s
r	Radius	m
s	Fractional rate of surface renewal	s^{-1}
s	Sample standard deviation	various
T	Temperature	K
t_e	Contact time	s
u	Superficial flow velocity	$m\,s^{-1}$
$u_{\overline{y}}$	Overall uncertainty of all repeat experiments for weighted output $\overline{y}$	various
$u_{x,i}$	Standard uncertainty of measured variable x_i	various
u_y	Standard uncertainty of calculated variable y	various
V	Vapor flow rate	$mol\,s^{-1}$
V	Volume	m^3
V^{discr}	Volume of a discrete element	m^3
V_i	$\pi \cdot (r_i)^2 \cdot h_p$, Volume inside the inner radius of the bed within packing height	m^3
v_{O2}	Molar volume of oxygen at its normal boiling point	$cm^3\,mol^{-1}$
V_o	$\pi \cdot ((r_{casing})^2 - (r_o)^2) \cdot h_p$, Volume between the outer radius of the bed and the stationary housing within packing height	m^3
V_p	Total RPB packing volume	m^3
V_t	$\pi \cdot (r_{casing})^2 \cdot h_p$, Volume of the RPB casing, bed and eye within packing height	m^3
w	Mass fraction	-
x	Liquid mole fraction	-
$x_{i,k}$	k^{th} measurement of i^{th} input variable for uncertainty calculation	various
y	Vapor mole fraction	-
y^*	Fictitious vapor mole fraction in equilibrium with bulk vapor	-
y_r	Calculated output variable for steady state repeat experiment r for uncertainty calculation	various
z	Mole fraction	-

Greek Symbols

Symbol	Description	Unit
αa_e	Volumetric heat transfer coefficient	$\mathrm{W\,m^{-3}\,K^{-1}}$
α	Heat transfer coefficient	$\mathrm{W\,m^{-2}\,K^{-1}}$
Δc_{rel}	Relative uncertainty of measured concentration	-
ΔP	Pressure drop	Pa
$\Delta P_{f,stat}$	Pressure drop contribution due to friction in the packed bed without rotation	Pa
Δw_{rel}	Relative uncertainty of measured mass fraction	-
Δx_i	Discretization step width of variable x_i	various
δ	Film thickness	m
$\delta_{m,n}$	Kronecker delta	-
ϵ	Porosity of packing	-
η	Dynamic viscosity	Pa s
$\eta_{CO2abs.}$	CO_2 absorption efficiency	-
Γ	Thermodynamic factor	-
γ	Activity coefficient	-
λ	Thermal conductivity	$\mathrm{W\,m^{-1}\,K^{-1}}$
ω	Angular velocity	$\mathrm{s^{-1}}$
$\overline{\delta}$	Numerical stability parameter for averaging	10^{-4}
Φ^L	Association factor of solvent	-
ψ^{Sphere}	Sphericity, 0.75 for metal foam	-
Ψ_0	Resistance coefficient for single-phase flow for classical, non-perforated packing elements	-
ρ	Density	$\mathrm{mol\,m^{-3}}$ or $\mathrm{kg\,m^{-3}}$
σ	Surface tension	$\mathrm{N\,m^{-1}}$
σ_{cr}	Critical surface tension of packing, 0.075 for metal foam	$\mathrm{N\,m^{-1}}$
σ_w	Surface tension of water at 298.15 K, =0.072	$\mathrm{N\,m^{-1}}$
φ	Form factor of dry packing	-
ϑ	Celsius temperature	°C
ζ_{CH}	Pressure drop contribution of centrifugal head	Pa

Superscripts

Symbol	Description
∞	Infinite dilution
$discr$	Discrete element
eq	Equilibrium

I	Interface
L	Liquid phase
LV	Saturation, liquid/vapor phase change
$mass$	Mass
mol	Molar
NJ	Number of discrete elements
V	Vapor phase
—	Average

Subscripts

Symbol	Description
∞	Total reflux
$\sum$	Constant mole fractions of all species except the n-th
B	Bottoms
b	Bead
$casing$	Casing
CH	Centrifugal head
cr	Critical point
D	Distillate
e	Effective
$empty$	Empty rotor
$exp.$	Experimental
$ext.$	External
f	Friction
$flood$	Flood point
G	Gas
$GCSM$	Generalized Corresponding States Method
i	Inner
in	Flow entering the packing
int	Integrated
$int.$	Internal
$loc.$	Local
$loss$	Loss
max	Maximum
min	Minimum
Mix	Mixture
o	Outer
obj	Objective
out	Flow exiting the packing
P	Constant pressure
p	Packing

$rand.$	Random
reb	Reboiler
$ref.$	Reference
rel	Relative
$sim.$	Simulation
$stat$	Static
$syst.$	Systematic
T	Constant temperature
t	Total
th	Theoretical

Indices

Symbol	Description
i	Uncertainty calculation: Index for input variable ($1...N_i$)
i,j,k	Index for component. ($1...NC$)
j	Index for stage. ($1...NJ$)
k	Index for experimental point. ($1...NE$)
k	Uncertainty calculation: Index for measurement within time series of one steady state point ($1...N_k$)
m,n	Index for component. ($1...NR = NC - 1$)
r	Uncertainty calculation: Index for repeat measurement of same steady state point ($1...N_r$)

List of Abbreviations

ANN	Artificial Neural Network
ATU	Area of a Transfer Unit
BUCT	Beijing University of Chemical Technology
BV	Besloten Vennootschap (Dutch private limited liability company)
CAPEX	CApital EXpenditure
CFD	Computational Fluid Dynamics
CO_2	carbon dioxide
convCT	conventional Computed Tomography
Cr	Chromium
CRB	Counterflow Concentric Ring Rotating Bed
CT	Computed Tomography
DGRL	German pressure-equipment directive
DOW	The Dow Chemical Company
ECHA	European Chemicals Agency
GC	Gas Chromatograph
GCSM	Generalized Corresponding States Method
HAZOP	Hazard and Operability Study
HETP	Height Equivalent of a Theoretical Plate
HIGEE	High Gravity
HTU	Height of a Transfer Unit
ICI	Imperial Chemical Industry

IPOPT	Interior Point OPTimizer
LSSVM	Least Squares Support Vector Machine
MEA	Mono-Ethanol-Amine
NBP	Normal Boiling Point
Ni	Nickel
NTHU	National Tsing Hua University
NTU	Number of Transfer Units
OPEX	OPerational EXpenditure
PFD	Process Flow Diagram
PIV	Particle Image Velocimetry
PTFE	PolyTetraFluoroEthylene
PVC	PolyVinyl Chloride
RPB	Rotating Packed Bed
RZB	Rotating Zigzag Bed
SE	Semi-Empirical
SLPM	Standard Liters Per Minute
SS	Stainless Steel
SVR	Support Vector Regression
tarCT	time-averaged angle-resolved Computed Tomography
TCD	Thermal Conductivity Detector
TM	Theoretical Mechanistic
TSBP	Two Stage Blade Packing
TSCC	Two Stage CounterCurrent
UK	United Kingdom of Great Britain and Northern Ireland
VOC	Volatile Organic Compound
VOF	Volume Of Fluid

1 Introduction

In search of answers to society's demands for cleaner, more energy efficient and innovative solutions directed at the chemical industry, the concept of process intensification has attracted much attention over recent years (Gorak and Stankiewicz, 2011). A key task in chemical engineering is the separation of process mixtures originating from reactions and other sources. The most prominent gas-liquid separation operations are distillation and absorption. Numerous works have therefore been targeted at intensification of these processes. Conventionally, distillation and absorption are conducted in large cylindrical columns filled with internals, such as trays or packings, to increase gas-liquid contact interfacial area. This results in a significant consumption of space and material. For distillation alone there are over 40 000 columns in operation worldwide (Kiss, 2013, p. 37). Furthermore, distillation is among the most energy demanding processes, accounting for up to 50 % of capital and operating costs in industrial processes (Gorak and Schoenmakers, 2014, p. vii). Approaches aiming to intensify distillation comprise e.g. Dividing Wall Columns, Reactive Distillation, Cyclic Distillation, Membrane Distillation, Heat Integrated Distillation Columns and HIGEE Distillation (Kiss, 2013). HIGEE, i.e. the operation in a centrifugal force field at high gravity ("high g"), has also been applied to intensify ab- and desorption processes (Agarwal et al., 2010), and is considered the origin of the research area of process intensification (Gorak and Stankiewicz, 2011).

Liquid traffic in a conventional column is governed by earth's gravity field. If gas flow rate is increased beyond a certain limit, liquid flow will be impeded, entrainment may occur, and a column may finally flood (Gorak and Olujic, 2014, p. 19). By increasing the driving force for liquid flow, much higher flow rates can be achieved in a smaller cross section, or packings with higher specific surface areas can be employed (Lockett, 1995). Mass transfer rates are influenced by available effective interfacial area and the magnitude of the mass transfer coefficients. Both can be increased through the intense mixing, surface renewal and shearing of liquid into small droplets and thin films that is induced through higher centrifugal forces (Burns and Ramshaw, 1996; Guo et al.,

2000; Rajan et al., 2011). The use of centrifugal force fields thus increases achievable throughputs of separation equipment and enhances mass transfer. The potential of applying centrifugal force fields has been realized already at the beginning of the 20th century (Elsenhans, 1906). Full use of the concept in form of a Rotating Packed Bed (RPB) including experimental confirmation was first made at Imperial Chemical Industry (ICI) by Ramshaw and co-workers (Ramshaw and Mallinson, 1981). Since then, several other types of HIGEE devices have been developed, such as spinning cone reactor (Huerta-Pérez and Pérez-Correa, 2018), spinning disc reactor (Meeuwse et al., 2012), rotating spiral fluid-phase contactor (MacInnes and Ayash, 2018) and different modifications of RPBs, such as Rotating Zigzag Beds (RZBs) (Wang et al., 2008a).

Compared to other HIGEE devices, RPBs allow for processing of large streams at comparably moderate pressure losses. Significant equipment size reductions are possible through use of RPBs (Rao et al., 2004; Agarwal et al., 2010). This is of interest especially where weight and size are limited, for example off-shore, in retrofit situations, or indoors (Fowler, 1989; Zheng et al., 1997). Several commercial applications of RPBs exist, mainly in China (Cortes Garcia et al., 2017; Guo et al., 2019) but also in the USA (Trent et al., 1999; Harbold and Park, 2008) and India (Rangaiah, 2016, p. 137).

The main components and the flow paths in a single block packing RPB for countercurrent gas-liquid flow are illustrated in Fig. 1.1. Such an RPB consists of a packing shaped in form of a hollow cylinder that is clamped between two rotor plates. One plate is connected through a shaft to a motor. The plates are housed in a casing with various inlets and outlets. The heavier phase, i.e. liquid, is fed to the center of the RPB, the so called "eye" of the rotor, and distributed through spraying nozzles onto the packing. Liquid is accelerated by the packing and driven outwards where it ejects from the packing as ligaments and droplets. The liquid is collected by the casing and routed outwards. The light phase, i.e. gas, is fed to the casing and driven inwards in countercurrent to the liquid by pressure difference. It exits the casing at the rotor eye. Two seals are required, one between shaft and casing to seal the device to the environment and another between the opposing rotor plate and the casing to avoid gas bypassing the packing. Different structured or random packing materials can be employed. Depending on the material, inner and outer support structures are needed to hold the packing in place and for spacing of the rotor plates.

Despite some successful industrial implementations of RPBs in China, the USA and India, no commercial installations of RPBs have so far been reported in Europe, aside

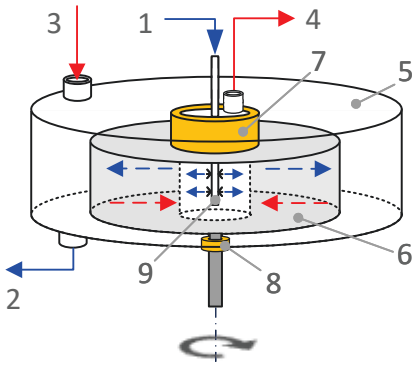


Fig. 1.1: Schematic of RPB with countercurrent gas-liquid flow paths and main components (1-liquid inlet, 2-liquid outlet, 3-gas inlet, 4-gas outlet, 5-casing, 6-packing, 7-upper seal, 8-lower seal, 9-liquid distributor) (Hilpert et al., 2022).

from the initial works at ICI. This is partially related to the chemical industry's reluctance to invest in technology where little or no in-house experience exists and a prevalent skepticism towards rotating equipment (Ramshaw, 1987), but also reflects the limited knowledge available on RPBs in general. While modeling of conventional distillation columns has reached great maturity, making the need for experiments in the design process often obsolete (Henley et al., 2011, p. 259) , this is not the case for RPBs. Especially the lack of proven design guidelines, scale-up rules as well as reliable and readily available models constitute a barrier (Cortes Garcia et al., 2017). The current work is a contribution in the effort to overcome these obstacles by developing and validating a rate-based model for multi-component distillation in RPBs. So far, to the best of the author's knowledge, no such model has been validated due to the lack of experimental data on multi-component distillation. However, most industrial separations involve mixtures with more than two components (Agrawal and Tumbalam Gooty, 2020). To gain industrially relevant insights, systematic experiments are conducted in a pilot-scale RPB test stand in this thesis. The data is subsequently evaluated and used to derive mass transfer correlations. The developed model is validated against further experimental data that was not part of the fit.

The thesis is structured as follows: In Chapter 2, the state-of-the-art of science and technology is summarized. Based on this, in Chapter 3 the research gap is analyzed, the objectives of the thesis laid out and the solution strategy presented. The choice of test systems, the development of the test stand as well as the experimental procedures are described in Chapter 4. The rate-based model for simulation of the experimental results is introduced in Chapter 5. Subsequently, desorption experiments conducted to obtain a liquid-side mass transfer correlation are presented along with the development of

this correlation in Chapter 6. In Chapter 7, the results of distillation experiments are analyzed and used to develop a correlation for gas-side mass transfer. Simulation results as well as the model validation are presented. The thesis closes with a conclusion and outlook in Chapter 8.

2 State-of-the-art

This chapter presents the state-of-the-art of science and technology with respect to the subject of this thesis. First, relevant fundamentals of the modeling and experimental investigation of mass transfer in gas-liquid systems are laid out. Next, a brief overview of hydrodynamics and mass transfer in RPBs is given, followed by an overview of modeling strategies for mass transfer in RPBs. Subsequently, a review of experimental and modeling studies of distillation in RPBs is presented. Finally, advantages and drawbacks of RPBs are described and related to industrial applications.

2.1 Fundamentals of mass transfer in gas-liquid systems

2.1.1 Mass transfer modeling

Key to most separation processes is the formation of an interface between adjoining phases (Henley et al., 2011, p. 5) at which properties, such as density or viscosity, undergo strong changes. For the purpose of this thesis, the considered phases are a gas or vapor phase and a liquid phase. Prerequisite for any separation process is the transport of material and energy across the interface. This can be modeled through two basic approaches, one equilibrium based and the other rate based (Taylor and Krishna, 1993, p. 397).

As opposed to equilibrium based modeling, where the final state of thermodynamic equilibrium is assumed to be reached through extremely fast heat and mass transfer, rate based modeling explicitly considers transport processes caused by driving forces between adjacent phases. It thus provides a more realistic representation of the occurring phenomena and is subsequently described in further detail. Exemplary local concentration profiles during mass transfer across a phase interface are illustrated in Fig. 2.1. The shown molar mass transfer rate N_i of a component i in a binary mixture with component j across the effective interfacial area A_e into phase L can be described

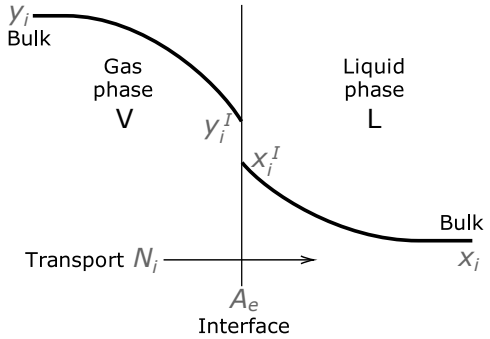


Fig. 2.1: Exemplary concentration profiles for mass transfer across a gas-liquid interface (adapted from Henley et al., 2011, p. 123).

by Eq. (2.1). It consists of a molecular diffusion contribution and a convective contribution that is caused by a net material flow between the phases that may or may not be zero (Henley et al., 2011, p. 86).

$$N_i = \underbrace{k_{i,j}^L \cdot A_e \cdot \rho_{Mix}^{L,mol} \cdot (x_i^I - x_i)}_{\text{diffusive part}} + \underbrace{x_i \cdot N_{net}}_{\text{convective part}} \tag{2.1}$$

The low flux mass transfer coefficient in this equation can accordingly be defined as in Eq. (2.2) (Taylor and Krishna, 1993, p. 141).

$$k_{i,j}^L = \lim_{N_i \to 0} \frac{N_i - x_i \cdot N_{net}}{A_e \cdot \rho_{Mix}^{L,mol} \cdot (x_i^I - x_i)} \tag{2.2}$$

Three main theories have been developed to describe heat and mass transfer. These are boundary layer theory, film theory and penetration theory. Furthermore, models for turbulent flow exist that are based on eddy diffusion, steady or unsteady state assumptions (Harriott, 1962).

Boundary layer theory postulates the existence of a boundary layer for external flows around objects, such as flat plates or spheres (Harriott, 1962): The changes of variables like velocity or temperature are confined to this boundary layer. The thickness of the layer can be defined as the point where a variable reaches 99 % of its bulk value. Thus layers for different variables may have different thicknesses. The layers can be laminar or turbulent (Kraume, 2012, p. 166). From solutions of boundary layer equations expressions for mass transfer coefficients or Sherwood number can be derived.

As Taylor and Krishna (1993, p. 152) summarize, film theory is based on the assumption that all resistance to heat and mass transfer lies in a thin film next to the phase interface. Only steady state diffusive transfer normal to the film occurs while in the bulk region all gradients are wiped out due to turbulence. Mass transfer parallel to the surface is assumed negligible. From these assumptions, Eq. (2.3) for the mass transfer coefficient follows, expressing a linear dependency between rate of mass transfer and molecular diffusivity. This is one of the main points of criticism of the film model, since experimental results show dependencies of $D_{i,j}^{0.5...0.75}$ as Henley et al. (2011, p. 120) point out. Furthermore, it can be seen that film thickness δ_i is component dependent. Concentration profiles in the film (without chemical reaction) are linear. In reality however, profiles are not linear. An example of more realistic profiles is provided by Fig. 2.1 (Henley et al., 2011, p. 123).

$$k_{i,j} = \frac{D_{i,j}}{\delta_i} \tag{2.3}$$

Film theory was extended to two phases by Whitman to obtain the two-film model. The interface is considered to be of infinitesimal thickness, not presenting any resistance to mass transfer. At the interface, phase equilibrium is assumed (Henley et al., 2011, p. 119). The two films on both sides of the interface pose resistances in series to mass transfer. The relation of resistances and mass transfer coefficients can be mathematically described by introducing an overall mass transfer coefficient that describes the mass transfer rate if all the resistance is thought to be located in one phase. To introduce an overall vapor side mass transfer coefficient $K_{i,j}^V$, a fictitious vapor mole fraction y_i^* at the interface is defined that is in equilibrium with the bulk liquid x_i. The molar diffusional flux of component i can then be described according to Eq. (2.4).

$$j_i = \rho_{Mix}^{V,mol} \cdot K_{i,j}^V \cdot (y_i - y_i^*) = \rho_{Mix}^{V,mol} \cdot k_{i,j}^V \cdot (y_i - y_i^I) = \rho_{Mix}^{L,mol} \cdot k_{i,j}^L \cdot (x_i^I - x_i) \tag{2.4}$$

From these expressions, Eq. (2.5) can be derived by means of reformulation (Henley et al., 2011, p. 125). The ratio of the differences of vapor and liquid mole fractions denotes the local slope m of the equilibrium curve between both phases. While it is often constant for ab- or desorption processes, i.e. can be replaced by a Henry coefficient, it changes significantly for distillation of mixtures.

$$\frac{1}{K_{i,j}^{V}} = \frac{1}{k_{i,j}^{V}} + \frac{\rho_{Mix}^{V,mol}}{\rho_{Mix}^{L,mol}} \cdot \frac{1}{k_{i,j}^{L}} \left(\frac{y_i^I - y_i^*}{x_i^I - x_i} \right) = \frac{1}{k_{i,j}^{V}} + \frac{\rho_{Mix}^{V,mol}}{\rho_{Mix}^{L,mol}} \cdot \frac{m}{k_{i,j}^{L}} \tag{2.5}$$

A more realistic picture of occurring processes is provided by penetration theory, developed by Higbie, that was extended by Danckwerts to the surface renewal theory (Henley et al., 2011, p. 120). Little packages of fluid, so called eddies, move to the interface and remain in contact for a short but defined exposure time t_e during which molecular unsteady-state diffusion occurs normal to the interface. Turbulence thus extends to the interface. The eddies subsequently return to the bulk phase and are replaced by other eddies from the fluid bulk that have bulk composition (Taylor and Krishna, 1993, p. 220). These assumptions lead to Eq. (2.6) for the mass transfer coefficient.

$$k_{i,j} = 2\sqrt{\frac{D_{i,j}}{\pi t_e}} \tag{2.6}$$

To obtain an even more realistic model, Danckwerts introduced a residence time distribution for the eddies at the interface (Henley et al., 2011, p. 121). The resulting Eq. (2.7) for mass transfer rate predicts the same dependency with respect to molecular diffusivity as penetration theory, but contains a different parameter s which is the fractional rate of surface renewal. Both t_e and s are, however, not directly accessible through experiments. Penetration theory has successfully been applied to applications involving droplet sprays (t_e equals total contact time of gas and liquid) or randomly packed columns (mixing when liquid film passes between different pieces of packing) (Henley et al., 2011, p. 121). Alternatively, correlations for t_e or s can be derived.

$$k_{i,j} = \sqrt{D_{i,j} \cdot s} \tag{2.7}$$

The framework provided by film theory, especially the assumption of equilibrium at the interface and the addition of resistances in series can be used in conjunction with mass transfer coefficients from other theories, such as penetration theory, or empirical correlations to obtain more realistic results (Henley et al., 2011, p. 123). For example, Rocha et al. (1996) used penetration theory with a correlation for exposure time and another correlation for gas side mass transfer coefficient. van Elk et al. (2007) used penetration theory for liquid side and film theory for gas side mass transfer modeling

of an absorption process. (Semi-) empirical correlations of dimensionless numbers are often used in situations with complicated flow patterns where a multitude of effects overlap. They typically achieve an accuracy around 30% (Cussler, 2000, p. 225).

Another important variable is the effective interfacial area mentioned earlier. This is the actual area where mass transfer between the phases takes place. It may be different from a geometrical area provided by internals of equipment, such as packings. Causes for differences between the areas may be regions of the packing that are not wetted, are covered in stagnant liquid and do not participate in mass transfer or additional area created by liquid droplets or rivulets not attached to the packing (Hegely et al., 2017). Usually the specific effective interfacial area a_e is used, which is calculated with respect to the total packing volume (Eq. (2.8)).

$$a_e = \frac{A_e}{V_p} \tag{2.8}$$

2.1.2 Mass transfer experiments

While for the rate based modeling of binary separation processes overall mass transfer coefficients may be sufficient, the design of an apparatus for separation of a multinary mixture through e.g. distillation requires knowledge of individual mass transfer coefficients of gas and liquid phase as well as the effective interfacial area. Separate values for these variables are accessible through chemical and physical ab- and desorption experiments. The following sections on the measurement of $k^L a_e$, $k^V a_e$ and a_e, which detail said methods, are based on the in-depth review by Hegely et al. (2017). Suitable test systems are recommended by VDI 3679-2.

The established methods for determining mass transfer coefficients have in common that volumetric coefficients are determined, i.e. the product of $k \cdot a_e$. Furthermore, the determined values are packing averaged, based on inlet and outlet concentrations of the streams. In conventional separation columns, special care is hence taken to avoid end effects and measure the mass transfer in the packing only. This enables the measured coefficient to be used in the design of greater packing heights. VDI 3679-2 gives guidelines for the design of such experiments to avoid end effects in conventional columns.

Determination of liquid side mass transfer coefficients

Liquid side volumetric mass transfer coefficients are measured by ab- or desorption of components with very low solubilities, e.g. oxygen in water. As can be seen from Eq. (2.5), gas side resistance becomes negligible for very high slopes m corresponding to low solubilities. Other systems are CO_2/air/water and desorption of toluene from water. In the case of high mass transfer coefficients or great packing heights, experimental uncertainty may increase due to saturation (in absorption experiments) or depletion (in desorption experiments) of the transferring component. Alternatively, chemical absorption can be used, but care has to be taken to control concentrations and stay in the reaction regime required for determining $k^L a_e$. One example is absorption of CO_2 in sodium hydroxide solution in the intermediate reaction rate regime to determine simultaneously a_e and k^L from the Danckwerts plot. However, such k^L values are associated with an increased uncertainty.

Determination of gas side mass transfer coefficients

Gas side volumetric mass transfer coefficients can be determined from chemical absorption with very fast reaction. Danckwerts (1970, p. 149) recommends an instantaneous irreversible second-order reaction, leading to a reaction plane at the gas-liquid interface and thus eliminating liquid side resistance and any back pressure. Danckwerts (1970, p. 209) advises to use the chemical absorption of SO_2 from air in aqueous sodium hydroxide solution, because very low concentrations of SO_2 can still be measured accurately, allowing for significant absorption to occur in the apparatus, and no increased corrosion of steel equipment is to be expected from the alkaline solution. Chemical absorption is the preferred method to determine $k^V a_e$ with SO_2/air/sodium hydroxide solution being extensively used. Gas side volumetric mass transfer coefficients could also be determined by vaporization of a pure liquid, e.g. air/water, as then no liquid side resistance exists. Care has to be taken not to saturate the gas phase. Thus only the investigation of short bed lengths is possible here. Physical absorption of components with high solubility at high liquid to gas ratios has been used, but there is always an influence of liquid side resistance. This needs to be accounted for by calculating $k^L a_e$ using other correlations.

Determination of specific effective interfacial area

Specific effective interfacial area can be determined using certain chemical absorption systems. The system CO_2/air/sodium hydroxide solution in the fast reaction regime has been almost exclusively used in the recent past (Hegely et al., 2017). Given a_e, the

mass transfer coefficients k^L and k^V can be calculated from $k^V a_e$ and $k^L a_e$. However, uncertainties of a_e are propagated to the mass transfer coefficients by this method. Hence, k^L and k^V correlations should only be used in conjunction with the corresponding a_e correlation from which they were determined (Song et al., 2018).

Transferability of mass transfer coefficients from ab- or desorption to distillation

The analogy and transferability of results obtained from absorption to distillation is subject of ongoing research. Some authors concluded that there is no significant difference in mass transfer coefficients determined from either absorption or distillation (Deed et al., 1947; Ovejero et al., 1992).

However, there are several differences between distillation and absorption processes that might hamper transferability. Especially the difference in surface tension between usually aqueous systems in absorption and usually organic systems in distillation seems to have to be taken into account (Yoshida and Koyanagi, 1962). This discrepancy results in different wettabilities of packing material between organic and aqueous systems. Studies tried to investigate these effects by addition of surfactants or modification of packing material or surfaces. Onda et al. (1968) reduced surface tension using a surfactant and observed a decrease in $k^L a_e$ values. Coughlin (1969) pointed out that addition of a surfactant often also influences other transport properties and may introduce a mass transfer resistance to the interface. Therefore, Coughlin measured $k^L a_e$ for packing materials with different contact angles. Coughlin concluded that the decrease in a_e with more hydrophobic material might be partly offset by increased surface renewal.

Differences in liquid viscosity between absorption and stripping, which usually occur near ambient temperature, and distillation at the boiling point are also significant. While viscosity in distillation is often in the range of 0.1 to 0.2 mPa s (Seider et al., 2004, p. 451), this is difficult to achieve experimentally with aqueous systems where viscosity is approximately 1 mPa s. Onda et al. (1968) investigated desorption of oxygen from methanol, Rejl et al. (2017) from methanol, ethanol, n-propanol and water to determine k^L. Rejl et al. (2017) found approximate proportionalities of k^L to $(D^L)^{0.5}$ (in agreement with penetration theory), $(\sigma^L)^{-0.5}$ and $(\eta^L)^{-0.3}$. Further studies exist that increase viscosity by addition of e.g. glycerol to standard aqueous test systems. Song et al. (2018) and Delaloye et al. (1991) found that k^L decreased with increasing viscosity due to reduced liquid diffusivity and due to a second influence (proportional to $(\eta^L)^{-0.4...-0.5}$) that Song et al. attributed to decreased liquid turbulence. Delaloye

et al. (1991) assumes that the uncertainties due to deviations in viscosity have only a moderate impact on distillation column design and are more important for absorption with viscous solvents.

Another major difference is the diffusion regime, with unidirectional diffusion occurring in ab- and desorption and approximately equimolar counterdiffusion occurring in distillation. Onda et al. (1968) assume that this, however, has little effect. More important are property changes along the packing, necessitating the integration of correlations. In modern works this integration is done by using correlations in discretized rigorous models.

Where alternative methods are not usable, employing correlations derived from ab- or desorption experiments to distillation modeling remains the best available option despite the associated uncertainties.

Direct measurement of liquid and gas mass transfer coefficients from distillation

To circumvent uncertainties associated with the use of correlations based on data from ab- or desorption experiments in distillation modeling, attempts have been made to obtain mass transfer coefficients directly from distillation experiments.

Edye (1955) investigated distillation in a laboratory column of low height (60 mm using benzene/n-heptane) to avoid large changes in concentration, enabling him to assign average values for concentrations to the results. Based on the HTU/NTU concept, Edye calculated the individual contributions of gas and liquid side to mass transfer resistance.

Blum (1995) employed a maximum likelihood function to fit simulated to experimental temperature and liquid composition profiles by adjusting either gas side, or both gas and liquid side mass transfer coefficients (one coefficient for the whole column length). He showed that liquid side mass transfer resistance is important especially in the stripping section where the equilibrium curve is steep. The method was used with binary and ternary mixtures of fatty alcohols at finite reflux to be closer to production conditions. Coefficients were more clearly identifiable when profiles were steep and thus the driving force $(y_i^I - y_i)$ or $(x_i - x_i^I)$ great, magnifying the influence of the mass transfer coefficient. Determination was more difficult in ternary systems, as the intermediate boiler develops a flat maximum in the concentration profile.

More recently, the group of Rejl presented another profile method (Linek et al., 2005; Rejl et al., 2006), which exploits the measured liquid composition profile from binary

distillation experiments at infinite reflux to simultaneously and directly deduce volumetric vapor and liquid side mass transfer coefficients $k^L a_e$ and $k^V a_e$. The method was extended to incorporate vapor composition profiles (Rejl et al., 2010). A column model is integrated over the height to obtain concentration profiles. By modifying existing correlations based on absorption, such as Onda et al. (1968) or Billet and Schultes (1999), through multiplication with a factor, the difference between measured and calculated concentration profiles is minimized. These three works showed considerable discrepancy between simulated profiles using existing absorption based correlations and experimental profiles from packed laboratory columns. Existing correlations multiplied with a factor were only able to describe experimental data when exponents of vapor and liquid velocity dependence were changed. To further investigate if the analogy of absorption and distillation results is valid, Rejl et al. (2016) employed the profile method in a wetted wall column. A wetted wall column has the advantage of a less complex hydrodynamic situation and a known interfacial area. Correlations from absorption runs in the column were determined and compared with mass transfer coefficients determined from the profile method for distillation runs in the same column. It was concluded that the analogy may be valid, as the deviations were within the relatively large uncertainties of the diffusion coefficients. First results of new investigations of profiles in a relatively large column ($d_i = 150\,\mathrm{mm}$) lead to the conclusion that $k^V a_e$ results (absorption of SO_2 from He, N_2 and SF_6 gas streams in sodium hydroxide solution) may be transferable, while $k^L a_e$ results from oxygen desorption from methanol/ethanol/n-propanol may not be well transferable to the distillation of these alcohols (Rejl et al., 2018).

Application of profile based methods to RPBs is difficult, as placement of temperature sensors along the radius into the packing of a single block RPB requires special telemetry due to the rotation of the packing (Hampel et al., 2020). Further advances on this technology might open new opportunities to determining mass transfer coefficients in RPBs. Alternatively, given a sufficiently long packing between inner and outer radius, it might be more easily possible to place temperature probes or even sample along the radius in a rotor-stator arrangement.

Summarizing, at the present time, the use of mass transfer coefficients from absorption and desorption experiments for the modeling of distillation processes is the most common method, despite some associated uncertainties. Alternative approaches exist, but are still in the development stage and of limited use for RPBs. Additional research is required in this area.

2.2 Hydrodynamics and mass transfer in RPBs

Key to designing RPBs is an understanding of their hydrodynamics and of the interaction between hydrodynamics and mass transfer. In this section, an introduction to important flow and mass transfer phenomena in RPBs is given. Only gas-liquid operation of RPBs is considered.

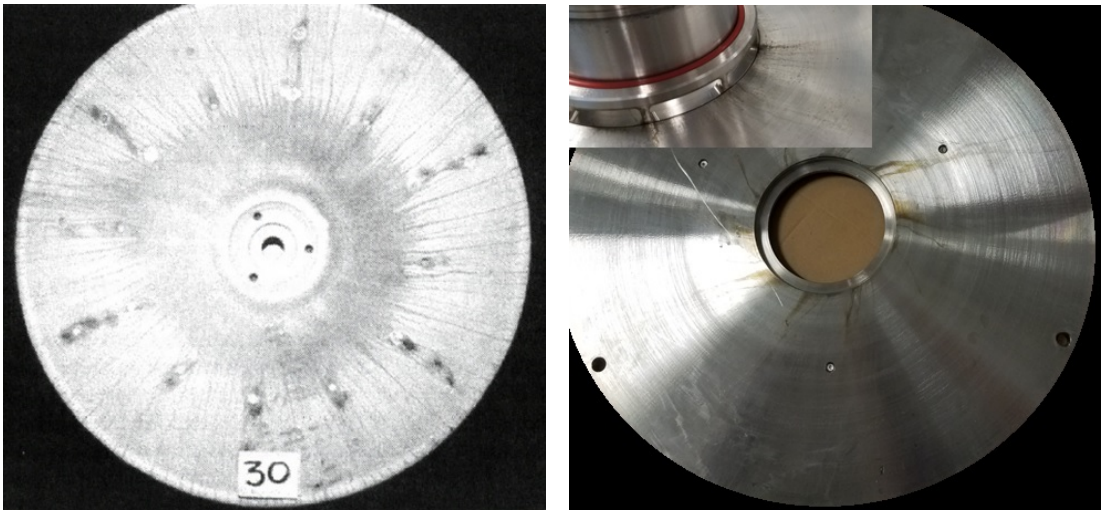
2.2.1 Hydrodynamics

The general flow pattern for a single block packing RPB in countercurrent operation has been described in the introduction based on Fig. 1.1. Several investigations have been conducted to resolve the occurring flow regimes of gas and liquid in further detail. Based on these investigations liquid flow, hold-up and residence time in RPBs are first detailed. Then, gas flow and pressure drop are described. Finally, the hydrodynamic operating window of RPBs is characterized.

Liquid flow, hold-up and residence time

Liquid enters the packing in a section known as the (inner) end effects zone. Due to the great difference in circumferential velocity between liquid and packing, strong shearing and break up of the liquid occurs. Not all liquid is immediately caught by the packing, with some flying further into the packing in the form of droplets, as observed by a camera mounted on a rotor (d_i =252 mm, d_o =452 mm, up to 1200 min^{-1}) packed with wire mesh and metal foam packings (Guo et al., 2000). Guo et al. (2014a) installed paper strips circumferentially at varying radial distances and investigated ink blot patterns to determine the length of the end effects zone. From this study, they concluded that flying droplets dominated within the end zone and transitioned to film flow in the packing bulk. Sang et al. (2019) optically measured the tangential angle with which droplets where ejected from the packing, adding wire mesh packing layer by layer. After a certain number of layers ejection angle remained constant, which was defined as the length of the inner end effects zone. Xu et al. (2019) investigated impacting of a liquid jet on a single layer of wire mesh packing using high-speed photography. They distinguished between a shearing action by vertical and a carrying action by horizontal fibers, resulting in a liquid film on the wire mesh of 21 to 32 µm thickness.

Salt precipitation in experiments of Trent and co-workers at DOW illustrate the liquid flow behavior in RPBs very well, as shown in Fig. 2.2a. Beyond the end effect zone,



(a) (b)

Fig. 2.2: Precipitates observed by (a) Trent et al. (1999) and (b) this work on rotor plates of RPBs.

it can be seen that liquid travels on a relatively straight path in radial direction. The same observation was made in the current investigation, where oil deposited on the rotor plates during initial experiments with a metal foam packing. Fig. 2.2b further illustrates that sections of the bed remain shadowed from the inner support ring, a spacer between upper and lower rotor plate. The phenomenon of shadowing is exacerbated for support rings with a low fraction of free area. Farther out in the rotor, the liquid travels as rivulets. This behavior was first reported from visual studies of flow in a PVC foam by Burns and Ramshaw (1996), who replaced a rotor plate by a transparent perspex cover. Thus, the assumption of complete wetting of the packing by film flow is not valid, as was confirmed through conductivity measurements of liquid hold-up in an RPB by Burns et al. (2000). Rather, radial rivulets made up of filled interconnected pores dominate at low rotational speeds and transition into droplet flow at higher rotational speeds, with a suspected onset of film flow (Burns and Ramshaw, 1996). Droplet flow was also reported by Yan et al. (2014) from ink stain experiments on paper strips placed in a packing of triangular spirals. They concluded that the frequency of droplet-packing collisions was very high and usually resulted in deposition of a droplet on the packing. From these experiments it can also be seen that little distribution of liquid in axial direction occurs (Yan et al., 2012; Yan et al., 2014). This is further supported by experiments of Rao et al. (2004). Any film that might be established is likely to break up at higher rotational speeds and radial positions farther from the center, leading to the formation of dry spots. This was observed by Moore

(1986, p. 46) for flow of water over rotating wire mesh sheets and is caused by the decrease in film thickness due to increased centrifugal acceleration and flow area at greater radial distances. An increased liquid flow rate delayed the film breakdown.

According to the tracer response experiments conducted by Burns et al. (2000), liquid velocity is high (around $1\,m\,s^{-1}$) and liquid hold-up low (in the range of 1 to 30 %). Consequently, residence time in the packing is below 1 s (Burns et al., 2000). This is in the same range as reported by Keyvani and Gardner (1989).

Further insights into liquid flow were gained through tomographic investigations using X-rays. Two technologies, namely conventional Computed Tomography (convCT) and time-averaged angle-resolved Computed Tomography (tarCT), were used (Groß et al., 2019). convCT depicts rotating parts as smeared (static observer) while tarCT depicts static parts as smeared (rotating observer). Yang et al. (2015a) employed convCT for liquid hold-up measurements in metal foam and wire mesh packings. They developed a correlation including measured influences of surface tension and viscosity based on a comprehensive review of existing hold-up correlations for RPBs. However, only a single-slit distributor and a lab-scale RPB were investigated. Residence times in the range of 0.1 to 1.6 s were calculated from liquid flow rate and hold-up. Groß et al. (2019) employed tarCT to measure liquid hold-up using a multi-point liquid distributor in a pilot-scale RPB with similar dimensions and an identical metal foam packing as used in this work. They observed a ring of liquid at a rotational speed of $300\,min^{-1}$ near the inner radius that gave way to better circumferential homogenization at $600\,min^{-1}$ and pronounced shadowing caused by the inner support ring at $1200\,min^{-1}$. Gas flow rate only influenced hold-up at low rotational speeds. The hold-up correlation of Burns et al. (2000) underpredicted observations by >30 %, probably due to the PVC foam having pores twice as large as the nickel-chromium foam investigated. The hold-up correlation of Yang et al. (2015a) on the other hand over-estimated measured values by >30 %, probably due to the much shorter bed length and thus greater influence of the inner end zone (Groß et al., 2019). Both CT investigations observed a maximum in liquid hold-up close to the eye of the RPB. This local accumulation of liquid was attributed to the packing capturing all the liquid injected by the distributor into the voids of the packing, prior to the spreading of the liquid due to increased flow area and centrifugal acceleration with increasing radial distance from the eye.

Visual studies of the liquid flow in the casing zone (the outer end effects zone) were conducted using high speed cameras. Sang et al. (2017b) studied droplet ejection from a wire mesh packing. They distinguished ligament flow at higher liquid flow rates and

lower rotational speeds that transitioned into droplet flow. Average droplet diameter was correlated to liquid initial velocity, rotational speed, outer packing radius as well as liquid surface tension and viscosity. Furthermore, Sang et al. (2017a) correlated droplet velocity to the influence of radius, rotational speed and liquid flow rate. Contact of so called mother droplets with the casing wall was studied. While the created liquid film at the casing wall was concluded to account for the greatest part of the generated effective surface area in the casing, mother droplets and so called daughter droplets resulting from back-splash contribute significantly as well. A model was proposed and validated using a_e values for the casing obtained from the CO_2/air/sodium hydroxide solution system following a procedure outlined by Guo et al. (2014b).

The above observations have several implications for RPB design:

- Free cross sectional area of the inner support ring should be kept as large as possible to avoid shadowing of sections of the bed (Rao et al., 2004).

- The ratio of outer to inner radius should not be increased too far because sections farther out are used less efficiently but add to power consumption and capital cost (Trent, 2004). The use of an additional rotor might prove more efficient.

- Liquid distributor nozzles should not be rotated with the packing, as the shearing and mixing of liquid upon first contact with the rotating packing becomes less intense, which decreases mass transfer efficiency (Trent et al., 1999).

- Care has to be taken to evenly distribute liquid in axial direction, especially for higher rotors (Rao et al., 2004).

- There is room for optimizing packing designs to exploit the phenomena.

Gas flow and pressure drop

Understanding gas flow in RPBs is key to modeling pressure drop. The following considerations pertain to a single block packing RPB with a vertical axis operated in countercurrent gas-liquid flow. In this mode, gas enters the casing and is set in circumferential motion by the rotation of the rotor. It has been observed that gas flow in the casing sets liquid at the casing bottom in circular motion due to the drag between gas and liquid (Rao et al., 2004). This warrants the installation of radial flow breakers at the casing bottom next to liquid outlets. Gas then enters the packing and accelerates

radially on its way inwards due to the decrease in flow area. At the rotor eye, gas has to perform a 90° turn to exit the rotor.

Gao et al. (2017) investigated gas flow in the absence of liquid in a lab-scale RPB (r_i =30 mm, r_o =100 mm, h_p =50 mm) packed with large glass beads (d_{bead} =16 to 25 mm) using 2D Particle Image Velocimetry (PIV). Particles employed stemmed from smoke. In the limited range of rotational speeds of 100 to 300 min^{-1}, gas velocity, radial and tangential slip velocity as well as turbulent kinetic energy in the packing were measured. Slip velocities in the range of 3 to 50 % of mean velocity were found. An increase in turbulent kinetic energy near the inner radius was viewed as an indicator of a gas inner end effect zone. Previously, only a gas outer end effect zone had been reported from CFD simulations (Liu et al., 2017).

Zheng et al. (2000) and Sandilya et al. (2001) concluded from analyzing equations of motion that gas in the RPB rotor undergoes a solid-body like rotation due to the drag between gas and packing. Zheng et al. (2000) investigated pressure drop in an RPB experimentally and developed a semi-empirical 1D model based on conservation equations of mass and momentum. The radial velocity component of the gas increases from outer to inner radius due to the decrease of the flow area and the conservation of mass. Regarding the angular velocity component of the gas, they deduced that it increases drastically once gas enters the rotor at the outer radius and quickly attains a velocity slightly above that of the rotating packing. The gas is decelerated by the packing on its way inwards, attaining an angular velocity slightly above that of the packing. Once the gas reaches the eye of the rotor, its angular velocity increases again due to the vortex formed in the eye by the Coriolis force. This behavior explained two observations. Pressure drop increases with an increasing inner radius since angular velocity of the exiting gas is greater. Pressure drop was observed to decrease with increasing liquid load at low liquid loads. Zheng et al. (2000) concluded that the liquid streams in the eye played the role of guide vanes, directing the gas flow in radial direction. This phenomenon was observed by several works on pressure drop in RPBs (Keyvani and Gardner, 1989; Liu et al., 1996; Sandilya et al., 2001). Whether the explanation suggested by Zheng et al. (2000) is correct has not been ascertained experimentally yet and other hypotheses have been suggested (e.g. Qi et al. (2016)).

Overall pressure drop can be considered to consist of several major contributions, namely pressure drop in the gas inlet and casing, RPB pressure drop and pressure drop in the eye and gas outlet (Rao et al., 2004). Agarwal et al. (2010) state that RPB pressure drop should be predominant for larger units, while the other components may

become significant for units with smaller outer diameters and axial heights. However, experimental determination of the individual contributions is difficult. RPB pressure drop can be subdivided in contributions of pressure drop due to momentum gain as flow area changes, frictional pressure drop and centrifugal pressure drop (Kumar and Rao, 1990). The latter is a predominant factor in RPBs (Agarwal et al., 2010) and can be calculated according to Eq. (2.9) (Kumar and Rao, 1990). A_{CH} is an empirical parameter with reported values ranging between 0.5 to 2 (Rao et al., 2004).

$$\zeta_{CH} = A_{CH} \cdot \frac{\rho_{Mix}^{V,mass} \cdot \omega^2}{2} \cdot \left((r_o)^2 - (r_i)^2 \right) \tag{2.9}$$

From the view point of a rotating observer, gas flow is similar to that in a conventional packed bed, but with decreasing flow area. Therefore, pressure drop equations of conventional beds can be adapted to describe frictional pressure drop in the packing (Rao et al., 2004). Pressure loss due to momentum gain as flow area changes accounts only for approximately 5 % of total pressure drop (Sandilya et al., 2001).

Suggested pressure drop models are either based on purely theoretical considerations (e.g. Kelleher and Fair (1996)) or contain empirical elements (e.g. Singh et al. (1992) and Neumann et al. (2017b)). Influence of liquid flow rate is often neglected. Neumann et al. (2017b) point out the limited transferability of available semi-empirical pressure drop correlations between RPBs of different sizes and the high number of required fitting parameters. They suggest a correlation with only two parameters (A_{CH} and a form factor) and fit these for different wire meshes and metal foams. The correlation performs better for their experimental data than the correlations of Kelleher and Fair (1996) and Singh et al. (1992).

Hydrodynamic operating window

Sudhoff (2015, pp. 232–234) described three phenomena limiting the hydrodynamic operating window of a single block packing RPB, namely flooding, impact and deflection. Based on theoretical considerations, he developed the corresponding graph shown in Fig. 2.3.

The most important phenomenon is flooding as it may impede operation entirely. Flooding occurs during operation with high gas and liquid loads at the inner radius of the packing where flow velocities are highest and centrifugal force is lowest. Liquid hold-up first increases until entrainment of liquid and finally flooding of the eye occur.

An increase of rotational speed increases the flooding limit significantly. Neumann et al. (2017a) compared different definitions and experimental strategies to determine RPB upper operating limit. Flooding limit can be described through a Wallis or Sherwood type correlation (Sudhoff et al., 2015). The knowledge of flood point is important for selection of the axial bed height to match design capacity, comparable to the choice of a proper diameter in conventional columns (Agarwal et al., 2010). Maximum allowable gas flow rate is lowered for nozzle types that create a spray and impart less energy on the liquid, such as flat jet tongue type nozzles compared to full jet nozzles, since entrainment occurs more easily as observed by Neumann et al. (2017a).

If liquid hits the packing with high initial velocities or the free area is small due to a support ring, part of the liquid is splashed back and creates a fine mist. The mist is entrained by the gas. Sudhoff termed this phenomenon "impact" and expected it to reduce the operating window more strongly at increased rotational speeds. Rao et al. (2004) describe the same phenomenon under the term "splashing", but cite an investigation that showed how splashing was reduced by an increased rotational speed. This was attributed to liquid clinging to the bars of the inner support ring and being accelerated into the bed.

At low initial liquid velocities and increased gas velocities deflection may occur, i.e. liquid is entrained with the gas stream prior to reaching the packing.

2.2.2 Mass transfer

Liquid side mass transfer in RPBs is enhanced as compared to conventional columns by the strong acceleration, shearing, impingement and mixing of the liquid, resulting in the formation of high specific effective surface areas and rapid surface renewal (Guo et al., 2000; Rao et al., 2004; Neumann et al., 2018).

Gas side mass transfer on the other hand is not intensified to the same extent. Due to the negligible difference in velocity between gas phase and the packing respectively the liquid, mass transfer coefficient on the gas side is expected to be similar to that in conventional columns (Sandilya et al., 2001). Chen and Liu (2002) attributed the increase of gas side volumetric mass transfer coefficient mainly to an increase in a_e. However, the a_e used to calculate k^V from the measured $k^V a_e$ were obtained from the correlation of Tung and Mah (1985), limiting their reliability. Gas side mass transfer coefficients in single block packing RPBs can be increased compared to conventional

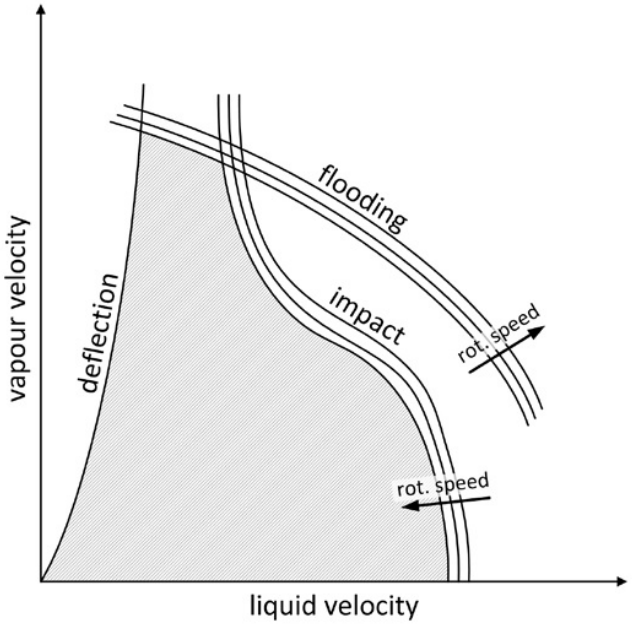


Fig. 2.3: Qualitative hydrodynamic operating window of a single block packing RPB (adapted from Sudhoff, 2015, p. 234).

columns due to the higher possible gas velocities that would cause flooding in columns (Trent, 2004, p. 37).

Some general trends that have been observed are an increase of mass transfer efficiency with increasing rotational speed, decreasing liquid flow rate and increasing gas-to-liquid ratio (Trent, 2004, p. 37). Of course there have been deviations from these trends, such as a maximum in separation efficiency with rotational speed (Kelleher and Fair, 1996; Liu et al., 2019a). Effective interfacial area has been found to increase with increasing rotational speed, liquid flow rate and gas-to-liquid ratio (Luo et al., 2012a; Neumann, 2018, p. 30). It appears high voidage packings are more advantageous to apply in RPBs than extremely high surface area packings due to their lower pressure drop but comparable mass transfer performance (Chen et al., 2006; Trent, 2004, p. 37). Especially wire meshes provide high separation efficiency (Chen et al., 2006; Qammar et al., 2019).

End effects

Mass transfer in RPBs is furthermore governed by the end effects which are a characteristic feature of single block packing RPBs. An inner and an outer end effects zone exist, as schematically indicated in Fig. 2.4.

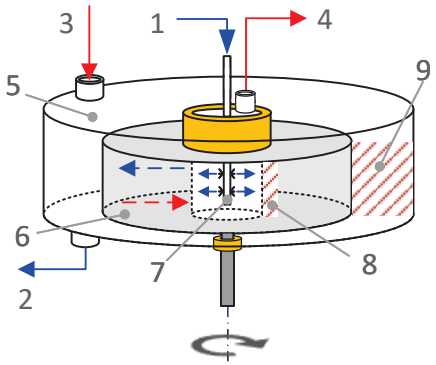


Fig. 2.4: Sketch of end effect zones in an RPB: 1 - liquid inlet, 2 - liquid outlet, 3 - gas inlet, 4 - gas outlet, 5 - casing, 6 - packed rotor, 7 - liquid distributor, 8 - inner end effects zone (within packing), 9 - outer end effects zone (in the casing).

The inner end effects zone of an RPB is characterized by the great velocity difference between the liquid and the rotating packing, resulting in strong shearing as described in the previous section. Furthermore, strong gas-liquid interaction is encountered here due to the highest gas flux being achieved in this smallest cross sectional area (Chu et al., 2014). The outer end effect zone is the casing in which additional interfacial surface is generated and additional mass transfer takes place. Possibly, there exists a third end effect zone, i.e. a gas side end effect zone which may occur in the outer layers of the packing where gas turbulence is increased as the gas enters the packing (Liu et al., 2017). It is not included in Fig. 2.4, since it has only been predicted based on CFD calculations but so far not been experimentally confirmed. Separation of these end effects from mass transfer in the bulk of the packing is difficult. Usually mass transfer due to end effects is attributed to the packing and included in reported results and also in developed correlations. Furthermore, mass transfer coefficients and effective surface area along the packing radius are not constant since flow velocities and centrifugal acceleration change. Shadowing and the formation of rivulets exacerbate the situation. Even without the presence of end effects, bed averaged values of mass transfer coefficients are thus usually obtained.

To alleviate the issue of outer end effects, different attempts have been made to separate these end effects from packing mass transfer. The simplest approach is sampling of liquid at the packing edge (Singh et al., 1992; Luo et al., 2012a; Chu et al., 2015) or of gas inside the casing (Reddy et al., 2006; Rajan et al., 2011). However, large fluctuations in measured gas concentrations in the casing have been reported compared to outlet gas concentrations (Rajan et al., 2011). Mass transfer has alternatively been restricted to the casing by blocking gas flow through the rotor: Guo et al. (2014b) used the

CO_2/sodium hydroxide system to measure a_e within the casing only, while purging the rotor from the inner radius with nitrogen gas. Reddy et al. (2006) connected both the inlet and outlet gas tubes to the casing to measure $k^V a_e$ within the casing using SO_2 absorption in aqueous sodium hydroxide solution. They reported good agreement between $k^V a_e$ within the casing obtained from this method and from gas sampling inside the casing under normal countercurrent operation inside the rotor. As a third approach, Reddy et al. (2006) first conducted experiments with a thin ring of packing near the inner radius serving as a liquid distributor to obtain $k^L a_e$ values of the casing. These values where then used to back-calculate concentration at the packing edge in packed rotor $k^L a_e$ measurements. However, this approach attributes inner end effects to the casing mass transfer. Munjal et al. (1989b) proceeded in a similar fashion but without any packing to distinguish between interfacial area provided by the packing and the outer end effects.

Inner end effects are desirable from an efficiency perspective since they contribute significantly to the overall mass transfer. It is possible to estimate the contribution from experiments with varying packed bed lengths (Singh et al., 1992). Chen et al. (2005a) attempted to account for inner and outer end effects in a correlation for $k^L a_e$ by varying inner and outer bed radii. A scaling term was incorporated in the correlation that includes the ratio of volume inside the rotor eye to total volume of the RPB and of volume between casing and rotor to total volume of the RPB. Usually such experiments are conducted in the same casing and possibly with the same rotor plates. This introduces additional effects, such as an increase of residence time of droplets flying in the outer cavity zone for decreased outer radii (Yang et al., 2011).

The extent to which end effects contribute to overall mass transfer depends on the exact geometry and operating conditions of a machine. To give an impression of the magnitude of end effects, some publications quantifying outer end effects are summarized in Tab. 2.1.

Tab. 2.1: Publications quantifying outer end effects in RPBs.

Reference	Contribution of cavity zone
Yang et al. (2011)	≈13 to 25 % of a_e
Luo et al. (2017)	≈9 % of a_e
Reddy et al. (2006)	≈30 to 40 % of $k^V a_e$, ≈60 to 70 % of $k^L a_e$
Chu et al. (2015)	≈1 to 40 % of $\eta_{CO2abs.}$

Comparing data from different HIGEE devices

To compare data from RPBs of different sizes, Trent (2004, p. 37) suggested to use centrifugal acceleration or tangential velocity instead of rotational speed. Sudhoff et al. (2015) demonstrated that centrifugal acceleration is not a unique measure to use for comparisons and suggested an integrated centrifugal acceleration instead. It can be interpreted as the energy input to an area of the rotor. Compared to a mean or maximum centrifugal acceleration it provides a unique value for a given rotor area.

Mass transfer in RPBs has been characterized using the above described (volumetric) mass transfer coefficients, HTU and HETP. As opposed to conventional columns, the latter two refer to the radial distance along the rotor (Sudhoff, 2015, p. 33) instead of the packing height. To account for the changes in flow velocities and centrifugal force in RPBs, different concepts have been suggested. Singh et al. (1992) introduced the Area of a Transfer Unit (ATU) in analogy to HTU in conventional columns. While this unit is more suited to describe RPBs, it cannot be used for comparisons with conventional columns.

While the ATU concept is often used in RPB literature, the reporting in terms of tangential velocity or (integrated) centrifugal acceleration has not yet been widely adopted.

As a consequence of the end effects in RPBs, use of well-known indicators, such as HETP, HTU, mass transfer coefficients or even ATU for performance comparison with differently sized RPBs or columns is problematic. While for a conventional column an additional section of packing will have a similar efficiency as the remainder of the unit and can equally be used to increase product purity, this is not the case for RPBs. Sections of bed further out will contribute less to overall separation efficiency. Special care has to be taken when considering data from RPBs with short radial bed lengths where end effects contribute disproportionately to the separation efficiency. Volumetric mass transfer coefficients may be up to an order of magnitude higher than those from larger RPBs. Thus, scale-up of an RPB using a correlation gained from a smaller machine may result in significant overprediction of efficiency, as will be shown in Sec. 6.2.1.

To date, the issue of comparing RPB performance indicators has not been solved. A possible approach lies in the use of a benchmark design for mass transfer and hydrodynamic investigations. Over time, experience could be gained as to how this relates to scale-up designs and suitable safety factors and rules of thumb could be obtained. Neumann (2018, pp. 105–110) proposed a first benchmark design of an RPB

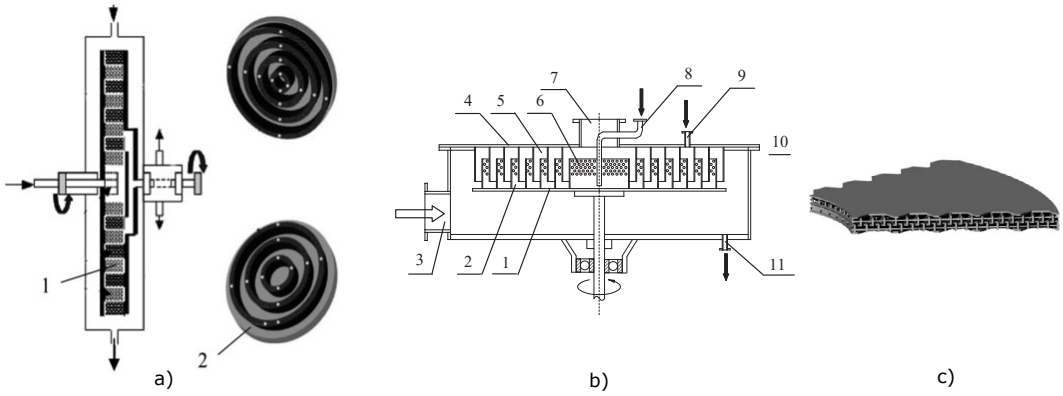


Fig. 2.5: Sketch of some HIGEE design modifications: a) split packing RPB, adapted from Rao (2015) (1 - sectional view, 2 - exploded view of the packing); b) RZB, adapted from Li et al. (2013b) (1 - rotor disk, 2 - rotating baffle, 3 - gas inlet, 4 - stator disk, 5 - stator baffle, 6 - perforations, 7 - gas outlet, 8 - liquid inlet, 9 - intermediate feed, 10 - casing, 11 - liquid outlet); c) Section of Zickzack packing, adapted from Qammar et al. (2019).

and defined knock-out criteria (major construction deficits) that would impede the use of a machine for benchmark measurements. Such a design could also serve to rate improvements from design changes. Possible reasons for the use of a benchmark design not having found application yet are the prototype nature of devices, the multitude of changes made to designs (described in the following section), the vast differences in periphery available in different experimental facilities and the lack of collaboration between different research groups.

2.2.3 RPB design modifications

Based on the above findings regarding RPB hydrodynamics and mass transfer, a series of modified designs have been proposed to further intensify heat and mass transfer, many of which are described in Cortes Garcia et al. (2017). Some developments are briefly presented here.

Chandra et al. (2005) proposed a split packing rotor made up of two co- or counter-rotating plates to which alternatingly rings of packing material are fixed with small annular gaps in between, as illustrated by Fig. 2.5 a). Metal foam was used as a packing material. The goal of the development was to increase the slip velocity between gas and rotor to enhance gas side mass transfer. First mass transfer experiments of Reddy et al. (2006) were not conclusive with small differences for $k^V a_e$ from co- and

counterrotation. Hence, two further investigations of split-packing RPBs were published by this workgroup: Rajan et al. (2011) measured $k^L a_e$ as well as a_e and found approximately 10 to 30 % higher values for counterrotation, likely due to improved liquid redistribution. Shivhare et al. (2013) investigated split packings and single block packings in comparison. While counterrotating packings performed only slightly better than corotating packings, $k^V a_e$ values were up to 50 % higher than for a single block packing. However, due to the increased cost of manufacture (tight tolerances) as well as operation (two motors) and the scale-up limitations (streams have to be routed through the shafts) this design has not found wide-spread use.

Some designs have attempted to recreate the inner end effect zone and the accompanying intense mass transfer. Luo et al. (2012b) constructed a blade packing RPB with alternating rings of wire mesh packing and angled metal blades. Increases of a_e up to 35 % and of k^L up to 100 % were reported as compared to a single block packing. A multi-liquid-inlet RPB was developed for absorption processes which had a lower pressure drop (Xing et al., 2014) as well as ≈23 % higher a_e and ≈8 % higher $k^L a_e$ (Chu et al., 2014) compared to a single block packing RPB.

Wang et al. (2008a) presented an RZB, comprised of a lower rotor plate and an upper stator plate to which alternatingly circular baffles are attached, as illustrated by Fig. 2.5 b). The upper parts of the rotating baffles are perforated (Wang et al., 2011). Gas and liquid are forced on a zigzag path. Liquid is stopped at every stator baffle and has to be accelerated anew. Gas velocity in the annular gaps can be kept constant by varying radial spacing of baffles. These characteristics cause a strong increase in pressure drop and motor power consumption compared to an RPB (Li et al., 2013a). On the other hand, mass transfer is enhanced due to increased relative velocities. The influence of geometrical details of RZBs was experimentally studied by Wang et al. (2019). k^V and a_e values were found to be slightly lower and k^L approximately 2.5 times higher than values from a single block RPB packed with stainless steel wire mesh (Li et al., 2017b). For distillation in RZBs, HETP values similar (Wang et al., 2008a; Chu et al., 2013) and up to 50 % lower than those achieved in single block packing RPBs have been reported (Qammar et al., 2019). Constructional advantages, such as no top seal, simple stacking of units to increase number of separation stages, no need for a liquid distributor and the possibility of a mid-feed have aided in establishing this mass transfer machine in China for commercial distillation applications (Wang et al., 2011). RZBs are, however, rarely used for ab- or desorption due to their high pressure drop.

Qammar et al. (2019) developed a Zickzack packing, shown in Fig. 2.5 c), and manufactured it by 3D printing. The Zickzack packing can be considered an RPB equivalent of a tray column to create a more uniform liquid hold-up throughout the rotor and constant gas velocity in the annular gaps. Concentric rings with weirs are alternatingly attached to the opposing rotor plates, forcing gas and liquid on a zigzag path. Since it is not a rotor-stator concept, pressure drop and power consumption are lower compared to RZBs. Mass transfer performance was studied by distillation of an ethanol/water mixture. The new packing was superior to conventional wire mesh only near its flooding point at very low rotational speeds ($\approx$200 min^{-1}).

In order to achieve more continuous velocities of gas and liquid and improve the utilization of the employed packing, a rotor with radial channels of constant cross sectional area was patented, with the channels being preferably tubes filled with packing (Schulz et al., 2019). No experimental tests were reported.

Further research has been directed at modifying surface properties (Zheng et al., 2016; Ma et al., 2019), employing corrosion resistant packing materials such as PTFE (Chen et al., 2016) or developing fouling resistant rotors (Liu et al., 2020).

2.3 CFD modeling of RPBs

To gain additional insights, especially into the hydrodynamics of RPBs, CFD modeling has been applied. An overview of CFD modeling works of RPBs has been given by Yang et al. (2019) and Xie et al. (2019). Xie et al. (2019) distinguish between CFD modeling approaches on three scales: Microscale modeling treats gas-liquid mass transfer between individual droplets or thin films. Mesoscale models, as used by Xie et al. (2019), are based on a representative elementary unit containing the important characteristics of the packing and can resolve gas-liquid-packing interaction. However, phenomena such as end effects and shadowing are not captured. Macroscale models encompass the entire RPB and are required to capture flow phenomena related to the overall structure.

Single phase 3D macroscale models provide insight into gas flow patterns and dry pressure drop. Due to the associated computational burden, most single phase simulations employ porous media models, not resolving the packing but treating it homogeneously. Momentum loss terms are introduced that are empirically correlated to packing porosity. Llerena-Chavez and Larachi (2009) investigated the influence of vapor inlet position

on gas maldistribution. They found that a radial inlet leads to considerable maldistribution, as seen in the radial velocities throughout the bed. Top feed and tangential feed perform significantly better. Yang et al. (2015b) showed that gas maldistribution with radial feed can be mitigated through placement of a perforated curved baffle between bed and gas inlet. Liu et al. (2017) resolved a structured wire mesh in detail and found a gas side end effect with increased turbulence near the outer packing radius.

Gas-liquid interaction is usually modeled using the Volume Of Fluid (VOF) method. To lower computational burden on the macroscale, mostly 2D simulations are performed with mesh structures simplified as square or circular blocks (Xie et al., 2017). Guo et al. (2017) created a 3D model using cylinders and the VOF method to obtain information on liquid flow regime, specific surface area and residence time. Xu et al. (2019) created a 3D simulation of a liquid jet impacting on a single layer of wire mesh and compared it to the results of a visual study.

CFD simulation of mass transfer in RPBs has only been done to a very limited extent. Guo et al. (2016) used a 2D CFD model to investigate micromixing efficiency in an RPB using the iodide-iodate reaction in Fluent. Yang et al. (2016) simulated in Fluent the isothermal vacuum deaeration of water using the VOF method for gas-liquid interface. They simplified the wire mesh as 2D four-square obstacles and neglected gas side mass transfer resistance. Liquid side mass transfer coefficients were obtained from the correlation of Chen et al. (2006). Results for removal efficiency agreed within 5% with experiments. This approach is not predictive and requires higher computational loads than mass transfer balance calculations. However, it is possible to investigate the influence of certain geometrical details, such as baffles, and possibly identify regions of higher mass transfer efficiency.

While CFD modeling provides valuable insights, it is not yet possible to represent the actual packing geometry and model the gas-liquid interaction, much less mass transfer, without input from experimental correlations. One conclusion that can be drawn from published investigations is that a vapor inlet can advantageously be placed on top of the RPB. Even though correlations for certain quantities, such as hold-up or pressure drop, have been derived from CFD simulation results, they should be used with caution due to the significant simplifications involved.

2.4 Modeling of mass transfer in RPBs

Modeling of mass transfer is required in order to design new units, improve designs and find optimal operating conditions. Rate-based or non equilibrium modeling is a physically more accurate approach than modeling assuming thermodynamic equilibrium between the phases, as it links equipment geometry and operational parameters with separation performance and accounts for mass transfer interactions occurring in multi-component systems (Kenig and Blagov, 2014, p. 399). The use of stage efficiencies, which may differ for each component in multi-component systems, is thus not necessary (Taylor and Krishna, 1993, p. 373). Consequently, most RPB modeling studies employ a rate-based modeling approach. This approach relies on material and possibly energy balances around the individual phases that are connected by rate equations for the transfering quantities, which have been described in Sec. 2.1.1. Different approaches for describing the involved mass transfer coefficients have been employed, which are summarized in the following. Parts of this section have been published in Hilpert and Repke (2021) and Hilpert et al. (2022).

Mass transfer coefficients that have been calculated by any one of the approaches described in the following Sec. 2.4.1 are then usually employed in discretized rate-based models (Gudena et al., 2013; Sudhoff, 2015, p. 49) or in differential equations (Yi et al., 2009; Agarwal et al., 2010) and numerically integrated. Models of RPBs are not available in commercial flowsheet simulators, so some studies attempted to modify commercially available models. Prada et al. (2012) incorporated RPB specific correlations in Aspen Plus using Fortran routines to model distillation of ethanol/water. It is, however, not clear if the changes in liquid velocities along the radius were incorporated. Joel et al. (2014) and Joel et al. (2015) used the same approach to model absorption of CO_2 in Mono-Ethanol-Amine (MEA). Variation in flow area was not accounted for but the RPB was modeled as an absorber of identical volume with the height equal to the distance from inner to outer radius. Gudena et al. (2012a) used the Aspen Plus RADFRAC unit by transforming the annular ring segments of the discretized rotor to cylinders of changing diameter and height of the equivalent column to preserve their flow area and volume. In a subsequent work using this approach, it is detailed that the rotor was discretized into 10 segments and RPB specific calculations were performed in a connected Excel spreadsheet (Gudena et al., 2013). In view of the associated difficulties, it becomes clear why most studies programmed RPB models from scratch.

2.4.1 Modeling of mass transfer coefficients in RPBs

Developed modeling approaches for mass transfer coefficients can be grouped in first principles models, semi-empirical correlations and machine learning-based approaches (Zhao et al., 2016) which are described and compared in the following.

First principles models

First principles modeling approaches were the first to be used to describe liquid side mass transfer in RPBs. Key to first principles modeling are assumptions regarding the liquid flow patterns (Cortes Garcia et al., 2017). Tung and Mah (1985) assumed a falling film in conjunction with penetration theory under the influence of the centrifugal field. Munjal et al. (1989b) assumed laminar film flow over randomly inclined plates to account for the random structure of packings coupled with penetration theory. Guo et al. (1997) employed an approach that accounted for the occurrence of both droplet and film flow in RPBs. To model the investigated cross-flow RPB, a surface renewal model was used in conjunction with results of hydrodynamic measurements of film thicknesses and droplet diameters. This approach was subsequently employed by a series of works at Beijing University of Chemical Technology: Luo et al. (2012a) modeled $k^L a_e$ for different zones in a blade and packing RPB incorporating results from hydrodynamic investigations like liquid holdup and droplet diameters in conjunction with surface renewal theory. The overall rotor mass transfer coefficient was additively determined from integration of mass transfer coefficients of the different zones. The same approach was followed by Zhao et al. (2017) for a rotor stator reactor and Liu et al. (2019b) for a mesh-pin rotor RPB, the latter incorporating a liquid holdup correlation based on performed X-Ray CT scans. To calculate the sectional $k^L a_e$ values, however, Liu et al. used geometrical mean radii of the individual rotor zones. The model was later amended to fit a scale-up mesh-pin rotor through use of droplet diameter correlations gathered from the up-scaled RPB (Liu et al., 2020).

Mostly absorption and desorption processes have been modeled using this approach. Development of first principles models for gas side mass transfer is difficult since here the strong link to observable flow patterns is missing. It has thus rarely been done. Usually, gas side resistance is neglected (Qian et al., 2009; Li et al., 2010; Zhang et al., 2011) or accounted for through a semi-empirical correlation (Yi et al., 2009; Sun et al., 2009). A theoretical derivation of $k^L a_e$ and $k^V a_e$ correlations for distillation is given by Li et al. (2014) for a Counterflow Concentric Ring Rotating Bed (CRB).

These correlations require determining a hydrodynamic fitting parameter based on distillation experiments that relates to the rate of gas surface renewal.

As shown, theoretical models based on considerations of flow patterns in RPBs have to rely on a series of strongly simplifying assumptions to enable mathematical modeling. This limits their ability to depict reality. Relaxation of certain assumptions and inclusion of relevant effects can make predictions more accurate. One example is the prediction of end effects in RPBs. So far, only one first principles model has been designed that captures end effects at the inner radius of the packing and models the mass transfer occurring in the casing separately (Sang et al., 2019). First principles models often require additional hydrodynamic data, such as droplet sizes or hold-up. Thus, their performance in turn depends on the accuracy and generalization capabilities of employed correlations for these quantities, and new measurements for a scale-up device may be necessary, as in the case of Liu et al. (2020).

Semi-empirical correlations

Most publications employ semi-empirical correlations based on dimensionless groups that can be found through dimensional analysis (Buckingham, 1914). Usually volumetric mass transfer coefficients are correlated since these are obtained directly from mass transfer experiments as described in Sec. 2.1.2. They are often of the general form shown in Eq. (2.10) with slight variations in the definitions of dimensionless groups, with x representing additional variables such as surface tension (Lin and Jian, 2007; Jiao et al., 2010; Zhang et al., 2011; Chen et al., 2016; Ma et al., 2019; Wen et al., 2020). While any of the exponents may be zero, the exponent on Sc^L is in lack of variation in experimental data often set equal to $1/2$ in accordance with penetration theory (Bird et al., 2002) and the findings of Onda et al. (1968) that $k^L \sim (D^L)^{1/2}$, while the exponent on Sc^V is often set equal to $1/3$ in accordance with the findings of Onda et al. (1968) that $k^V \sim (D^V)^{2/3}$.

$$Sh = c_1 Re^{c_2} Ga^{c_3} Fr^{c_4} We^{c_5} Sc^{c_6} \left(\frac{x}{x_{ref}}\right)^{c_7} \tag{2.10}$$

Singh et al. (1992) developed one of the first semi-empirical mass transfer correlations, correlating overall liquid ATU using specific geometric packing area as characteristic

length. Reynolds and Galilei[1] number were incorporated. Due to a lack of variation in data, Sc^L was not included. A series of correlations was developed and published by the work group of Chen from the Republic of China: They studied influence of end effects by varying inner and outer radii and included the effects through terms incorporating volumes of RPB, eye, and outer cavity of casing (Chen et al., 2005a). Furthermore, they investigated influences of viscosity and packing material (Chen et al., 2005b; Chen et al., 2006). All these works were carried out in lab scale RPBs with radii ranging from 10 to 60 mm. Correlations for split packing RPBs in co- and counter-rotation made from metal foam packing have been developed by Reddy et al. (2006), Rajan et al. (2011), and Shivhare et al. (2013). Reddy et al. presented a correlation of k^La_e and the first correlation for k^Va_e in RPBs. Reddy et al. and Rajan et al. regressed correlations of local $k_{loc}a_e$ values that are integrated according to Eq. 2.11 to obtain the average ka_e value of the rotor. Shivhare et al. regressed a correlation for average k^La_e and k^Va_e values that employ Re and Ga calculated at the arithmetic mean radius of the bed.

$$ka_e = \frac{\int_{r_i}^{r_o} k_{loc}a_e r dr}{\int_{r_i}^{r_o} r dr} \tag{2.11}$$

Fewer correlations for gas side than for liquid side (volumetric) mass transfer coefficients have been published. Investigated processes often had a non-negligible liquid side mass transfer limitation so that only overall gas side coefficients were obtained and correlated. Chen (2011) developed a correlation for k^Va_e based on data for K^Va_e from the publications of Liu et al. (1996), Ramshaw and Mallinson (1981), Chen and Liu (2002), Lin et al. (2004), and Chiang et al. (2009) by back-calculating k^Va_e using the previously developed correlation for k^La_e of Chen et al. (2006). This k^Va_e correlation also includes a term containing the ratio of volumes of outer casing cavity to the total RPB volume to account for outer end effects. It has been used in conjunction with the liquid side correlations of Chen et al. in several modeling studies (Gudena et al., 2012a; Gudena et al., 2013; Joel et al., 2015; Li et al., 2017a; Oko et al., 2019).

Among the reasons for the widespread use of semi-empirical correlations is that deep understanding of all the physical processes is not necessary, but instead complicated phenomena can be lumped together. The correlations are easy to implement and the

[1] Influence of centrifugal acceleration is captured by a Galilei number. In RPB literature this is often misleadingly termed a Grashoff number. Grashoff number is commonly used to describe free convection and is defined differently (VDI Heat Atlas 2010, pp. 11–12). The term "Galilei number" will be used throughout this work even if original publications use "Grashoff number".

associated computational burden is low. Important proportionalities of the process can be analyzed directly from fitted correlations. However, there are also some drawbacks. Empirical correlations often fail to capture all dependencies and interconnections in the data. This fact and the uncertainty introduced through experimental error lead to typical accuracies in the range of 30 % (Cussler, 2000, p. 225). Generalization performance of correlations depends on the choice of the right mathematical arrangement of dimensionless groups and of the contained variables. Delaloye et al. (1991) point out that, for example, liquid density and viscosity have often been used as a means to obtain coherent dimensionless groups but have not actually been varied over significant ranges. Another important point is the choice of proper reference lengths. Singh et al. (1992) encountered this issue while attempting to apply an existing correlation developed for a different packing type to a metal foam. Empirical correlations are limited to operating conditions and fluid properties of original experimental data. Uncertainties introduced through extrapolation of such correlations beyond the region where they were fitted have to be accounted for by use of over design factors. Depending on the variables included, transferability to other operating conditions and geometries is further limited. Many correlations for mass transfer in RPBs, for example, do not incorporate geometrical variables of the casing or liquid distributor.

Machine learning-based approaches

Some publications employed machine learning algorithms to predict mass transfer behavior of RPBs. In those approaches, an algorithm "learns" from a large training data set. The predictive ability can be checked on a testing data set that was formerly excluded from the training data. As in empirical approaches, the quantities to be correlated with each other have to be selected.

Saha (2009) used three different Artificial Neural Networks (ANNs) to predict overall volumetric mass transfer coefficients $K^V a_e$ for gas and liquid side limited absorption and stripping processes in RPBs from three different sources based on gas flow, liquid flow and rotational speed. To increase the number of data points available for training, new points were generated by interpolating between experimental data. ANN-predictions were better than from the empirical correlations proposed by the experimenters. Zhao et al. (2014) used Support Vector Regression (SVR) to correlate Sherwood number of CO_2-absorption in sodium hydroxide solution with dimensionless groups based on data from several different authors. On the same dataset, they performed multiple nonlinear regression for an empirical correlation and used an ANN with back-propagation. Comparison of results of the three approaches showed

that SVR performed vastly superior to the empirical correlation and also better than the ANN. Zhang et al. (2021) developed a Least Squares Support Vector Machine (LSSVM) model to predict $K^V a_e$ for CO_2-absorption in sodium hydroxide solution obtained from different RPBs. A comparison to multiple nonlinear regression and artificial neutral networks showed better performance of the LSSVM.

There are two major drawbacks to machine learning approaches. Firstly, there is a need for large training data samples in order to fully exploit the potential of machine learning algorithms (Schmidt et al., 2019). Experimental generation of large data sets is expensive and time consuming, and experimental data in literature is not comprehensively reported, but rather reported in a post-processed way, thus limiting its use. Secondly, the models possess a black-box-nature. While black box modeling can capture hidden dependencies and interconnections, these do not become visible to the researcher and can thus not be readily exploited for design purposes (Schmidt et al., 2019). Utilizing the captured information could be done by mathematical optimization. Furthermore, several modeling related parameters, like the number of neural network layers, have to be chosen properly (Zhao et al., 2016), requiring knowledge and experience in the use of such algorithms. Extrapolation capability of such models is limited. Advances in the field of equation learning might help overcome the black box nature and limits of extrapolation in the future (Sahoo et al., 2018).

Summary of the mass transfer coefficient modeling approaches

First principles models, semi-empirical correlations and machine learning-based approaches have all been used for mass transfer coefficient modeling of RPBs. Due to the required larger datasets and their increased mathematical complexity, machine learning models have only been used experimentally in a few publications. First principles models have been used especially for liquid side modeling, but require additional data from hydrodynamic experiments. The majority of publications uses semi-empirical models for liquid and gas side which are easy to implement and directly reveal important proportionalities.

2.4.2 Comparison of the modeling of ab- or desorption and distillation in RPBs

Ab- and desorption processes usually occur with little changes in gas and liquid flow rates. Furthermore, steady state temperature of a system where an aqueous absorbens

is recycled between absorber and desorber is usually equal to the wet bulb temperature (VDI 3679-2). Consequently, average mass transfer coefficients are often employed in the design of conventional columns in conjunction with the HTU/NTU-concept. A similar approach can be chosen for RPBs. Here, however, local and average mass transfer coefficients differ significantly due to changes of flow area and thus liquid and gas velocities as well as centrifugal acceleration with radial position. Still, an average mass transfer coefficient for a certain rotor at a representative radial position can be calculated. Instead of the HTU/NTU concept the ATU/NTU-concept can be employed here to iteratively design the required geometry of a rotor (Singh, 1989).

In the case of distillation, however, strong variations in composition, temperature and consequently slope of the equilibrium curve occur along the rotor. Thus, it is not meaningful to use an average coefficient for the whole rotor, and a rigorous rate-based approach with local $k^L a_e$ and $k^V a_e$ values should be used instead.

2.5 Experimental and modeling studies of distillation in RPBs

As outlined in the introduction, the focus of this work is on distillation in RPBs. In this section, a literature review of experimental and modeling studies of distillation in RPBs is presented. Parts of this section have been published in Hilpert et al. (2022).

Distillation was the first reported process to be investigated in RPBs. Colin Ramshaw and co-workers conducted during the 1970s and 1980s at ICI in the UK intensive studies on distillation in RPBs. These works cumulated in the construction of a $2.5-million pilot plant (Short, 1983) and the filing of a comprehensive patent (Ramshaw and Mallinson, 1981). Aside from a few lab-scale measurements in the patent, no actual operating data was released and only little information published in three articles in popular scientific engineering journals (Ramshaw, 1983; Ramshaw and Arkley, 1983; Short, 1983). In the ICI pilot unit ($d_i = 200\,\mathrm{mm}$, $d_o = 800\,\mathrm{mm}$, $h_p = 150\,\mathrm{mm}$) using the metal foam Retimet ($a_p = 2000\,\mathrm{m^2/m^3}$) and operating at rotational speeds up to $1800\,\mathrm{min^{-1}}$, 18 theoretical stages were achieved for ethanol/iso-propanol separation (Short, 1983; Reay et al., 2013, p. 11). Up to $3\,\mathrm{t\,h^{-1}}$ could be processed at total reflux. The pilot plant accumulated more than 3500 h of trouble-free operation. Using two RPBs for rectifying and stripping section with a mid-feed, up to 40 theoretical stages could be obtained, enabling fine cuts and demonstrating the potential of RPBs for distillation (Short, 1983). Besides distillation, some absorption experiments were also conducted

at lab scale. In 1984, ICI granted an exclusive world-wide license to Glitsch Inc. (USA). Glitsch realized a few commercial applications and pilot plants in the following years, mainly absorption and stripping processes for water and natural gas treatment (Fowler, 1989). Since then, several experimental studies of distillation using different types of HIGEE units, such as RPB, RZB or CRB, have been published (Cortes Garcia et al., 2017). A comprehensive list of publications can be found in Tab. 2.2.

Kelleher and Fair (1996) were the first to publish distillation experiments in a scientific journal. They distilled cyclo-hexane/n-heptane at infinite reflux and pressures of 1.655 bar(a) and 4.137 bar(a) in a rather large rotor with 15 cm bed height. So far, it is the only investigation operating an RPB for distillation at elevated pressure. The rotor was packed with a Ni-Cr-foam ("Celmet" by Sumitomo Electric Industries Ltd.) with a specific surface area of 2500 m^2/m^3 and a porosity of 0.92. They reported NTU according to Singh's ATU/NTU-concept and derived $k^V a_e$ by using $k^L a_e$ from the ATU-correlation of Singh et al. (1992). The $k^V a_e$-values were correlated using the same form as the Onda-correlation for conventional columns, assuming the same exponent on Sc^V (Onda et al., 1968)[2]. However, parameters were not fitted to minimize error in $k^V a_e$, but to minimize error in ATU.

Another investigation in distillation using a single block packing RPB, packed with a stainless steel wire mesh, was presented by Lin et al. (2002). They reported an HETP-correlation for distillation of methanol/ethanol at infinite reflux. Li et al. (2008) and Li and Liu (2010) presented investigations on continuous distillation using one RPB for the stripping section and one RPB for the rectifying section. They did not clearly state the system used, but it is presumably ethanol ("alcohol")/water. A correlation for obtained number of theoretical stages was presented. However, the theoretical stages were evaluated using a formula derived by Dodge and Huffman (1937) for mixtures with constant relative volatility. The equation used is thus not strictly valid for any alcohol/water system. Nascimento et al. (2009) published ATU and $K^V a_e$ values for distillation of n-hexane/n-heptane at infinite reflux in a single block packing RPB filled with stainless steel wire mesh and ceramic Raschig rings at speeds up to 2500 min^{-1}. Li et al. (2017a) conducted vacuum distillation of ethanol/water mixtures at infinite reflux in a single block packing RPB packed with stainless steel wire mesh. Qammar et al. (2018) investigated distillation of ethanol/water in an RPB with and without a knit mesh packing. They found that the empty rotor contributed significantly to the

[2] An exponent of -1/3 is reported for Sc^V in the fitted correlation which should be +1/3. This is assumed to be a typing error since the original Onda correlation was reproduced correctly in the paper.

separation performance, especially at rotational speeds greater than 800 min^{-1}. Furthermore, an attempt was made to determine the casing contribution to mass transfer for experiments with the packed rotor by inferring vapor composition from temperature measurements, assuming a well mixed gas phase. A casing contribution ranging from 20 to 80 % was estimated over the range of rotational speeds investigated.

Since 2008 several papers on distillation in special types of RPBs were published. Wang et al. (2008a) and Wang et al. (2008b) reported experiments in a new type of RPB, called RZB, which consists of a rotor-stator arrangement of concentric, partially perforated baffles. Pressure loss and energy consumption of this type of machine are significantly higher than in single block packing RPBs due to the inefficient liquid usage with decelerations and accelerations at each rotor/stator baffle pair and higher entrainment (Li et al., 2013b). To overcome these deficiencies, a Crossflow Concentric-Baffle Rotating Bed (Wang et al., 2014a; Wang et al., 2014b) and a Counterflow Concentric-Ring Rotating Bed (Li et al., 2014) were suggested by the authors. Mondal et al. (2012) used a split-packing RPB to enhance gas side mass transfer, which is often dominating in distillation. They suggested a correlation for $K^V a_e$, based on F-factor and rotational speed. Shi et al. (2011) conducted a reactive distillation experiment for n-butylacetate synthesis in a Two-Stage Counter-Current RPB. The rotating catalyst-filled packing rings alternate with stationary baffles. Reports of this are not available in English, but only in a Chinese language journal. The rotor-stator concept of the device that enables stacking of rotors also enables introduction of a mid-feed and thus continuous distillation in one machine. Three subsequent works investigated distillation at finite reflux using two-stage RPBs of the same basic design as for the reactive distillation runs with intermediate feed and different packings (Luo et al., 2012b; Chu et al., 2013; Luo et al., 2016). In 2019, Qammar et al. (2019) published a rotor design with baffles functioning as trays fixed alternatingly to one or the other rotor plate, the so called Zickzack Packing. This design aims at generating a more uniform liquid hold-up throughout the rotor by the use of weirs on each tray and at creating a more uniform gas flow along the radial direction by varying the spacing between individual trays. The design showed a higher mass transfer performance as compared to knit mesh packing, but only in the region close to its flood point which was lower than for knit mesh packing, limiting the new design's capacity.

Both Agarwal et al. (2010) and Prada et al. (2012) presented design studies for binary distillation tasks without validation of the employed models. Sudhoff et al. (2014) developed and validated a simplified mass transfer correlation for overall volumetric mass transfer coefficient $K^V a_e$ using literature data from binary distillation experi-

ments in RPBs. They applied this correlation to a modeling study of methanol/water separation. However, their approach is not usable for multi-component distillation problems. A few modeling studies of multi-component distillation in RPBs have been published by Gudena and co-workers. Gudena et al. (2012b) and Gudena et al. (2013) modeled reactive stripping processes, while Gudena et al. (2012a) modeled a reactive distillation process. These studies have used correlations for gas and liquid side mass transfer coefficients developed from absorption or desorption experiments in RPBs, as it is common practice for design of conventional distillation columns. Due to a lack of data, the applicability of the developed models could not be validated for distillation applications. Li et al. (2017a) modeled results of vacuum distillation of ethanol/water mixture using the literature correlations of Chen et al. (2006) for $k^L a_e$ and Chen (2011) for $k^V a_e$.

Tab. 2.2: Overview of experimental investigations of distillation in RPBs. Operation at infinite reflux where not noted otherwise.

Author (Year)	RPB-Type, Packing	RPB Dimensions ($d_i/d_o/h_p$, in mm)	Component System	Remarks
Ramshaw and Mallinson (1981)	single block, Stainless Steel (SS) wire mesh	120/180/12...25[a]	methanol/ethanol	report $K^V a_e$
Short (1983), Ramshaw (1983), Ramshaw and Arkley (1983), Reay et al. (2013, p. 11)	single block, metal wire meshes	lab: n.a./190/12...25	various	lab: HETP=10...20mm at around 3500 min^{-1}
	single block, metal foam	demo: 200/800/150	ethanol/iso-propanol	demo: 3 $\mathrm{t\,h}^{-1}$, two RPBs for continuous distillation
Kelleher and Fair (1996)	single block, Ni-Cr foam	175/600/150	cyclo-hexane/n-heptane	report ATU/NTU, correlation for $k^V a_e$, 1.66 bar(a) & 4.14 bar(a)
Lin et al. (2002)	single block, SS wire mesh	122/294/50 & 95	methanol/ethanol	correlation for HETP, rotors showed different dependence of HETP on F-factor
Li et al. (2008)	single block, SS corrugated disk/wire mesh/wave thread	60/110/63	"alcohol"/water	correlation for N_{th},[b] two RPBs for continuous distillation
Wang et al. (2008a)	Rotating Zigzag Bed	52/100/78	methanol/water	report HETP
Wang et al. (2008b)	Rotating Zigzag Bed with 2 rotors in casing	200/630/80	ethanol/water	report N_{th}

Continued on next page

Tab. 2.2 (continued).

Author (Year)	RPB-Type, Packing	RPB Dimensions ($d_i/d_o/h_p$, in mm)	Component System	Remarks
Nascimento et al. (2009)	single block, ceramic Raschig rings/SS wire mesh	44/160/40	n-hexane/n-heptane	report ATU and $K^V a_e$, rotating liquid distributor
Li and Liu (2010)	RPB with SS fin-baffle packing	60/110/30	"alcohol"/water	report N_{th}/HETP[b], two RPBs for continuous distillation
Shi et al. (2011)	Two Stage CounterCurrent (TSCC) RPB, SS wire mesh and catalyst filling in rotating rings	145/373/46, ring thickness 16mm	n-butanol/acetic acid/ water/n-butyl acetate	in Chinese, reactive distillation (n-butyl acetate synthesis) in TSCC RPB with intermediate feed, report conversion, x_D & x_B of ester
Mondal et al. (2012)	split packing, wire mesh	60/310/27 (vapor draw at 150)	methanol/ethanol	two counter-rotating disks, report HETP and ATU, correlation for $K^V a_e$
Luo et al. (2012b)	TSCC RPB, SS wire mesh	145/355/46	acetone/water	TSCC RPB with intermediate feed for continuous distillation, report N_{th}

Continued on next page

Tab. 2.2 (continued).

Author (Year)	RPB-Type, Packing	RPB Dimensions ($d_i/d_o/h_p$, in mm)	Component System	Remarks
Chu et al. (2013)	TSCC RPB, SS wire mesh packing	145/365/58	methanol/water	TSCC RPB with intermediate feed for continuous distillation, report N_{th}
Li et al. (2014)	Counterflow Concentric-Ring Rotating Bed	140/272/15 & 45	ethanol/water	theoretical derivation of correlations for k^V, k^L, a_e, $K^V a_e$, HETP (only k^L & a_e predictive), fit of empirical correlations for $K^V a_e$
Wang et al. (2014a) and Wang et al. (2014b)	Crossflow Concentric-baffle Rotating Bed	240/469.6/72	ethanol/water	report stage efficiency
Luo et al. (2016)	Two Stage Blade Packing (TSBP) RPB, SS wire mesh	128/348/40 (upper) 158/348/40 (lower)	methanol/water	TSBP RPB with intermediate feed for continuous distillation, report N_{th}
Li et al. (2017a)	single block, SS wire mesh	360/570/310	ethanol/water	report x_D and HETP, 0.11 to 1.0 bar(a), modeling using literature correlations

Continued on next page

Tab. 2.2 (continued).

Author (Year)	RPB-Type, Packing	RPB Dimensions ($d_i/d_o/h_p$, in mm)	Component System	Remarks
Qammar et al. (2018)	single block, SS wire mesh	146/400/10	ethanol/water	report ATU/NTU, quantify fraction of mass transfer in packing and in casing/empty rotor
Qammar et al. (2019)	single block, SS wire mesh, metal foam, Zickzack packing	146/380/10	ethanol/water	introduction of Zickzack packing, comparison of N_{th}/HETP and Δp for different packings (metal foams, knit mesh, Zickzack)
Wang et al. (2019)	Rotating Zig-Zag Bed	118/285/50	ethanol/water	investigation of influence of geometry on N_{th}, Δp and motor power consumption

[a] Axial height taken from Ramshaw (1983): "The early laboratory experiments used rotors having an outside diameter of 190 mm and an axial depth of 12 to 25 mm."
[b] Reported „NTU" are not calculated from HTU/NTU concept, but from formula for N_{th} derived by Dodge and Huffman (1937) for constant relative volatility (which is not fulfilled for ethanol/water, assuming "alcohol" means ethanol).

2.6 Characteristics and exemplary industrial applications of HIGEEs

In this section advantages and disadvantages of HIGEEs are summarized and related to potential and realized industrial applications of HIGEEs.

Ramshaw and Arkley (1983), Mersmann et al. (1986), and Fowler (1989) derive several potential situations where the application of RPBs may be advantageous due to their specific properties. These also apply to similar types of HIGEE devices, such as RZBs.

- Due to the high specific surface area generated in RPBs and the increased mass transfer coefficients, RPBs can be built several times smaller and thus lighter than conventional columns. This favors applications where space is limited, such as retrofits or off-shore installations. Furthermore, it provides an additional cost advantage when capital expenditure is high, for example where high operating pressures or especially corrosion resistant alloys are required. Small size also increases mobility and modularity of plants, which may be beneficial for fast on-site transportation and start-up, e.g. in case of a retrofit. It could also prove advantageous when sterilization of equipment is required, i.e. in food and pharmaceutical industry.

- The centrifugal force field provided by the RPB is several times that of earth's gravity, which makes RPBs to a certain degree insensitive to motion. This property may again be useful in off-shore applications but also for operation at zero gravity, i.e. in space.

- RPBs can be constructed to have very little hold-up. This is especially interesting for processing of hazardous (e.g. toxic or explosive), corrosive or expensive materials. Combined with the high throughputs allowable in RPBs, the low hold-up leads to short residence times. This enables processing of unstable and heat sensitive materials, and may aid in obtaining higher selectivities in cases where fast consecutive reactions consume a desired product. The low residence times also lead to fast dynamics of the RPB itself. If the equipment connected to the RPB has similarly small time constants, this can reduce off-spec material during start-up and be beneficial for dynamic and intermittent processes.

- RPBs display a greater flexibility than conventional mass transfer equipment, since they exhibit relatively high turn-down ratios, and their mass transfer efficiency can be adjusted to a certain degree through rotational speed.

- The high g-forces and shear forces acting in the RPB make it a potential device to process viscous media, media with foaming tendencies or conduct liquid/liquid extraction processes between liquids with small differences in density.

Cortes Garcia et al. (2017) list the main drawbacks of HIGEEs, especially the additional power consumption, wear and maintenance caused by the rotating parts. HIGEEs are unsuitable for deep vacuum operation due to their pressure drop. Further barriers to RPB deployment in industry are the reluctance of businesses to invest in a new technology where little experience exists when benefits or savings are small compared to the perceived risks (Kletz and Amyotte, 1998, p. 42). Furthermore, not all phenomena in HIGEEs are yet fully understood and proven design strategies and modeling capabilities are still lacking.

In situations where advantages of HIGEEs strongly outweigh the drawbacks, devices have been industrially applied. Zheng et al. (1997) reported the application of RPBs in water deaeration for off-shore enhanced oil recovery, reducing oxygen content from between 6 and 14 ppm to below 50 ppb in a 50 $t\,h^{-1}$ and a 300 $t\,h^{-1}$ unit. Here, the reduced volume and weight cause significant capital cost savings. Trent et al. (1999) report the application of RPBs for a reactive stripping process in the production of hypochloric acid. The short residence time of RPBs enabled the production of an unstable intermediate product with an increase in yield from 80 % to 90 %. Harbold and Park (2008) report the installation of eight RPBs for vacuum water deaeration in the soft-drink bottling industry. Reliability of achieved residual oxygen concentrations could be increased whilst reducing strip gas consumption, leading to significant operating cost savings. Guo et al. (2019) present a review of HIGEE applications for gas purification, most of which have been installed in China. Examples include H_2S removal, where mass transfer intensifications lead to regeneration steam savings or where equipment size reduction lead to successful off-shore implementation. RPBs were used for particulate matter removal from coal gas and proved vastly superior to the previously installed conventional purification. Shut downs of a downstream compressor due to blockages could be decreased from once per week to once per half year. Finally, Wang et al. (2011) present a series of industrial applications of RZBs for distillation, some of which had been operated sucessfully for several years already. Photos show the

installation of devices indoors where available heights are limited, highlighting the volume reduction benefits of HIGEEs.

3 Research gap, objective and approach

In this chapter the research gap is analyzed, the objective of the thesis is defined, and the chosen approach to achieve the outlined goal is presented. Parts of this chapter have been previously published in Hilpert et al. (2022).

3.1 Analysis of the research gap

As outlined in Chapter 1, distillation is one of the most important unit operations in the process industry, with more than 40 000 columns in operation worldwide (Kiss, 2013, p. 37), accounting for up to 50 % of capital and operating costs in industrial processes (Gorak and Schoenmakers, 2014, p. vii). The potential of RPBs for process intensification of distillation was for the first time demonstrated by Ramshaw and co-workers (Reay et al., 2013, p. 11). HETP values between 1/2 and 1/10 of those in conventional columns have since been reported (Qammar et al., 2019). Achievable reductions in size may be of interest especially in environments where space and weight are an issue, such as off-shore applications, retrofits or indoor situations with limited heights (Fowler, 1989; Zheng et al., 1997). Further advantages of RPBs include a high turn-down ratio, short time to steady-state, and increased flexibility by influencing product composition through rotational speed (Wang et al., 2008a; Fowler, 1989; Sudhoff et al., 2015).

Nevertheless, reports of applications of RPBs in the Western process industry are scarce. Some of the associated reasons were identified to be the deficiency of proven models, design and scale-up rules (Neumann, 2018, p. 33), the lack of demonstration plants in Europe (Neumann, 2018, p. 32), a skepticism towards rotating equipment (Ramshaw, 1987), as well as risk aversion of industry in view of uncertainties associated to new technologies (Kletz and Amyotte, 1998, p. 42).

It is thus necessary to improve existing modeling capabilities for distillation operation in RPBs to provide means of evaluating RPBs as a possible alternative when designing distillation equipment.

A review of experimental studies investigating distillation in RPBs showed that fewer than 25 publications exist in English language literature (cf. Tab. 2.2). All studies with a focus on separation performance investigated binary mixtures, mostly ethanol/methanol and ethanol/water. There is no data available on distillation of multinary mixtures. Multicomponent distillation data is however required to verify the application of vapor and liquid side mass transfer coefficient correlations for RPBs to multicomponent distillation modeling. Validated multicomponent models are needed to broaden the scope of possible applications of RPBs, as real-world engineering problems usually involve multicomponent separation tasks (Agrawal and Tumbalam Gooty, 2020). Potential applications of RPBs which would benefit from such investigations besides distillation of multicomponent mixtures include reactive applications, such as reactive distillation. As shown in Sec. 2.5, machines investigated in literature differ strongly in types (single block packing, split packing, RZB, multi-rotor arrangements...), packing (wire mesh, metal foam, Zickzack...) and geometric dimensions, hindering direct comparison and derivation of correlations based on data from different machines. Furthermore, geometrical details or information on key operating parameters are sometimes missing. Concentration measurements are generally not available. Data is rather reported in a processed form, e.g. as HETP, NTU, or $K^V a_e$. A few publications present simplified correlations for some of these quantities which are applicable only to the binary case. Examples are a correlation for HETP in dependence of vapor Reynolds and Galilei number proposed by Lin et al. (2002) or a correlation for $K^V a_e$ developed by Mondal et al. (2012) in dependence of F-factor and relative volatility. Development of alternative correlations based on literature data is thus difficult.

Existing simulation studies for distillation in RPBs used either simplified correlations (e.g. for $K^V a_e$) to model the separation of binary mixtures or they used literature correlations for $k^L a_e$ and $k^V a_e$ from ab- or desorption experiments to model multicomponent distillation (cf. Sec. 2.5). In the latter case, validation was not possible due to a lack of data.

A closer inspection of published literature on binary distillation experiments reveals that an optimal rotational speed with a corresponding maximum in separation efficiency is repeatedly reported (Nascimento et al., 2009; Luo et al., 2012b; Chu et al., 2013; Luo et al., 2016; Li et al., 2017a; Qammar et al., 2018; Qammar et al., 2019). This

behavior is often attributed to a trade-off between an intensification of heat and mass transfer on the one hand, and a decrease in contact time on the other hand, as centrifugal acceleration increases (Nascimento et al., 2009; Luo et al., 2016; Qammar et al., 2019). Capturing this maximum is important for proper design, choice of operating speed or optimization of RPBs for separation tasks. A study presented by Li et al. (2017a) investigated distillation of ethanol/water mixtures at vacuum and ambient pressure. The experiments were modeled with the Aspen BatchSep module, using the mass transfer correlations of Chen et al. (2006) for $k^L a_e$ and Chen (2011) for $k^V a_e$, shown in Tab. 7.2. The maximum in separation efficiency observed by Li et al. (2017a) appears to be well predicted. Unfortunately, throughput is not provided, hindering a reproduction of the results. A possible reason for the model to reproduce the maximum may be the incorporation of liquid hold-up into the model mentioned by the authors. However, the authors do not further specify how liquid hold-up was used to modify mass transfer rate equations. Another reason might be the influence of the strong differences in transport properties between ethanol and water on the calculated mass transfer coefficients. When applied to thermodynamically near-ideal systems, however, the correlations for gas and liquid-side mass transfer in RPBs used by Li et al. (2017a) do not capture the maximum in separation efficiency as observed in the present study (cf. Sec. 6.2.1 and Sec. 7.2.2). Instead, they predict a continuous increase of separation performance with centrifugal acceleration.

3.2 Objective and approach

This thesis aims to further narrow the described research gap, i.e. the lack of multicomponent distillation data from RPBs and the need for correlations capable of capturing the maximum in separation efficiency. To this end, a rate-based model for multicomponent distillation of miscible liquids in single block packing RPBs is developed and validated. Since no data is available for distillation of multicomponent mixtures, a test stand is constructed and own experiments are conducted. The test stand is of pilot-scale to increase the value of derived conclusions for industrial scale applications. The design of the test stand allows for investigation of increased throughputs with F-factors at the eye of up to $5\,\mathrm{Pa}^{0.5}$ which most publications do not achieve due to the required high reboiler duties. For modeling, one correlation each is needed for the vapor and liquid side mass transfer coefficients. Literature review revealed the issue of limited transferability of mass transfer correlations between different devices. Thus,

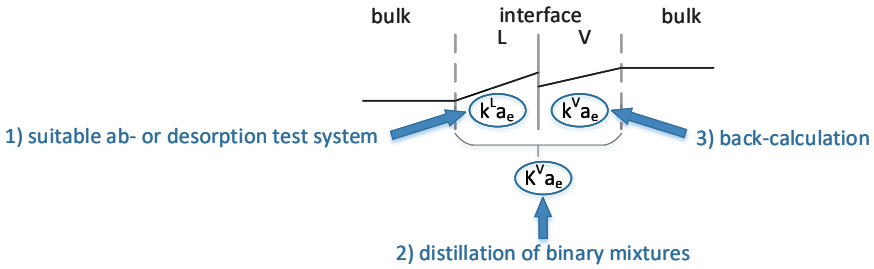


Fig. 3.1: Schematic representation of the strategy applied to obtain volumetric mass transfer coefficients following the resistances in series model based on two-film theory.

correlations for liquid and vapor side mass transfer coefficients are developed for this specific test stand. Especially the observed maximum in separation efficiency of RPBs at varying rotational speeds will be studied and incorporated in the model.

The employed methodology aims to reduce experimental effort. Hence, specific effective surface area will not be measured separately, but volumetric mass transfer coefficients will be correlated, as is common practice. The approach chosen to develop the required correlations is based on the resistances in series model derived from two-film theory. The correlations themselves are not necessarily restricted to adhere to the assumptions of two-film theory, as outlined in Sec. 2.1.1.

Mass transfer coefficients can be determined either from ab- or desorption experiments or directly from distillation experiments. Since temperature and concentration profiles are not readily available for single block packing RPBs, only the mass transfer coefficient of either liquid or vapor phase can be determined from top and bottoms composition measurements of infinite reflux distillation runs (Pelkonen, 1997, p. 44). The other one needs to be determined e.g. through absorption or desorption experiments in the same device, or taken from literature correlations. Some authors neglect liquid side resistance based on the assumption that most of the mass transfer resistance in distillation lies on the vapor side (Pelkonen, 1997, p. 44). Others conclude that liquid side resistance can account for more than 50 % of total resistance in distillation, and that contributions may change over the concentration range depending on the examined mixture (Edye, 1955; Onda et al., 1968; Linek et al., 2005). As evidence does not allow for safely neglecting liquid side resistance, it should be accounted for. The gas side resistance will therefore be derived from distillation experiments with the aid of $k^L a_e$ values obtained from ab- or desorption experiments.

In summary, as shown in Fig. 3.1, $k^L a_e$ is measured from a suitable test system and correlated. In the second step, $K^V a_e$ is obtained from distillation of binary mixtures. Based on these results $k^V a_e$ is back-calculated and correlated. This approach is similar to that taken by Kelleher and Fair (1996). It possesses the advantage of minimizing the experimental effort by eliminating a campaign to separately measure gas side mass transfer coefficients. The rate-based model is then validated against results from binary and ternary distillation experiments.

The goal of the current work is to demonstrate the applicability of the chosen approach illustrated in Fig. 3.1 and develop a model suitable for multicomponent distillation in pilot-scale RPBs. In the process, an experimental database will be generated that can be used by other works for validation purposes or development of scale-up correlations. This is aided by publishing data of concentration measurements and relevant sensors along with processed data, such as volumetric mass transfer coefficients.

The remainder of the thesis is structured as follows: In Chapter 4, the choice of test systems, development of the test stand and the experimental procedure are outlined. The developed rate-based distillation model of the RPB is introduced in Chapter 5. Chapter 6 describes the results of experiments for measurement of the liquid-side mass transfer coefficient as well as the development of a $k^L a_e$ correlation. Results of distillation experiments, the development of a $k^V a_e$ correlation and the model validation are presented in Chapter 7. Finally, results of this thesis are summarized in Chapter 8.

4 Generation of an experimental data basis for modeling of mass transfer in RPBs

In this chapter, the material and methods required to generate an experimental data basis for the subsequent model development and validation are presented. First, the choice of component systems for the mass transfer measurements is described. Based on the selected component systems and the findings of the literature review in Chapter 2, a test stand is designed and the experimental procedure outlined. Parts of the sections describing the test stand and the experimental procedure have previously been published in Hilpert and Repke (2021) and Hilpert et al. (2022).

4.1 Selection of suitable component test systems

The choice of component systems for the mass transfer experiments is a critical point. Several aspects are to be considered which are subsequently treated in this chapter in more detail, resulting in the choice of proper test systems. Most important is the suitability of the component system for the task, i.e. if the required mass transfer coefficients can be determined using the selected system. Further aspects include:

- availability of property data
- analyzability
- toxicity
- commercial availability and price
- use in literature (availability of reference data).

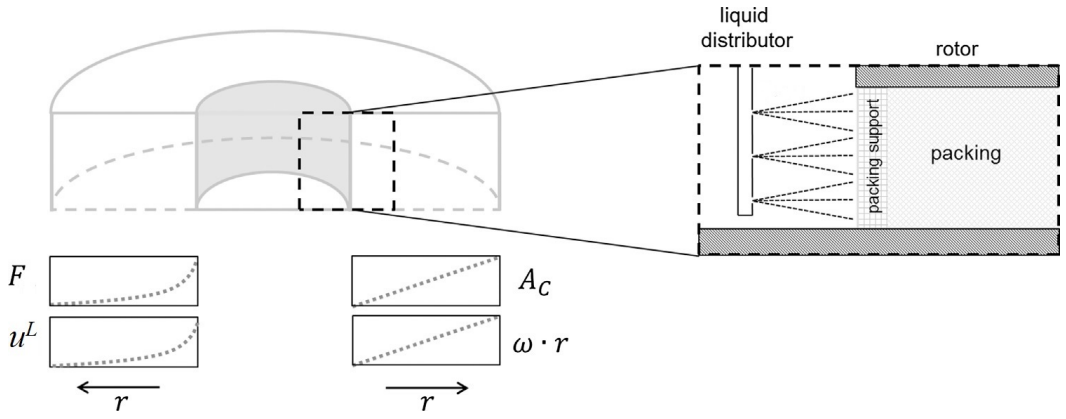


Fig. 4.1: Change of local values of F-factor F, liquid superficial velocity u^L, cross sectional area A_c and centrifugal acceleration $\omega \cdot r$ along the radius of an RPB (adapted from Neumann et al., 2017a).

4.1.1 Distillation test systems

The goal of this work is to systematically develop mass transfer correlations for distillation in RPBs from binary test mixtures and apply them to other binary and ternary mixtures.

Suitability for the task

Pelkonen (1997, pp. 43–45) presents some considerations regarding the choice of suitable test systems for column distillation experiments aimed at determining mass transfer coefficients. His main goal is obtaining constant mass transfer coefficients over the column height, so that global mass transfer coefficients based on in- and outlet streams are valid for the whole column. With constant mass transfer coefficients, the reporting of a single HETP value for the whole column is also valid. Precondition is that phase velocities, physical properties, and packing geometry are constant along the column. While in an RPB packing geometry may be kept approximately constant, the condition of constant phase velocities is per se not fulfilled in homogeneous packings, such as metal foams or wire meshes. Furthermore, the acceleration varies along the bed in radial direction, as illustrated in Fig. 4.1. It is thus necessary to deal with these changes either through integration of correlations for local coefficients (Onda et al., 1968; Reddy et al., 2006; Rajan et al., 2011), or by using rigorous models that use correlations for local coefficients (Sudhoff et al., 2015). However, following the suggestions of Pelkonen allows to observe characteristic behavior of the RPB without being overshadowed by effects introduced through non-idealities of the component system.

Pelkonen suggests distillation of ideal, organic, narrow boiling binary mixtures at infinite reflux for the determination of mass transfer coefficients and validation of correlations. However, as RPBs at the investigated scale provide only a small number of theoretical stages, very narrow boiling mixtures should not be used for measuring mass transfer coefficients since the influence of analysis error grows with smaller changes in concentration. For validation of mass transfer coefficients Pelkonen (1997, p. 43) suggests non-ideal, aqueous and wide boiling component systems. Here, the thermodynamic correction matrix and non-zero net mole flux become relevant. High flux correction factor in distillation is usually close to unity and can be neglected for both types of systems (Taylor and Krishna, 1993, p. 151).

Arlt and Onken (1990) describe eight recommended test systems for distillation equipment at atmospheric pressure that serve as a starting point to find a suitable component system. Based on data published for an RPB of comparable geometry at TU Dortmund (Qammar et al., 2018), 3 to 5 theoretical stages were expected in the RPB test stand. Out of the test systems recommended by Arlt and Onken, the four systems displayed in Tab. 4.1 match the expected range of theoretical stages. Except for methanol/water, these systems are thermodynamically near-ideal.

Tab. 4.1: Recommended test systems for atmospheric distillation with low numbers of theoretical stages (Arlt and Onken, 1990).

System	Number of theoretical stages
Toluene/Chlorobenzene	3…7
cyclo-Hexane/n-Heptane	3…7
Methanol/Water	1…4
Methanol/Ethanol	4…8

For the design of the test stand, it is necessary to identify a ternary near-ideal system A-B-C. A fourth component is required which forms non-ideal subsystems with at least one of the other components and can thus produce a non-ideal ternary system A-B-D by substituting one of the three components, as illustrated in Fig. 4.2.

Linear (i.e. non-branched) organic components of a homologous series display near-ideal behavior. Therefore, the simple component classes of alkanes and alcohols are further considered to identify near-ideal test systems. The components n-hexane to n-octane and methanol to n-propanol have normal boiling points in the moderate temperature range below and slightly above 100 °C. The alcohol system can easily be expanded to a non-ideal system by addition of water. It is desirable to restrict the

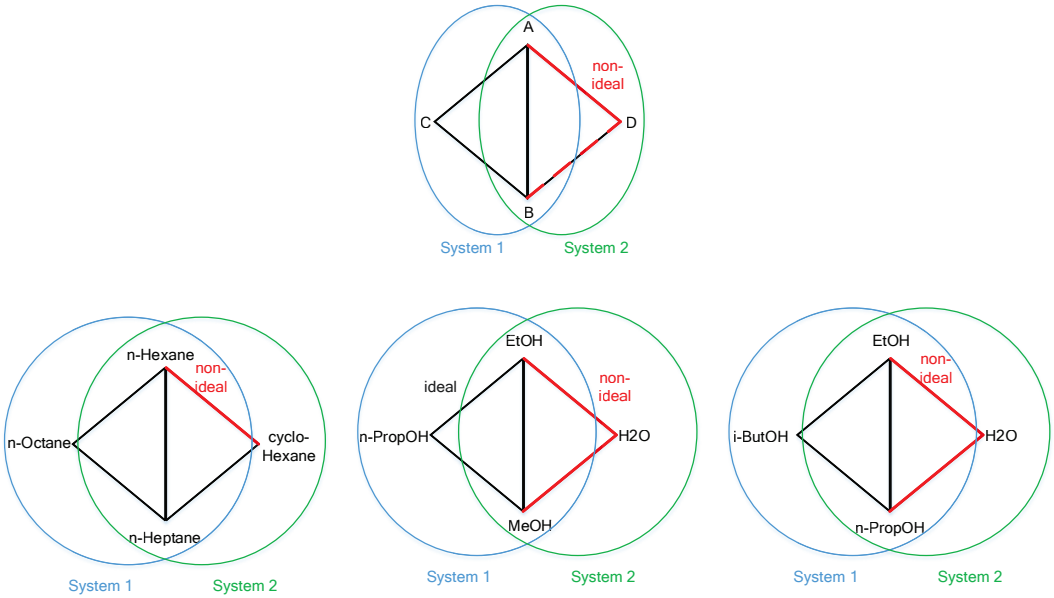


Fig. 4.2: Potential component test systems for distillation in the RPB test stand.

first distillation experiments to homogeneous mixtures. Thus, for the non-ideal system involving the alkanes an additional component other than water is needed. While cyclo-hexane and n-heptane behave thermodynamically near ideal, cyclo-hexane and n-hexane form an azeotrope. It is thus possible to introduce the desired non-ideality to the alkane system without the formation of two liquid phases by addition of cyclo-hexane.

Flooding in a comparably sized RPB was observed at a rotational speed of 1200 $\mathrm{min^{-1}}$, liquid loads of 26 to 39 $\mathrm{m^3\,m^{-2}\,h^{-1}}$ and F-factors of 2.4 to 3.4 $\mathrm{Pa^{0.5}}$ at the eye of the RPB (Neumann et al., 2017a, see also Section 4.2.3). In order to investigate F-factors up to this range, relatively high gas flow rates are required, leading to large reboiler duties. Alkanes offer the advantage of an enthalpy of vaporization which is about half of that of alcohols, enabling higher F-factors for a given reboiler duty.

Availability of property data

For both the alcohol/water system and the alkane system, pure component and mixture transport and thermodynamic data are available. Availability of diffusion coefficients for alcohols is slightly better.

Analyzability

While for alcohols and alkanes gas chromatography is the method of choice, water is not so well analyzable with a Gas Chromatograph (GC). For binary mixtures of water and alcohols, density or refractive index can be used to determine concentrations. To verify low water contents in multicomponent mixtures, Karl-Fischer-titration may be used.

Toxicity

All considered organic components are highly flammable, and pose some health hazard, such as skin irritation, eye damage or causing of dizziness. The alkanes are classified by European Chemicals Agency (ECHA) as posing a serious health hazard, since they are fatal if swallowed or inhaled (European Chemicals Agency, 2020). They are very toxic to aquatic life with long lasting effects. Of the alcohols, only methanol is similarly hazardous, being classified by ECHA as acutely toxic and posing a serious health hazard if ingested, inhaled or in contact with skin. Alternatively, the system ethanol/n-propanol/i-butanol may be used, avoiding methanol. The choice of i-butanol over n-butanol is dictated by the 10 K lower normal boiling point, while near-ideal behavior of the mixtures is maintained. A lower boiling point of the high boiler produces a lower spread between minimum and maximum operating temperature in the RPB. A narrow temperature range is necessary because the upper RPB seal, which prevents gas bypass, is designed to have a certain leakage rate at the design temperature. At temperatures significantly below design, leakage increases due to the lacking thermal expansion of the seal.

Commercial availability and price

All components are available through commercial suppliers in sufficient quality and quantity. However, pure n-alkanes are two to three times more expensive than the alcohols.

Use in RPB literature

The majority of experimental works on distillation in RPBs in literature have used short-chained alcohols and water (cf. Tab. 2.2), providing some reference for experimental results.

Tab. 4.2: Selected properties of the chosen components for design of the RPB test stand.

Component	NBP in °C	σ in mN/m	η in mPas	Remarks
Methanol (PubChem, 2020d)	65	22 (25°C)	0.5 (25°C)	high separation factor with n-propanol and water
Ethanol (PubChem, 2020c)	78	22 (25°C)	1.1 (25°C)	homogenous azeotrope with water
n-Propanol (PubChem, 2020a)	97	24 (20°C)	2.3 (20°C)	homogenous azeotrope with water
i-Butanol (PubChem, 2020b)	108	23 (20°C)	4.0 (20°C)	heterogeneous azeotrope with water
Water (PubChem, 2020f)	100	72 (25°C)	0.9 (25°C)	
n-Heptane (PubChem, 2020e)	*98*	*20 (25°C)*	0.3 (25°C)[a]	*non-polar reference*

[a] Cooper (1988)

Choice of test systems

Given the above considerations, the ideal system ethanol/n-propanol/i-butanol and the miscible non-ideal system ethanol/n-propanol/water are chosen to design the test stand. In case the number of theoretical stages achieved in the RPB is lower than expected, i-butanol may be replaced by methanol. Main reasons are lower toxicity, lower price, and the broader availability of literature data as compared to the alkane system. An overview of the components and the important properties Normal Boiling Point (NBP), surface tension and viscosity is given in Tab. 4.2.

4.1.2 Test system for determination of $k^L a_e$

Suitable test systems for measurements of liquid side mass transfer coefficients require no or a negligible gas side resistance to mass transfer, as discussed in Sec. 2.1.2. Among the systems used for $k^L a_e$ measurements in RPBs are absorption of CO_2 from air in sodium hydroxide solution (e.g. Rajan et al. (2011) and Luo et al. (2012a)), absorption of CO_2 from air in water (Keyvani and Gardner, 1988) and desorption of Volatile Organic Compounds (VOCs) (Singh et al., 1992). However, most studies used oxygen desorption from water in a nitrogen gas stream (cf. Tab. D.1). This is also one of the recommended test systems of VDI 2761-2. As it is well analyzable, easily available and

associated with low hazards, oxygen desorption from water into nitrogen gas will be used to determine $k^L a_e$ in this study as well.

The selected test systems for both distillation and desorption mass transfer investigations are summarized in Tab. 4.3.

Tab. 4.3: Summary of the chosen component systems for experimental mass transfer investigations in the RPB test stand.

Target variable	Component system	Remarks
$k^L a_e$	oxygen desorption from water into nitrogen	
$K^V a_e$	infinite reflux distillation of ethanol/n-propanol/i-butanol	thermodynamically near-ideal, if max. $N_{th} \geq 5$
$K^V a_e$	infinite reflux distillation of methanol/ethanol/n-propanol	thermodynamically near-ideal, if max. $N_{th} < 5$
$K^V a_e$	infinite reflux distillation of ethanol/n-propanol/water	thermodynamically non-ideal

4.2 Design of the test stand

The test stand should provide great flexibility for various investigations while capturing a maximum of information about the process. Specifically, the design should enable the investigation of the following:

- stripping and absorption,
- distillation at infinite reflux,
- distillation at various V/L ratios,
- influence of RPB design (e.g. packing type, bed height, liquid distributor),
- end effects.

In this section, the basic design considerations are described. First, the design of the RPB is briefly explained. Next, the process flow diagram is developed. Finally, considerations regarding the temperature and pressure range of the test stand are laid out.

More information on the basic and detail engineering can be found in Vlaminck (2019). Details of the safety concept developed in a Hazard and Operability Study (HAZOP), the implementation of the process control system and the commissioning of the plant are described in Krink (2019).

4.2.1 Design of the RPB

Systematic design procedures for RPBs are scarce. The most comprehensive methodology is presented by Agarwal et al. (2010). First, an RPB type, packing material and operating speed are selected. To determine rotor geometry, the inner radius is chosen based on space requirements for the liquid distributor and the required size of the gas outlet. Axial packing height is determined from desired throughput and approach to flooding limit using RPB-specific flood point correlations. Finally, outer radius is chosen based on mass transfer calculations to satisfy desired product purities. This is comparable to conventional column design, with column diameter corresponding to RPB axial packing height and column height corresponding to the RPB radial bed length.

In case of the RPB test stand, the design procedure is different since the goal is not the separation of a certain mixture, but to conduct mass transfer experiments. Special attention is paid to incorporate conclusions from Sec. 2.2, p. 17, in details of the RPB design. Furthermore, the design recommendations of Neumann (2018, p. 110) were taken into consideration.

Even though the design procedure is different for this test stand, the reasoning of Agarwal et al. (2010) regarding the inner bed radius still applies. Based on the space requirements of a liquid distributor that can accommodate different types of nozzles and allow for their adjustment, an inner radius of 60 mm is chosen. To avoid a dominating influence of end effects, the rotor should have a sufficient radial length. An outer radius of 225 mm is chosen, which is in the upper range of RPBs used for investigation of distillation (cf. Tab. 2.2). The selection of axial packing height determines the sizing of the periphery, such as reboiler, condenser and pumps. To be able to achieve liquid loads and F-factors in a meaningful range of the RPB hydrodynamic window whilst not exceeding feasible dimensions of periphery in a lab environment, axial height is chosen as low as possible. Lowest investigated packing heights are in the range of 10 to 25 mm (cf. Tab. 2.2). The RPB is consequently designed for this range of heights. A set of different rotor spacers for the eye and outer periphery allow for investigation



Fig. 4.3: NCX1116 metal foam packing (inner diameter 120 mm, segment diameters 190 mm/260 mm/ 330 mm, outer diameter 450 mm).

of packing heights of 10, 15, 20 and 25 mm. The support rings are designed to have a large free cross section(≈90 %), to avoid shadowing of sections of the bed as much as possible. To minimize interference with mass transfer, only three spacers of 20 mm diameter each are employed at the rotor outer radius.

Different types of packing can be employed. The RPB is initially equipped with NCX1116 Cr-Ni metal foam supplied by Recemat BV, which has a specific geometric surface area of 1000 $m^2\,m^{-3}$, a porosity of 0.92 and an average pore size of 1.4 mm (RECEMAT BV, 2014). The foam is segmented in rings, as shown in Fig. 4.3, to allow for variations in radial bed length. Two sets of rings with a height of 10 mm are initially procured, allowing for bed heights of 10 mm or 20 mm. The use of metal foam allows for better reproducibility as compared to wire meshes, when repacking the rotor. Wire meshes would need to be wound anew around the inner packing support ring after having been removed. This process is tedious and entails the risk of a non-uniform packing with respect to packing density and rotor balancing.

Liquid is distributed evenly by two nozzles over the packing height, which are positioned 180° apart. Either full jet nozzles, that are typically employed in RPBs, or flat fan nozzles, that allow for a more even distribution of liquid over the axial packing height, are used. The flow patterns of the nozzles are shown in Fig. 4.4.

Two samplers made from PTFE are positioned in the RPB casing to investigate outer end effects. The liquid sampler collects liquid ejected from the RPB packing edge

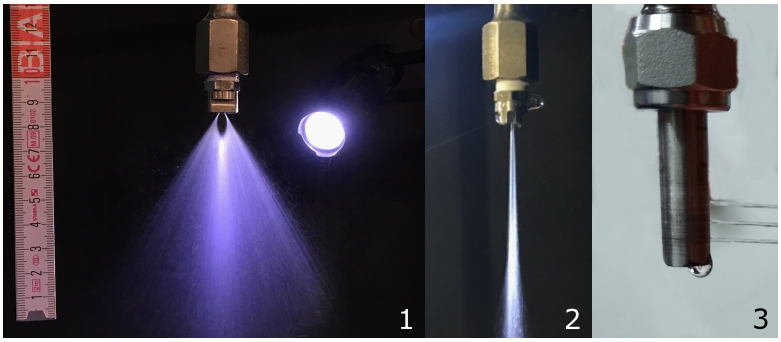


Fig. 4.4: Spraying characteristics of flatfan (1 - front view, 2 - side view) and fulljet nozzles (3).

over an axial height of 11 mm and is positioned 2.5 mm from the rotor. The inlet of the gas sampler is oriented tangential to the rotor and located above the upper rotor plate, with the opening facing away from the direction of rotation to avoid capturing entrained liquid droplets. The casing inner diameter is set to 533 mm to allow space for the samplers.

The casing is designed to minimize liquid hold-up and thus liquid residence time. The floor is angled towards the outside and it is further equipped with three liquid outlets next to which radial wipers are installed. These direct the liquid towards the outlets and prevent a churning of the liquid on the casing floor.

Gas inlet is located on top of the RPB casing near the outer radius for ease of manufacture and in accordance with results of the CFD study of Llerena-Chavez and Larachi (2009) that showed low radial gas maldistribution for such a configuration. The gas outlet is located centrally on the top cover.

The rotational speed of the RPB can be adjusted through a variable speed drive in the range of 0 to 2800 min^{-1}. This exceeds the range of most RPBs investigated in literature. An overview of the RPB specifications is given in Tab. 4.4. A photograph of the test rig is shown in Fig. 4.5.

4.2.2 Development of the process flow diagrams

In this section, the basic Process Flow Diagrams (PFDs) are presented. An overview of employed measurement devices and their associated accuracies is given in Tab. 4.5.

Tab. 4.4: Rotating Packed Bed geometry, packing and liquid distributor specifications.

Item	Specification
Casing inner diameter / height	533 mm / 105 mm
Packing inner / outer diameter / height	120 mm / 450 mm / 10 or 20 mm
Packing inner support ring	10 vertical ribs, ≈90 % free area
Packing outer support	3 cylindrical disc spacers (diameter 20 mm)
Packing	Ni-Cr metal foam Recemat NCX1116 ($\epsilon = 0.92, a_p = 1000\ m^2/m^3$, average pore diameter 1.4 mm) (RECEMAT BV, 2014)
Gas inlet/outlet diameter (both top of casing)	63 mm
Liquid outlet diameter (3x bottom of casing)	25 mm
Liquid distributor	2 nozzles, 180° apart
- full jet nozzles with 3 jets each	nozzle tube inner diameter 6 mm hole diameter 0.7 mm or hole diameter 1.0 mm
- flat fan nozzles (Spraying Systems Co.)	HB 1/8 VV-316SS-65 0033 (≤0.3 kg/min) or HB 1/8 VV-316SS-65 0067 (0.75 kg/min) or HB 1/8 VV-316SS-65 015 (1.25 kg/min) or HB 1/8 VV-316SS-65 025 (≥1.8 kg/min)

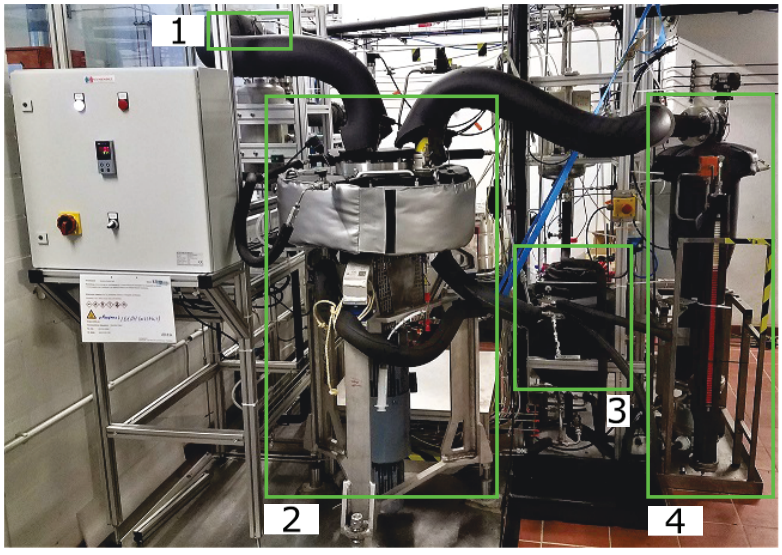


Fig. 4.5: Photograph of the RPB test stand (1 - condenser, 2 - RPB, 3 - drum D-01, 4 - reboiler).

Tab. 4.5: Overview of employed measurement devices.

PID Tag	Measurement	Measurement Principle	Accuracy
TI01...TI12	Temperature	PT100	Class A $(0.15 + 0.002\vartheta\ (^\circ C))K$
PI01, PI02	Absolute pressure	Piezoresistive	6 mbar
PDI01	Pressure drop	Piezoresistive	0.5 mbar
SI01	Rotational speed	Optical incremental encoder	n.a.
FI02	Liquid mass flow rate	Coriolis	0.15%
QI01	Dissolved Oxygen	Optical	$\lvert\Delta c_{rel}\rvert = 4\%$
QI02	Dissolved Oxygen	Optical	$\lvert\Delta c_{rel}\rvert = \max\left(4\% + \frac{0.125\ \mu mol/L}{c\ (\mu mol/L)}, 5\%\right)$
S-01...S-06	Liquid samples	GC-TCD	$\lvert\Delta w_{rel}\rvert = 2\%/\sqrt{w}$

Distillation operation

Experiments for evaluation of separation efficiency are commonly conducted at infinite reflux. The flow sheet configuration for this operating mode is shown in Fig. 4.6. In this mode, liquid is evaporated in the electrical reboiler, enters the RPB casing on the outside, is driven by pressure gradient inwards through the packing and exits the RPB at the eye. The top seal prevents vapor bypassing the rotor. Vapor is then routed to a total condenser, subcooled to avoid cavitation of the reflux pump, and collected in a reflux drum. From here, it is pumped by P-02 via a Coriolis flowmeter FI02 (Endress+Hauser Cubemass C100 DN04) and a reflux preheater to the spraying nozzles that evenly distribute it on the packing inner radius. Pump speed is manipulated through a controller cascade involving a flow rate controller and a level controller of vessel D-02. Liquid catches on to the packing and is driven outwards by centrifugal force countercurrently to the vapor, undergoing intense heat and mass transfer. Liquid is ejected from the packing as a shower of ligaments and droplets, splashes against the casing and is subsequently collected to be routed directly to the reboiler. A series of sampling points enables assessment of mass transfer performance. A liquid (S-03) and a vapor sample (S-02) can be taken from within the RPB casing. For inertization

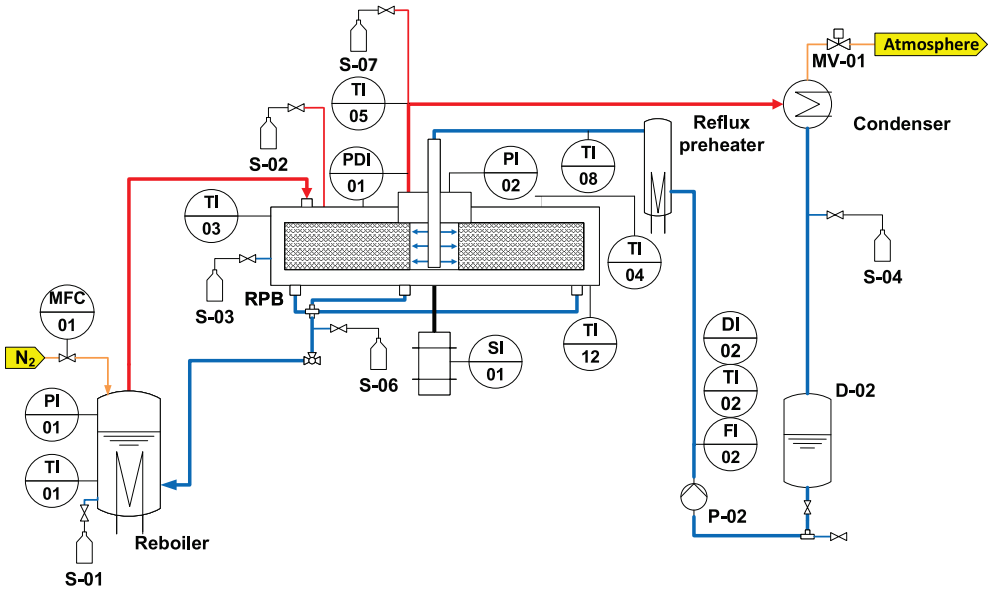


Fig. 4.6: Process flow diagram of the test stand configured for distillation at infinite reflux.

purposes, nitrogen can be dosed to the reboiler via thermal mass flow controller MFC-01 (BROOKS SLA5850) and routed to atmosphere through magnet valve MV-01.

For continuous separation of liquid mixtures by distillation, finite reflux is required. A conventional column is usually separated through the feed stream in a rectifying section above the feed and a stripping section below the feed. In a single block packing RPB, a radial mid-feed is not possible. Therefore, two rotors are required for rectifying and stripping section, either mounted on the same shaft or in two different machines, as illustrated in Fig. 4.7. Assuming a liquid feed stream, in the rectifying section vapor molar flow rate is greater than liquid molar flow rate, while in the stripping section liquid molar flow rate is greater than vapor molar flow rate. These hydrodynamic conditions could potentially influence mass transfer efficiency in RPBs, as it has been observed to be the case for conventional columns (Williams et al., 1950). It is thus desirable to be able to study the effect of vapor to liquid ratio.

However, continuous operation of the RPB as either a rectifying or stripping section would require large quantities of chemicals and large storage tanks, increasing risk and cost. Therefore, the idea of Edye (1955) is seized to operate the plant with bypass streams to vary the V/L ratio within a certain range, while maintaining a closed cycle. The resulting flowsheet is shown in Fig. 4.8. Liquid exiting the RPB is now collected in vessel D-01, subcooled to avoid cavitation and pumped into the reboiler. Pump

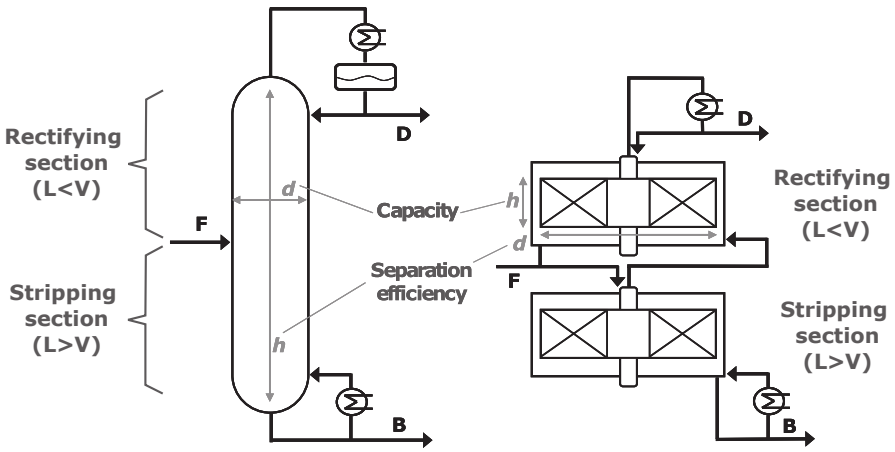


Fig. 4.7: Analogy between distillation column and two RPBs configured for distillation at finite reflux (adapted from Cortes Garcia et al., 2017).

speed is manipulated through a level controller of vessel D-01. In stripping mode, P-01 is required since part of this liquid stream is bypassed around the reboiler and pumped to the distillate drum D-02. The split ratio is calculated from the mass flow rates measured by Coriolis flow meters FI01 and FI03 and controlled by valve CV-02. Thus, the molar ratio of V/L inside the RPB is less than one. In rectifying mode, part of the reflux liquid is routed to vessel D-01, where it is mixed with the liquid exiting the RPB and subsequently pumped to the reboiler. The reflux ratio is calculated based on measurements of Coriolis flow meters FI02 and FI04 and controlled by valve CV-01. Thus, a molar ratio of V/L inside the RPB of greater than one can be achieved. These bypasses constitute a second stage of expansion of the test stand and have not been constructed as a part of this thesis.

Desorption operation

In desorption mode, water is pre-saturated by sparging either with air or pure oxygen in a 220 L barrel. From there it is pumped by pump P-02 via the optical dissolved oxygen sensor QI01 (OXROB10 of Pyroscience GmbH) and the Coriolis mass flow meter FI02 to the nozzles located in the eye of the RPB. Flow rate is controlled by manipulation of pump speed. Oxygen is desorbed from the water traveling through the rotating packing, collects in the casing and is routed past a second optical dissolved oxygen sensor QI02 (TROXROB10) for trace ranges of oxygen to vessel D-01. From there, it is pumped by P-01 to a second barrel. Pump speed of P-01 is manipulated by a level controller of vessel D-01. Nitrogen from a cylinder is introduced on the outside of the RPB casing and flows countercurrently to the water inwards to the eye

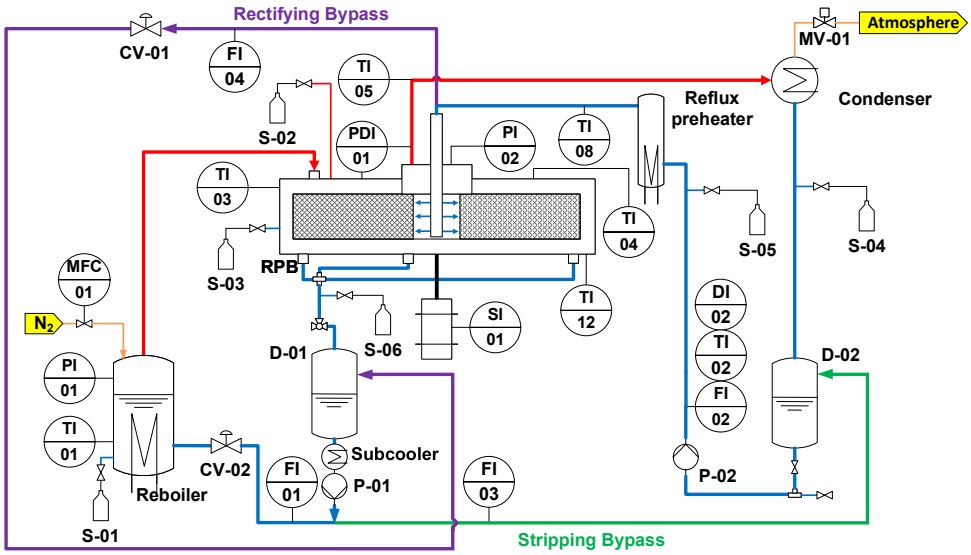


Fig. 4.8: Process flow diagram of the test stand configured for distillation in rectifying or stripping mode.

of the RPB. From there it is routed to the atmosphere. Nitrogen flow rate is controlled through thermal mass flow controller MFC01. For cocurrent desorption, the flow path of the nitrogen gas stream is reversed. Oxygen levels in the outlet gas stream can be monitored through a µGC.

4.2.3 Operating range of the RPB test stand

The operating range of the RPB test stand regarding pressure, temperature and hydrodynamics is selected based on the following considerations.

Operating pressure and temperature

The RPB is normally operated at ambient pressure. In distillation, elevated pressure leads to an increase in gas density and thus a decrease in gas velocity, since the increase in gas density is not compensated through the accompanying increase in boiling temperature. This results in overall lower F-factors for comparable reboiler duties when increasing pressure. Since F-factor is a determining criterion in operation and realizable reboiler duties are limited, operation at significantly elevated pressures is not planned. Furthermore, limiting the operating range to a maximum pressure of 1.5 bar(a) facilitates construction of the plant, as below this pressure the German

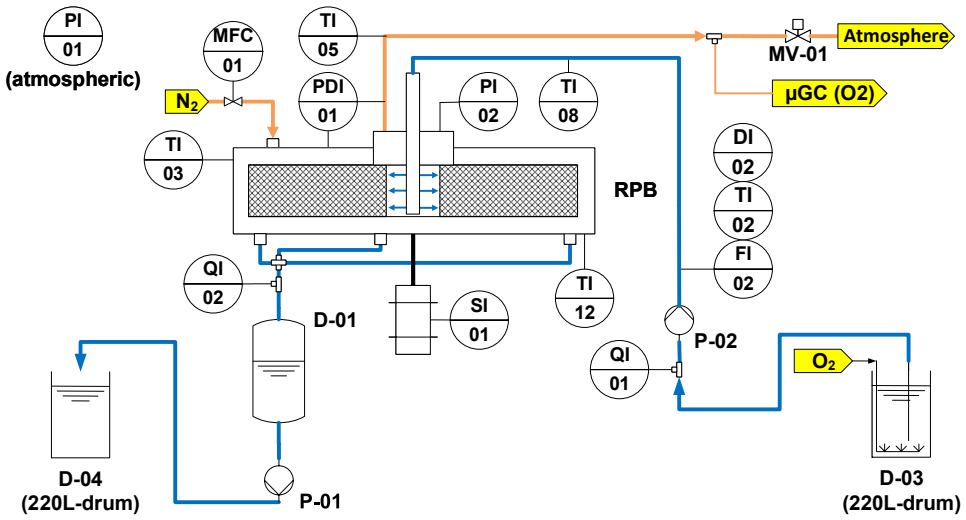


Fig. 4.9: Process flow diagram of the test stand configured for oxygen desorption from water countercurrent to a nitrogen gas stream (Hilpert and Repke, 2020).

pressure-equipment directive (DGRL) is not applicable. For the maximum bed height, operation at partial vacuum of approximately 0.75 bar(a) is planned, to produce higher F-factors with realizable reboiler duties.

The lowest operating temperature is ambient temperature for oxygen stripping from water. The chosen maximum operating pressure of ambient pressure determines the highest expected operating temperature. Based on the boiling point of the highest boiling component i-butanol this is 107.6 °C at 1.013 bar(a) (VDI-Wärmeatlas 2013, p. 362).

Hydrodynamic operating range

It is desirable to be able to operate the RPB up to its flood point. Hydrodynamics in RPBs are described by the F-factor and the liquid load. Both vary along the radius since the cross section of the RPB depends on the radial position in the bed (cf. Fig. 4.1). Several publications use the maximum F-factor according to Eq. (4.1) which is found at the inner packing edge, the so-called eye of the RPB, where flooding initiates (Kelleher and Fair, 1996; Neumann, 2018). Neumann et al. (2017a) define the corresponding liquid load at the eye of the RPB according to Eq. (4.2).

$$F_{max} = \frac{\dot{V}_{G,i}}{2\pi r_i h_p} \sqrt{\rho_{Mix,i}^{V,mass}} \tag{4.1}$$

$$LL_{max} = \frac{\dot{V}_{L,i}}{2\pi r_i h_p} \tag{4.2}$$

In Tab. 4.6, a selection of F-factors that have been reported in RPB literature is summarized. From these, no typical operating range can be identified. This is likely due to the variety of influencing variables on feasible operating region, such as type and geometry of liquid distributor, type of RPB and packing material, operating pressure, and liquid flow rates. Furthermore, the studies might not have utilized the full hydrodynamic operating range possible in the respective RPBs.

Tab. 4.6: Selected F-factors for experimental investigations of distillation in RPBs from literature.

Author (Year)	RPB-Type, packing	RPB dimensions (d_i / d_o / h_p, in mm)	F_{max} in $Pa^{0.5}$
Kelleher and Fair (1996)	single block, Ni-Cr foam	175/600/150	0.6...1.3[a]
Lin et al. (2002)	single block, SS wire mesh	122/294/50 & 95	1...3
Wang et al. (2008a)	Rotating Zigzag Bed	52/100/78	4.1...20.5[b]
Mondal et al. (2012)	split packing, wire mesh	60/310/27 (vapor draw at 150)	0.36...0.6
Li et al. (2014)	Counterflow Concentric-Ring Rotating Bed	140/272/15 & 45	0.3...3.8
Wang et al. (2014a) and Wang et al. (2014b)	Crossflow Concentric-baffle Rotating Bed	240/469.6/72	1.3...6.6

[a] Investigations at pressures of 1.7 bar(a) and 4.1 bar(a). Flooding was observed.
[b] Reported F-factors for RZBs are significantly higher since they are calculated with respect to the smaller annular area between two adjacent baffles as opposed to the lateral surface at the eye for RPBs.

The approximate optimal operating range of conventional distillation columns is between 50 to 90 % of flood point (Schönbucher, 2002, p. 470). Recommended F-factors for design point of towers with structured and random packings are found around the load point, and range from 60...80% of flood point (Goedecke, 2006, p. 762; Turton, 2003, p. 349; Towler and Sinnott, 2008, p. 758). From the limited information available on the investigations at ICI, RPBs can be operated at up to 70 % of flood point without significant decrease in performance (Wem, 2012).

Neumann et al. (2017a) investigated flooding in an RPB with the same packing material, RECEMAT NCX1116, chosen for the designed RPB test stand in this work. A bed with inner radius of 73 mm, 10 mm height and a full jet liquid distributor positioned 20 mm from the bed were used, which is similar to the RPB design in this study. For the water/air system, accumulation of a rotating liquid film at the gas outlet and entrainment of liquid droplets towards the gas outlet were first observed at a rotational speed of 1200 min^{-1}, $F_{max,flood}$ =3.4 $Pa^{0.5}$ and a liquid load at the inner packing edge of 39.2 $m^3/(m^2h)$ (corresponding to a jet velocity of 2.9 $m\,s^{-1}$).

Taking the operating range of $0.5...0.9 \cdot F_{max,flood}$ as a rough guideline for distillation in RPBs, this results in an operating range of 1.7 to 3.1 $Pa^{0.5}$ for the designed RPB, based on the experimentally determined $F_{max,flood}$ of Neumann et al. (2017a).

For infinite reflux operation, a given F-factor corresponds to a certain liquid load, which can be calculated by means of Eq. (4.3).

$$LL_{max,\infty} = \frac{\sqrt{\rho_{Mix,i}^{V,mass}}}{\rho_{Mix,i}^{L,mass}} F_{max,\infty} \tag{4.3}$$

For the mixtures to be investigated, the corresponding minimum liquid load for F_{max} =3.4 $Pa^{0.5}$ is approximately 17 $m^3/(m^2h)$, occurring for n-propanol/water system, while the maximum liquid load is approximately 25 $m^3/(m^2h)$, occurring for n-propanol/iso-butanol. Densities have been calculated assuming distillation at infinite reflux at 1 bar(a) with 4 theoretical stages and a bottoms concentration of 20 mol % light key. Those liquid loads are lower than the one in the quoted air/water experiment. Assuming a variation of L/V molar flow ratio through stripping and rectifying mode within the range of 0.5...2, LL_{max} would vary approximately between $0.5...2 \cdot LL_{max,\infty}$. This corresponds to a further reduction of liquid load below the $LL_{max,flood}$ reported by (Neumann et al., 2017a) in case of rectifying, and an increase in liquid load beyond the one reported for flooding in case of stripping mode. Comparison of the maximum liquid load for stripping mode, roughly 50 $m^3/(m^2h)$, to the literature value of 39.2 $m^3/(m^2h)$ suggests that a L/V of 1.5 should still be achievable without flooding. Furthermore, rotational speed can be increased beyond 1200 min^{-1}. Therefore, even higher actual maximal F-factors and liquid loads at flooding could be achievable.

Based on the above considerations, the RPB and its periphery are designed for a range of F-factors of 1 to 3 $Pa^{0.5}$ for a bed of 10 mm height. This is comparable to the range of

operation of various conventional structured packings at atmospheric pressure (Sulzer Chemtech, 2012) and falls within the range of F-Factors reported in RPB literature.

For a bed height of 20 mm or 25 mm, the maximum F-factor envisioned is 2 $Pa^{0.5}$ to minimize required reboiler duty. Maximum reboiler duty is estimated from Eq. (4.4) for a bed height of 25 mm and an F-factor at the eye of 2 $Pa^{0.5}$ at 0.75 bar(a) for the considered mixtures to be in the range of 16 to 22 kW without heat losses. To allow for heat losses, the reboiler is designed with a duty of 25 kW.

$$\dot{Q}_{reb} \approx \Delta h_{Mix,reb}^{LV,mass} \sqrt{\rho_{Mix,i}^{V,mass}} F_{max,\infty} \pi d_i h_p + \dot{Q}_{loss} \tag{4.4}$$

The design operating ranges of the RPB test stand are summarized in Tab. 4.7.

Tab. 4.7: Summary of design operating ranges of the RPB test stand.

Parameter	Design Range	Remarks
Operating Pressure	0.75 to 1.1 bar(a)	permissible range 0.1 to 1.5 bar(a)
Operating Temperature	15 to 110 °C	permissible range −25 to 150 °C
Rotational Speed	0. . . 2800 RPM	
F_{max} [a]	1 to 3 $Pa^{0.5}$	Distillation with $h_p = 10$ mm
	0.5 to 2 $Pa^{0.5}$	Distillation with $h_p = 20$ mm & 25 mm
LL_{max}	5 to 50 $m^3\,m^{-2}\,h^{-1}$	

[a] Achievable ranges at infinite reflux operation are greater since stripping or rectifying operation require larger duties for the same F-factors.

4.3 Experimental procedure

In this section, the experimental procedures for oxygen desorption (Hilpert and Repke, 2021) and distillation experiments (Hilpert et al., 2022) are described.

4.3.1 Experimental procedure for desorption experiments

A two-point calibration of the dissolved oxygen sensors was conducted according to the procedure outlined by the manufacturer. For zero point, deionized water was first sparged with nitrogen for ten minutes. To scavenge residual oxygen, sodium sulfite was dissolved to obtain a 30 g/L solution. The covered flask, which had negligible gas head space, sat for 15 min. before oxygen sensors and a PT100 were pierced

through the cover. Zero point was recorded upon reaching constant readings. The second calibration point was obtained by sparging compressed air through water in a flask for ten minutes and adding the oxygen and temperature sensors afterwards. The calibration point was again recorded upon reaching constant readings.

Prior to experimentation, the nozzle positions were adjusted to properly position the jet impact points or the flat fan spray over the height of the packing. Tightness of the device was established (pressure loss typically <6 mbar/h at 1.5 bar(a)) and the system was rendered inert using pressure cycling with nitrogen (purity >99.999%). Oxygen level was checked using an online µGC. During operation, plant pressure was typically 40 to 100 mbar above ambient pressure, depending on nitrogen gas flow rate. Water in the barrel was sparged using pure oxygen to obtain oxygen levels close to saturation. This was necessary since oxygen content in the outlet drops to very low levels, increasing analytical error strongly when sparging with air. Only for the data series measured in the packed rotor with the flat fan nozzles at a liquid load of 28.7 $m^3\,m^{-2}\,h^{-1}$ air was used for sparging[3]. After saturation, nitrogen and water flow were started and different operating points investigated.

To establish a steady state point, desired values of rotational speed, nitrogen flow rate and water flow rate were set. After reaching constant readings of flow rate, levels, pressures and dissolved oxygen concentration, readings required for the calculation of results were averaged over a time period of approximately ten minutes. Most operating points were repeated twice, usually on a different day, to demonstrate reproducibility. No fixed procedure regarding the order of set point changes was followed, as hysteresis effects could not be observed in preliminary tests.

4.3.2 Experimental procedure for distillation experiments

Ethanol (ROTIPURAN $\geq$ 99.8%, pro analysi) and n-propanol ($\geq$ 99.5%, pro synthesis), purchased from Carl Roth GmbH + Co. KG, and demineralized water were used in the experiments. Analysis of all samples was carried out using an Agilent Technologies 6850 Network GC System with an HP-PLOT Q capillary column (30.0 m x 320 µm x 20.0 µm nominal) and a Thermal Conductivity Detector (TCD). Iso-propanol (ROTISOLV $\geq$ 99.8%, Pestilyse) was used as solvent and helium as carrier gas. Calibration was done using the method of external standard. Relative error in analyzed mass

[3]This was the first flow rate investigated. Afterwards, oxygen was used for sparging.

percent can be described through the trumpet curve given in Eq. 4.5 for all three components (cf. Appendix C of Gottheil (2021)).

$$|\Delta w_{rel}| = \frac{2\%}{\sqrt{w}} \tag{4.5}$$

Prior to experimentation, the nozzle positions were adjusted to properly position the jet impact points over the height of the packing. Tightness of the device was established (pressure loss typically $<$ 6 mbar/h at 1.5 bar(a)) and the system was rendered inert using pressure cycling with nitrogen (purity >99.8%). Establishment of steady state after start-up took approximately 1 h, mainly governed by the heat capacities of the RPB and periphery. Time between steady states was governed by the liquid holdups in the periphery of the RPB, mainly the reboiler and the reflux drum, and took depending on the flow rate and the amount of change in set points approximately 30 min.

To establish a steady state point, desired values of rotational speed, reboiler duty and an estimated pre-heater temperature were set. A sub-cooling of reflux fed to the RPB of approximately 0.5 K was targeted. After reaching constant readings of flow rate, levels, pressures and temperatures, a bubble point calculation based on distillate composition and pressure at the eye of the RPB was carried out. The set point for the pre-heater was set 0.5 K below the calculated value. Three test systems were investigated. For the ethanol/water system, composition for the bubble point calculation was determined based on the density and temperature readings of the Coriolis flow meter using the correlation of Khattab et al. (2012) for density of ethanol/water mixtures. For ethanol/n-propanol and ethanol/n-propanol/water systems this was not possible due to the similarity in densities of the two alcohols. Here, samples of distillate (S_4) were taken and analyzed immediately in a GC to perform the bubble point calculation.

After reaching the desired set point of the pre-heater and again obtaining constant values for all readings, another 30 min. was waited prior to taking all targeted samples. Samples were taken through septa using syringes and transferred to sampling vials covered with screw caps with septa. Sampling procedure took approximately 6 min. After another 10 min. a second round of samples was taken to verify steady state conditions. A steady state was accepted if deviations between these samples were within the measurement uncertainty of the GC analytics. Sensor readings required in the calculation of results were averaged over the time period of sampling. Each operating point used for model development was repeated once, usually on a different day, to demonstrate reproducibility. No fixed procedure regarding the order of set

point changes was followed, as hysteresis effects could not be observed in preliminary tests.

5 Rate-based mass transfer model of the RPB

In this chapter, the formulated rate-based mass transfer model of the RPB is described. As outlined in Sec. 2.4, compared to the equilibrium model, this model provides a more accurate representation of the physical phenomena. The link provided between geometry, operating conditions and performance is particularly important in the case of RPBs, for which mass transfer is highly dependent on parameters such as rotational speed. This chapter has previously been published in Hilpert et al. (2022).

In the rate-based model, the considered device is divided into a series of NJ discrete elements. For every element, the balance equations for mass and energy are set up individually for the liquid and vapor phase. Both phases are linked through mass and energy balances around the interface. The equilibrium constants are determined by the interface compositions and temperature.

The following assumptions were made to simplify the model:

- The process is at steady state.
- Each bulk phase is completely mixed on each stage.
- Vapor and liquid balance region of the same non-equilibrium stage j are in mechanical equilibrium, i.e. $P_j^L = P_j^V = P_j$.
- The phase interface itself poses no resistance to mass transfer.
- There is no accumulation of material and energy at the interface.
- There are no reactions in the system.
- Vapor phase is treated as ideal due to operation at atmospheric pressure and the type of components simulated.

- Liquid phase is considered as non-ideal for equilibrium calculations. Heat of mixing is neglected, since it amounts to less than 3 % of enthalpy of vaporization (Larkin, 1975; Byval'tsev and Perelygin, 1970; Ramalho and Ruel, 1968; Counsell et al., 1970; Majer et al., 1978).

- For calculation of the mass transfer rates, it is assumed that the finite flux mass transfer coefficients are equal to the low flux mass transfer coefficients. Accordingly, the high flux correction factor matrix is set equal to the identity matrix, as it has been found to be close to unity in distillation (Taylor and Krishna, 1993, p. 292).

- All mass transfer occurs within the rotor, i.e. mass transfer occurring in the casing or the eye of the rotor is not separately considered but ascribed to the rotor.

- There is no heat exchange between the rotor and the environment as the rotor is surrounded by hot vapor in the casing.

- Flow and hence mass transfer within the rotor are point symmetric, allowing for the use of averaged heat and mass transfer coefficients per discrete element. tarCT measurements showed that this is an acceptable assumption for symmetric liquid distribution at sufficiently high rotational speeds beyond $\approx$600 min^{-1} (Groß et al., 2019).

The condenser and reboiler are considered as total heat exchangers, i.e. there is no further separation by means of these apparatuses. They represent stages $j = 0$ and $j = NJ + 1$, respectively, and are modeled as equilibrium stages (Taylor and Krishna, 1993, p. 405).

The model, which is described in detail in the subsequent sections, was set up using MOSAICmodeling[4] environment (Tolksdorf et al., 2019) and exported to AMPL (Fourer et al., 2009) to be solved using IPOPT (Wächter and Biegler, 2006). It is an advanced development of the model presented in Calvillo Aranda (2020). The parameters required for property and equilibrium models are taken from Aspen Plus V10 databanks *PURE32* and *VLE-IG*. An overview of the associated MOSAICmodeling elements is given in Appendix G.

[4] https://mosaic-modeling.de/

5.1 MERSHQ-equations

Following the well-known approach to rigorous rate-based column modeling, for each discrete element or non-equilibrium stage, as sketched in Fig. 5.1, **M**aterial balances, **E**nergy balances, **R**ate equations, **S**ummation equations, **H**ydraulic equations and e**Q**uilibrium equations at the interface are set up (Taylor and Krishna, 1993, p. 404).

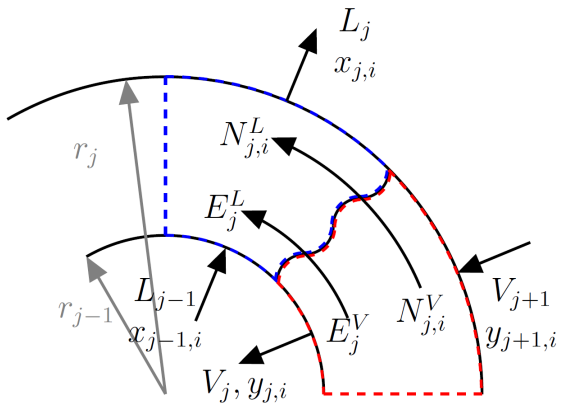


Fig. 5.1: Schematic representation of the j-th non-equilibrium stage of an RPB for counter-current gas-liquid mass transfer. Vapor and liquid phase are shown separated for ease of representation, even though they are interspersed in the RPB (Hilpert et al., 2022).

M Material balances

The component material balances on any non-equilibrium stage are given by Eq. 5.1 to 5.3.

Liquid
$$L_{j-1} \cdot x_{j-1,i} + N^L_{j,i} = L_j \cdot x_{j,i} \tag{5.1}$$

Vapor
$$V_{j+1} \cdot y_{j+1,i} = V_j \cdot y_j + N^V_{j,i} \tag{5.2}$$

Interface
$$N^L_{j,i} = N^V_{j,i} \tag{5.3}$$

E Energy balances

The energy balances are described through Eq. 5.4 to 5.6 for $j = 1,2,..,NJ$.

Liquid
$$L_{j-1} \cdot h^L_{j-1} + E^L_j = L_j \cdot h^L_j \tag{5.4}$$

Vapor
$$V_{j+1} \cdot h^V_{j+1} = V_j \cdot h^V_j + E^V_j \tag{5.5}$$

Interface
$$E^L_j = E^V_j \tag{5.6}$$

Liquid molar streams exiting non-equilibrium stage j are denoted by L_j, with the associated mole fraction of component i being $x_{j,i}$; vapor or gas molar flow rates are denoted by V_j with mole fractions $y_{j,i}$. The transfering molar flow rate of species i between vapor and liquid is $N_{j,i}$, while the rate of energy transfer is indicated as E_j.

R Transfer rate equations

The mass transfer rate equations on any non-equilibrium stage are Eq. 5.7 and 5.8 for $i = 1, 2..., NC - 1$, with NC representing the total number of components.

Liquid
$$\left(N_j^L\right) = \rho_{Mix,j}^{L,mol} \cdot \left[k^L a_{e,j}\right] \cdot V_j^{discr} \cdot \left(x_j^I - x_j\right) + \sum_{i=1}^{NC} N_{j,i}^L \cdot \left(x_j\right) \tag{5.7}$$

Vapor
$$\left(N_j^V\right) = \rho_{Mix,j}^{V,mol} \cdot \left[k^V a_{e,j}\right] \cdot V_j^{discr} \cdot \left(y_j - y_j^I\right) + \sum_{i=1}^{NC} N_{j,i}^V \cdot \left(y_j\right) \tag{5.8}$$

Superscript I indicates values at the liquid-vapor or liquid-gas interface. $\left(N_j^L\right)$ and $\left(N_j^V\right)$ represent the vectors of elements $N_{j,i}^L$ and $N_{j,i}^V$, respectively. $\left[ka_{e,j}\right]$ is the matrix of volumetric low-flux mass transfer coefficients, i.e. the product of the mass-transfer coefficients and the specific effective surface area. Since ka_e is treated as one variable, it is assigned a joint stage index j ($ka_{e,j}$ instead of $k_j a_{e,j}$). This implementation is chosen as literature correlations for RPBs are usually available for the volumetric coefficients. Furthermore, only volumetric coefficients and no specific effective surface areas are experimentally determined in this work. $\left(x_j^I - x_j\right)$ and $\left(x_j\right)$ represent vectors with elements $x_{j,i}^I - x_{j,i}$ and $x_{j,i}$; this similarly applies to Eq. 5.8.

The energy transfer rate equations on any non-equilibrium stage are Eq. 5.9 and 5.10.

Liquid
$$E_j^L = \alpha^L a_{e,j} \cdot V_j^{discr} \cdot \left(T_j^I - T_j^L\right) + \sum_{i=1}^{NC} N_{j,i}^L \cdot \overline{h}_{j,i}^L \tag{5.9}$$

Vapor
$$E_j^V = \alpha^V a_{e,j} \cdot V_j^{discr} \cdot \left(T_j^V - T_j^I\right) + \sum_{i=1}^{NC} N_{j,i}^V \cdot \overline{h}_{j,i}^V \tag{5.10}$$

The $\overline{h}$ denote the partial molar enthalpies and αa_e the volumetric heat transfer coefficients. As with ka_e, αa_e is considered as one variable and hence it is assigned a joint index j. The volume of a discrete element is given by Eq. 5.11 and depends on the

discretization approach. Further details on the rotor discretization are presented in Sec. 7.2.1.

$$V_j^{discr} = \pi \cdot \left(\left(r_j\right)^2 - \left(r_{j-1}\right)^2 \right) \cdot h_p \tag{5.11}$$

S Summation equations

$$\sum_{i=1}^{NC} x_{j,i} - 1 = 0, \qquad \sum_{i=1}^{NC} y_{j,i} - 1 = 0 \tag{5.12}$$

$$\sum_{i=1}^{NC} x_{j,i}^I - 1 = 0, \qquad \sum_{i=1}^{NC} y_{j,i}^I - 1 = 0 \tag{5.13}$$

H Hydraulic equations

$$P_{j+1} = P_j + \Delta P_j \tag{5.14}$$

Pressure of adjacent non-equilibrium stages is related through Eq. 5.14. The pressure drop ΔP_j is calculated using the model of Neumann et al. (2017b), Eq. (5.15) to Eq. (5.20), which was developed for a similarly sized RPB employing the same packing material. Pressure of the first stage $P_{j=1}$ is set equal to the pressure of the condenser $P_{j=0}$.

The model of Neumann et al. (2017b) contains terms for centrifugal head ζ_{CH}, which is the pressure difference across the rotor induced through rotation, and frictional pressure drop of the gas flowing through the packing, as shown in Eq. 5.15. Influence of liquid flow, which is expected to be minor, is not included.

$$\Delta P_j = \zeta_{CH,j} + \Delta P_{f,stat,j} \tag{5.15}$$

Centrifugal head is calculated according to Eq. 5.16, where A_{CH} is an RPB configuration dependent parameter. Frictional pressure drop is calculated from Eq. 5.17, where φ is the form factor of the packing. The authors regressed these values to 0.85 and 0.32, respectively, for NCX1116 metal foam packing material used in an RPB of similar size to the one in the current study (Neumann et al., 2017b). $\overline{F}_{int,j}^V$ is the average value of the integrated gas capacity factor.

$$\zeta_{CH,j} = A_{CH} \cdot \frac{\rho_{Mix,j}^{V,mass} \cdot \omega^2}{2} \cdot \left(\left(r_j\right)^2 - \left(r_{j-1}\right)^2 \right) \tag{5.16}$$

$$\Delta P_{f,stat,j} = \Psi_{0,j} \cdot (1-\varphi) \cdot \frac{1-\epsilon}{\epsilon^3} \cdot \frac{\overline{F}^{V}_{int,j}}{d_p} \cdot \left(r_j - r_{j-1}\right) \tag{5.17}$$

$$\overline{F}^{V}_{int,j} = \frac{V/\rho^{V,mol}_{Mix,j}}{2 \cdot \pi \cdot h_p \cdot (r_j - r_{j-1})} \cdot \ln\left(\frac{r_j}{r_{j-1}}\right) \cdot \sqrt{\rho^{V,mass}_{Mix,j}} \tag{5.18}$$

$$\Psi_{0,j} = \frac{725.6}{\overline{Re}^{V}_{int,j}} + 3.203 \tag{5.19}$$

$$\overline{Re}^{V}_{int,j} = \frac{d_p}{(1-\epsilon) \cdot \frac{\eta^{V}_{Mix,j}}{\rho^{V,mass}_{Mix,j}}} \cdot \frac{\overline{F}^{V}_{int,j}}{\sqrt{\rho^{V,mass}_{Mix,j}}} \tag{5.20}$$

Q Interface equilibrium equation

$$y^{I}_{j,i} \cdot P_j = x^{I}_{j,i} \cdot \gamma_{j,i} \cdot P^{LV}_{j,i} \tag{5.21}$$

In the equilibrium relationship Eq. 5.21, valid at the interface, $P^{LV}_{j,i}$ is the vapor pressure of pure component i on stage j and $\gamma_{j,i}$ its respective activity coefficient which is calculated using the NRTL model.

5.2 Calculation of mass transfer coefficients

The values of the volumetric multi-component mass transfer coefficients are predicted from RPB-specific binary mass transfer correlations by use of the R-matrix and the matrix of thermodynamic correction factors Γ according to Eq. 5.22 (Taylor and Krishna, 1993, pp. 165, 215). The linearized theory of Toor, Stewart and Prober is applied for distillation modeling (Taylor and Krishna, 1993, p. 184). Accordingly, in calculating the Γ-matrix, the elements of the R-matrix and in evaluating the correlations of binary mass transfer coefficients, arithmetic mean values of mole fractions between interface and bulk are employed. Furthermore, arithmetic mean values of temperatures between interface and bulk are used for those calculations.

$$\left[ka_{e,j}\right] = \left[R_j\right]^{-1} \cdot \left[\Gamma_j\right] \tag{5.22}$$

The elements of $[R_j]$ are calculated according to Eq. 5.23 and Eq. 5.24.

$$R_{j,m,m} = \frac{z_{j,m}}{ka_{e,j,m,NC}} + \sum_{\substack{k=1 \\ k \neq m}}^{NC} \frac{z_{j,k}}{ka_{e,j,m,k}} \tag{5.23}$$

$$R_{j,m,n} = -z_{j,m} \cdot \left(\frac{1}{ka_{e,j,m,n}} - \frac{1}{ka_{e,j,m,NC}} \right) \tag{5.24}$$

$z_{j,m}$ and $z_{j,k}$ represent the arithmetic mean molar composition of component m or k on stage j between bulk and interface in liquid or vapor phase (e.g. $z_{j,m} = 0.5(y^I_{j,m} + y_{j,m})$). $ka_{e,j,m,n}$ is the binary volumetric mass transfer coefficient for the binary $m-n$ pair and can be estimated by a correlation.

The thermodynamic correction matrix $[\Gamma_j]$ is defined by Eq. 5.25 with the Kronecker delta specified by Eq. 5.26. The $\sum$ next to the partial derivative indicates that all mole fractions are kept constant except the NCth which is adjusted to satisfy the summation equation (Taylor and Krishna, 1993, p. 542). As in the equilibrium equations, the NRTL model is used to calculate the elements of the Gamma-matrix.

$$\Gamma_{j,m,n} = \delta_{m,n} + x_{j,m} \cdot \frac{\partial \ln \gamma_{j,m}}{\partial x_{j,n}}\Big|_{T,P,\sum} \tag{5.25}$$

$$\delta_{m,n} = \begin{cases} 1 & \text{if } m = n \\ 0 & \text{if } m \neq n \end{cases} \tag{5.26}$$

Liquid mixture viscosity is calculated using the Generalized Corresponding States Method (GCSM) of Teja and Rice (1981) (see also Poling et al., 2001, p. 9.85). The Teja and Rice (1981) model for liquid mixture viscosity yields different results depending on the choice of the two reference fluids in multi-component mixtures. There is no clear indicator as to what the best choice is (Wu and Asfour, 1992). Reference fluids should be similar to the components to be described (Viswanath et al., 2007, p. 419). Thus, selected reference components for liquid mixture viscosity calculation with the GCSM are the respective binary pairs for binary mixtures and ethanol/water for the ternary mixture. Binary diffusion coefficients at infinite dilution are estimated using the Wilke-Chang and Wilke-Lee correlations for liquid and vapor phase, respectively (Poling et al., 2001, pp. 11.21, 11.10). Liquid diffusion coefficients at finite dilution are calculated according to Eq. 5.27, which is a geometrically consistent generalization of the Vignes equation (Taylor and Krishna, 1993; Kooijman and Taylor, 1991, p. 91).

$$D^{L}_{j,i,k} = \left(D^{\infty}_{j,i,k}\right)^{(1+x_{j,k}-x_{j,i})/2} \cdot \left(D^{\infty}_{j,k,i}\right)^{(1+x_{j,i}-x_{j,k})/2} \tag{5.27}$$

5.3 Estimation of volumetric heat transfer coefficients

Volumetric heat transfer coefficients are estimated from averaged volumetric mass transfer coefficients and diffusivities according to Eq. 5.28 for vapor and liquid phase, respectively. Eq. 5.28 is derived from the Chilton-Colburn analogy Eq. 5.29 (Taylor and Krishna, 1993, p. 278), which is often used in modeling of packed columns (Krishnamurthy and Taylor, 1985). Krishnamurthy and Taylor (1985) found that uncertainties introduced through use of the Chilton-Colburn analogy have little influence on composition profiles in rate-based distillation modeling.

Averaged diffusivities $\overline{D}$ are calculated according to Eq. 5.30, which is also used for averaging of the volumetric mass transfer coefficients $\overline{ka}_e$ (Aspen Plus V10). In this equation, $\overline{\delta}$ is a numerical stability parameter set to 10^{-4}. Analogously to the calculation of mass transfer coefficients, required transport properties are evaluated using arithmetic mean values of mole fractions and temperatures between interface and bulk for distillation modeling, as recommended by Chilton and Colburn for significant concentration or temperature differences (Henley et al., 2011, p. 116).

$$\alpha a_{e,j} = \rho^{Mass}_{Mix,j} \cdot c^{Mass}_{p,Mix,j} \cdot \overline{ka}_{e,j} \cdot \left(\frac{\lambda_{Mix,j}}{\rho^{Mass}_{Mix,j} \cdot c^{Mass}_{p,Mix,j} \cdot \overline{D}_j}\right)^{2/3} \tag{5.28}$$

$$St_{\alpha} Pr^{2/3} = StSc^{2/3} \tag{5.29}$$

$$\overline{D}_j = \frac{\sum_{m=1}^{NC-1}\sum_{n=m+1}^{NC}(x_{j,m}+\overline{\delta})(x_{j,n}+\overline{\delta})D_{j,m,n}}{\sum_{m=1}^{NC-1}\sum_{n=m+1}^{NC}(x_{j,m}+\overline{\delta})(x_{j,n}+\overline{\delta})} \tag{5.30}$$

6 Investigation of liquid-side mass transfer

As described in Chapter 4, volumetric liquid-side mass transfer coefficients are measured in this study from desorption experiments of oxygen from water into a nitrogen gas stream. This is not only a suitable test system for measurement of $k^L a_e$ values, but also of industrial relevance. Water with low oxygen contents is required for corrosion prevention, e.g. as boiler feed water or in enhanced oil recovery (Zheng et al., 1997; Beer et al., 2018). Furthermore, water needs to be deaerated for certain applications in the beverage industry, involving carbonation of drinks such as soft-drinks or beer (Harbold and Park, 2008). Results of this chapter are thus also of practical relevance for the application of RPBs in these areas.

In this chapter experimental results are first presented and discussed. Next, literature correlations are evaluated with respect to their ability to reproduce the experimental results. Finally, a correlation for $k^L a_e$ is developed and applied to experimental and literature data. Parts of the experimental results of this chapter have previously been published in Hilpert and Repke (2021).

The experiments have usually been conducted in the rotor packed with NCX1116 metal foam of 10 mm height, 60 mm inner and 225 mm outer radius. In the graphs, this is indicated as "packed rotor". Any changes, i.e., no packing material ("empty rotor") or different height or radii, are indicated where applicable.

6.1 Evaluation of the experiments

Besides rotational speed, the two key operating parameters are water flow rate and nitrogen gas flow rate. To characterize water flow rate, liquid load at the inner cross sectional area of the rotor is used. Reporting of the location is necessary because flow area changes along the radius of the RPB. Nitrogen flow rate is reported in Standard Liters Per Minute (SLPM), i.e. at 0 °C and 1.013 25 bar(a).

An expression for calculation of volumetric liquid-side mass transfer coefficients can be derived by integration of a differential material balance of oxygen in the liquid phase combined with an overall material balance of oxygen in the rotor to calculate oxygen concentration in the exiting gas stream. A series of assumptions is made, including a process at steady state, negligible change in liquid flow rate $\dot{V}_L$ along the rotor, negligible gas-side resistance to mass transfer, validity of Henry's Law, constant temperatures (leading to constant Henry coefficients He along the rotor), the water stream being the only source of oxygen (i.e. a tight device), and an ideal gas phase. Furthermore, a constant, i.e. a bed-averaged volumetric liquid-side mass transfer coefficient $k^L a_e$, is assumed. The resulting equations are Eq. 6.1 for countercurrent operation (Chen et al., 2005a) and Eq. 6.2 for cocurrent gas-liquid flow (Beer et al., 2018).

Countercurrent flow:

$$k^L a_e = \frac{\dot{V}_L}{h_p \pi \left(r_o^2 - r_i^2\right)} \frac{1}{1 - \frac{RT}{He}\frac{\dot{V}_L}{\dot{V}_G}} \ln\left(\frac{c_{L,in} - \frac{RT}{He}\left(c_{G,in} + \frac{\dot{V}_L}{\dot{V}_G}(c_{L,in} - c_{L,out})\right)}{c_{L,out} - \frac{RT}{He}c_{G,in}}\right) \tag{6.1}$$

Cocurrent flow:

$$k^L a_e = \frac{\dot{V}_L}{h_p \pi \left(r_o^2 - r_i^2\right)} \frac{1}{1 + \frac{RT}{He}\frac{\dot{V}_L}{\dot{V}_G}} \ln\left(\frac{c_{L,in} - \frac{RT}{He}c_{G,in}}{c_{L,out} - \frac{RT}{He}\left(c_{G,in} + \frac{\dot{V}_L}{\dot{V}_G}(c_{L,in} - c_{L,out})\right)}\right) \tag{6.2}$$

The reference volume for the packed rotor is that of the packing, while the reference volume for the empty rotor is chosen to be that of the empty rotor plates, i.e. the same volume is used for both cases. Due to the location of the oxygen sensors in the inlet and outlet lines, end effects are attributed to the packing by use of Eqs. 6.1 and 6.2. Henry coefficients used in evaluation of the experimental results are calculated based on the fit of Garcia and Gordon (1992) for equilibrium dissolved oxygen concentration in water.

Experimental uncertainties reported and error bars shown are the results of an uncertainty calculation taking into account uncertainties stemming from measurement devices, analytics and repeat runs. Details of the procedure are given in Appendix A.

6.1.1 Influence of pre-saturation of nitrogen with water vapor

VDI 2761-2, a norm treating the "Measurement and evaluation of fluid dynamics and mass transfer in packed columns" through absorption and desorption, recommends to pre-saturate the employed gas stream with water vapor. This is to ensure isothermal operation of the packing, constant flow rates of gas and liquid throughout the packing and to avoid distortion of measured mass transfer by convective mass transfer through Stefan diffusion. The recommendation is based on investigations of ammonia absorption from air in water that showed a significant influence of air pre-saturation for low liquid loads. The norm recommends to limit changes in molar flows to $<3\,\%$ and in temperature to $<5\,\mathrm{K}$ along the packing.

In the investigated process of water deoxygenation in a nitrogen gas stream, no significant influence of pre-saturation of the gas is expected. Water flow rate in the conducted experiments is very high compared to the employed nitrogen flow rates. At the lowest water flow rate of $0.25\,\mathrm{kg\,min^{-1}}$ combined with the highest nitrogen flow rate of 12.3 SLPM, approximately 0.2 % of the water would evaporate, resulting in a 1 K decrease in water temperature. Both is well within the acceptable changes according to VDI 2761-2. Distortion of temperature profiles occurs to a far greater extent through heat generated by friction of the top seal of the RPB. The temperature increase between liquid inlet (TI08) and liquid outlet (TI12) depends on the rotational speed, the duration of operation and the water flow rate. Only for the lowest investigated liquid load at the eye of $4.8\,\mathrm{m^3\,m^{-2}\,h^{-1}}$ and a rotational speed of $2300\,\mathrm{min^{-1}}$ a temperature difference of 6 K was observed. For all other operating conditions, the temperature rise remained below 5 K, as recommended by VDI 2761-2. The heat production due to top seal friction will need to be remedied through constructional changes in the future.

To obtain experimental confirmation of the above assessment, a series of experiments is conducted with and without pre-saturation of the gas stream for comparison. To saturate the gas stream, it is bubbled through a water bottle. The comparison of the resulting $k^L a_e$ values is shown in Fig. 6.1. Taking into account the experimental uncertainties, no appreciable influence of pre-saturation of the nitrogen gas stream can be observed. Further experiments are conducted without pre-saturation of the gas stream.

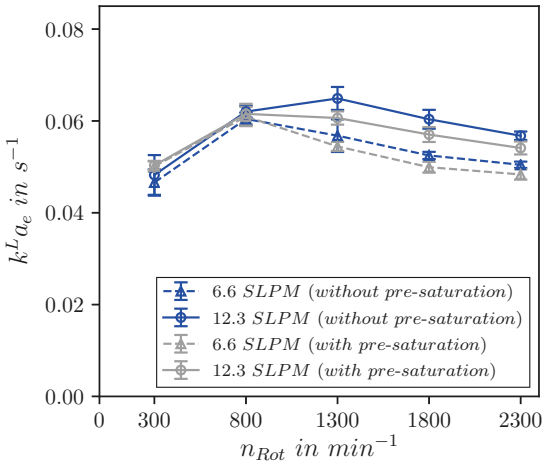
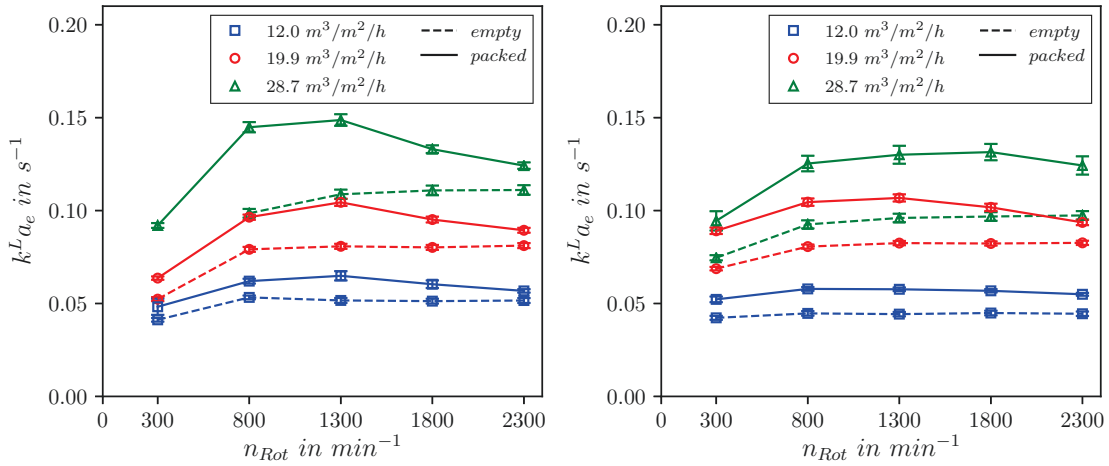


Fig. 6.1: Comparison of $k^L a_e$ values with and without pre-saturation of the nitrogen gas stream with water vapor at a liquid load at the eye of 12 $m^3\,m^{-2}\,h^{-1}$ in dependence of RPB rotational speed for countercurrent desorption in the packed rotor with 0.7 mm jet nozzles.

6.1.2 Investigation of spraying nozzle type and the influence of packing material

Due to the strong centrifugal forces acting on the liquid in the packed rotor, little distribution of liquid occurs in axial and circumferential direction (Rao et al., 2004). Even initial liquid distribution is thus of great importance in the investigated type of single block packing RPBs. Most publications employ full jet nozzles which are easy to fabricate and to adjust with respect to the packing. The current work compared the performance of full jet nozzles and flat fan nozzles that have the potential to create a more uniform wetting of the packing (cf. Fig. 4.4). Furthermore, the influence of the packing material on mass transfer performance and its interplay with the spraying nozzle type was studied. The mass transfer performance for both types of nozzles with and without metal foam packing, characterized by $k^L a_e$, is shown in Fig. 6.2 in dependence of RPB rotational speed.

The general trends observable with both nozzle types are identical: In the presence of packing material, $k^L a_e$ values increase with rotational speed to a maximum around 1300 min^{-1} and slightly decline afterwards. This clear maximum cannot be observed without packing material. Here, a plateau is reached where further increase of centrifugal acceleration does not further improve mass transfer. Especially with full jet nozzles, $k^L a_e$ values with packing seem to converge towards those without at high cen-



(a) full jet nozzle.

(b) flat fan nozzle.

Fig. 6.2: Comparison of $k^L a_e$ values at a nitrogen gas flow rate of 12.3 SLPM using (a) full jet and (b) flat fan nozzles in dependence of RPB rotational speed for countercurrent desorption in the empty and packed rotor at different liquid loads at the eye (Hilpert and Repke, 2021).

trifugal accelerations. The observed maximum in separation efficiency is thus a result of increased interaction of gas and liquid phase due to the presence of the packing. The phenomenon has been observed mainly in distillation (Nascimento et al., 2009; Luo et al., 2012b; Chu et al., 2013; Luo et al., 2016; Li et al., 2017a; Qammar et al., 2018; Qammar et al., 2019). Papers investigating water deaeration usually report an increase or a plateau (Chen et al., 2005a; Reddy et al., 2006; Lin and Jian, 2007; Rajan et al., 2011; Chen et al., 2016; Wen et al., 2020). A publication investigating water ozonation (Liu et al., 2019a) also reported a maximum. A possible explanation often cited in distillation literature (Nascimento et al., 2009; Luo et al., 2016; Qammar et al., 2019) is a trade-off between enhancement of mass transfer due to increased micro-mixing and increased specific effective surface area on the one hand, and a shortened residence time available for mass transfer at higher centrifugal accelerations on the other hand. For very high centrifugal accelerations, the lower limit of separation efficiency, represented by the empty rotor, is approached. The reason why this phenomenon has not been observed in publications on oxygen desorption so far, is probably related to the smaller size of the investigated RPBs compared to the pilot-scale unit in this work (cf. Tab. D.1 and 4.4), resulting in lower centrifugal accelerations at the investigated comparable rotational speeds.

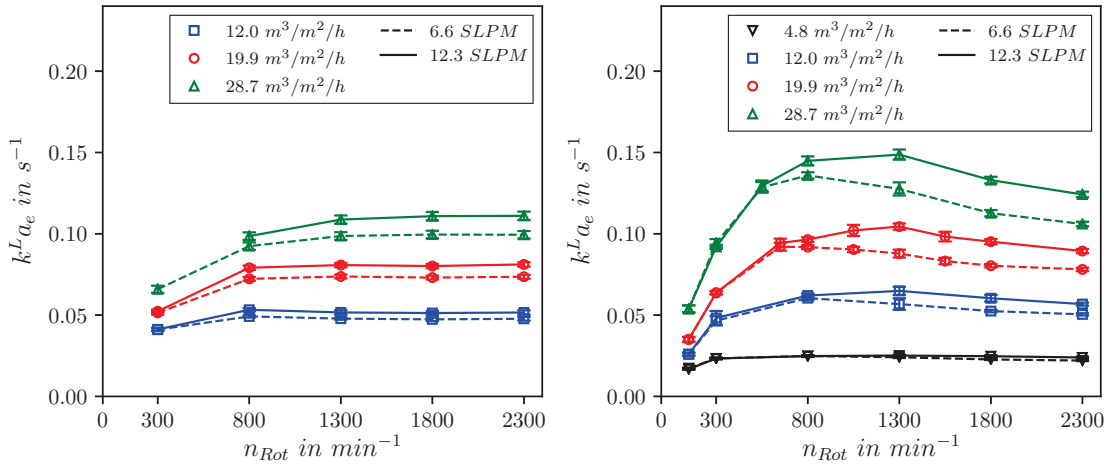
For flat fan nozzles, the maximum is less pronounced compared to full jet nozzles. The absolute values reached are slightly lower, both with and without packing. Full jet nozzles create liquid streams with distinct impact locations on the packing. The impacting streams may enter deeper into the packing before a flow regime transition, governed by centrifugal acceleration, occurs. This is visible in ink blot experiments and tomographic measurements of liquid flow in RPBs (Guo et al., 2014a; Yang et al., 2015a). Flat fan nozzles create a spray of droplets with an elliptic impact region. Thus, the mass transfer area created in the eye of the rotor by the spray prior to contact with the packing is larger than that of the full jets. Wetting of the packing is more uniform for a properly positioned flat fan nozzle. However, since the packed bed height investigated was only 10 mm, this likely has no significant influence. On the other hand, the transition to packing flow regime may occur closer to the packing inner radius. The thus shortened length of the inner end effects zone probably outweighs the mass transfer occurring in the eye due to droplet spray, resulting in slightly lower separation efficiencies compared to full jet nozzles. Finally, the flooding limit of flat fan nozzles is lower and entrainment of droplets at increased gas flow rates is more likely to occur, as observed by Neumann et al. (2017a) for flat jet tongue type nozzles. However, this phenomenon does not play a role for the investigated low gas flow rate, corresponding to an F-factor at the inner packing edge of 0.06 $Pa^{0.5}$.

To achieve optimal wetting over the packed bed height, flat fan nozzle position has to be adjusted for different liquid flow rates since spraying angle depends on flow rate. Due to this disadvantage, the associated lower flooding limit and the slightly inferior performance of the flat fan nozzles, only full jet nozzles are further discussed.

Observed pressure drops during oxygen desorption experiments depended almost exclusively on rotational speed and ranged approximately between 0 and 17 mbar for rotational speeds between 300 and 2300 min^{-1} in the packed rotor. The use of flat fan or full jet spraying nozzles did not show a measurable impact on pressure drop across the rotor.

6.1.3 Influence of gas flow rate

Using the full jet nozzles, experiments at two different nitrogen gas flow rates of 6.6 SLPM and 12.3 SLPM were conducted. The results are depicted in Fig. 6.3 for the empty and packed rotor. It can be seen that at increased rotational speeds beyond approximately 500...800 min^{-1} slightly higher $k^L a_e$ values are achieved at the increased



(a) empty rotor.

(b) packed rotor.

Fig. 6.3: Comparison of $k^L a_e$ values at two nitrogen gas flow rates for countercurrent desorption in the (a) empty and (b) packed rotor in dependence of RPB rotational speed using full jet nozzles at different liquid loads at the eye (Hilpert and Repke, 2021).

gas flow rate both for the empty and packed rotor. Furthermore, in the packed rotor, the location of the maximum in separation efficiency is shifted from ≈800 min^{-1} to a higher rotational speed of ≈1300 min^{-1} at the higher gas flow rate. With increasing liquid flow rate, the maximum becomes more pronounced. At the lowest investigated liquid flow rate, neither a maximum nor an appreciable difference in $k^L a_e$ for the two gas flow rates can be observed.

Most literature studies do not investigate the influence of gas flow rate on liquid-side volumetric mass transfer coefficients, since it is assumed to have negligible influence on a liquid-side controlled process (Hegely et al., 2017). This is also true for investigations in RPBs. Among the few studies varying gas flow, some did not observe an influence (Lin and Jian, 2007; Wen et al., 2020) while others report an increase of separation efficiency (Chen et al., 2004; Chen et al., 2016; Dutra e Mello, Marcus V. and Huang, 2018).

At higher gas flow rates, oxygen in the gas phase is more strongly diluted, which leads to an increase in driving force for mass transfer. Eq. 6.1 and 6.2 account for this effect. Hence, the observed increase in $k^L a_e$ at higher gas flow rates is an actual mass transfer phenomenon. $k^L a_e$ values may be increased by either an increase in specific effective surface area or an enhancement of mass transfer. Several studies of a_e have found an increase in interfacial area with increasing gas flow rate (Yang et al.,

2011; Chen et al., 2016; Luo et al., 2017; Ma et al., 2019). It is furthermore known that gas-liquid interaction can enhance mass transfer on a micro-scale (Kapoustina et al., 2019). Possibly, a similar phenomenon is observed here. The observed influence of gas flow rate is potentially due to a combination of the two factors. The effect becomes slightly more pronounced at higher liquid loads due to the increased liquid hold-up and thus greater gas-liquid interaction for the same rotational speeds. When rotational speed is too low, no sufficient liquid dispersion is generated by the rotor for the phenomenon to be observed. For higher gas flow rates the improvement of mass transfer due to gas-liquid interaction is sufficiently strong to move the maximum in mass transfer efficiency to higher rotational speeds before the shortening in residence time outweighs the improvements. Operation at even higher gas flow rates might move the maximum to centrifugal accelerations where it can no longer be observed. At some point, entrainment and finally flooding will occur, lowering separation efficiency again and eventually impeding operation.

While the $k^L a_e$ plots may convey that the greatest separation efficiency is achieved for the highest liquid flow rates, it can be seen from the plot of the number of overall liquid-phase transfer units, Fig. 6.4, that the opposite is the case. It becomes apparent that separation efficiency changes only slightly with liquid flow rate and peaks at about 7 transfer units at a rotational speed of 1300 $1/\text{min}^{-1}$. An increase in liquid flow rate leads to a slight decrease in NTU_{OL}. Possibly the higher liquid hold-up associated with higher flow rates leads to thicker films and larger droplets or filling of small pores where liquid interacts less intensely with passing gas.

Especially at low centrifugal accelerations, larger amounts of liquid are not sufficiently dispersed at high flow rates, causing the difference to be more pronounced. In the region of maximum efficiency, differences between different flow rates diminish, to re-appear at higher centrifugal accelerations. Possibly, there exists a limit to effective interfacial area that can be created at high centrifugal accelerations. This area available to mass transfer is similar for high and low liquid flow rates. The amount of oxygen that needs to be transferred is however greater at high flow rates. Thus the realized NTU_{OL} decreases more strongly for higher liquid loads. To gain further understanding of the causes of the observed phenomena, additional investigations are required on the interplay of hydrodynamics and mass transfer, potentially supported by CFD modeling.

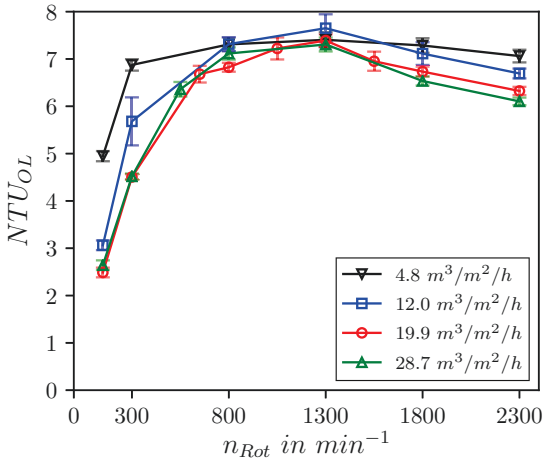


Fig. 6.4: NTU_{OL} in dependence of rotational speed of RPB for countercurrent desorption in the packed rotor using full jet nozzles at a nitrogen gas flow rate of 12.3 SLPM at different liquid loads at the eye.

6.1.4 Influence of cocurrent operating mode

To gain additional insight into the gas-liquid interaction in the packed rotor, desorption experiments were conducted with cocurrent flow of gas and liquid phase. The results are shown in Fig. 6.5 in comparison to results of countercurrent desorption experiments. For cocurrent flow, no significant influence of gas flow rate can be observed. In this regime, there is less gas-liquid interaction as liquid does not impede gas flow, resulting in no measurable influence of the employed low gas flow rates. Furthermore, there is no maximum, but a plateau in $k^L a_e$ values. This is in line with the findings of Groß et al. (2020), who investigated cocurrent water deaeration in a comparably sized pilot-scale RPB. The absolute magnitude of $k^L a_e$ values is the same as in countercurrent operation, since the intensity of mass transfer of the overall similar processes is comparable.

6.2 Modeling and simulation of $k^L a_e$

For the rate-based model introduced in Chapter 5, a mathematical description of $k^L a_e$ is required. Among the modeling approaches for mass transfer described in Sec. 2.4.1 the development of a semi-empirical correlation is chosen, since the hydrodynamic data required for the development of a mechanistic model is not available and there is not sufficient data to develop a machine learning model.

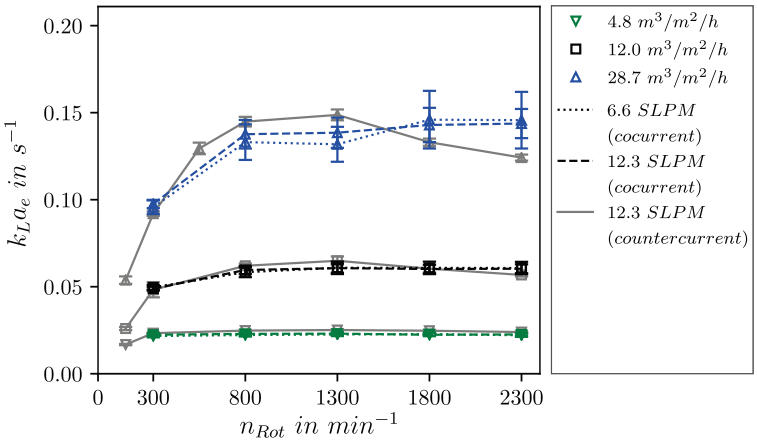


Fig. 6.5: $k^L a_e$ in dependence of rotational speed of the RPB for cocurrent desorption in the packed rotor using full jet nozzles at two nitrogen gas flow rates at different liquid loads at the eye. Data from countercurrent experiments at 12.3 SLPM gas flow rate added in grey and connected with lines (—) for comparison (Hilpert and Repke, 2021).

Transport properties were calculated as follows: Liquid diffusion coefficients were approximated by the infinite dilution diffusion coefficients calculated from the Wilke-Chang method due to the low concentrations of dissolved oxygen (Perry and Green, 2008). Liquid viscosity and density were calculated using PPDS equations, liquid surface tension using DIPPR 106 equation, all using coefficients for pure water from VDI-Wärmeatlas 2013. Further details are presented in Appendix C.

6.2.1 Evaluation of literature correlations

Prior to developing a correlation, a comprehensive set of available literature correlations for $k^L a_e$ in RPBs is more closely investigated regarding their capability to predict the measured data. An overview of the literature correlations is given in Tab. E.1. The corresponding parity plots are shown in Appendix E. For three correlations (cf. Tab. 6.1), results are subsequently presented in greater detail. These are the semi-empirical correlations for volumetric binary liquid-side mass transfer coefficients of Chen et al. (2005a), Chen et al. (2006) and Reddy et al. (2006). The correlation of Chen et al. (2005a) is based on an extensive amount of data, including variations in fluid properties and packing geometry to account for end effects, while the correlation of Chen et al. (2006) additionally takes into account packing material. Both have therefore been used for mass transfer modeling by several other publications (Gudena et al., 2012a; Groß et al., 2020; Beer et al., 2018; Li et al., 2017a; Li et al., 2020).

The correlation developed by Reddy et al. has been obtained from an RPB employing metal foam packings similar to the material employed in the current study. Since the investigation was conducted in a split-packing RPB, the correlation for co-rotation is used to describe the single block packing in the current study. In the development of the Chen correlations no metal foams were investigated. The sphericity of the metal foam packing required in the Chen correlations is taken to be equal to $\psi^{Sphere} = 0.75$, a value experimentally determined for a metal foam with pores of 0.3 mm (Gangoso Posadas, 2018). The critical surface tension of metal of 75 mN/m is used for the foam's chromium-nickel material (Kelleher and Fair, 1996). The Chen correlations are evaluated at the arithmetic mean radius $0.5(r_i + r_o)$. Even though the Chen publications do not state which radius was used for evaluating the dimensionless numbers, the original data of Chen can be reproduced well using the arithmetic mean.

Tab. 6.1: Literature correlations for the estimation of volumetric liquid-side mass transfer coefficients, all based on oxygen desorption experiments.

Author	Correlation
Reddy et al. (2006) (co-rotating split-packing RPB)	$k^L_{loc} a_e = 0.152 \cdot \left(Re^L\right)^{0.569} \cdot \left(Ga''^L\right)^{0.14} \cdot \left(Sc^L\right)^{0.5} \cdot \left(\frac{a_p \cdot D^L}{d_p}\right)$
Chen et al. (2005a) (single block RPB)	$k^L a_e = 0.65 \cdot \left(Sc^L\right)^{0.5} \cdot \left(Re^L\right)^{0.17} \cdot \left(Ga'^L\right)^{0.3} \cdot \left(We^L\right)^{0.3} \cdot \left(\frac{a_p \cdot D^L}{d'_p}\right) \cdot \left(1 - 0.93 \cdot \frac{V_o}{V_t} - 1.13 \cdot \frac{V_i}{V_t}\right)^{-1}$
Chen et al. (2006) (single block RPB)	$k^L a_e = 0.35 \cdot \left(Sc^L\right)^{0.5} \cdot \left(Re^L\right)^{0.17} \cdot \left(Ga'^L\right)^{0.3} \cdot \left(We^L\right)^{0.3} \cdot \left(\frac{a_p}{a_b}\right)^{-0.5} \cdot \left(\frac{\sigma_{cr}}{\sigma_w}\right)^{0.14} \cdot \left(\frac{a_p \cdot D^L}{d'_p}\right) \cdot \left(1 - 0.93 \cdot \frac{V_o}{V_t} - 1.13 \cdot \frac{V_i}{V_t}\right)^{-1}$

The results of the comparison are shown in Fig. 6.6. Both Chen correlations produce very similar results since the correlation from 2006 is developed through slight modification of the 2005 correlation. Therefore, only the results of the 2006 correlation are shown. All three correlations overpredict the experimental $k^L a_e$ values. Investigated RPBs in all three studies had significantly smaller geometries resulting in stronger influence of end effects on the rotor-averaged $k^L a_e$ values. That behavior is especially pronounced for the Chen correlations, where investigated RPBs had radii between

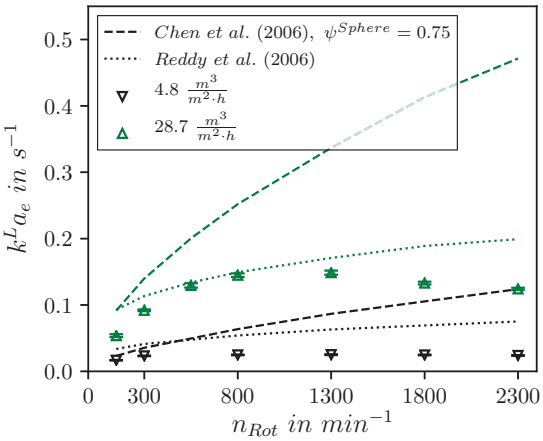


Fig. 6.6: Performance of literature correlations for $k^L a_e$ in comparison to the experimental data for countercurrent desorption at a nitrogen gas flow rate of 12.3 SLPM in the packed rotor in dependence of RPB rotational speed using full jet nozzles at the highest and lowest investigated liquid loads at the eye.

$r_{i,min} = 10mm$ and $r_{o,max} = 60mm$. The literature correlations are not capable of describing a maximum. This is inherent to the structure of the correlations, with centrifugal acceleration only contained in one term raised to a constant power. It is also the case for the other semi-empirical correlations from investigations of RPBs, listed in Tab. E.1, the parity plots of which are shown in Figs. E.1 and E.2.

6.2.2 Suggestion of a correlation for $k^L a_e$ capable of producing a maximum in separation efficiency

It is thus necessary to develop a correlation suitable for predicting liquid-side volumetric mass transfer coefficients in the investigated pilot-scale RPB that also accounts for the local maximum in separation efficiency in dependence of rotational speed. From the observed convergence of $k^L a_e$ values of the packed rotor towards those of the empty rotor, a correlation is derived consisting of additive contributions for both. The reference lengths used are the length of the liquid flow path $r_o - r_i$ for the empty rotor and the specific geometric surface area of the metal foam packing for the packed rotor. The choice of reference length of the empty rotor is identical to that of Munjal et al. (1989a) for a rotating disk, while the choice for the packed rotor is identical to that of Singh (1989) for an RPB packing. The general form of the correlation is chosen similar to that employed by Reddy et al., with contributions of liquid flow rate represented

through Re^L and centrifugal acceleration represented through Ga^L. The obtained experimental data does not contain significant variation in physical properties. Hence, the exponent of Sc^L is set equal to 1/2 to preserve the often observed proportionality of $k^L a_e \sim (D^L)^{1/2}$ which is in accordance with penetration theory (Onda et al., 1968; Bird et al., 2002, p. 708). The maximum observed for the packed rotor in countercurrent operation is accounted for by introducing the product of $(Ga^L)^{c_6} \cdot \exp(c_7 \cdot Ga^L)$ in the packed rotor term. The final form of the correlation is shown in Eq. 6.4. This correlation for local volumetric liquid-side mass transfer coefficients is integrated using Eq. 6.3 to obtain bed averaged values. The integral is numerically evaluated using Romberg's method (Romberg, 1955), as implemented in the Python SciPy-package (Virtanen et al., 2020).

$$k^L a_e = \frac{\int_{r_i}^{r_o} k^L_{loc} a_e r dr}{\int_{r_i}^{r_o} r dr} \tag{6.3}$$

$$k^L_{loc} a_e = c_1 \cdot (Re^{L,empty})^{c_2} \cdot (Ga^{L,empty})^{c_3} \cdot \frac{D^L}{(r_o - r_i)^2} \cdot (Sc^L)^{0.5} + c_4 \cdot (Re^L)^{c_5} \cdot (Ga^L)^{c_6} \cdot \exp(c_7 \cdot Ga^L) \cdot (a_p)^2 \cdot D^L \cdot (Sc^L)^{0.5} \tag{6.4}$$

The suggested correlation does not account for the influence of gas flow rate. That could be accomplished e.g. by introducing Re^V raised to some power as a factor in both terms. This was not done due to the limited variation in the data regarding gas velocity. Correlations are subsequently presented for the highest gas flow rate experimentally investigated, i.e. 12.3 SLPM. A correlation for $k^L a_e$ which takes Re^V into account based on literature data and own experiments is presented by Hilpert and Repke (2021).

6.2.3 Parameters for the suggested $k^L a_e$ correlation based on full jet nozzles

First, a correlation is obtained from data measured using full jet nozzles. The coefficients c_1...c_3 are obtained from regression analysis of the $k^L a_e$ data measured in the empty rotor. Using these fixed values, the coefficients c_4...c_7 are obtained from a second regression based on packed rotor data. The liquid loads at the inner radius used in the fits were 12.0 $m^3/m^2/h$, 19.9 $m^3/m^2/h$ and 28.7 $m^3/m^2/h$, since the lowest load was not investigated in the empty rotor. The values of the coefficients obtained are

shown in Eq. (6.5). The goodness of fit is illustrated in the parity plot and the plot of $k^L a_e$ over RPB rotational speed in Fig. 6.7 and 6.8. Agreement is well within $\pm 30\%$, demonstrating the capability of the correlation to capture the observed maximum in $k^L a_e$. This correlation has previously been presented in Appendix A of Hilpert et al. (2022).

$$k^L_{loc} a_e = 41.81 \cdot (Re^L_{empty})^{0.8160} \cdot (Ga^L_{empty})^{0.06993} \frac{D^L}{(r_o - r_i)^2} \cdot (Sc^L)^{0.5} + 1.955 \cdot 10^{-6} \cdot (Re^L)^{1.258} \cdot (Ga^L)^{0.8739} \cdot \exp(-4.963 \cdot 10^{-7} \cdot Ga^L) \cdot (a_p)^2 \cdot (D^L) \cdot (Sc^L)^{0.5} \tag{6.5}$$

6.2.4 Parameters for the suggested $k^L a_e$ correlation based on flat fan nozzles

For flat fan nozzles, parameters were fitted for the same basic correlation of local $k^L a_e$ that is again integrated according to Eq. 6.3. The correlation Eq. 6.6 is shown containing the parameters.

$$k^L_{loc} a_e = 113.9 \cdot (Re^{L,empty})^{0.7964} \cdot (Ga^{L,empty})^{0.03846} \cdot \frac{D^L}{(r_o - r_i)^2} \cdot (Sc^L)^{0.5} + 2.016 \cdot 10^{-6} \cdot (Re^L)^{1.203} \cdot (Ga^L)^{0.8643} \cdot \exp(-3.772 \cdot 10^{-7} \cdot Ga^L) \cdot (a_p)^2 \cdot D^L \cdot (Sc^L)^{0.5} \tag{6.6}$$

The parity plots and plots of $k^L a_e$ in dependence of rotational speed are shown in Fig. 6.9 and 6.10 for the empty and packed rotor, respectively. The goodness of fit is slightly inferior to that obtained for the full jet nozzles. This is due to the use of a different flat fan nozzle for each flow rate. The nozzles have slightly different spraying characteristics regarding the produced droplet size and droplet energy. These discrete changes introduce a disturbance that the correlation cannot account for.

Two additional sets of data are available to test the performance of the correlation regarding changes in bed geometry. One set of experiments was performed at an axial bed height of 20 mm, i.e. twice that investigated in obtaining the correlation. Another set of experiments was conducted with a shortened packing length with an

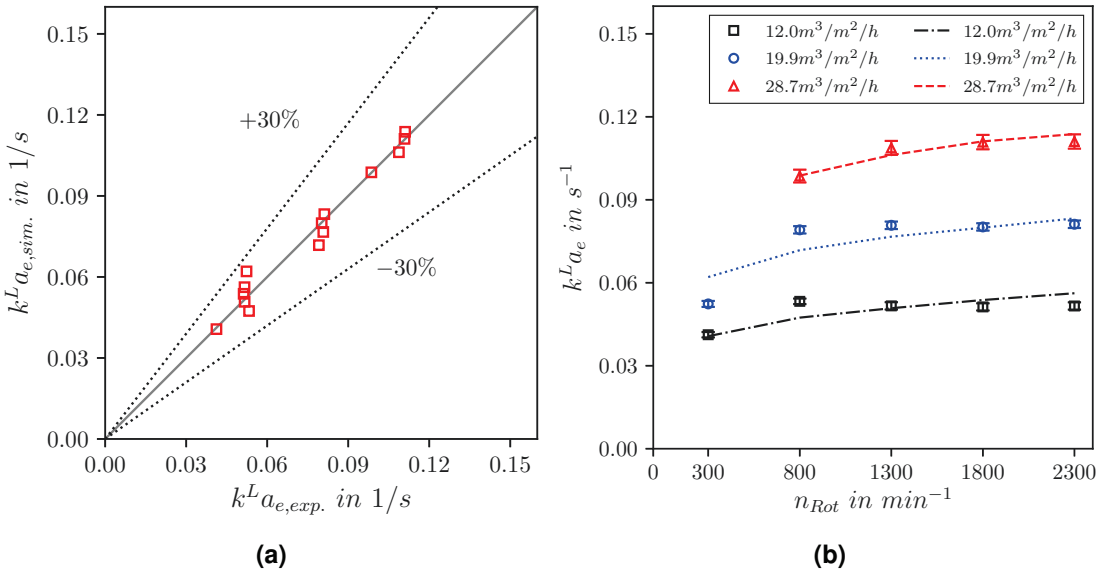


Fig. 6.7: Comparison of experimental and calculated data using estimated parameters of the developed local $k^L a_e$ correlation: (a) Parity plot of $k^L a_e$ and (b) Plot of $k^L a_e$ in dependence of RPB rotational speed for countercurrent desorption at a nitrogen gas flow rate of 12.3 SLPM in the empty rotor in dependence of RPB rotational speed using full jet nozzles at different liquid loads at the eye (Hilpert et al., 2022).

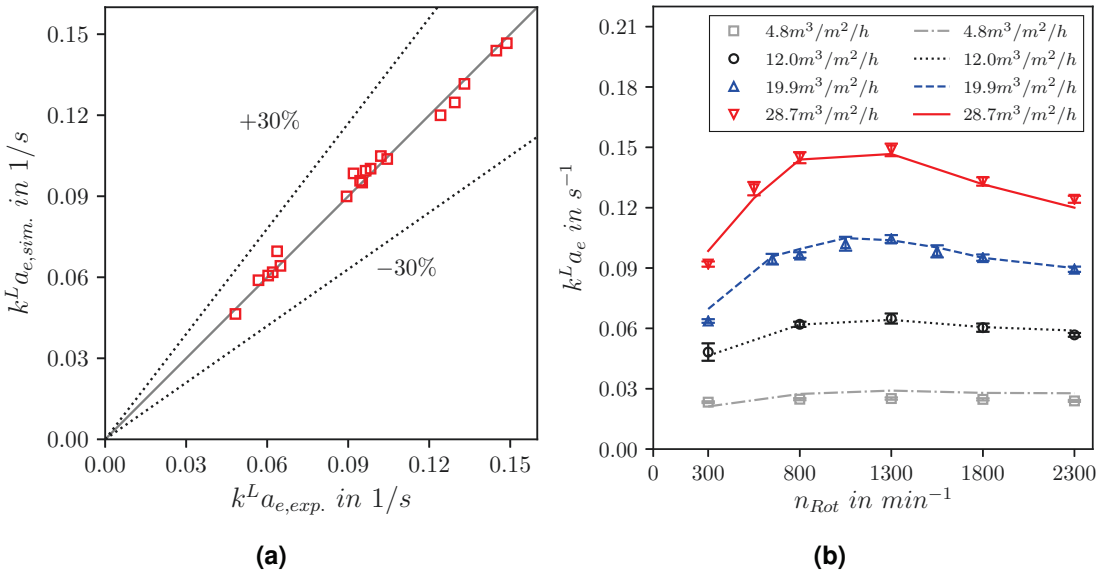


Fig. 6.8: Comparison of experimental and calculated data using estimated parameters of the developed local $k^L a_e$ correlation: (a) Parity plot of $k^L a_e$ and (b) Plot of $k^L a_e$ in dependence of RPB rotational speed for countercurrent desorption at a nitrogen gas flow rate of 12.3 SLPM in the packed rotor in dependence of RPB rotational speed using full jet nozzles at different liquid loads at the eye. Liquid load of 4.8 $m^3/m^2/h$ was not part of fit (Hilpert et al., 2022).

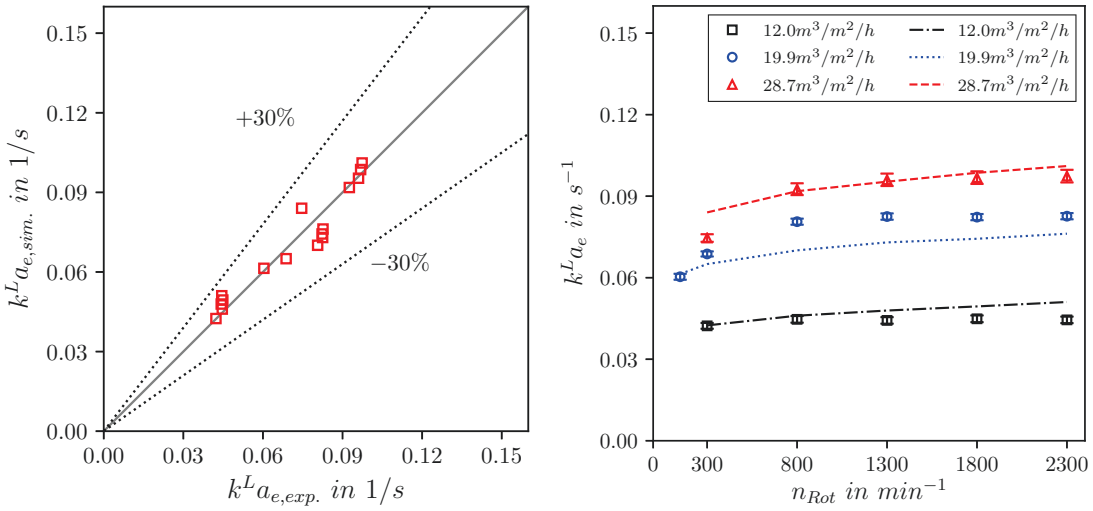


Fig. 6.9: Comparison of experimental and calculated data using estimated parameters of the developed local $k^L a_e$ correlation: (a) Parity plot of $k^L a_e$ and (b) Plot of $k^L a_e$ in dependence of RPB rotational speed for counter-current desorption at a nitrogen gas flow rate of 12.3 SLPM in the empty rotor in dependence of RPB rotational speed using flat fan nozzles at different liquid loads at the eye.

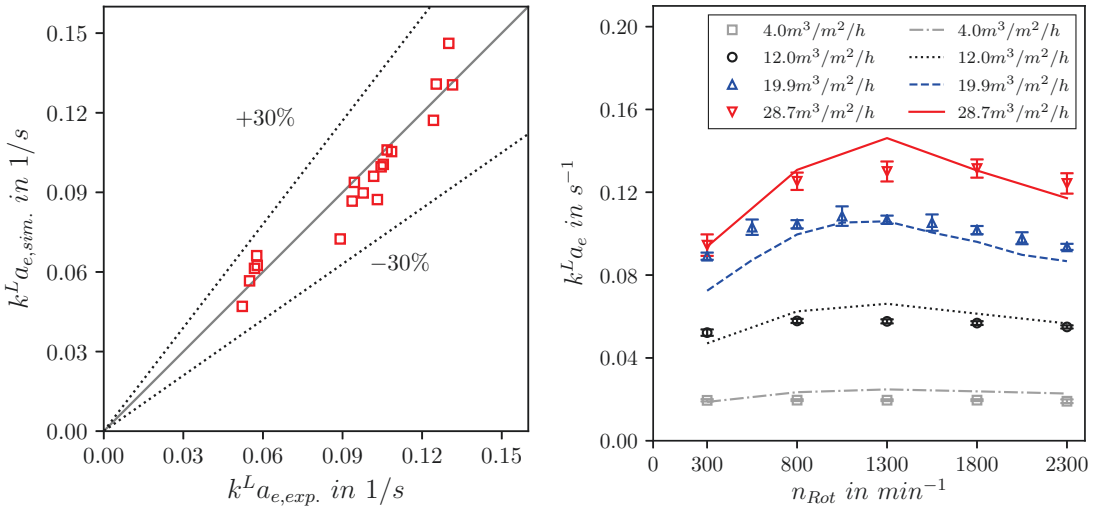


Fig. 6.10: Comparison of experimental and predicted data using estimated parameters of the developed local $k^L a_e$ correlation: (a) Parity plot for $k^L a_e$ and (b) Plot of $k^L a_e$ in dependence of RPB rotational speed for counter-current desorption at a nitrogen gas flow rate of 12.3 SLPM in the packed rotor in dependence of RPB rotational speed using flat fan nozzles at different liquid loads at the eye. Liquid load of 4.0 $m^3/m^2/h$ was not part of fit.

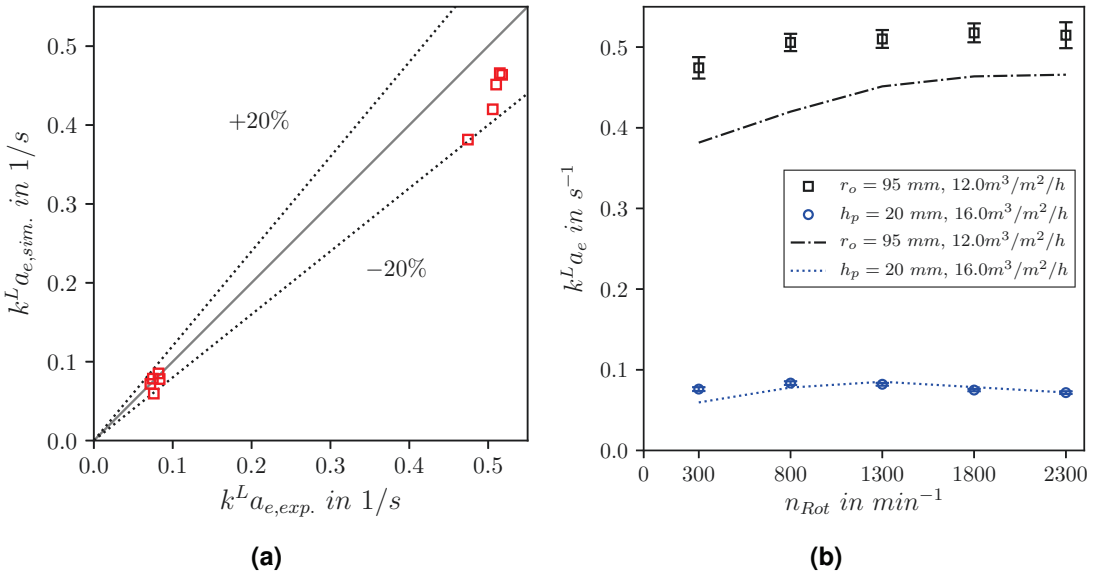


Fig. 6.11: Comparison of experimental and predicted data using estimated parameters of the developed local $k^L a_e$ correlation: (a) Parity plot and (b) Plot of $k^L a_e$ in dependence of RPB rotational speed for counter-current desorption at a nitrogen gas flow rate of 12.3 SLPM in the packed rotor in dependence of RPB rotational speed using flat fan nozzles at different liquid loads at the eye. Deviations from basic rotor geometry ($r_i = 60\ mm$, $r_o = 225\ mm$, $h_p = 10\ mm$) are given in the legend.

outer radius of 95 mm, i.e. approximately 1/5th of the packing length at which the correlation was developed. All experimental points were repeated once with exception of the experiments at 300 min^{-1} and 2300 min^{-1} at $r_o = 95\ mm$. The averaged results are shown in Fig. 6.11.

The correlation performs similarly well in predicting the data at increased axial packing height as in the original fit. This was expected since flow regime should not change for an even liquid distribution. It further confirms that no significant wall effects are present. The prediction of the $k^L a_e$ values for the smaller outer radius is acceptable, but experimental values are continuously underpredicted by up to 20%. The deviation is still within the original goodness of fit, but the underprediction indicates a stronger relative contribution of end effects to the total mass transfer in the shorter bed.

6.3 Conclusion for the investigation of liquid-side mass transfer

Water deaeration experiments for the measurement of $k^L a_e$ using full jet and flat fan nozzles revealed the existence of a maximum in separation efficiency at intermediate

rotational speeds of the RPB. A possible explanation is a trade-off between an enhancement of mass transfer and an increase in effective interfacial area with increasing rotational speeds on the one hand, and the associated decrease of available contact time for mass transfer on the other hand. This phenomenon has been observed mainly in distillation in RPBs, but rarely in $k^L a_e$ measurements. Hence, existing literature correlations for $k^L a$ could not capture the described maximum. Consequently, a new correlation was suggested, capable of mathematically describing this maximum.

Furthermore, a slight positive influence of strip gas flow rate on $k^L a_e$ could be identified, which is likely due to the known slight increase in effective interfacial area caused by stronger gas-liquid interaction. This effect has not been incorporated in the developed $k^L a_e$ correlation due to the low variation in investigated gas flow rates.

Based on the obtained correlation for $k^L a_e$, $k^V a_e$ values can now be obtained from subsequent distillation experiments, using the model described in Chap. 5.

7 Investigation of distillation

In this chapter, experimental data of binary and ternary distillation experiments at infinite reflux is presented and discussed. Subsequently, two sets of literature correlations are employed to assess their capability of describing the data, using the rate-based model introduced in Chapter 5. Due to the limitations of the literature correlations, a new correlation for $k^V a_e$ is developed from distillation data of the thermodynamically near-ideal mixture ethanol/n-propanol. The correlation is validated against the data from distillation of ethanol/water and ethanol/n-propanol/water, and the simulation results are discussed. The contents of this chapter have been published in part in Hilpert et al. (2022).

7.1 Evaluation of the experiments

In the following, throughputs will be characterized by F-factor and liquid load, as all experiments have been conducted at infinite reflux. The reference location for both is at the inner cross sectional area of the rotor, as is common practice in RPB literature. At the inner radius, both F-factor and liquid load are highest, while centrifugal acceleration is lowest. Consequently, flooding first occurs at this location, making it important in characterizing RPB operation (Neumann et al., 2017a).

As for the desorption experiments, experimental uncertainties reported and error bars shown are the results of an uncertainty calculation taking into account uncertainties stemming from measurement devices, analytics and repeat runs. Details of the procedure are given in Appendix A.

To assess and compare separation efficiency between different experiments, overall volumetric mass transfer coefficients $K^V a_e$ are calculated based on Eq. 7.1 according to the ATU-NTU concept shown in Eq. 7.2. The concept of Area per Transfer Unit was developed by Singh (1989) in analogy to the established HTU-NTU concept in conventional distillation and absorption. It accounts for the mass transfer in an RPB

taking place along the radius, with which radial acceleration, gas and liquid loads vary along the flow path. The integral was numerically evaluated using Romberg's method (Romberg, 1955), as implemented in the Python SciPy-package (Virtanen et al., 2020). The value of y^{eq} corresponding to y is obtained from a vapor-liquid equilibrium calculation for the average bed pressure and $x = y$ due to operation at total reflux. The same parameters as in the rate-based model are used for calculating P^{LV} and γ. The integration boundaries correspond to the concentrations measured at sampling locations S-04 and S-06 if not stated otherwise (cf. Fig. 4.6).

$$K^V a_e = \frac{\dot{V}_G}{h_p \pi \left(r_o^2 - r_i^2\right)} \int_{y_i}^{y_o} \frac{dy}{y^{eq} - y} \tag{7.1}$$

$$\pi \left(r_o^2 - r_i^2\right) = ATU_{og} NTU_{og} = \frac{\dot{V}_G}{h_p K^V a_e} \int_{y_i}^{y_o} \frac{dy}{y^{eq} - y} \tag{7.2}$$

To compare the observed separation performance to literature, the frequently reported HETP($= N_{th}/(r_o - r_i)$) was calculated. N_{th} was obtained based on the McCabe-Thiele method (Henley et al., 2011, pp. 261–270). As in the literature studies referenced in Tab. 7.1, HETP is based on the concentrations of the liquid reflux and the liquid leaving the casing (sampling locations S-04 and S-06, cf. Fig. 4.6). Mass transfer in the casing is thus ascribed to the rotor.

In case of a ternary mixture, there exists a 2x2 matrix of NTU_{og} values (Krishna et al., 1977). To still compare the separation efficiency using a single variable, the number of theoretical stages to achieve the observed separation performance for the key component ethanol, i.e. the distillation line, has been calculated: Starting from the measured composition of the liquid leaving the casing, a step-wise series of vapor-liquid equilibrium calculations is performed. The resulting vapor composition of one calculation serves as the liquid composition for the next vapor-liquid equilibrium calculation (total reflux conditions), until the distillate mole fraction of ethanol is exceeded.

All experiments were either conducted without any packing material ("empty rotor") or with the NCX1116 metal foam packing of 10 mm height, 60 mm inner and 225 mm outer radius ("packed rotor").

7.1.1 Influence of initial liquid jet velocity

Liquid is evenly distributed on the packing at the inner radius of the rotor by two jet nozzles with three holes each. Agarwal et al. (2010) recommend an initial jet velocity in the range of 4 to 5 $\mathrm{m\,s^{-1}}$. For counter-current operation, two limiting hydrodynamic conditions are influenced by the liquid distributor: impact and deflection (cf. Fig. 2.3) (Sudhoff, 2015, pp. 232–234). Impact may occur for very high jet velocities and is characterized by impacting liquid splashing back and forming a fine mist that is carried away by the gas. At extremely low jet velocities deflection may occur, i.e. the liquid is carried away by the vapor prior to reaching the packing. Finally, initial liquid jet velocity has an influence on the length of the inner end effects zone where transition of flow regimes occurs with intense shearing and mixing of liquid as it hits the rotating packing for the first time (Guo et al., 2014a). Initial jet velocity is therefore expected to have a certain influence on mass transfer efficiency, even within the hydrodynamic operating window.

Based on the design recommendation by Agarwal et al., two nozzle sizes with 0.7 mm and 1.0 mm hole diameter were tested to check if operation is within the limits of deflection and impact, and to determine if a significant influence of the jet velocity on mass transfer efficiency could be observed. This would necessitate a change of nozzles for different desired throughputs. The runs were conducted with an ethanol/n-propanol binary mixture at the highest F-factor of 3.0 $\mathrm{Pa^{0.5}}$ investigated with this mixture, corresponding to an average liquid load of 18.4 $\mathrm{m^3\,m^{-2}\,h^{-1}}$. The resulting initial jet velocities were 4.1 $\mathrm{m\,s^{-1}}$ and 8.3 $\mathrm{m\,s^{-1}}$ for the 1.0 mm and 0.7 mm nozzles, respectively.

As can be seen in Fig. 7.1, the results agree within the experimental uncertainties. Thus, impacting does not occur, which would cause $K^V a_e$ to be lower for higher initial jet velocities, i.e. the smaller nozzle. Also, the deflection phenomenon does not occur, as it would result in a decrease of separation performance with the larger nozzle, regardless of rotational speed. Deflection is governed by the ratio of kinetic energy of the liquid stream to the gas stream, shown in Eq. (7.3). This ratio depends only on the liquid and vapor densities and not on mass flow rate for infinite reflux operation. As the densities do not change drastically for the investigated systems, the ratio remains relatively constant. Thus, if deflection does not occur at one throughput, it will not occur at any other for distillation at infinite reflux, as long as a proper liquid jet capable of reaching the packing is generated. Also, it can be concluded that the change in the length of inner end effects zone does not significantly impact the measured separation performance for the investigated RPB configuration.

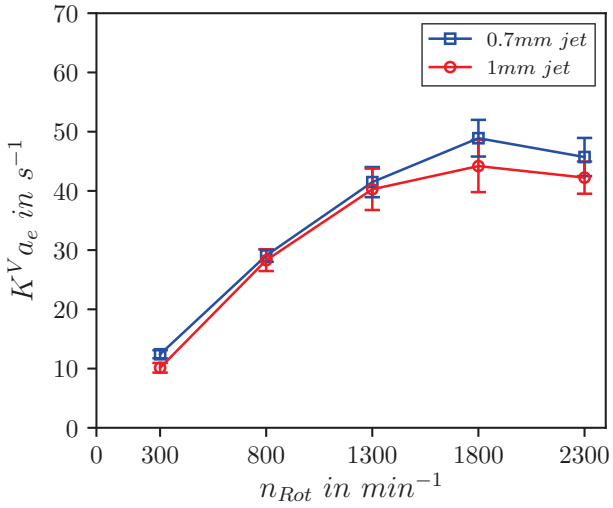


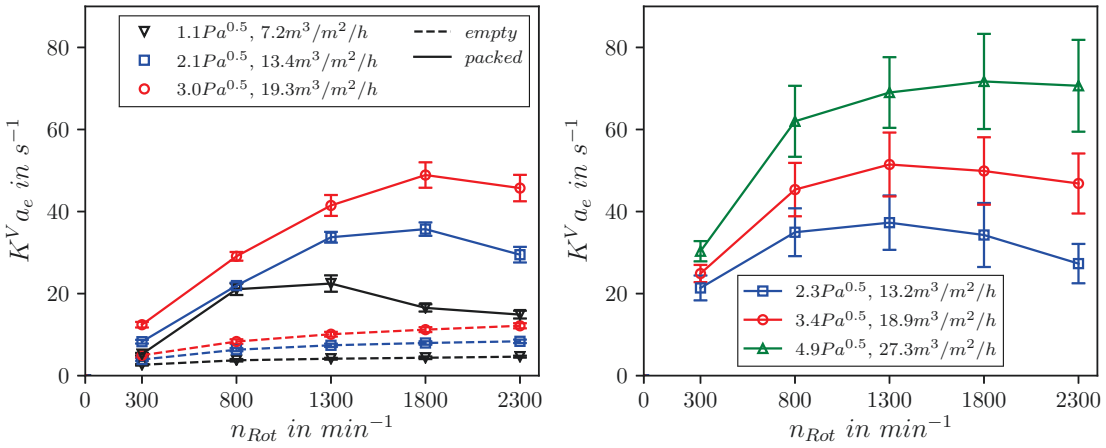
Fig. 7.1: Comparison of the behavior of $K^V a_e$ values of 0.7 mm jet nozzles and 1.0 mm jet nozzles using ethanol/n-propanol system at 3.0 $Pa^{0.5}$ and 18.4 $m^3\,m^{-2}\,h^{-1}$ with the packed rotor.

$$\frac{\dot{E}^L_{kin}}{\dot{E}^V_{kin}} = \frac{1/2\dot{m}(u^L)^2}{1/2\dot{m}(u^V)^2} = \frac{\left(\dot{m}/(\rho^L A_{jets})\right)^2}{\left(\dot{m}/(\rho^V A_{eye})\right)^2} \tag{7.3}$$

Based on these findings, further experiments are conducted with the 0.7 mm nozzle only. Resulting initial liquid jet velocities of the ethanol/n-propanol mixture for the investigated range of F-factors of 1.1 to 3.0 $Pa^{0.5}$ are thus in the range of 2.3 to 8.8 $m\,s^{-1}$.

7.1.2 Distillation of binary mixtures

Using the binary mixture of ethanol and n-propanol, experiments were conducted with and without packing material to assess the mass transfer performance of the packed rotor in comparison to the empty rotor and casing. The resulting overall gas-side volumetric mass transfer coefficients $K^V a_e$ are shown for three different F-Factors in Fig. 7.2a. $K^V a_e$ values for the empty rotor are calculated using the empty rotor volume as a reference. Without packing material inside the rotor, the $K^V a_e$ values reach approximately 20 to 30% of the values with packing, except for the lowest rotational speed, where they reach up to 50% of $K^V a_e$ with packing. Mass transfer coefficients of the empty rotor show a slight yet monotonous increase with increasing centrifugal accelerations. For the packed rotor, $K^V a_e$ first increases more strongly and a maximum



(a) *ethanol / n − propanol.* **(b)** *ethanol / water.*

Fig. 7.2: Comparison of the behavior of $K^V a_e$ values of (a) ethanol/n-propanol system with and without packing and (b) ethanol/water system with packing at different F-factors and flow rates (Hilpert et al., 2022).

in $K^V a_e$ can be observed. The maximum shifts to higher rotational speeds as gas and liquid loads increase. It appears thus less pronounced in the studied range of rotational speeds. These observations are confirmed by the experiments with the packed rotor using an ethanol/water mixture shown in Fig. 7.2b. Instead of the data series at an F-factor of 1.1 $Pa^{0.5}$, a higher throughput of 4.9 $Pa^{0.5}$ was investigated. Error bars are significantly larger compared to experiments with ethanol/n-propanol due to distillate concentrations approaching the azeotropic point. At the highest throughput of 4.9 $Pa^{0.5}$ combined with the lowest rotational speed of 300 min^{-1}, the upper end of the hydrodynamic operating range was approached. Liquid hold-up started to increase near the eye of the rotor, leading to an increase in pressure drop compared to operation at 800 min^{-1}, as illustrated in Fig. 7.3. At lower throughputs, pressure drop always decreased with decreasing rotational speed.

$K^V a_e$ values increase with increasing throughput, yet NTU_{og}, measuring the separation efficiency, is highest for lowest flow rates, as shown in Fig. 7.4. Only at high centrifugal accelerations NTU_{og} of high flow rates exceed those at lower flow rates for both binary mixtures. Maximum NTU_{og} values achieved for both mixtures at comparable F-factors of 2 $Pa^{0.5}$ to 3 $Pa^{0.5}$ are in a similar range of ≈7 for ethanol/water and ≈8 for ethanol/n-propanol. Error bars in Fig. 7.4a increase at the lowest F-factor for ethanol/n-propanol mixtures as concentrations near the pure substances are reached.

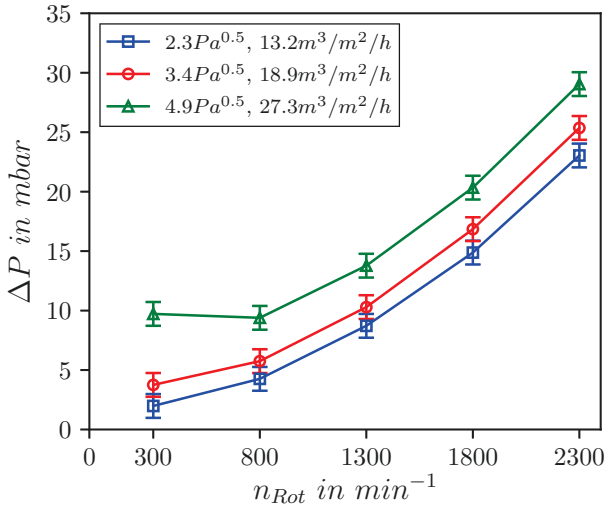


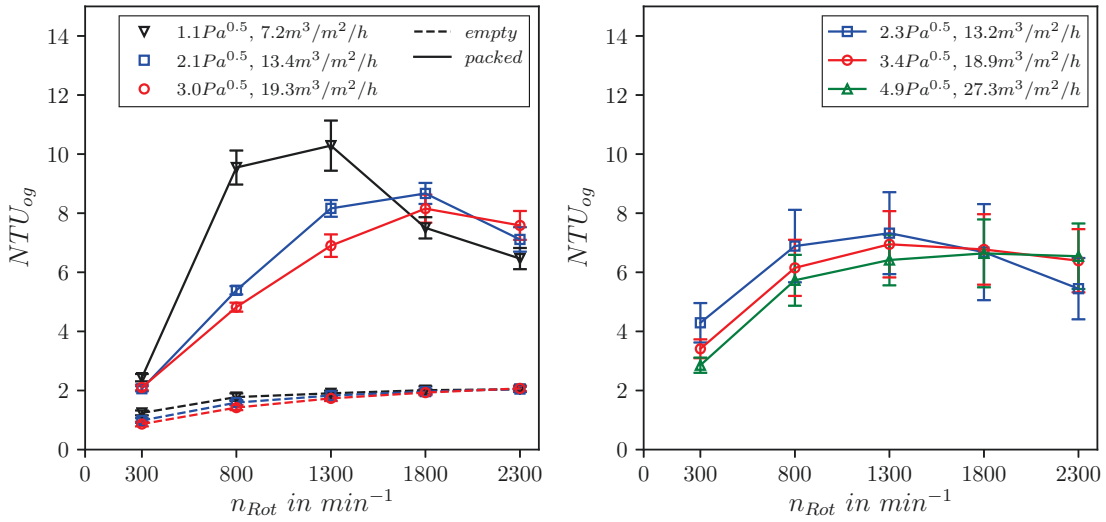
Fig. 7.3: Pressure drop (PDI01) across the packing for distillation of ethanol/water using 0.7 mm jet nozzles at different rotational speeds of the RPB rotor. Flood point is approached at 300 min^{-1} and 4.9 $Pa^{0.5}$.

The achieved separation performance is equivalent to N_{th} ranging from 1.9 to 9.7 for ethanol/n-propanol and 1.9 to 5.7 for ethanol/water. This corresponds to HETP values ranging from 17 to 87 mm and 29 to 87 mm, respectively. These values are in the typical range for RPBs, as shown in Tab. 7.1.

Tab. 7.1: Overview of some published ranges of HETP values for distillation of binary mixtures in RPBs at infinite reflux and atmospheric pressure.

Reference	r_i (mm)	r_o (mm)	$r_o - r_i$ (mm)	HETP (mm)	Remarks
Lin et al. (2002)	61	147	86	40...80	
Mondal et al. (2012)	30	155	125	25...150	split-packing
Li et al. (2017a)	90	142.5	52.5	20...85	
Qammar et al. (2019)	73	190	117	65...84	metal foam NCX1116
present study	60	225	165	17...87	

A possible explanation of the formation of a maximum in $K^V a_e$ with increasing rotational speed is suggested in literature (Nascimento et al., 2009; Luo et al., 2016; Qammar et al., 2019): On the one hand, mass transfer is intensified through an increase in specific effective surface area and micro-mixing efficiency with increasing centrifugal acceleration (Yang et al., 2011; Chen et al., 2016; Luo et al., 2017; Ma et al., 2019). On the other hand, residence time available for mass transfer decreases (Burns et al., 2000; Guo et al., 2000). Furthermore, liquid maldistribution through shadowing and rivulet



(a) *ethanol / n − propanol.*

(b) *ethanol / water.*

Fig. 7.4: Comparison of the behavior of NTU_{og} values of (a) ethanol/n-propanol system with and without packing and (b) ethanol/water system with packing at different F-factors and flow rates.

formation may increase at higher centrifugal accelerations (Burns and Ramshaw, 1996). The absence of a maximum in the $K^V a_e$ curve of the empty rotor appears to be due to the missing intense contact between gas and liquid that occurs in the pores of the packing. This behavior is identical to that observed during the $k^L a_e$ measurements (cf. Sec. 6.1).

The observed maximum in the $K^V a_e$ curve of the packed rotor is shifted to higher rotational speeds as throughput increases. An increase in gas flow increases the specific effective surface area available for mass transfer (Yang et al., 2011; Chen et al., 2016; Luo et al., 2017; Ma et al., 2019). An increase in liquid flow rate increases liquid hold-up in the packing (Burns et al., 2000; Yang et al., 2015a), but also leads to shorter residence times (Burns et al., 2000; Guo et al., 2000). However, the increased liquid hold-up might additionally cause a stronger gas-liquid interaction and thus intensify the mass transfer overall. As a result, the point where a shortened residence time outweighs the improvements in mass transfer at higher centrifugal accelerations may be moved to higher accelerations with increased throughput. Further studies could operate the RPB as a rectifier and a stripper, i.e. not at infinite reflux, to enable an independent discussion of the effects of gas and liquid flow rate on mass transfer.

At high rotational speeds and low liquid flow rates, the $K^V a_e$ curve of the packed rotor displays an inflection point after the maximum over centrifugal acceleration (Fig. 7.2a, 1.1 $Pa^{0.5}$). The packed rotor appears to adopt a behavior similar to that of the empty rotor which has a very low liquid hold-up. Possibly, the performance of the empty rotor poses a limit to which the separation performance of the packed rotor converges at very high centrifugal accelerations. This behavior was observed by Qammar et al. (2018) for lower F-factors of 0.35 $Pa^{0.5}$ and 0.65 $Pa^{0.5}$ with an ethanol/water system in an RPB of comparable dimensions using a metal knit-mesh packing at rotational speeds of 1200 min^{-1}.

The slightly lower NTU_{og} for increased throughputs as seen in Fig. 7.4 may be caused by a lower effective surface area due to pore filling and local formation of thicker films. This effect diminishes at higher rotational speeds. The experiments at the F-factor of 0.35 $Pa^{0.5}$ in the study of Qammar et al. showed a higher maximum efficiency compared to experiments at 0.65 $Pa^{0.5}$, indicating the same trend of an efficiency increase at lower loads observed in Fig. 7.4. While NTU_{og} values reported by Qammar et al. (2018) for the empty rotor were in the same range of 1 to 2, maximum values achieved with packing did not exceed 4 transfer units. The lower values of 4 compared to 7 overall gas transfer units achieved with ethanol/water in the study of Qammar et al. and this study, respectively, are thus likely due to differences in packing material and geometry of the RPB as well as the liquid distributor (details of which are not provided) employed by Qammar et al. (2018).

7.1.3 Distillation of ternary mixtures

To provide a basis for validation of the multi-component distillation model for RPBs, experiments using the ternary mixture ethanol/n-propanol/water have been carried out. The system exhibits two binary temperature-minimum azeotropes, between ethanol and water as well as n-propanol and water. Consequently, there exists a distillation boundary which divides the composition space in two distillation regions. Experiments were conducted in both distillation regions, as illustrated in Fig. 7.5. Balance lines between top and bottoms compositions obtained from experiments at 300 min^{-1} and 1800 min^{-1}, corresponding to the extremes in separation performance, are displayed to visualize the range of compositions covered.

On the ethanol/n-propanol side of the distillation boundary, i.e. the upper distillation region ("region 2"), experiments were carried out at an F-factor of 3.5 $Pa^{0.5}$ and rota-

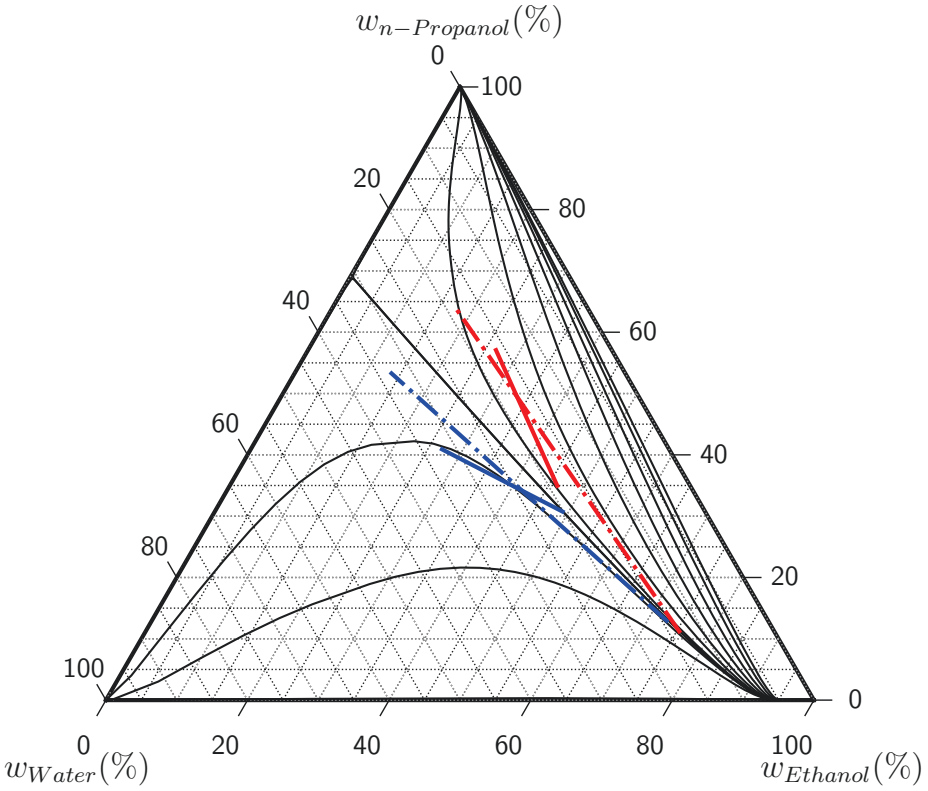


Fig. 7.5: Residue curve map of weight fractions of ethanol/n-propanol/water system at 1.013 bar(a) with balance lines of experiments at 300 min^{-1} (−) and 1800 min^{-1} (·−), at 3.5 $Pa^{0.5}$ and 18 to 19 $m^3/(m^2h)$ with the packed rotor (Hilpert et al., 2022).

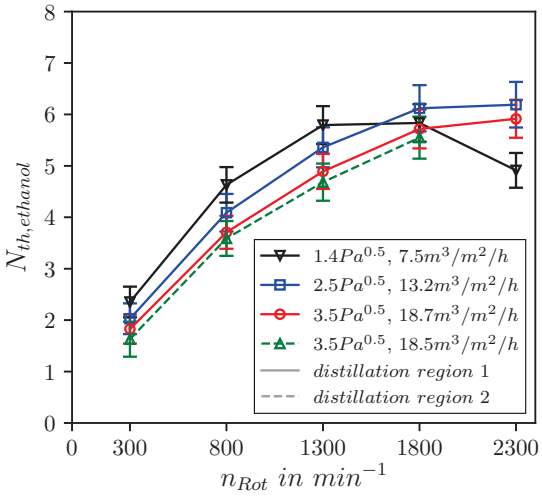


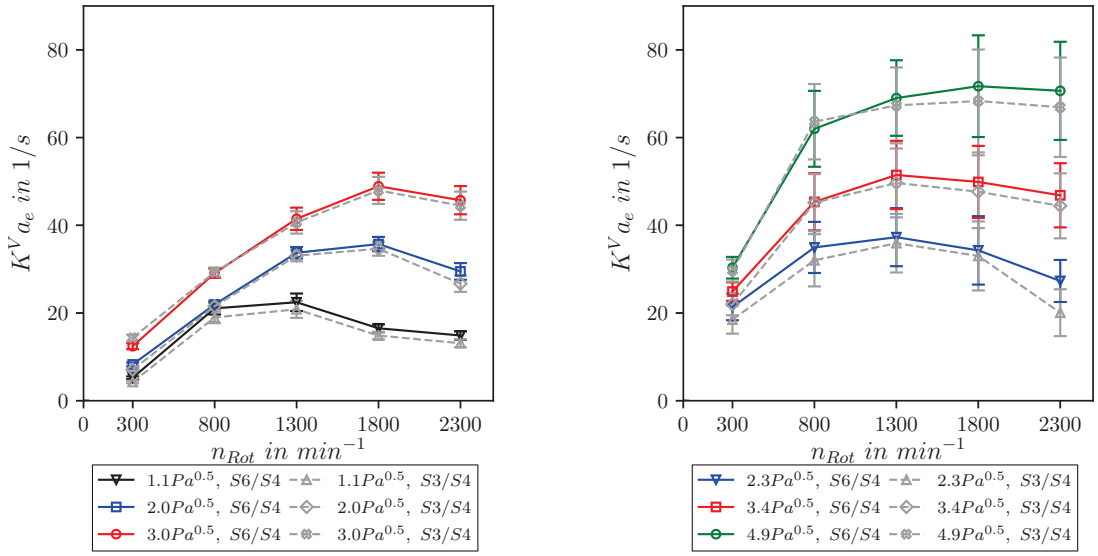
Fig. 7.6: Numbers of theoretical stages achieved in ternary distillation of ethanol/n-propanol/water system (calculated based on ethanol concentrations) with the packed rotor (Hilpert et al., 2022).

tional speeds ranging from 300 to 1800 min^{-1} in steps of 500 min^{-1}. On the ethanol/water side of the distillation boundary, i.e. in the lower region, additional experiments at throughputs of 1.4 $Pa^{0.5}$ and 2.5 $Pa^{0.5}$ and the additional rotational speed of 2300 min^{-1} have been conducted.

The results in Fig. 7.6 exhibit the same trends as the binary experiments. At low throughputs slightly higher numbers of theoretical stages are achieved. Also, at low throughputs a maximum can be observed while at higher throughputs the investigated centrifugal accelerations are not sufficiently high to observe the expected decline in the numbers of theoretical stages. For both distillation regions, a similar separation performance is achieved due to the similar composition ranges covered.

7.1.4 Investigation of outer end effects

As described in Sec. 2.2.2, total mass transfer is made up of contributions of the packing and of the outer end effects, i.e. mass transfer in the casing. This is due to additional effective surface area generated by droplets that are ejected from the packing and splash back from the casing, as well as liquid on the casing walls and bottom plate. To enable an investigation of the contribution of outer end effects to overall mass transfer, a liquid sampler was designed which collects liquid 2.5 mm from the packing edge over an axial height of 11 mm. For the bed height of 10 mm investigated in all distillation



(a) ethanol/n-propanol. **(b)** ethanol/water.

Fig. 7.7: Plot of $K^V a_e$ in dependence of RPB rotational speed, calculated based on sampling locations S3/S4 (packing contribution to mass transfer) and locations S6/S4 (packing and casing contribution to mass transfer) for (a) ethanol/n-propanol and (b) ethanol/water.

experiments, this corresponds to sampling the full bed height. A comparison of $K^V a_e$ values calculated based on samples from liquid outlet (S6) and liquid ejected from the packing (S3) is shown in Fig. 7.7, both using the same distillate sample (S4) (cf. PFD in Fig. 4.6).

$K^V a_e$ values calculated using both pairs of sampling locations yield almost identical results, especially in view of the associated measurement uncertainties. The contribution of the packing typically amounts to 90 to 100 % of total mass transfer of packing and casing.

Since the dissolved oxygen sensor QI02 used for calculation of $k^L a_e$ values was also located in the liquid outlet line, $K^V a_e$ values calculated based on sampling locations S6/S4 are subsequently used for model development.

For additional comparison, $K^V a_e$ values were calculated using samples of vapor drawn from the casing (S2) and the eye (S7) at F-factors of 3.4 $Pa^{0.5}$ and 4.9 $Pa^{0.5}$ investigated using the ethanol/water mixture. Obtained values agreed with those shown in Fig. 7.7b well within the measurement uncertainties (deviation $<\pm 7$ %, with exception of an outlier at 3.4 $Pa^{0.5}$ and 300 min^{-1}). The data is shown in Appendix F. Due to the

associated additional effort involved and the similarity to the results obtained from the liquid samples, no vapor samples were taken for the remainder of the experiments.

7.2 Simulation using literature correlations

The rate-based RPB distillation model used in this study requires a discretization approach, as outlined in Ch. 5. The selection of a suitable approach and the number of discrete elements is described in Sec. 7.2.1. To simulate the experimental results, correlations for $k^L a_e$ and $k^V a_e$ are required in Eq. 5.23 and Eq. 5.24 of the introduced rate-based stage model. Two promising sets of correlations (cf. Tab. 7.2) were chosen from RPB literature to predict the experimental results of the thermodynamically near-ideal ethanol/n-propanol system. The results of these simulations are presented in Sec. 7.2.2.

Tab. 7.2: Employed literature correlations for the estimation of volumetric mass transfer coefficients.

Reference	Correlation	
Reddy et al. (2006) (co-rotating split-packing RPB)	$k^L_{loc} a_e = 0.152 \cdot \left(Re^L\right)^{0.569} \cdot \left(Ga''^L\right)^{0.14} \cdot \left(Sc^L\right)^{0.5} \cdot \left(\frac{a_p \cdot D^L}{d_p}\right)$	[a]
	$k^V_{loc} a_e = 7.62 \cdot 10^{-3} \cdot \left(Re^V\right)^{0.852} \cdot \left(Ga''^V\right)^{0.194} \cdot \left(Sc^V\right)^{1/3} \cdot \left(\frac{a_p \cdot D^V}{d_p}\right)$	[b]
Chen et al. (2006), Chen (2011) (single block RPB)	$k^L a_e = 0.35 \cdot \left(Sc^L\right)^{0.5} \cdot \left(Re^L\right)^{0.17} \cdot \left(Ga'^L\right)^{0.3} \cdot \left(We^L\right)^{0.3} \cdot \left(\frac{a_p}{a_b}\right)^{-0.5} \cdot \left(\frac{\sigma_{cr}}{\sigma_w}\right)^{0.14} \cdot \left(\frac{a_p \cdot D^L}{d'_p}\right) \cdot \left(1 - 0.93 \cdot \frac{V_o}{V_t} - 1.13 \cdot \frac{V_i}{V_t}\right)^{-1}$	[a]
	$k^V a_e = 0.023 \cdot \left(Re^V\right)^{1.13} \cdot \left(Re^L\right)^{0.14} \cdot \left(Ga'^V\right)^{0.31} \cdot \left(We^L\right)^{0.07} \cdot \left(\frac{a_p}{a_b}\right)^{1.4} \cdot \left(a_p\right)^2 \cdot \left(D^V\right) \cdot \left(1 - 0.9 \cdot \frac{V_o}{V_t}\right)^{-1}$	[c]

[a] Based on measurements using oxygen desorption from water into nitrogen gas; [b] Based on measurements using SO_2 absorption from air into aqueous NaOH; [c] Based on $k^V a_e$ calculated using $K^V a_e$ from various publications and the $k^L a_e$ correlation of Chen et al. (2006)

7.2.1 Discretization of the RPB rotor in the rate-based model

Two approaches have so far been used in literature, namely the equidistant and the equiareal discretization (Sudhoff et al., 2014). In the former approach, the RPB's rotor is discretized into ring segments in such a way that all elements have the same radial length, while in the latter approach the rotor is discretized into segments where all elements have the same volume. Since the height of the packing is constant, the segments will have the same area as well. This causes the radial distance between discrete elements to decrease with increasing diameter, as illustrated in Fig. 7.8.

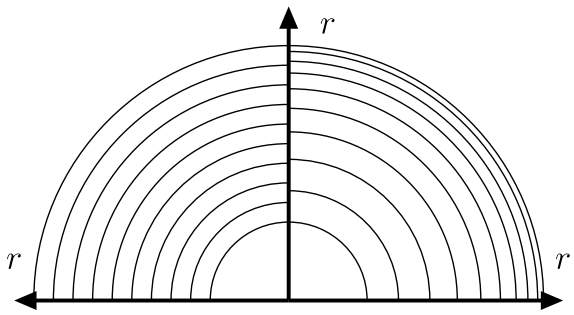


Fig. 7.8: Discretization approaches (left: equidistant; right: equiareal discretization).

A more even distribution of calculated points in radial composition and temperature profiles is obtained using the equidistant approach. Sudhoff et al. (2015) claim that the equiareal approach would require a lower number of discrete rings. A comparison of convergence behavior of both approaches did not confirm this. Both approaches converged equally well to a similar solution. Therefore, the equidistant approach is selected.

In order to chose a suitable number of discrete elements for which no appreciable change in calculated outlet weight fractions in comparison to a finer discretization does occur, a study was conducted using the literature correlations for $k^L a_e$ and $k^V a_e$ of Reddy et al. (2006) (cf. Tab. 7.2). They were obtained for co-rotation of a split-packing RPB and are capable of reproducing the experimental results to a certain extent as illustrated by Fig. 7.10.

To quantify the influence of the number of discrete elements, simulations were performed for the ethanol/n-propanol system at the three flow rates experimentally investigated and rotational speeds between $300\,\mathrm{min}^{-1}$ and $2300\,\mathrm{min}^{-1}$ with different numbers of elements ranging between 30 and 200. In Fig. 7.9, the relative deviation

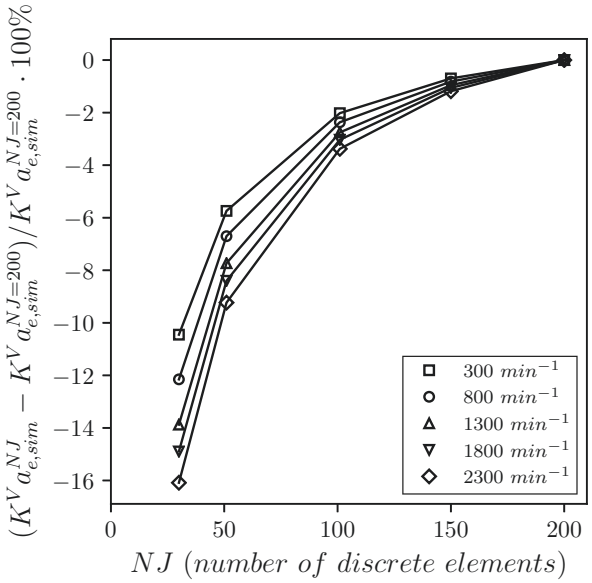


Fig. 7.9: Relative change in simulated $K^V a_e$ compared to 200 discrete elements with increasing number of discrete elements for distillation of ethanol/n-propanol in an RPB at infinite reflux using the correlations for $k^L a_e$ and $k^V a_e$ of Reddy et al. (2006) at an F-factor of 1.1 $Pa^{0.5}$(corresponding to the operating points of ethanol/n-propanol distillation from this study).

of simulated $K^V a_e$ using a certain number of discrete elements with respect to the value calculated using 200 elements is shown for the F-factor of 1.1 $Pa^{0.5}$, for which the slowest convergence was observed. While there is still considerable change when increasing the number of discrete elements to 101, the average relative deviation at 101 elements as compared to 200 elements amounts to −2.4%. This is acceptably small in view of the relative experimental uncertainty of approximately 13% for $K^V a_e$ of ethanol/n-propanol experiments in the packed rotor. For reasons of computational economy, further simulations where thus conducted using 101 elements.

7.2.2 Evaluation of the predictive capabilities of selected literature correlations

To compare model predictions with results of binary distillation experiments, $K^V a_e$ is calculated twice using Eq. 7.1: First, $K^V a_{e,exp.}$ is calculated with experimental distillate and experimental casing outlet composition. Secondly, $K^V a_{e,sim.}$ is calculated with experimental distillate composition and the casing outlet composition simulated using the rate-based stage model with input variables summarized in Tab. 7.3. If the

correlations are capable of predicting the experimental results, simulated casing outlet concentrations are identical to the experimental ones and consequently $K^V a_{e,sim.}$ are identical to $K^V a_{e,exp.}$.

Tab. 7.3: Input variables and results for simulations in this work.

Input Variables	PFD-Tag	Results	PFD-Tag
Distillate flow rate	FI02	Bottoms pressure	PI01
Condenser pressure	PI02	Bottoms composition	S-06
Temperature of reflux	TI08	Temperature profiles	-
Rotational speed	SI01	Concentration profiles	-
Distillate composition	S-04		
Packing geometry (a_p, ϵ...)[a]	-		
RPB geometry (r_i, r_o, h_p...)[a]	-		

[a] Additional variables may be required depending on the correlation used.

The first set of literature correlations by Chen et al. (2006) and Chen (2011) is chosen since it has been used in several literature modeling studies of distillation in RPBs (Li et al., 2017a; Gudena et al., 2012c; Li et al., 2020). The parity plot of $K^V a_e$ values calculated from experimental and simulated data in Fig. 7.10a shows that the correlations of Chen et al. massively overpredict separation performance in the investigated RPB. At higher rotational speeds, calculated ethanol concentration at the outer radius approaches zero, preventing a reliable evaluation of the NTU-integral in Eq. (7.1). Thus, $K^V a_e$ values for rotational speeds $>1300\,\mathrm{min}^{-1}$ are not shown in in Fig. 7.10b. The strong overprediction is also observed for the ethanol/water and ternary experiments. The correlations developed by Chen et al. contain terms that are supposed to account for the RPB geometry and associated inner and outer end-effects at the eye and in the casing. This makes them attractive for scale-up purposes. However, the RPBs on which the Chen correlations are based had comparatively small dimensions as shown in Tab. 7.4. This may be part of the reason for the massive overprediction observed for the investigated pilot-scale RPB. In the experimental data of Chen et al., the inner end-effects zone, i.e. the zone of increased mass transfer near the eye of the rotor where liquid first contacts the rotating packing, contributes more strongly to the overall observed mass transfer. This contribution is less pronounced in larger RPBs. In larger RPBs, outer regions of the rotor have a lower mass transfer efficiency. These regions are additionally often not fully wetted due to shadowing by support structures at the inner radius and rivulet formation (Burns and Ramshaw, 1996). Furthermore, different packing types from the one employed here were used in these studies, mainly stainless

steel wire mesh. This has been shown to have a slightly higher efficiency compared to metal foams (Qammar et al., 2019).

Tab. 7.4: Comparison of dimensions of RPBs used in studies for derivation of the tested mass transfer correlations from literature.

	$r_{i,min}$ (m)	$r_{o,max}$ (m)	r_{casing} (m)	h_p (m)
Chen et al. (2006) $k^L a_e$	0.01	0.06	0.075	0.02
Chen (2011) $k^V a_e$ [a]	0.02...0.045	0.04...0.09	0.06...0.15	0.02...0.035
Reddy et al. (2006)	0.0405	0.0855 & 0.148[b]	0.25...0.275[c]	0.03
current work	0.06	0.225	0.2665	0.01

[a] Data from RPBs of different sources; [b] Packing with lower outer radius used for $k^L a_e$ due to analytics detection limit; [c] Rectangular box

The second set of correlations by Reddy et al. (2006) is chosen for the similarity of the investigated RPB and packing material to the one studied here. The RPB of Reddy et al. was a split packing design with metal foam rings alternatingly fixed to both rotor plates. The correlations employed were derived from experiments with co-rotating rotor plates, simulating a single block packing RPB. The correlations of Reddy et al. enable better prediction of the mass transfer in the investigated RPB. The magnitude of $K^V a_e$ values is met, but with increased scatter, since the maximum in separation efficiency is not captured, as illustrated by Fig. 7.10. The improved performance of these correlations may be due to the similarity in packing material and the larger rotor geometry used in determination of $k^V a_e$ values. Reddy et al. furthermore attempted to exclude casing contributions from $k^V a_e$ by measuring gas concentrations directly in the casing and for $k^L a_e$ by conducting separate experiments with the innermost packing ring only.

The failure of both sets of correlations to describe a maximum in separation efficiency for a near-ideal system is inherent to their structure, which does not account for any adverse effect of centrifugal acceleration on mass transfer coefficients. This is also the case for the other semi-empirical mass transfer correlations available in RPB literature.

7.3 Suggestion of a correlation for $k^V a_e$ capable of producing a maximum in separation efficiency

As outlined in the previous section, available literature correlations are not capable of reproducing the observed maximum in RPB separation efficiency at increasing

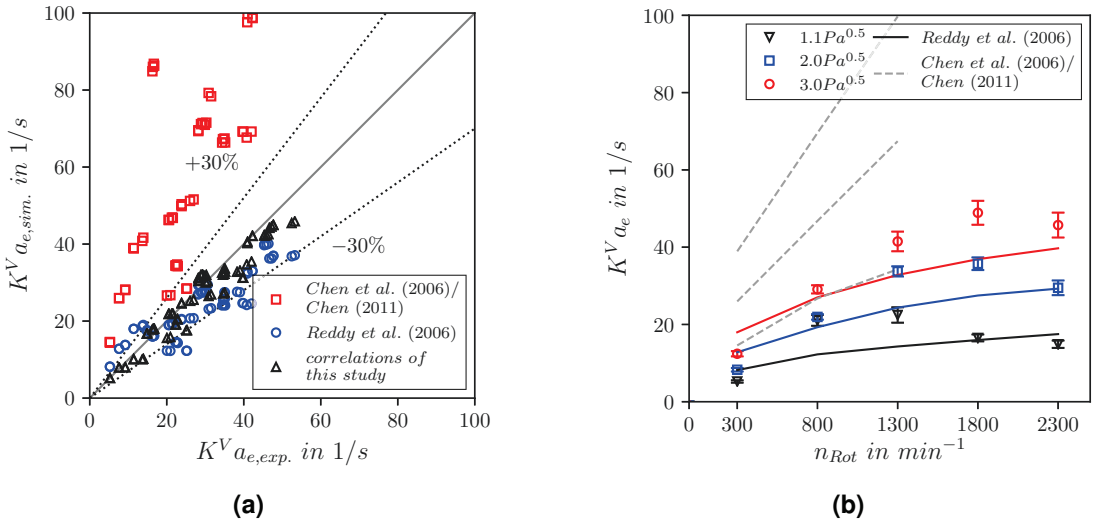


Fig. 7.10: Comparison of experimental and simulated data of binary ethanol/n-propanol system in the packed rotor, using correlations of Chen et al. (2006) and Chen (2011), Reddy et al. (2006) and this study: (a) Parity plot for $K^V a_e$ and (b) Plot of $K^V a_e$ in dependence of RPB rotational speed (literature correlations only).

centrifugal accelerations for thermodynamically near-ideal component systems. Hence, it is necessary to derive a correlation which is mathematically capable of generating such a maximum.

Two-film theory relates overall, liquid- and vapor-side volumetric mass transfer coefficients according to Eq. 7.4. However, due to the significant changes in local slope m of the equilibrium curve and in properties between inlet and outlet of the RPB, a $k^V a_e$ representative of the whole rotor cannot be obtained from this equation.

$$\frac{1}{K^V a_e} = \frac{1}{k^V a_e} + \frac{m \cdot \rho_{Mix}^{V,mol}}{k^L a_e \cdot \rho_{Mix}^{L,mol}} \tag{7.4}$$

Instead, the rate-based stage model with the underlying correlations for local $k^L a_e$ (Eq. 6.4) and $k^V a_e$ (Eq. 7.6) is used to simulate the casing outlet concentrations of ethanol based on the experimental distillate concentrations and the other input variables in Tab. 7.3. From experimental distillate and simulated outlet concentrations, $K^V a_{e,sim.}$ is calculated using Eq. 7.1. As outlined in section 7.1, $K^V a_{e,exp.}$ is calculated from experimental distillate and experimental outlet concentrations using Eq. 7.1. The objective function Eq. 7.5 for fitting of the parameters in the $k^V a_e$ correlation is chosen to minimize deviation between $K^V a_{e,sim.}$ and $K^V a_{e,exp.}$, and consequently of experi-

mental and simulated outlet concentration. The minimization is carried out using the Interior Point OPTimizer (IPOPT). Details of the developed software framework and optimization are given by Gerakis (2021).

$$f_{obj} = \sum_{k=1}^{NE} \left(\frac{K^V a_{e,sim,k} - K^V a_{e,exp,k}}{K^V a_{e,exp,k}} \right)^2 \tag{7.5}$$

The correlation for $k^V a_e$ is developed from distillation experiments at infinite reflux with the thermodynamically near-ideal system ethanol/n-propanol. For $k^L a_e$, the correlation Eq. 6.5 is used, developed in Sec. 6.2.3. It is based on oxygen desorption experiments from water in a nitrogen gas stream in the same RPB using full jet nozzles.

$$\begin{aligned} k^L_{loc} a_e = {} & 41.81 \cdot (Re^L_{empty})^{0.8160} \cdot (Ga^L_{empty})^{0.06993} \frac{D^L}{(r_o - r_i)^2} \cdot (Sc^L)^{0.5} + \\ & 1.955 \cdot 10^{-6} \cdot (Re^L)^{1.258} \cdot (Ga^L)^{0.8739} \cdot \exp(-4.963 \cdot 10^{-7} \cdot Ga^L) \cdot (a_p)^2 \cdot (D^L) \cdot (Sc^L)^{0.5} \end{aligned} \tag{6.5}$$

As a starting point for the development of a local gas-side mass transfer correlation serves the $k^V a_e$ correlation of Reddy et al. (2006), which is shown in Tab. 7.2. Contributions to $k^V a_e$ are assumed to stem from a combination of the empty rotor and the packed rotor, based on the observations shown in Fig. 7.2 and presented by Qammar et al. (2018). These contributions are represented through two additive terms. The packed rotor term is modified to contain the product of $(Ga^V)^{c_6} \cdot \exp(c_7 \cdot Ga^V)$. This structurally enables the formation of a local maximum. The reference lengths chosen for the dimensionless expressions are the length of the liquid flow path $r_o - r_i$ for the empty rotor, as done by Munjal et al. (1989a) for a rotating disk, and the specific geometric surface area a_p of the packing for the packed rotor, as done by Singh (1989). Due to insufficient variation in the Schmidt numbers of the experimental data in this study, its exponent is set to 1/3. This preserves the proportionality of $k^V a_e \sim (D^V)^{2/3}$ observed by Onda et al. (1968). The resulting correlation is shown in Eq. 7.6.

$$k_{loc}^V a_e = c_1 \cdot (Re_{empty}^V)^{c_2} \cdot (Ga_{empty}^V)^{c_3} \frac{D^V}{(r_o - r_i)^2} \cdot (Sc^V)^{1/3} + c_4 \cdot (Re^V)^{c_5} \cdot (Ga^V)^{c_6} \cdot \exp(c_7 \cdot Ga^V) \cdot (a_p)^2 \cdot (D^V) \cdot (Sc^V)^{1/3} \quad (7.6)$$

The fitting of parameters in the $k^V a_e$ correlation was done using the previously described rate-based RPB distillation model. First, parameters of the empty rotor term were fitted based on data obtained from distillation of ethanol/n-propanol in the empty rotor and subsequently fixed. Only the first summand of the $k^L a_e$ correlation Eq. 6.4, i.e. for the empty rotor, is used in this step. In a second step, parameters for the packed rotor term were estimated based on the packed rotor data for distillation of ethanol/n-propanol.

A parity plot created from data simulated using the resulting $k^V a_e$-correlation Eq. 7.7 and the $k^L a_e$-correlation Eq. 6.4 is shown in Fig. 7.11a. In the parity plot, all repeat experiments and duplicate samples are shown. For clarity's sake only the uncertainty-weighted averages of experimental data along with a representative set of simulations are displayed in Fig. 7.11b. Deviations of $K^V a_e$ are within ±30 %. Fig. 7.10a shows that performance of the correlations fitted to the experimental data from this study is as expected superior to the literature correlations when applied to the investigated RPB. Gerakis (2021, p. 67) demonstrated that the model is also capable of properly simulating data obtained at F-factors of 0.8 $\mathrm{Pa}^{0.5}$ and 3.9 $\mathrm{Pa}^{0.5}$ with the ethanol/n-propanol system, which were not used for the fit.

$$k_{loc}^V a_e = 0.02986 \cdot (Re_{empty}^V)^{0.8861} \cdot (Ga_{empty}^V)^{0.1954} \frac{D^V}{(r_o - r_i)^2} \cdot (Sc^V)^{1/3} + 2.6 \cdot 10^{-6} \cdot (Re^V)^{0.3431} \cdot (Ga^V)^{1.315} \cdot \exp(-1.0 \cdot 10^{-5} \cdot Ga^V) \cdot (a_p)^2 \cdot (D^V) \cdot (Sc^V)^{1/3} \quad (7.7)$$

It has to be remarked that by the applied method uncertainties in $k^L a_e$ are propagated to $k^V a_e$. Especially the independence of $k^L a_e$ of gas flow rate, that is commonly assumed for conventional columns (Hegely et al., 2017), is likely not valid for RPBs (cf. Sec. 6.1.3). The current method of fit will attribute such dependencies to $k^V a_e$. It is therefore recommended to use the developed correlation Eq. 7.7 for $k^V a_e$ only in conjunction with the employed correlation Eq. 6.4 for $k^L a_e$. Gerakis (2021, pp. 75–78) discusses in

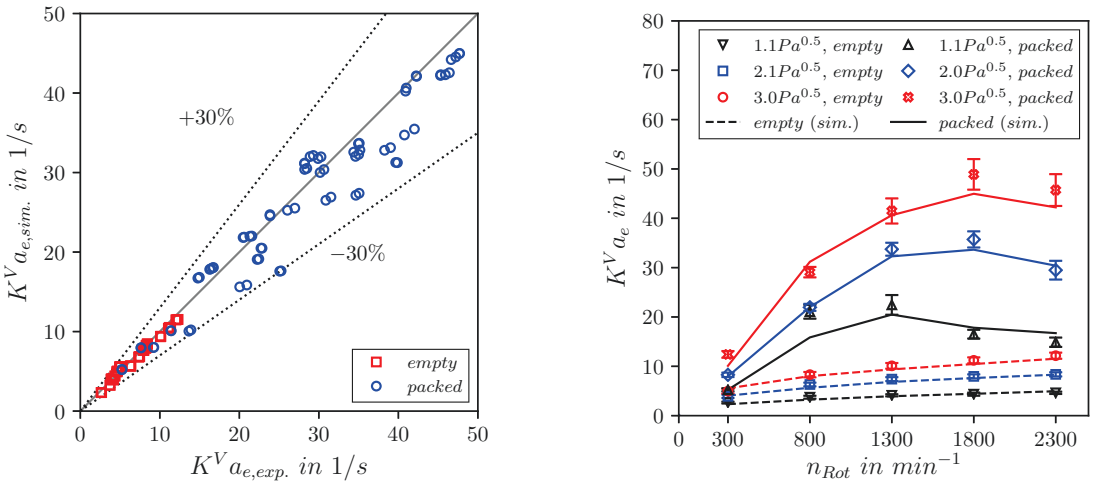


Fig. 7.11: Comparison of experimental and simulated data using estimated parameters of the developed $k^V a_e$ correlation: (a) Parity plot for $K^V a_e$ and (b) Plot of $K^V a_e$ in dependence of RPB rotational speed of binary ethanol/n-propanol system in empty and packed rotor. Lines represent simulation results (Hilpert et al., 2022).

more detail uncertainties in the model prediction of the contribution of the vapor and liquid phase resistances to the overall mass transfer resistance.

Uncertainties in the mass transfer model have to be accounted for by applying appropriate safety factors, as is common practice in conventional distillation column design. Such factors are usually obtained from statistical analysis of deviations obtained by applying a given model to a broad database of experimental data (Kister, 1992; Souza et al., 2016, p. 529). As an example, Bravo and Fair (1982) determined a safety factor of 1.6 for their model from a database of 231 points from 11 distillation component systems for a 95 % confidence interval. Unfortunately, such comprehensive data sets for distillation in RPBs are not yet available. Hence, pilot-scale experiments will likely continue to constitute an important step in the design of RPBs for new separation tasks.

7.4 Model validation

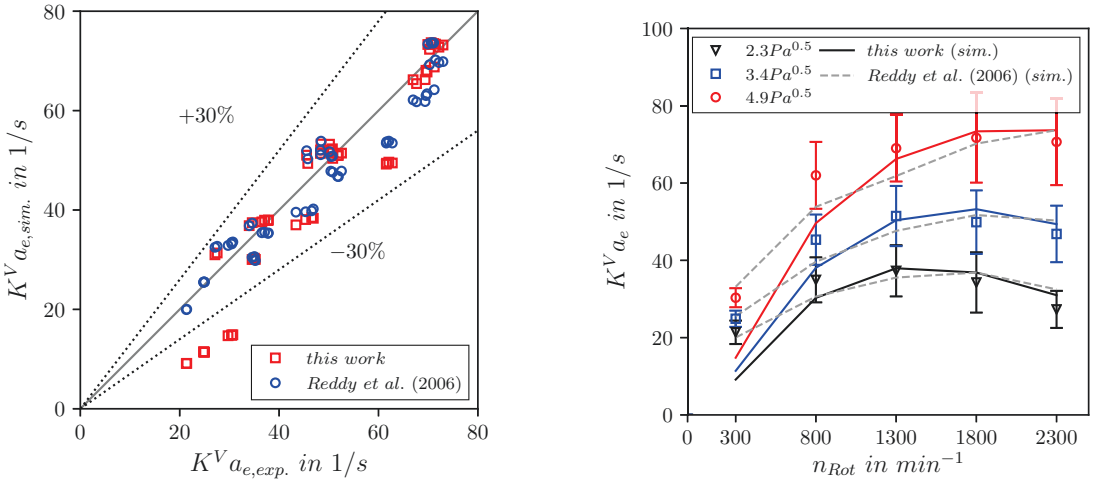
To validate the model, its performance in predicting the separations of the thermodynamically non-ideal system ethanol/water and the ternary system of ethanol/n-propanol/water is evaluated. These systems were not used for fitting the parameters.

For comparison, the performance of the literature correlations of Reddy et al. (2006) is shown.

7.4.1 Simulation of the distillation experiments with ethanol/water

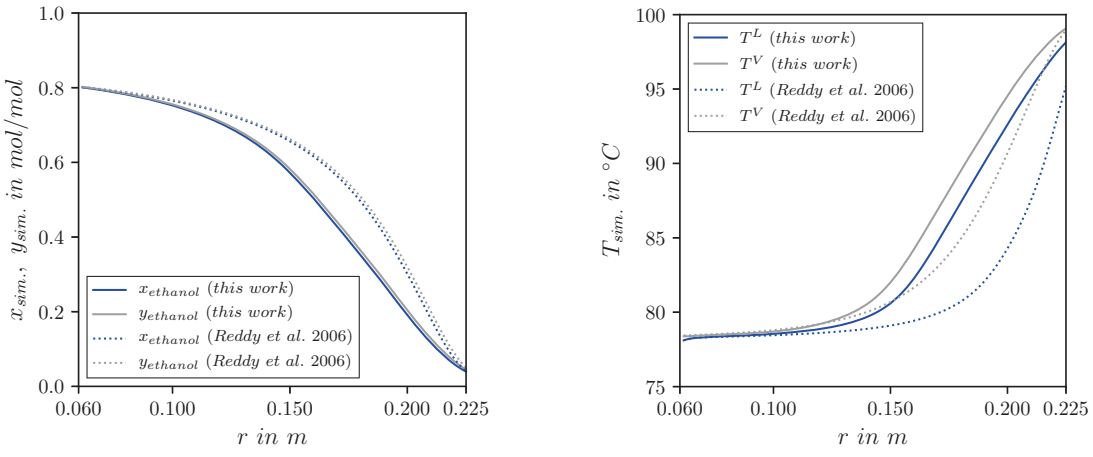
Results of the validation with ethanol/water are very promising. From the plots of $K^V a_e$ values in Fig. 7.12 it can be seen that most of the data of the ethanol/water system is represented within ±30 % with exception of the values at the lowest rotational speed of 300 min^{-1}. Operation at these low rotational speeds is not of interest for commercial operation due to the associated low separation efficiency. The trends of the maximum in separation efficiency, especially its location and shift with rotational speed, are well captured.

The Reddy et al. correlations are capable of reproducing the separation efficiency of the ethanol/water system surprisingly well. For this non-ideal system, a maximum in separation efficiency is produced by the model. This is likely due to the strong changes in transport properties along the rotor. For one operating point, where both, the Reddy model and the model developed in this work, yield almost identical outlet concentrations, the rotor profiles of vapor and liquid bulk mole fraction as well as vapor and liquid bulk temperatures predicted by the two models are shown in Fig. 7.13. Especially near the outer radius predicted profiles differ significantly. This underlines the need to measure further information along the radius, such as temperature profiles, to improve the models. From outlet concentrations alone it is not clear whether one or the other model is closer to reality. Hampel et al. (2020) have shown first results of radial temperature profile measurements in RPBs. It is important to determine whether measured temperatures in the packing are closer to vapor or liquid temperature, since both profiles can differ significantly due to vapor side resistance to heat transfer (cf. Fig. 7.13b). Experiments to determine this in a conventional column are described by Blum (1995, pp. 64–66). A temperature sensor was shielded through a rotatable glass vial with a cut-out either from vapor or from liquid. Displayed temperature of sensors in the packing was close to liquid temperature, with vapor temperature being 1.5 to 2 K above liquid temperature. A similar test should be conducted in an RPB prior to using a radial profile to improve model predictions.



(a) (b)

Fig. 7.12: Comparison of experimental and simulated data using correlations of Reddy et al. (2006) and this study: (a) Parity plot for $K^V a_e$ and (b) Plot of $K^V a_e$ in dependence of RPB rotational speed of binary ethanol/water system in the packed rotor.



(a) (b)

Fig. 7.13: Comparison of simulated radial packing profiles of (a) liquid and vapor bulk mole fractions of ethanol and (b) liquid and vapor bulk temperatures for operating point 033 (1800 min^{-1}, 2.3 $Pa^{0.5}$) using correlations of Reddy et al. (2006) and this study.

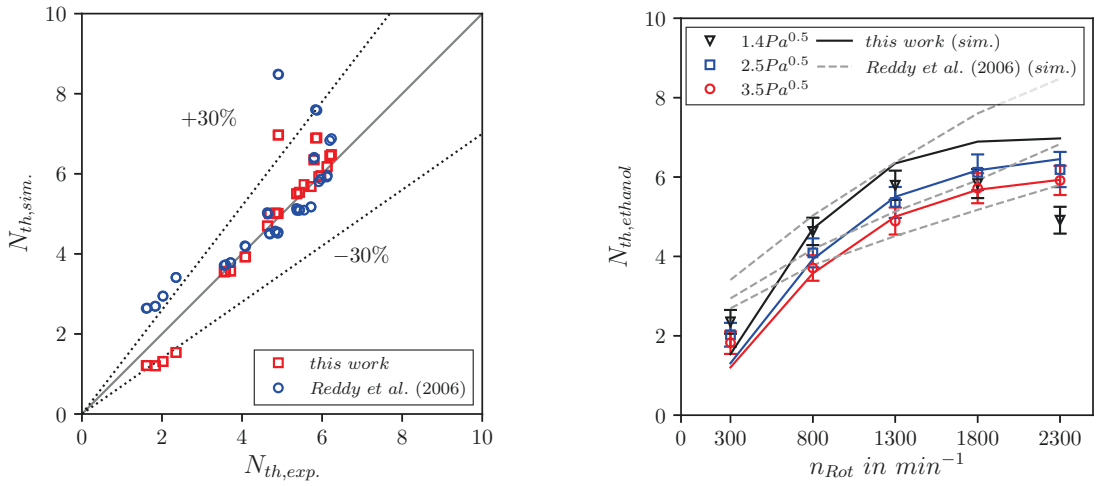


Fig. 7.14: Comparison of experimental and simulated data using correlations of Reddy et al. (2006) and this study: (a) Parity plot for $N_{th,ethanol}$ and (b) Plot of $N_{th,ethanol}$ in dependence of RPB rotational speed of ternary ethanol/n-propanol/water system in the packed rotor.

7.4.2 Simulation of the distillation experiments with ethanol/n-propanol/water

For the ternary distillation experiments, the rate-based stage model is likewise used to simulate the bottoms compositions for the experimental distillate composition and the other input variables (cf. Tab. 7.3). Using the experimental distillate composition and the bottoms composition simulated with the rate-based stage approach, $N_{th,ethanol}$ is calculated as a measure of separation efficiency. $N_{th,ethanol}$ is determined through a series of flash calculations for comparison with the experimental $N_{th,ethanol}$, i.e. through calculation of the distillation line. Again most of the data is described with deviations of ±30 % and less, as shown in Fig. 7.14. However, there is a tendency to overpredict separation performance at higher rotational speeds and decreased flow rates. For clarity's sake, the four data points from distillation region 2 are not shown in Fig. 7.14b. Their $N_{th,ethanol}$ values are also predicted with deviations below ±30 %. For the ternary system, the Reddy et al. correlations are not capable of reproducing the drop in separation efficiency and show an increased overprediction of separation efficiency.

7.5 Sources of deviations of model predictions

Reasons for increased deviations when modeling different component systems may stem from the exponents on Schmidt numbers Sc^L and Sc^V, which are based on literature and have not been fitted. As Delaloye et al. (1991) point out, properties such as viscosity or density are often used to obtain consistent dimensionless groups but are not varied significantly when fitting correlations. This is also the case in the present study. Hence, further improvement of predictions could be achieved by optimized positioning of physical properties in the correlations. To this end, additional experiments with different component systems are required.

Inaccuracies introduced through submodels for the calculation of mixture properties, such as viscosity or diffusion coefficients, further contribute to deviations. As an example, Tab. 7.5 shows a comparison of experimental and predicted liquid viscosity values using the simple mixture model of Arrhenius (1887) (cf. Eq. (7.8)) and the GCSM model of Teja and Rice (1981) used in this work. Experimental data was measured for the ternary mixture ethanol/n-propanol/water at 30 °C (Papaioannou et al., 1991). While the Teja and Rice model provides improved predictions, there are still appreciable deviations. Experimental liquid viscosity data for validation at temperatures relevant in distillation are not available. For the binary subsystems, both models provide accurate predictions for ethanol/n-propanol, while predictions for ethanol/water show similar deviations as the ternary system.

$$\eta^L_{Mix,j} = \prod_{i=1}^{NC} \left(\eta^L_{j,i}\right)^{x_{j,i}} \tag{7.8}$$

To illustrate the influence of the liquid diffusion coefficient at finite dilutions as a second example, simulations were performed using the model of Leffler and Cullinan (1970) in Eq. (7.9) and compared to the previously employed model of Taylor and Krishna (1993, p. 77) in Eq. (5.27).

$$D^L_{j,i,k} = \left(D^\infty_{j,i,k}\right)^{(1+x_{j,k}-x_{j,i})/2} \cdot \left(D^\infty_{j,k,i}\right)^{(1+x_{j,i}-x_{j,k})/2} \tag{5.27}$$

$$D^L_{j,i,k} = \frac{\left(D^\infty_{j,i,k} \cdot \eta^L_{j,k}\right)^{x_{j,k}/(x_{j,k}+x_{j,i})} \cdot \left(D^\infty_{j,k,i} \cdot \eta^L_{j,i}\right)^{x_{j,i}/(x_{j,i}+x_{j,k})}}{\eta^L_{Mix,j}} \tag{7.9}$$

Tab. 7.5: Comparison of liquid mixture viscosity data for ethanol/n-propanol/water at 30 °C (Papaioannou et al., 1991) to predictions of the model of Arrhenius (1887) and the GCSM model of Teja and Rice (1981).

$x_{ethanol}$ (mol/-mol)	$x_{n\text{-}propanol}$ (mol/-mol)	x_{water} (mol/-mol)	η^L (mPa s)	$\eta^L_{Arrhenius}$ (mPa s)	$\Delta\eta^L_{Arrhenius}$	η^L_{GCSM} (mPa s)	$\Delta\eta^L_{GCSM}$
4%	6%	89%	1.8	0.9	-51%	1.3	-27%
5%	16%	79%	2.2	0.9	-57%	1.6	-25%
7%	30%	64%	2.2	1.0	-53%	1.8	-19%
10%	59%	31%	1.9	1.3	-30%	1.5	-19%
9%	7%	83%	2.0	0.9	-56%	1.5	-25%
12%	19%	69%	2.1	1.0	-55%	1.8	-18%
16%	34%	50%	2.0	1.1	-45%	1.7	-14%
20%	51%	29%	1.8	1.2	-29%	1.5	-16%
18%	14%	68%	2.1	0.9	-55%	1.8	-16%
25%	30%	45%	1.9	1.1	-42%	1.7	-10%
30%	43%	27%	1.7	1.2	-28%	1.4	-14%
28%	16%	56%	1.9	1.0	-50%	1.8	-8%
33%	24%	44%	1.8	1.0	-42%	1.7	-7%
39%	34%	27%	1.6	1.1	-29%	1.4	-9%
28%	10%	62%	2.0	0.9	-53%	1.8	-9%
36%	16%	49%	1.8	1.0	-45%	1.7	-4%
45%	26%	29%	1.6	1.1	-31%	1.5	-6%
34%	5%	61%	1.9	0.9	-53%	1.8	-5%
40%	11%	49%	1.8	1.0	-46%	1.7	-2%
47%	19%	34%	1.6	1.0	-35%	1.6	-2%
46%	5%	49%	1.7	0.9	-46%	1.7	1%
55%	13%	32%	1.5	1.0	-34%	1.5	1%
62%	6%	31%	1.5	1.0	-34%	1.5	5%
80%	4%	16%	1.2	1.0	-21%	1.3	4%

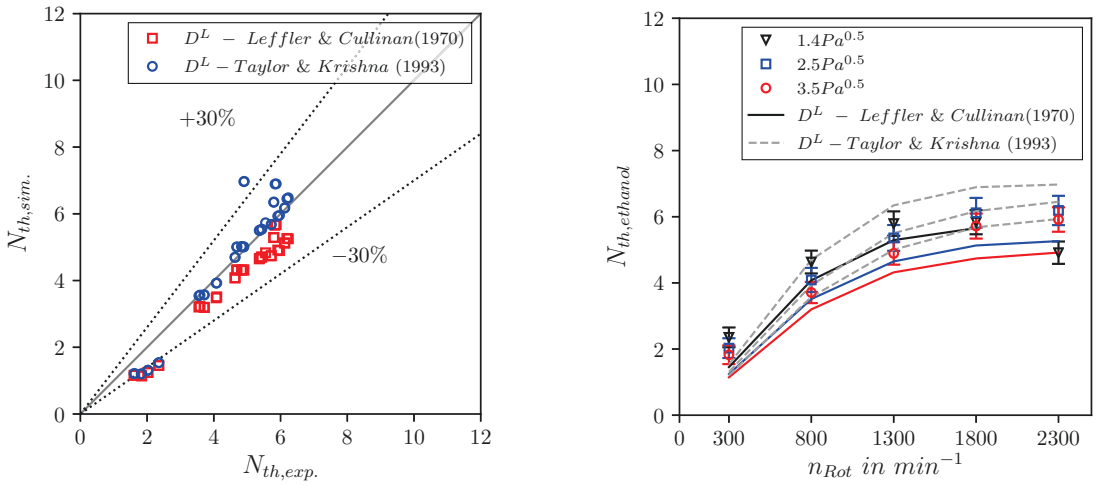


Fig. 7.15: Comparison of experimental and simulated data using correlations of this study and $D^L_{j,i,k}$ models of Leffler and Cullinan (1970) and Taylor and Krishna (1993, p. 77): (a) Parity plot for $N_{th,ethanol}$ and (b) Plot of $N_{th,ethanol}$ in dependence of RPB rotational speed of ternary ethanol/n-propanol/water system in the packed rotor. (Note: Simulations at 2300 min^{-1} and 1.4 $Pa^{0.5}$ with Leffler & Cullinan D^L model did not converge).

For the mixture of the structurally similar components ethanol/n-propanol, this change has no appreciable impact. However, the choice of the diffusivity model becomes increasingly important for multi-component mixtures. This is illustrated by Fig. 7.15 which shows simulation results using the two diffusivity models in comparison to experimental data. Calculation using the Leffler and Cullinan (1970) model results in $N_{th,ethanol}$ values which are on average ≈10 % lower than those obtained from the model of Taylor and Krishna (1993, p. 77). These two examples underline the importance to use the most suitable property models available.

7.6 Transferability of the developed model to different RPB machines

The influence of various geometry details, such as inner and outer packing supports or the liquid distributor, is so far not contained in the correlations. For example, the developed correlations are fitted for an RPB with a large free cross sectional area at the inner (≈90 %) and outer packing supports. This information is not available for

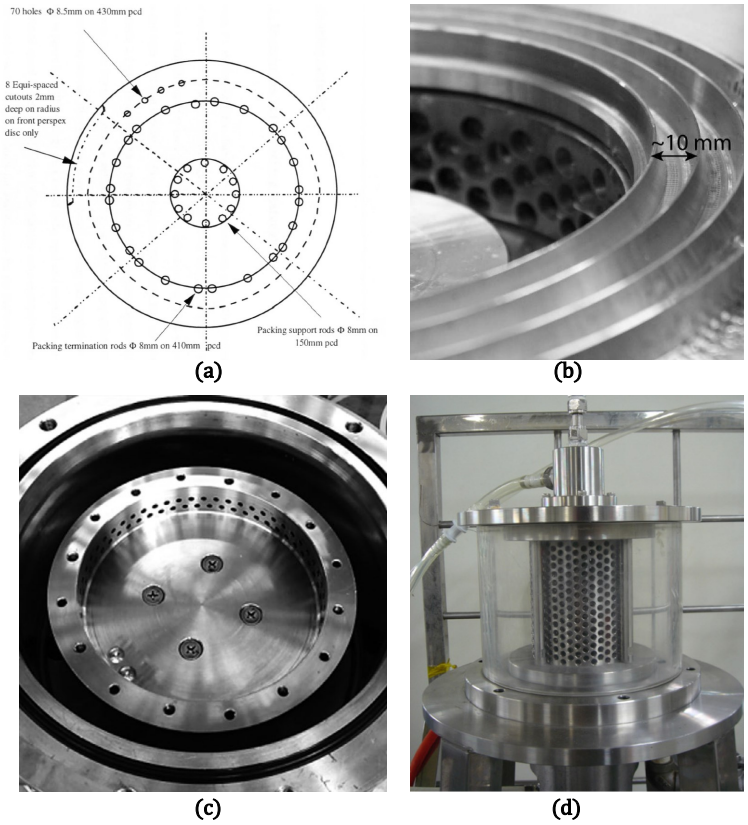
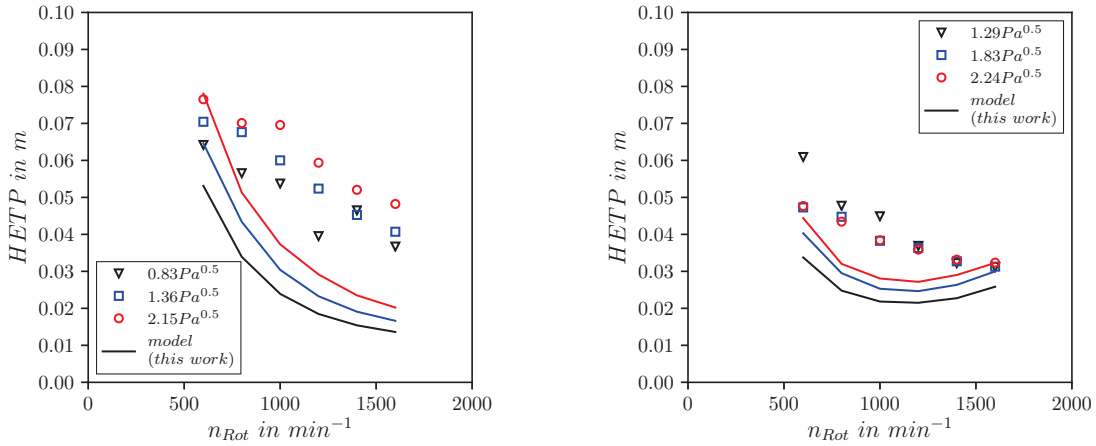


Fig. 7.16: Examples of (a) support rods with ≈80 % free area at the eye (Hassan-Beck, 1997, p. 41), (b) an inner perforated support ring with ≈60 % free area (Neumann, 2018, p. 194), and outer perforated support rings for RPB packings used by (c) Lukin et al. (2021) and (d) Lin and Chen (2011).

most publications, such as Lin et al. (2002) for which simulation results are presented in Fig. 7.17. Often, these supports are made of perforated metal sheets with a low fraction of free area (Neumann et al., 2017a) or support rods, as illustrated in Fig. 7.16. Neumann worked with RPBs from the NTHU in Taiwan (≈50 % free area) and BUCT in China (≈60 % free area) (Neumann, 2018, pp. 190–195). A change in free area at the inner support would alter the separation performance, i.e. the shape and magnitude of experimentally measured curves such as in Fig. 7.17. A low free area compared to the RPB used to develop the correlations in the current study would likely cause an underprediction of HETP due to incomplete wetting of the packing. Additionally, the influence of the liquid distributor design is not explicitly contained in the developed correlations. These factors limit the applicability of the model to different RPB machines. Furthermore, the developed correlations are not valid for extreme hydrodynamic conditions, for example close to the flood point.



(a) Rotor RP1. **(b)** Rotor RP2.

Fig. 7.17: Comparison of experimental data of Lin et al. (2002) for distillation of methanol/ethanol at infinite reflux and simulated data using correlations of this study. HETP shown in dependence of n_{Rot} for various F-factors at the eye (a) measured in rotor RP1 (h_p =95 mm, a_p =982 $m^2\,m^{-3}$, ϵ =0.946), (b) measured in rotor RP2 (h_p =25 mm, a_p =519 $m^2\,m^{-3}$, ϵ =0.971), both with r_i =61 mm, r_o =147 mm and packed with wire mesh.

To illustrate this, the model is applied to the available literature data of single block packing RPBs that were used for distillation at infinite reflux. In Fig. 7.17, the comparison of predicted and experimental HETP is shown for the data of Lin et al. (2002). A mixture of methanol and ethanol was distilled in two rotors of same radii but different heights and types of wire mesh. The magnitude of measured HETP values and general trends of the influential factors rotational speed and F-factor are captured. Details of observed trends are, however, not well predicted, leading to deviations of up to 60 %. Results of the modeling of data published by Kelleher and Fair (1996), who operated near the flood point, Nascimento et al. (2009), who employed a very different type of liquid distributor, and Qammar et al. (2019), who operated at much lower F-factors, are presented in Appendix H. Similarly to the data of Lin et al. (2002), considerable deviations exist. To describe data of a different RPB with good accuracy, a new fit of the correlation parameters using data obtained from the RPB to be modeled would hence be required.

7.7 Conclusion for the investigation of distillation

Distillation in an RPB has been investigated using two binary and a ternary component system. The maximum in separation efficiency observed in literature for distillation at intermediate rotational speeds could be confirmed. As literature correlations were not capable of simulating this behavior for all the test systems, a new correlation for $k^V a_e$ was suggested. Using the correlations for $k^L a_e$ and $k^V a_e$ developed in this work with a rate-based model, the experimental data was successfully simulated.

Sensitivities of the rate-based model towards the submodels for transport properties were illustrated, underlining the importance of a proper selection. Finally, the developed model was used to simulate literature data from distillation in other RPBs. Transferability of the model is limited through differences in the RPB designs, such as the design of packings supports and liquid distributors, which are not contained explicitly in the suggested correlations. A critical point remains that correlations developed for one type of packing are not valid for changed RPB packing geometries. Furthermore, the influence of hydrodynamics on separation performance in general requires additional research. This includes the upper and lower operating limit as well as the gas/liquid ratio which is influenced by feed state and reflux ratio in distillation operation.

The present work has demonstrated an efficient method for creating a model based on pilot-scale experiments. However, the ultimate goal has to be to further minimize experimentation to speed up development and reduce costs. In the future, the advancement of CFD models may play a key role to this end by reducing the need for experimental investigations.

8 Conclusion and Outlook

Distillation, absorption and desorption are three of the key separation unit operations in chemical industry which are conventionally carried out in large packed or trayed columns. The demand for safer, more efficient and less resource consuming equipment is a main driver for research in process intensification of such separation processes. RPBs hold significant potential for intensification of distillation and absorption processes through intensification of heat and mass transfer, leading to substantially smaller equipment. Furthermore, flexibility is increased through a larger hydrodynamic operating window, fast dynamics and the additional degree of freedom of rotational speed. RPBs thus offer a promising alternative to conventional columns for e.g. off-shore applications, retrofits or mobile plants. While considerable research has been directed at ab- and desorption processes in RPBs, a literature review revealed that few studies investigated distillation processes. Especially, data of multicomponent distillations is not available in English language literature. Hence, a validation of existing models for multicomponent separations was so far not possible, despite the importance of multicomponent separations which constitute the majority of technical separation tasks.

This study therefore aimed to develop and validate a model for distillation of multicomponent mixtures in RPBs. Since literature data is scarce and often incomplete, and transferability of data between different RPBs is still difficult, the required database was obtained from a pilot-scale RPB test stand designed and constructed during this study. For simulation of the distillation process, a rate-based approach was chosen. It allows for coupling of geometric and operational conditions to mass and heat transfer, and explicitly accounts for diffusional interactions occurring in multicomponent systems. The required binary volumetric mass transfer coefficients of gas and liquid side are described through newly developed empirical correlations of dimensionless groups. The parameters of the liquid side correlation were fitted to mass transfer coefficient measurements using desorption of oxygen from water in a nitrogen gas stream. The parameters of the gas side mass transfer correlation were fitted based on data obtained

from distillation of the thermodynamically near-ideal system ethanol/n-propanol at total reflux. This was done by solving the rate-based model with the previously obtained liquid side correlation and the gas side correlation with variable parameters until good agreement of calculated and observed separation performance was achieved. Subsequently, the model was successfully validated by simulating distillation experiments of ethanol/water and ethanol/n-propanol/water. Predicted and experimental separation performance, expressed as overall volumetric mass transfer coefficient or number of theoretical stages, usually agreed within ±30 %.

A maximum in separation performance was observed at intermediate rotational speeds in both the desorption and distillation experiments. This phenomenon has previously been reported in literature but was not incorporated into existing empirical mass transfer correlations. The developed correlations incorporate terms enabling the mathematical description of such a maximum. It was found that the formation of the maximum in separation efficiency is strongly related to the gas-liquid interaction caused by the presence of packing material. In the empty rotor without packing material or with cocurrent gas-liquid flow, no maximum was observed. Furthermore, it was found that mass transfer coefficients of gas and liquid side can be modeled through additive contributions of the empty rotor and the packed rotor. The empty rotor term was correlated using experiments conducted without packing. At high centrifugal accelerations, mass transfer efficiency declines and appears to converge to values of the empty rotor. Separation efficiency is then dominated by mass transfer occurring in the casing and at the inner support ring of the packing. The correct modeling of the maximum in separation efficiency directly impacts the choice of the proper operating speed during design of an RPB.

Unfortunately, in the case of RPBs extensive databases of experimental data, especially under industrial operating conditions, are not available and will not be in the near future. Pilot-scale experimental investigations will thus likely remain an important step in unit design for specific applications. The present thesis has demonstrated a potential procedure to obtain a rate-based multicomponent mass transfer model for pilot-scale RPBs. For the first time, mass transfer correlations have been developed which are capable of describing the centrifugal acceleration dependent maximum in separation efficiency of countercurrently operated RPBs. Finally, operating data is made available which can be used for future validation or development of new models of RPBs. Besides data of water deoxygenation and distillation data of the binary systems ethanol/water as well as ethanol/n-propanol, distillation data of a ternary component system in an RPB, i.e. ethanol/n-propanol/water, is published for the first time.

Several areas requiring further research were identified in the course of this study. Transfer of models developed for one RPB to a different RPB remains difficult. This is largely due to non-uniform mass transfer within the rotor, i.e. the occurrence of inner and outer end effects as well as rivulet formation and shadowing. The issue of end effects could be addressed through modeling of the mass transfer in different zones of the RPB by dedicated correlations. The applied method of fitting a correlation solely based on concentrations at the ends of the RPB packing does not uniquely identify a specific profile within the packing, i.e. two different correlations could produce the same concentrations at the ends of the packing but different profiles. Thus, a method for measurement of temperature and possibly concentration profiles within the rotor should be devised and incorporated in the model development workflow. Correct modeling of the actual rotor profiles would potentially also improve transferability of simulation results to different RPBs. Another area to be further researched is the influence of hydrodynamics on mass transfer. The test stand has been designed to allow for distillation operation as a stripping or rectifying section to study the influence of the gas to liquid ratio in future works. Further research is also required to incorporate the influence of RPB packing support and liquid distributor design in mass transfer correlations. To improve design rules and judge existing models regarding their scale-up capabilities, industrial data of RPBs is required. Besides accurate mass transfer models of RPBs, correlations for estimation of CAPEX and OPEX are required to assess RPBs as potential equipment alternatives and enable the full utilization of their potential in industry.

Appendix A

Measurement uncertainty calculation

The following description of the uncertainty calculation has previously been published in part in the Supporting Information of Hilpert and Repke (2021).

All measurements are associated with random and possibly also systematic errors, i.e. deviations from the true value (Gränicher, 1996, p. 1-2): Random or statistic errors stem from random changes over the time in the investigated process. They thus decrease for repeat runs or an increased measurement period. They often have a low amplitude and a high frequency ("white noise") (Narasimhan and Jordache, 2010, p. 2). Systematic errors produce the same off-set for measurements under the same conditions. They will thus not be minimized through repetition of the experiments. Systematic errors cause a non-random change of deviations for changes in experimental conditions. Examples are erroneous calibration, improper installation of a sensor, and wear or fouling (if sufficiently slow) (Narasimhan and Jordache, 2010, p. 2). Gross errors, i.e. outliers, caused for example by sensor failures, leakages etc. have been removed from the data prior to its use for evaluation and discussion. They are therefore not part of the measurement uncertainty calculation (Gränicher, 1996, p. 1-3).

Measurement uncertainty, the quantity to be determined here, is in contrast to measurement error a measure of the probable deviation from the measured value within which the true value falls (GUM 1995). It may be significant even if the measured value is close to its true unknown value.

The propagated measurement uncertainty is calculated based on calibration data, vendor information on sensor accuracy, recorded statistical fluctuations of sensor signal in steady state and several repeat experiments (where available). This is done in two stages. First, uncertainties of individual experiments are determined. Second, individual values calculated for experiments at identical set-points of the operating variables

and their respective uncertainties are combined to give an averaged value (averaging of repeat experiments).

DIN 1319-4 serves as a guideline for the first part. The main steps in the process of uncertainty calculation are:

- Pre-processing of own and third-party data (calculate mean and standard uncertainties of inputs)
- Model development
- Uncertainty propagation (calculate outputs and their uncertainties)
- Reporting of results

For all input variables of an experimental point (denoted by index i) the mean (Eq. A.1) and standard uncertainty (Eq. A.3) based on empirical variance (Eq. A.2) are calculated for the duration of the steady state. As opposed to the empirical variance, standard uncertainty will converge to zero for a large number of measurement values.

$$\overline{x}_i = \frac{1}{N_k} \sum_{k=1}^{N_k} x_{i,k} \tag{A.1}$$

$$s_i^2 = \frac{1}{N_k - 1} \sum_{k=1}^{N_k} (x_{i,k} - \overline{x}_i)^2 \tag{A.2}$$

$$u_{x,i} = \frac{s_i}{\sqrt{N_k}} \tag{A.3}$$

While random error, here represented through standard uncertainty according to Eq. A.3, is often considered as uncorrelated (Narasimhan and Jordache, 2010, p. 33), sensor errors could potentially be of a systematic nature and could continuously show a constant off-set within the manufacturer supplied accuracy. Calibration and sensor accuracy related uncertainties are therefore considered as systematic uncertainties. Values of these uncertainties are tabulated in Tab. 4.5.

The model of the process, here generally denoted as M, is represented by the equations for calculation of mass transfer coefficients or theoretical stages based on measured flow rates, concentrations, temperatures and pressures.

For uncertainty propagation, correlated and uncorrelated input variables have to be distinguished. Due to the lack of information, the inputs are considered as uncorrelated (DIN 1319-4). Gaussian uncertainty propagation is used to propagate random uncertainties (Eq. A.4). Systematic uncertainties are linearly propagated according to Eq. A.5, providing a conservative estimate (Gränicher, 1996, p. 2-8). The partial derivatives required are numerically approximated by Eq. A.6. A step size Δx_i of about half the respective relative uncertainty is chosen. The total uncertainty is determined through addition of the two contributions (Eq. A.7).

$$u_{y,rand.} = \sqrt{\sum_{i=1}^{N_i} \left(\frac{\partial M}{\partial x_i}\right)^2 u_{x,i}^2} \tag{A.4}$$

$$u_{y,syst.} = \sum_{i=1}^{N_i} \left| \frac{\partial M}{\partial x_i} u_{x,i} \right| \tag{A.5}$$

$$\frac{\partial M}{\partial x_i} = \frac{1}{\Delta x_i} \left(M(x_1, ..., x_i + 0.5\Delta x_i, ..., x_{N_i}) - M(x_1, ..., x_i - 0.5\Delta x_i, ..., x_{N_i}) \right) \tag{A.6}$$

$$u_y = u_{y,rand.} + u_{y,syst.} \tag{A.7}$$

In the second step, i.e., the averaging of N_r repeat experiments, a weighted mean (Eq. A.8) and uncertainty are calculated. The corresponding uncertainty is taken to be the greater one of the uncertainties calculated based on internal (Eq. A.9) and external consistency (Eq. A.10) (Gränicher, 1996, p. 6-3).

$$\overline{y} = \frac{\sum_{r=1}^{N_r} \left(y_r / u_{y,r}^2 \right)}{\sum_{r=1}^{N_r} 1/u_{y,r}^2} \tag{A.8}$$

$$u_{\overline{y},int.}^2 = \left(\sum_{r=1}^{N_r} \frac{1}{u_{y,r}^2} \right)^{-1} \tag{A.9}$$

$$u_{\overline{y},ext.}^2 = \frac{\sum_{r=1}^{N_r} \left((y_r - \overline{y})^2 / u_{y,r}^2 \right)}{(N_r - 1) \sum_{r=1}^{N_r} 1/u_{y,r}^2} \tag{A.10}$$

$$u_{\overline{y}} = \max(u_{\overline{y},int.}, u_{\overline{y},ext.}) \tag{A.11}$$

The overall uncertainty (Eq. A.11) of the weighted means of the repeat experiments (Eq. A.8) is presented in form of error bars in the graphs.

Appendix B

Experimental data of water deoxygenation experiments

The data in this appendix has partly been published in the supporting information of Hilpert and Repke (2021).

Full jet nozzle data

Tab. B.1: $k^L a_e$ data measured in the empty rotor with full jet nozzles in countercurrent operation.

Data Set No.	No. of averaged individual exps.	n_{Rot} min^{-1}	$\dot{V}_G$ $SLPM$	$\dot{m}_L$ kg/min	T^L $°C$	$k^L a_{e,exp.}$ $1/s$	$\Delta k^L a_{e,exp.}$ $1/s$	$NTU_{ol,exp.}$ $-$	$\Delta NTU_{ol,exp.}$ $-$	$ATU_{ol,exp.}$ m^2	$\Delta ATU_{ol,exp.}$ m^2
1	2	300	6,6	0,75	24,4	0,041	0,001	4,84	0,10	0,0305	0,0006
2	3	800	6,6	0,75	25,2	0,049	0,001	5,80	0,08	0,0255	0,0003
3	3	1300	6,6	0,75	24,7	0,048	0,001	5,64	0,07	0,0262	0,0003
4	1	1800	6,6	0,75	25,3	0,047	0,001	5,59	0,12	0,0264	0,0006
5	1	2300	6,6	0,75	26,2	0,048	0,001	5,63	0,13	0,0262	0,0006
6	2	300	6,6	1,25	24,3	0,051	0,001	3,63	0,07	0,0406	0,0008
7	2	800	6,6	1,25	24,4	0,072	0,001	5,11	0,08	0,0289	0,0004
8	2	1300	6,6	1,25	24,7	0,074	0,001	5,22	0,08	0,0283	0,0004
9	2	1800	6,6	1,25	24,4	0,073	0,001	5,17	0,08	0,0286	0,0004
10	2	2300	6,6	1,25	24,6	0,074	0,001	5,21	0,08	0,0284	0,0004
11	1	300	6,6	1,80	25,7	0,066	0,002	3,24	0,10	0,0457	0,0015
12	1	800	6,6	1,80	25,8	0,092	0,002	4,54	0,10	0,0326	0,0007
13	1	1300	6,6	1,80	25,6	0,099	0,002	4,84	0,11	0,0305	0,0007
14	1	1800	6,6	1,80	25,2	0,100	0,002	4,89	0,11	0,0302	0,0007
15	1	2300	6,6	1,80	24,5	0,099	0,002	4,89	0,11	0,0302	0,0007
16	1	300	12,3	0,75	24,1	0,041	0,001	4,86	0,11	0,0304	0,0007
17	2	800	12,3	0,75	24,8	0,053	0,001	6,28	0,11	0,0235	0,0004
18	1	1300	12,3	0,75	24,9	0,052	0,001	6,09	0,15	0,0243	0,0006
19	1	1800	12,3	0,75	25,4	0,051	0,001	6,04	0,14	0,0244	0,0006
20	1	2300	12,3	0,75	25,8	0,052	0,001	6,08	0,15	0,0243	0,0006
21	2	300	12,3	1,25	24,4	0,052	0,001	3,70	0,07	0,0399	0,0008
22	2	800	12,3	1,25	24,7	0,079	0,001	5,60	0,09	0,0264	0,0004
23	2	1300	12,3	1,25	24,6	0,081	0,001	5,71	0,09	0,0259	0,0004
24	2	1800	12,3	1,25	24,4	0,080	0,001	5,67	0,09	0,0260	0,0004
25	2	2300	12,3	1,25	24,8	0,081	0,001	5,74	0,09	0,0257	0,0004
26	1	800	12,3	1,80	25,7	0,099	0,002	4,84	0,11	0,0305	0,0007
27	1	1300	12,3	1,80	25,9	0,109	0,003	5,34	0,12	0,0277	0,0006
28	1	1800	12,3	1,80	25,9	0,111	0,003	5,44	0,12	0,0271	0,0006
29	1	2300	12,3	1,80	25,4	0,111	0,003	5,46	0,12	0,0271	0,0006

Tab. B.2: $k^L a_e$ data measured in the packed rotor with full jet nozzles in countercurrent operation.

Data Set No.	No. of averaged individual exps.	n_{Rot} min^{-1}	$\dot{V}_G$ $SLPM$	$\dot{m}_L$ kg/min	T^L °C	$k^L a_{e,exp.}$ $1/s$	$\Delta k^L a_{e,exp.}$ $1/s$	$NTU_{ol,exp.}$ –	$\Delta NTU_{ol,exp.}$ –	$ATU_{ol,exp.}$ m^2	$\Delta ATU_{ol,exp.}$ m^2
1	1	150	6,6	0,30	25,5	0,017	0,000	5,12	0,11	0,0289	0,0006
2	3	300	6,6	0,30	25,2	0,023	0,001	6,89	0,17	0,0215	0,0005
3	3	800	6,6	0,30	24,6	0,025	0,001	7,33	0,15	0,0202	0,0004
4	3	1300	6,6	0,30	25,5	0,024	0,000	7,10	0,13	0,0208	0,0004
5	3	1800	6,6	0,30	25,5	0,023	0,000	6,70	0,10	0,0220	0,0003
6	3	2300	6,6	0,30	25,9	0,022	0,000	6,50	0,10	0,0227	0,0003
7	1	150	6,6	0,75	24,3	0,026	0,001	3,06	0,10	0,0483	0,0016
8	3	300	6,6	0,75	24,7	0,047	0,003	5,49	0,34	0,0269	0,0016
9	4	800	6,6	0,75	23,6	0,060	0,001	7,12	0,16	0,0207	0,0005
10	2	1300	6,6	0,75	23,8	0,057	0,004	6,69	0,42	0,0221	0,0014
11	3	1800	6,6	0,75	24,6	0,052	0,001	6,19	0,09	0,0239	0,0004
12	3	2300	6,6	0,75	25,6	0,050	0,001	5,95	0,08	0,0248	0,0003
13	1	150	6,6	1,25	24,2	0,035	0,001	2,47	0,10	0,0598	0,0025
14	2	300	6,6	1,25	23,9	0,064	0,001	4,51	0,07	0,0327	0,0005
15	1	650	6,6	1,25	24,7	0,092	0,002	6,51	0,16	0,0227	0,0006
16	4	800	6,6	1,25	23,6	0,092	0,001	6,50	0,08	0,0227	0,0003
17	2	1050	6,6	1,25	24,1	0,090	0,002	6,39	0,11	0,0231	0,0004
18	3	1300	6,6	1,25	24,1	0,088	0,002	6,21	0,17	0,0238	0,0007
19	1	1550	6,6	1,25	24,5	0,083	0,002	5,89	0,13	0,0251	0,0006
20	3	1800	6,6	1,25	24,6	0,080	0,001	5,69	0,07	0,0260	0,0003
21	3	2300	6,6	1,25	25,8	0,078	0,001	5,52	0,07	0,0267	0,0003
22	1	150	6,6	1,80	24,2	0,054	0,002	2,65	0,10	0,0558	0,0022
23	3	300	6,6	1,80	24,5	0,094	0,002	4,64	0,12	0,0318	0,0008
24	1	550	6,6	1,80	24,3	0,129	0,003	6,32	0,15	0,0234	0,0006
25	4	800	6,6	1,80	24,4	0,136	0,002	6,68	0,09	0,0221	0,0003
26	3	1300	6,6	1,80	24,4	0,128	0,004	6,27	0,20	0,0236	0,0008
27	3	1800	6,6	1,80	24,6	0,113	0,002	5,54	0,10	0,0267	0,0005
28	3	2300	6,6	1,80	23,9	0,106	0,001	5,21	0,06	0,0283	0,0004
29	1	150	12,3	0,30	24,5	0,017	0,000	4,95	0,11	0,0299	0,0006
30	3	300	12,3	0,30	24,9	0,023	0,000	6,87	0,12	0,0215	0,0004
31	3	800	12,3	0,30	24,6	0,025	0,001	7,31	0,15	0,0202	0,0004
32	3	1300	12,3	0,30	25,6	0,025	0,001	7,40	0,16	0,0200	0,0004
33	3	1800	12,3	0,30	25,6	0,025	0,001	7,29	0,15	0,0203	0,0004
34	3	2300	12,3	0,30	26,3	0,024	0,000	7,06	0,13	0,0209	0,0004
35	1	150	12,3	0,75	24,3	0,026	0,001	3,06	0,10	0,0482	0,0016
36	2	300	12,3	0,75	24,9	0,048	0,004	5,68	0,51	0,0260	0,0023
37	3	800	12,3	0,75	23,8	0,062	0,001	7,31	0,15	0,0202	0,0004
38	2	1300	12,3	0,75	23,9	0,065	0,002	7,65	0,29	0,0193	0,0007
39	3	1800	12,3	0,75	24,7	0,060	0,002	7,11	0,24	0,0208	0,0007
40	3	2300	12,3	0,75	25,8	0,057	0,001	6,69	0,10	0,0221	0,0003
41	1	150	12,3	1,25	24,2	0,035	0,001	2,49	0,10	0,0594	0,0024
42	3	300	12,3	1,25	23,5	0,064	0,001	4,51	0,06	0,0328	0,0004
43	1	650	12,3	1,25	24,7	0,094	0,003	6,68	0,18	0,0221	0,0006
44	4	800	12,3	1,25	23,7	0,096	0,001	6,82	0,09	0,0216	0,0003
45	1	1050	12,3	1,25	24,0	0,102	0,003	7,22	0,23	0,0205	0,0007
46	4	1300	12,3	1,25	24,3	0,104	0,002	7,39	0,13	0,0200	0,0004
47	1	1550	12,3	1,25	25,0	0,098	0,003	6,95	0,20	0,0212	0,0006
48	3	1800	12,3	1,25	24,8	0,095	0,002	6,73	0,11	0,0219	0,0003
49	3	2300	12,3	1,25	25,4	0,089	0,001	6,32	0,09	0,0234	0,0003
50	1	150	12,3	1,80	24,1	0,054	0,002	2,64	0,10	0,0559	0,0022
51	3	300	12,3	1,80	24,5	0,092	0,001	4,52	0,06	0,0327	0,0004
52	1	550	12,3	1,80	24,3	0,129	0,003	6,36	0,15	0,0232	0,0006
53	3	800	12,3	1,80	24,5	0,145	0,003	7,12	0,13	0,0208	0,0004
54	3	1300	12,3	1,80	24,4	0,149	0,003	7,31	0,15	0,0202	0,0004
55	3	1800	12,3	1,80	24,9	0,133	0,002	6,53	0,10	0,0226	0,0003
56	3	2300	12,3	1,80	24,1	0,124	0,002	6,10	0,08	0,0242	0,0003

Tab. B.3: $k^L a_e$ data measured in the packed rotor with full jet nozzles in cocurrent operation.

Data Set No.	No. of averaged individual exps.	n_{Rot} min^{-1}	$\dot{V}_G$ $SLPM$	$\dot{m}_L$ kg/min	T^L $°C$	$k^L a_{e,exp.}$ $1/s$	$\Delta k^L a_{e,exp.}$ $1/s$	$NTU_{ol,exp.}$ $-$	$\Delta NTU_{ol,exp.}$ $-$	$ATU_{ol,exp.}$ m^2	$\Delta ATU_{ol,exp.}$ m^2
1	1	300	6,6	0,30	24,5	0,022	0,001	6,39	0,23	0,0231	0,0008
2	1	800	6,6	0,30	23,8	0,022	0,001	6,55	0,25	0,0225	0,0009
3	1	1300	6,6	0,30	25,6	0,023	0,001	6,65	0,27	0,0222	0,0009
4	1	1800	6,6	0,30	25,8	0,023	0,001	6,71	0,29	0,0220	0,0009
5	1	2300	6,6	0,30	26,6	0,022	0,001	6,51	0,25	0,0227	0,0009
6	3	300	6,6	0,75	23,4	0,050	0,001	5,86	0,16	0,0252	0,0007
7	2	800	6,6	0,75	23,3	0,058	0,003	6,88	0,33	0,0215	0,0010
8	2	1300	6,6	0,75	23,6	0,061	0,004	7,18	0,42	0,0206	0,0012
9	2	1800	6,6	0,75	24,7	0,061	0,004	7,17	0,42	0,0206	0,0012
10	2	2300	6,6	0,75	25,4	0,061	0,004	7,16	0,41	0,0206	0,0012
11	1	300	6,6	1,80	24,9	0,096	0,004	4,70	0,19	0,0314	0,0012
12	2	800	6,6	1,80	24,8	0,133	0,010	6,54	0,50	0,0226	0,0017
13	2	1300	6,6	1,80	25,0	0,132	0,010	6,47	0,49	0,0228	0,0017
14	2	1800	6,6	1,80	24,6	0,146	0,017	7,17	0,81	0,0206	0,0023
15	2	2300	6,6	1,80	24,6	0,146	0,016	7,16	0,79	0,0206	0,0023
16	1	300	12,3	0,30	24,4	0,022	0,001	6,61	0,23	0,0223	0,0008
17	1	800	12,3	0,30	24,3	0,023	0,001	6,75	0,24	0,0219	0,0008
18	1	1300	12,3	0,30	25,7	0,023	0,001	6,79	0,26	0,0218	0,0008
19	1	1800	12,3	0,30	26,0	0,022	0,001	6,60	0,24	0,0224	0,0008
20	1	2300	12,3	0,30	26,7	0,023	0,001	6,66	0,25	0,0222	0,0008
21	2	300	12,3	0,75	23,4	0,049	0,001	5,76	0,12	0,0256	0,0006
22	2	800	12,3	0,75	23,5	0,060	0,002	7,03	0,28	0,0210	0,0008
23	2	1300	12,3	0,75	24,0	0,061	0,003	7,16	0,30	0,0206	0,0009
24	2	1800	12,3	0,75	24,7	0,060	0,003	7,10	0,29	0,0208	0,0009
25	2	2300	12,3	0,75	25,4	0,060	0,003	7,11	0,29	0,0208	0,0009
26	2	300	12,3	1,80	24,9	0,098	0,002	4,79	0,11	0,0308	0,0007
27	2	800	12,3	1,80	24,9	0,138	0,008	6,76	0,40	0,0219	0,0013
28	2	1300	12,3	1,80	25,0	0,138	0,009	6,80	0,42	0,0217	0,0013
29	2	1800	12,3	1,80	24,9	0,143	0,010	7,02	0,48	0,0210	0,0014
30	3	2300	12,3	1,80	25,0	0,144	0,008	7,06	0,41	0,0209	0,0012

Tab. B.4: $k^L a_e$ data measured in the packed rotor with full jet nozzles in countercurrent operation, with pre-saturation of the N2 gas stream.

Data Set No.	No. of averaged individual exps.	n_{Rot} min^{-1}	$\dot{V}_G$ $SLPM$	$\dot{m}_L$ kg/min	T^L $°C$	$k^L a_{e,exp.}$ $1/s$	$\Delta k^L a_{e,exp.}$ $1/s$	$NTU_{ol,exp.}$ $-$	$\Delta NTU_{ol,exp.}$ $-$	$ATU_{ol,exp.}$ m^2	$\Delta ATU_{ol,exp.}$ m^2
1	1	300	6,6	0,75	22,7	0,050	0,001	5,91	0,13	0,0250	0,0006
2	1	800	6,6	0,75	23,1	0,061	0,002	7,20	0,24	0,0205	0,0007
3	2	1300	6,6	0,75	22,2	0,054	0,001	6,43	0,11	0,0230	0,0004
4	1	1800	6,6	0,75	23,1	0,050	0,001	5,89	0,13	0,0251	0,0006
5	1	2300	6,6	0,75	23,7	0,048	0,001	5,71	0,13	0,0259	0,0006
6	2	300	12,3	0,75	22,5	0,050	0,001	5,94	0,09	0,0249	0,0004
7	1	800	12,3	0,75	22,9	0,062	0,002	7,26	0,25	0,0203	0,0007
8	2	1300	12,3	0,75	22,5	0,061	0,001	7,16	0,16	0,0206	0,0005
9	1	1800	12,3	0,75	23,1	0,057	0,002	6,73	0,18	0,0219	0,0006
10	1	2300	12,3	0,75	23,7	0,054	0,001	6,39	0,16	0,0231	0,0006

Flat fan nozzle data

Tab. B.5: $k^L a_e$ data measured in the empty rotor with flat fan nozzles in countercurrent operation.

Data Set No.	No. of averaged individual exps.	n_{Rot} min^{-1}	$\dot{V}_G$ $SLPM$	$\dot{m}_L$ kg/min	T^L °C	$k^L a_{e,exp.}$ $1/s$	$\Delta k^L a_{e,exp.}$ $1/s$	$NTU_{ol,exp.}$ –	$\Delta NTU_{ol,exp.}$ –	$ATU_{ol,exp.}$ m^2	$\Delta ATU_{ol,exp.}$ m^2
1	2	300	6,6	0,75	24,6	0,044	0,001	5,14	0,13	0,0288	0,0007
2	2	800	6,6	0,75	24,7	0,046	0,001	5,39	0,15	0,0274	0,0008
3	2	1300	6,6	0,75	25,0	0,046	0,001	5,44	0,15	0,0272	0,0008
4	2	1800	6,6	0,75	25,5	0,046	0,001	5,43	0,15	0,0272	0,0008
5	2	2300	6,6	0,75	25,7	0,046	0,001	5,39	0,15	0,0274	0,0008
6	2	150	6,6	1,25	25,4	0,059	0,001	4,15	0,07	0,0356	0,0006
7	3	300	6,6	1,25	25,4	0,065	0,001	4,62	0,06	0,0320	0,0004
8	3	800	6,6	1,25	25,5	0,074	0,001	5,22	0,07	0,0283	0,0004
9	3	1300	6,6	1,25	25,3	0,075	0,001	5,27	0,07	0,0280	0,0004
10	3	1800	6,6	1,25	25,3	0,075	0,001	5,27	0,07	0,0280	0,0004
11	3	2300	6,6	1,25	25,3	0,074	0,001	5,27	0,07	0,0280	0,0003
12	4	300	6,6	1,80	23,7	0,070	0,002	3,46	0,09	0,0427	0,0011
13	6	800	6,6	1,80	24,0	0,088	0,001	4,31	0,05	0,0343	0,0004
14	3	1300	6,6	1,80	24,8	0,090	0,002	4,44	0,08	0,0333	0,0006
15	3	1800	6,6	1,80	24,9	0,091	0,002	4,45	0,08	0,0332	0,0006
16	4	2300	6,6	1,80	25,2	0,091	0,001	4,48	0,07	0,0330	0,0005
17	1	300	9,5	0,75	24,1	0,041	0,001	4,81	0,16	0,0307	0,0010
18	1	800	9,5	0,75	24,3	0,042	0,002	5,01	0,18	0,0295	0,0011
19	1	1300	9,5	0,75	24,6	0,042	0,002	4,99	0,18	0,0296	0,0011
20	1	1800	9,5	0,75	25,0	0,044	0,002	5,14	0,19	0,0287	0,0011
21	1	2300	9,5	0,75	25,7	0,045	0,002	5,34	0,20	0,0277	0,0010
22	4	300	9,5	1,80	24,3	0,074	0,001	3,65	0,06	0,0405	0,0006
23	2	800	9,5	1,80	24,5	0,091	0,002	4,45	0,10	0,0332	0,0007
24	2	1300	9,5	1,80	24,5	0,094	0,002	4,60	0,10	0,0321	0,0007
25	2	1800	9,5	1,80	24,9	0,094	0,002	4,64	0,10	0,0319	0,0007
26	2	2300	9,5	1,80	25,2	0,095	0,002	4,66	0,10	0,0317	0,0007
27	2	300	12,3	0,75	24,6	0,042	0,001	4,99	0,12	0,0296	0,0007
28	2	800	12,3	0,75	24,8	0,045	0,001	5,27	0,14	0,0280	0,0007
29	2	1300	12,3	0,75	25,0	0,044	0,001	5,22	0,14	0,0283	0,0007
30	2	1800	12,3	0,75	25,3	0,045	0,001	5,29	0,14	0,0279	0,0007
31	2	2300	12,3	0,75	25,9	0,044	0,001	5,24	0,14	0,0282	0,0007
32	2	150	12,3	1,25	25,3	0,060	0,001	4,27	0,07	0,0346	0,0006
33	3	300	12,3	1,25	25,5	0,069	0,001	4,86	0,06	0,0304	0,0004
34	3	800	12,3	1,25	25,5	0,081	0,001	5,70	0,07	0,0259	0,0003
35	3	1300	12,3	1,25	25,6	0,083	0,001	5,83	0,08	0,0253	0,0003
36	3	1800	12,3	1,25	25,3	0,082	0,001	5,82	0,08	0,0254	0,0003
37	3	2300	12,3	1,25	25,6	0,083	0,001	5,84	0,08	0,0253	0,0003
38	3	300	12,3	1,80	23,9	0,075	0,001	3,67	0,07	0,0403	0,0007
39	2	800	12,3	1,80	24,5	0,093	0,002	4,55	0,10	0,0325	0,0007
40	2	1300	12,3	1,80	24,5	0,096	0,002	4,72	0,11	0,0313	0,0007
41	2	1800	12,3	1,80	24,9	0,097	0,002	4,76	0,11	0,0311	0,0007
42	2	2300	12,3	1,80	25,2	0,097	0,002	4,78	0,11	0,0309	0,0007

Tab. B.6: $k^L a_e$ data measured in the packed rotor with flat fan nozzles in countercurrent operation.

Data Set No.	No. of averaged individual exps.	n_{Rot} min^{-1}	$\dot{V}_G$ $SLPM$	$\dot{m}_L$ kg/min	T^L °C	$k^L a_{e,exp.}$ $1/s$	$\Delta k^L a_{e,exp.}$ $1/s$	$NTU_{ol,exp.}$ –	$\Delta NTU_{ol,exp.}$ –	$ATU_{ol,exp.}$ m^2	$\Delta ATU_{ol,exp.}$ m^2
1	1	150	6,6	0,25	24,5	0,018	0,000	6,30	0,15	0,0234	0,0006
2	2	300	6,6	0,25	24,0	0,019	0,001	6,78	0,26	0,0218	0,0008
3	2	800	6,6	0,25	23,9	0,018	0,001	6,18	0,37	0,0239	0,0014
4	2	1300	6,6	0,25	24,5	0,018	0,001	6,45	0,24	0,0229	0,0008
5	2	1800	6,6	0,25	25,0	0,018	0,000	6,40	0,16	0,0231	0,0006
6	3	2300	6,6	0,25	26,0	0,019	0,001	6,56	0,18	0,0225	0,0006
7	1	150	6,6	0,75	26,0	0,044	0,001	5,15	0,11	0,0287	0,0006
8	4	300	6,6	0,75	24,5	0,055	0,002	6,46	0,18	0,0229	0,0007
9	2	400	6,6	0,75	25,9	0,060	0,002	7,02	0,19	0,0210	0,0006
10	2	600	6,6	0,75	26,0	0,060	0,002	7,08	0,22	0,0209	0,0007
11	4	800	6,6	0,75	24,7	0,062	0,001	7,27	0,13	0,0203	0,0004
12	3	1000	6,6	0,75	25,3	0,060	0,001	7,04	0,13	0,0210	0,0004
13	4	1300	6,6	0,75	24,7	0,061	0,001	7,20	0,12	0,0205	0,0004
14	5	1800	6,6	0,75	25,4	0,056	0,001	6,55	0,08	0,0226	0,0003
15	1	2000	6,6	0,75	25,8	0,054	0,001	6,36	0,16	0,0232	0,0006
16	4	2300	6,6	0,75	26,0	0,053	0,001	6,19	0,08	0,0239	0,0003
17	3	150	6,6	1,25	24,5	0,059	0,002	4,18	0,17	0,0353	0,0015
18	5	300	6,6	1,25	24,8	0,088	0,002	6,26	0,12	0,0236	0,0005
19	1	550	6,6	1,25	24,7	0,103	0,004	7,25	0,24	0,0204	0,0007
20	5	800	6,6	1,25	24,8	0,104	0,002	7,37	0,12	0,0201	0,0003
21	2	1050	6,6	1,25	25,1	0,105	0,003	7,40	0,19	0,0200	0,0005
22	5	1300	6,6	1,25	24,7	0,097	0,001	6,88	0,09	0,0215	0,0003
23	1	1550	6,6	1,25	24,5	0,090	0,002	6,37	0,15	0,0232	0,0006
24	4	1800	6,6	1,25	25,2	0,086	0,001	6,09	0,07	0,0243	0,0003
25	1	2050	6,6	1,25	24,3	0,083	0,002	5,86	0,13	0,0252	0,0005
26	4	2300	6,6	1,25	25,9	0,081	0,001	5,73	0,06	0,0258	0,0003
27	1	300	6,6	1,78	20,8	0,091	0,003	4,52	0,14	0,0327	0,0010
28	1	800	6,6	1,79	25,8	0,141	0,013	6,94	0,64	0,0213	0,0020
29	1	1300	6,6	1,79	26,0	0,134	0,010	6,62	0,49	0,0223	0,0017
30	1	1800	6,6	1,79	22,4	0,121	0,006	6,00	0,28	0,0246	0,0012
31	5	300	6,6	1,80	23,1	0,096	0,004	4,73	0,20	0,0312	0,0013
32	10	800	6,6	1,80	23,1	0,120	0,003	5,90	0,17	0,0250	0,0007
33	5	1300	6,6	1,80	24,0	0,128	0,003	6,27	0,16	0,0236	0,0006
34	8	1800	6,6	1,80	23,6	0,114	0,002	5,63	0,08	0,0263	0,0004
35	3	2300	6,6	1,80	24,0	0,107	0,002	5,27	0,11	0,0280	0,0006
36	1	300	9,5	1,78	20,9	0,091	0,003	4,51	0,14	0,0327	0,0010
37	1	1800	9,5	1,78	22,4	0,142	0,013	7,05	0,64	0,0210	0,0019
38	2	800	9,5	1,79	23,3	0,132	0,007	6,54	0,33	0,0226	0,0011
39	2	1300	9,5	1,79	23,5	0,145	0,011	7,15	0,52	0,0207	0,0015
40	1	1800	9,5	1,79	21,1	0,136	0,010	6,72	0,48	0,0220	0,0016
41	3	300	9,5	1,80	22,8	0,094	0,005	4,64	0,24	0,0318	0,0016
42	5	800	9,5	1,80	22,5	0,117	0,005	5,74	0,24	0,0257	0,0011
43	4	1300	9,5	1,80	23,8	0,128	0,005	6,28	0,22	0,0235	0,0008
44	4	1800	9,5	1,80	23,6	0,124	0,003	6,08	0,16	0,0243	0,0006
45	3	2300	9,5	1,80	25,0	0,117	0,003	5,77	0,15	0,0256	0,0007
46	1	150	12,3	0,25	24,3	0,018	0,000	6,30	0,15	0,0235	0,0006
47	2	300	12,3	0,25	24,2	0,020	0,001	6,90	0,19	0,0214	0,0006
48	2	800	12,3	0,25	24,6	0,020	0,000	6,93	0,14	0,0213	0,0004
49	2	1300	12,3	0,25	24,9	0,020	0,000	6,93	0,14	0,0213	0,0004
50	2	1800	12,3	0,25	25,6	0,020	0,000	6,93	0,14	0,0213	0,0004
51	2	2300	12,3	0,25	26,1	0,019	0,001	6,74	0,31	0,0219	0,0010
52	4	300	12,3	0,75	24,6	0,052	0,002	6,15	0,18	0,0240	0,0007
53	4	800	12,3	0,75	24,8	0,058	0,001	6,82	0,12	0,0217	0,0004
54	4	1300	12,3	0,75	25,0	0,058	0,001	6,79	0,11	0,0217	0,0004
55	4	1800	12,3	0,75	25,5	0,057	0,001	6,70	0,11	0,0221	0,0004
56	4	2300	12,3	0,75	26,1	0,055	0,001	6,48	0,09	0,0228	0,0003
57	3	150	12,3	1,25	24,9	0,062	0,001	4,39	0,09	0,0337	0,0007
58	5	300	12,3	1,25	24,8	0,089	0,002	6,30	0,12	0,0234	0,0005
59	1	550	12,3	1,25	24,7	0,103	0,004	7,29	0,25	0,0203	0,0007
60	4	800	12,3	1,25	24,9	0,105	0,002	7,39	0,13	0,0200	0,0004
61	1	1050	12,3	1,25	24,8	0,108	0,005	7,67	0,32	0,0193	0,0008
62	5	1300	12,3	1,25	25,2	0,107	0,002	7,55	0,13	0,0196	0,0003
63	1	1550	12,3	1,25	24,5	0,105	0,004	7,45	0,27	0,0198	0,0007
64	3	1800	12,3	1,25	25,4	0,102	0,002	7,20	0,13	0,0205	0,0004
65	1	2050	12,3	1,25	24,6	0,098	0,003	6,92	0,19	0,0214	0,0006
66	3	2300	12,3	1,25	25,9	0,094	0,001	6,62	0,10	0,0223	0,0003
67	1	800	12,3	1,79	21,1	0,111	0,004	5,49	0,21	0,0269	0,0010
68	3	300	12,3	1,80	22,8	0,094	0,005	4,64	0,25	0,0318	0,0017
69	5	800	12,3	1,80	22,6	0,125	0,004	6,16	0,21	0,0240	0,0008
70	5	1300	12,3	1,80	24,3	0,130	0,005	6,39	0,24	0,0231	0,0009
71	4	1800	12,3	1,80	23,6	0,131	0,004	6,46	0,21	0,0229	0,0007
72	2	2300	12,3	1,80	25,1	0,124	0,005	6,11	0,23	0,0242	0,0009

Tab. B.7: $k^L a_e$ data measured in the packed rotor with an outer radius of 95 mm instead of 225 mm with flat fan nozzles in countercurrent operation.

Data Set No.	No. of averaged individual exps.	n_{Rot} min^{-1}	$\dot{V}_G$ $SLPM$	$\dot{m}_L$ kg/min	T^L °C	$k^L a_{e,exp.}$ $1/s$	$\Delta k^L a_{e,exp.}$ $1/s$	$NTU_{ol,exp.}$ –	$\Delta NTU_{ol,exp.}$ –	$ATU_{ol,exp.}$ m^2	$\Delta ATU_{ol,exp.}$ m^2
1	1	300	6,6	0,75	24,6	0,454	0,011	6,17	0,15	0,0028	0,0001
2	2	800	6,6	0,75	24,4	0,486	0,009	6,61	0,12	0,0026	0,0000
3	2	1300	6,6	0,75	24,6	0,480	0,009	6,53	0,12	0,0026	0,0000
4	2	1800	6,6	0,75	25,0	0,472	0,009	6,42	0,11	0,0027	0,0000
5	2	2300	6,6	0,75	25,6	0,466	0,008	6,33	0,11	0,0027	0,0000
6	1	300	12,3	0,75	25,6	0,474	0,013	6,45	0,17	0,0026	0,0001
7	2	800	12,3	0,75	24,4	0,506	0,011	6,88	0,14	0,0025	0,0000
8	2	1300	12,3	0,75	24,6	0,510	0,011	6,94	0,14	0,0025	0,0001
9	2	1800	12,3	0,75	25,0	0,518	0,012	7,04	0,15	0,0024	0,0001
10	1	2300	12,3	0,75	25,7	0,515	0,016	7,00	0,21	0,0024	0,0001

Tab. B.8: $k^L a_e$ data measured in the packed rotor with a packing height of 20 mm instead of 10 mm with flat fan nozzles in countercurrent operation.

Data Set No.	No. of averaged individual exps.	n_{Rot} min^{-1}	$\dot{V}_G$ $SLPM$	$\dot{m}_L$ kg/min	T^L °C	$k^L a_{e,exp.}$ $1/s$	$\Delta k^L a_{e,exp.}$ $1/s$	$NTU_{ol,exp.}$ –	$\Delta NTU_{ol,exp.}$ –	$ATU_{ol,exp.}$ m^2	$\Delta ATU_{ol,exp.}$ m^2
1	2	150	6,6	2,00	24,0	0,036	0,001	3,22	0,12	0,0458	0,0017
2	1	225	6,6	2,00	24,1	0,050	0,001	4,44	0,10	0,0333	0,0008
3	2	300	6,6	2,00	24,8	0,076	0,002	6,72	0,22	0,0220	0,0007
4	3	800	6,6	2,00	23,6	0,078	0,001	6,89	0,11	0,0214	0,0004
5	2	1300	6,6	2,00	23,8	0,068	0,001	6,05	0,10	0,0244	0,0004
6	2	1800	6,6	2,00	25,3	0,063	0,001	5,58	0,09	0,0265	0,0004
7	2	2300	6,6	2,00	26,0	0,060	0,001	5,31	0,08	0,0278	0,0004
8	1	150	12,3	2,00	24,1	0,035	0,001	3,12	0,10	0,0473	0,0016
9	2	300	12,3	2,00	24,4	0,076	0,002	6,72	0,21	0,0220	0,0007
10	2	800	12,3	2,00	23,4	0,083	0,002	7,38	0,19	0,0200	0,0005
11	3	1300	12,3	2,00	24,5	0,082	0,002	7,25	0,14	0,0204	0,0004
12	2	1800	12,3	2,00	25,0	0,075	0,001	6,62	0,12	0,0223	0,0004
13	2	2300	12,3	2,00	25,8	0,072	0,002	6,34	0,15	0,0233	0,0005

Appendix C

Transport property methods for calculation of $k^L a_e$ for water deoxygenation

The following description of the property calculation for $k^L a_e$ has previously been published in the Supporting Information of Hilpert and Repke (2021). For calculation of $k^L a_e$ from oxygen desorption from water, mixture properties were taken equal to those of pure water due to the low concentrations of the solute. Transport properties were calculated using Eqs. C.1 to C.3 with parameters as shown in Tab. C.1 (VDI-Wärmeatlas 2013, p. 357):

$$\rho^L = \rho_{cr} + c_1 \left(1 - \frac{T}{T_{cr}}\right)^{0.35} + c_2 \left(1 - \frac{T}{T_{cr}}\right)^{2/3} + c_3 \left(1 - \frac{T}{T_{cr}}\right) + c_4 \left(1 - \frac{T}{T_{cr}}\right)^{4/3} \tag{C.1}$$

$$\eta^L = c_5 \exp\left(c_1 \left(\frac{c_3 - T}{T - c_4}\right)^{1/3} + c_2 \left(\frac{c_3 - T}{T - c_4}\right)^{4/3}\right) \tag{C.2}$$

$$\sigma^L = c_1 \left(1 - \frac{T}{T_{cr}}\right)^{c_2 + c_3 \frac{T}{T_{cr}} + c_4 \left(\frac{T}{T_{cr}}\right)^2 + c_5 \left(\frac{T}{T_{cr}}\right)^3} \tag{C.3}$$

Binary diffusion coefficients of oxygen in water were estimated using the Wilke-Chang method shown in eq C.4 (Perry and Green, 2008, pp. 5–54). The association factor ϕ^L, which accounts for hydrogen bonding of the solvent, is equal to 2.26 for water (Perry and Green, 2008, pp. 5–54). Molar mass of the solvent M^L equals 18.015 g mol^{-1}, v_{O2}, the molar volume of the solute at its normal boiling point of 90 K, equals 27.9 cm^3 mol^{-1} in

Tab. C.1: Coefficients for calculation of transport properties of water (VDI-Wärmeatlas 2013, Ch. D3.1).

Property	ρ^L	η^L	σ^L
T_{cr}	647.10 K		647.10 K
ρ_{cr}	322 kg m^{-3}		
c_1	1094.0233 kg m^{-3}	0.45047	0.154 88 N m^{-1}
c_2	−1813.2295 kg m^{-3}	1.39753	1.64129
c_3	3863.9557 kg m^{-3}	613.181 K	-0.75986
c_4	−2479.8130 kg m^{-3}	63.697 K	-0.85291
c_5		0.000 068 96 Pa s	1.14113

the case of oxygen (Poling et al., 2001, A-34). With T in K and η^L in Pa s, D^L is obtained in m^2 s^{-1}.

$$D^L = \frac{7.4 \cdot 10^{-15} (\phi^L M^L)^{1/2} T}{\eta^L v_{O2}^{0.6}} \tag{C.4}$$

Appendix D

Literature overview of experimental investigations of $k^L a_e$ in RPBs using water deoxygenation

The following table has previously been published in Hilpert and Repke (2021).

Tab. D.1: Overview of experimental investigations of $k^L a_e$ in RPBs using oxygen desorption from water (Hilpert and Repke, 2021). Countercurrent operation if not indicated otherwise. Packing Material: Stainless Steel (SS), Modeling Approaches: Theoretical Mechanistic (TM), Semi-Empirical (SE).

Author (Year)	RPB-Type, Packing Material	RPB Dimensions ($d_i/d_o/h_p$, in mm)	Modeling Approach	Remarks
Ramshaw and Mallinson (1981)	single-block, glass beads/copper gauze	80/180/n.a.	TM[a]	patent, 8 data points
Guo et al. (1997)	cross-flow perforated rotor, wire gauze	64/164/200	TM	
Zheng et al. (1997)	single-block, wire reticulated Ni-Cr-alloy	300/600/250	none	pilot scale
Chen et al. (2004)	single-block, SS metal sheets	77/165/20, 46/118/20	SE	O_2 desorption and ozonation
Chen et al. (2005a)	single-block, SS wire mesh/plastic beads	20…100/60…120/20	SE	influence of bed geometry
Chen et al. (2005b)	single-block, SS wire mesh	20/120/20	SE	varying viscosity, Newtonian and non-Newtonian fluids
Chen et al. (2006)	single-block, various packings (beads, Raschig rings, mesh…)	20/120/20	SE	various internals
Reddy et al. (2006)	co-/counter-rotating split packing, Ni-Cr metal foam	81/171[b]/30	SE	local correlation
Lin and Liu (2007)	single-block, SS wire mesh	76/160/20	none	
Lin and Jian (2007)	blades, covered with SS wire mesh	39/125/29.5	SE	
Shivhare et al. (2013)	single-block & co-/counter-rotating split packing, Ni-Cr metal foam	81/121…171/30	SE	
Tsai and Chen (2015)	Blade-baffle RPB	36/156/18	none	

Continued on next page

Tab. D.1 (continued).

Author (Year)	RPB-Type, Packing Material	RPB Dimensions ($d_i/d_o/h_p$, in mm)	Modeling Approach	Remarks
Yang et al. (2016)	single-block, steel wire mesh	86/252/35	none	operation at 30 mbar
Chen et al. (2016)	single-block, SS and PTFE wire meshes	80/164/15	SE	
Zhao et al. (2017)	rotor-stator (static pins, perforated rotating rings)	70/190/65	TM	
Zhao et al. (2018)	rotor-stator (static pins, perforated rotating rings)	70/190/65	SE	atmospheric and vacuum
Beer et al. (2018)	single-block, SS wire mesh	130/154/50, 100/152/50	none	cocurrent flash degassing
Liu et al. (2019b)	Mesh-pin rotor, Full Mesh Rotor	37/82/15	TM	
Groß et al. (2020)	single-block, SS wire mesh, metal foam	146/200...460/10, 100/160/50	none	cocurrent operation, pilot-scale
Wen et al. (2020)	single-block, polyamide wire mesh	40/80/16.7	SE	3D printed packing

[a] Model for k^L by Tung and Mah (1985); [b] Only four rings of the whole rotor were used since else outlet oxygen levels dropped too far (Reddy et al., 2006).

Appendix E

Assessment of the predictive capabilities of literature correlations for $k^L a_e$ data measured in this study

Various literature correlations for $k^L a_e$ have been compared to the experimental $k^L a_e$ data obtained in this study using full jet nozzles. An overview of the correlations is presented in Tab. E.1. The resulting parity plots of the comparison are shown in Figs. E.1 and E.2. None of the correlations can reproduce the experimental data satisfactorily. This comparison has been presented in the Supporting Information of Hilpert and Repke (2021).

The correlation of Chen et al. (2004) does not contain dimensionless numbers and thus lacks transferability to other separation processes, such as distillation. The correlations of Chen et al. (2016) and Wen et al. (2020) were developed for structured wire mesh packings, which are characterized through the square mesh opening size c and fiber thickness d. Those are not applicable to the packing materials of the pilot scale RPB investigated in this study. The study of Zhao et al. (2018) investigated a different type of RPB without continuous packing. Consequently, no parity plots were created for the correlations from those investigations.

Tab. E.1: Overview of semi-empirical correlations for volumetric liquid-side mass transfer coefficients in RPBs obtained from desorption of oxygen or VOCs from water. Packing Material abbreviation: Stainless Steel (SS) (Hilpert and Repke, 2021).

Author (Year)	RPB-Type, Packing Material	RPB Dimensions ($d_i/d_o/h_p$, in mm)	No. of Data Points[a]	Remarks
Singh (1989)	single-block, SS wire mesh, metal foam $k^L a_e = \frac{\dot{V}^L}{h_p \cdot ATU}$ with $ATU = \frac{337143.86}{a_p^2} \cdot \left(\frac{\rho^L \ \dot{v}^{L,avg}}{a_p \ \eta^L}\right)^{0.6} \cdot \left(\frac{(\rho^L)^2 \ a_c^{avg}}{(\eta^L)^2 \ a_p^3}\right)^{-0.15}$ $\dot{v}^{L,avg} = \frac{\dot{V}^L}{2\pi h_p} \frac{\ln(r_o/r_i)}{r_o - r_i}$, $a_c^{avg} = \frac{r_o^2 - r_i^2}{2(r_o - r_i)}\omega^2$	254/457, 610, 762/127	≈36	based on o-xylene, $d_o = 457mm$ rotor
Chen et al. (2004)	single-block, SS metal sheets $k^L a_e = 3.38 u^L(r_i)^{0.747} u^V(r_o)^{0.282} \omega^{0.311} 1.016^{\vartheta - 20}$	77/165/20, 46/118/20	17	not suitable for other component systems (no dimensionless groups)
Chen et al. (2005a)	single-block, SS wire mesh/plastic beads $k^L a_e = 0.65 \cdot \left(Sc^L\right)^{0.5} \cdot \left(Re^L\right)^{0.17} \cdot \left(Ga'^L\right)^{0.3} \cdot \left(We^L\right)^{0.3} \cdot \left(\frac{a_p \cdot D^L}{d'_p}\right) \cdot \left(1 - 0.93 \cdot \frac{V_o}{V_t} - 1.13 \cdot \frac{V_i}{V_t}\right)^{-1}$	20…100/60…120/20	≈320	influence of bed geometry
Chen et al. (2005b)	single-block, SS wire mesh $k^L a_e = 0.9 \cdot \left(Sc^L\right)^{0.5} \cdot \left(Re^L\right)^{0.24} \cdot \left(Ga''^L\right)^{0.29} \cdot \left(We^L\right)^{0.29} \cdot \left(\frac{a_p \cdot D^L}{d_p}\right)$	20/120/20	≈100	varying viscosity, Newtonian and non-Newtonian fluids

Continued on next page

Tab. E.1 (continued).

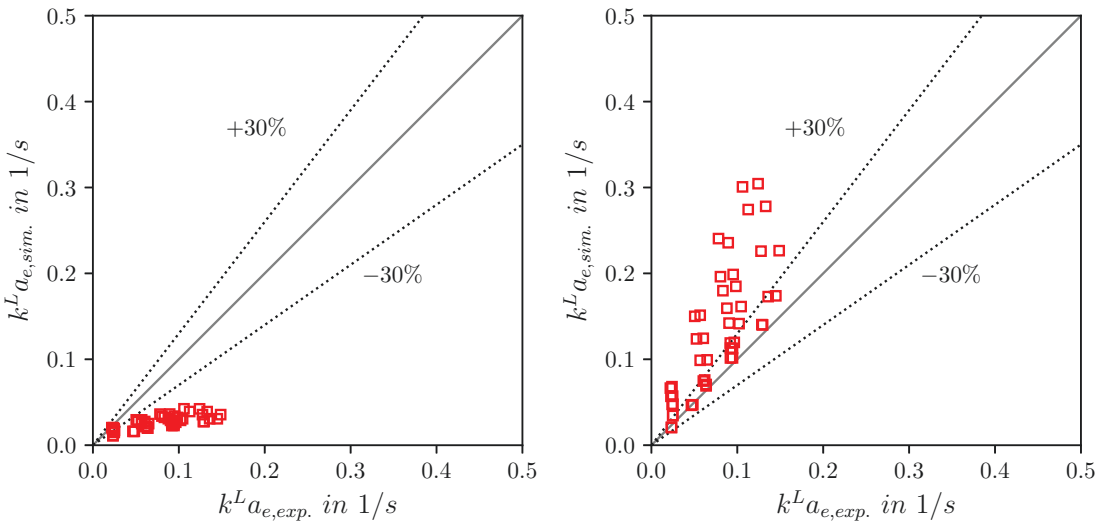
Author (Year)	RPB-Type, Packing Material	RPB Dimensions ($d_i/d_o/h_p$, in mm)	No. of Data Points[a]	Remarks
Chen et al. (2006)	single-block, various packings (beads, Raschig rings, mesh...)	20/120/20	≈240(+320)	various internals
	$k^L a_e = 0.35 \cdot \left(Sc^L\right)^{0.5} \cdot \left(Re^L\right)^{0.17} \cdot \left(Ga'^L\right)^{0.3} \cdot \left(We^L\right)^{0.3} \cdot \left(\frac{a_p \cdot D^L}{d'_p}\right) \cdot \left(1 - 0.93 \cdot \frac{V_o}{V_t} - 1.13 \cdot \frac{V_i}{V_t}\right)^{-1} \cdot \left(\frac{a_p}{a_b}\right)^{-0.5} \cdot \left(\frac{\sigma_{cr}}{\sigma_w}\right)^{0.14}$			
Reddy et al. (2006)	co-/counter-rotating split packing, Ni-Cr metal foam	81/171[b]/30	18	local correlation for co-rotation shown
	$k^L_{loc} a_e = 0.152 \cdot \left(Re^L\right)^{0.569} \cdot \left(Ga''^L\right)^{0.14} \cdot \left(Sc^L\right)^{0.5} \cdot \left(\frac{a_p \cdot D^L}{d_p}\right)$			
Lin and Jian (2007)	blades, covered with SS wire mesh	39/125/29.5	20	
	$k_L a_e = 0.478 \cdot \left(Re^L\right)^{0.906} \cdot \left(Ga''^L\right)^{0.275} \cdot \left(\frac{a_p \cdot D^L}{d_p}\right)$			
Shivhare et al. (2013)[c]	single-block & co-/counter-rotating split packing, Ni-Cr metal foam	81/121...171/30	36	correlation for single block shown
	$k^L a_e = 2.59 \cdot \left(Sc^L\right)^{0.5} \cdot \left(Re^L\right)^{0.93} \cdot \left(Ga''^L\right)^{0.25} \cdot \left((r_o^2 - r_i^2) \cdot \frac{a_p}{d_p}\right)^{-1.01} \cdot \left(\frac{a_p \cdot D^L}{d_p}\right)$			

Continued on next page

Tab. E.1 (continued).

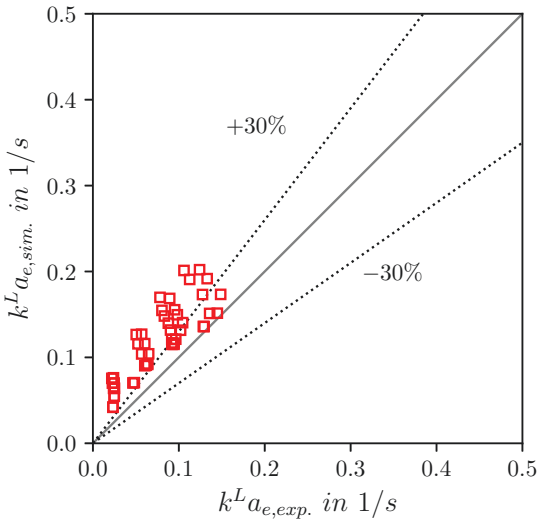
Author (Year)	RPB-Type, Packing Material	RPB Dimensions ($d_i/d_o/h_p$, in mm)	No. of Data Points[a]	Remarks
Chen et al. (2016)	single-block, SS and PTFE wire meshes $k^L a_e = 25.237 \cdot \left(Re'^L\right)^{0.815} \cdot \left(We'^L\right)^{0.214} \cdot \left(Fr^L\right)^{-0.270} \cdot (\varphi)^{-0.154} \cdot \left(\frac{\sigma}{\sigma_{cr}}\right)^{0.936} \cdot \left(\frac{a_p \cdot D^L}{d_p}\right)$	80/164/15	≈36	correlations for structured wire meshes, for plain-woven packing shown, mesh form factor $\varphi = c^2/(c+d)^2$
Zhao et al. (2018)	rotor-stator (static pins, perforated rotating rings) $k^L a_e = c_1 \cdot \left(Re''^L\right)^{c_2} \cdot \left(Re'^V\right)^{c_3} \cdot \left(We''^L\right)^{c_4} \cdot \left(We^V\right)^{c_5} \cdot \left(Fr'^L\right)^{c_6} \cdot \left(Sc^L\right)^{c_7} \cdot \left(Sc^V\right)^{c_8} \cdot \left(Eu^L\right)^{c_9} \cdot \left(Eu^V\right)^{c_{10}} \cdot \left(\frac{D^L}{r_i^2}\right)$	70/190/65	>45[d]	atmospheric and vacuum
Wen et al. (2020)	single-block, polyamide wire mesh $k^L a_e = 7.749 \cdot \left(Re'^L\right)^{1.171} \cdot \left(We'^L\right)^{0.086} \cdot \left(Fr^L\right)^{-0.234} \cdot (\varphi)^{-0.291} \cdot \left(\frac{\sigma}{\sigma_{cr}}\right)^{-0.851} \cdot \left(\frac{a_p \cdot D^L}{d_p}\right)$	40/80/16.7	≈75	correlation for structured wire meshes, mesh form factor $\varphi = c^2/(c+d)^2$

[a] Approximate number of data points used in fit of correlation; [b] Only four rings of the whole rotor were used since else outlet oxygen levels dropped too low (Reddy et al., 2006); [c] Factor was changed from 2.59 to 308.6 to be able to represent the data in the original paper of Shivhare et al. (2013). This also improved representation of the data from this study. Possibly the original paper is erroneous; [d] Data and coefficients given only in Supplementary Information, which is not available in the print journal. Experimental data probably taken largely from Zhao et al. (2017).

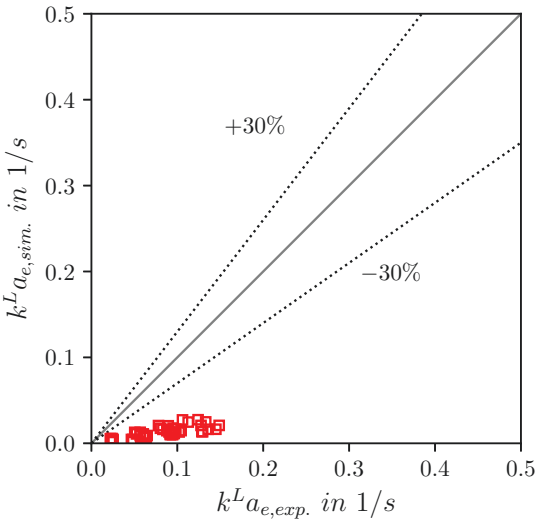


(a) Singh (1989).

(b) Lin and Jian (2007).

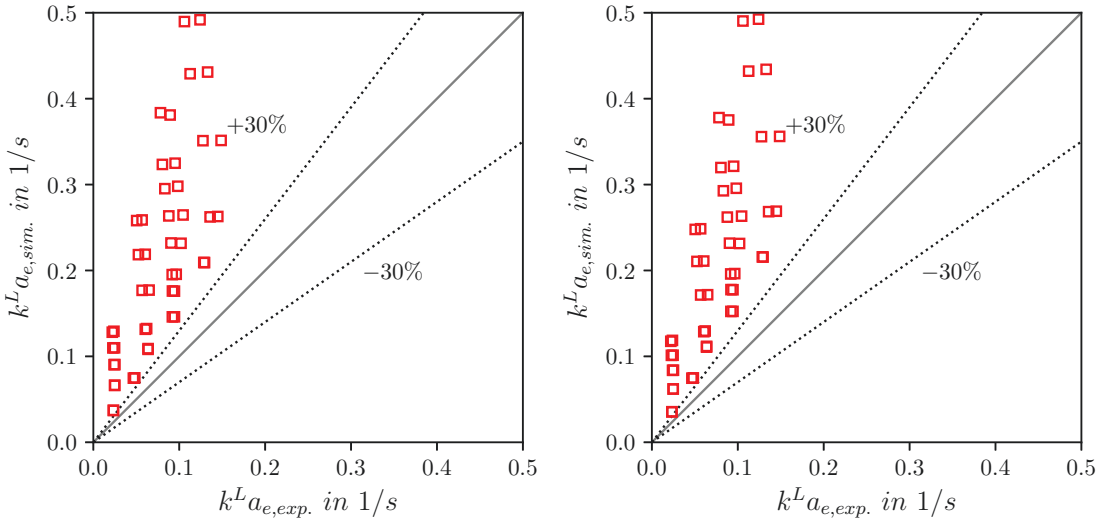


(c) Reddy et al. (2006).



(d) Shivhare et al. (2013).

Fig. E.1: Performance of literature correlations for $k^L a_e$ in comparison to the experimental data from this study for countercurrent desorption using full jet nozzles.



(a) Chen et al. (2005a).

(b) Chen et al. (2005b).

(c) Chen et al. (2006).

Fig. E.2: Performance of literature correlations for $k^L a_e$ in comparison to the experimental data from this study for countercurrent desorption using full jet nozzles (contd.).

Appendix F

Experimental data of distillation experiments

The data in this appendix has partly been published in the Supporting Information of Hilpert et al. (2022).

Averaged values - Ethanol/n-Propanol (no packing), Sample locations S6/S4, 0.7mm jet nozzle

	no. of averaged steady states	nRot	RPB effective motor power	std RPB_Peff	Qreb	mDist	std mDist	PI01	std PI01	PI02	std PI02	F	delta F	LLeye	delta LLeye	KGa	delta KGa	NTUg	delta NTUg	ATUg	delta ATUg	Nth_oi	delta Nth_oi	HETP_oi	delta HETP_oi
Unit		RPM	kW	kW	kW	kg/min	kg/min	mbar	mbar	mbar	mbar	Pa^0.5	Pa^0.5	m3/m2/h	m3/m2/h	1/s	1/s			m2	m2			m	m
Remark / No.		of RPB		standard deviation over repeat experiments	reboiler duty	FI02	standard deviation over repeat experiments		standard deviation over repeat experiments		standard deviation over repeat experiments	at eye	uncertainty of F		uncertainty of LLeye		uncertainty of KGa									
1	4	300	0,056	0,000	6	0,332	0,002	1020	6	1019	6	1,1	0,0	7,2	0,0	2,6	0,2	1,2	0,1	0,119	0,008	1,2	0,1	0,136	0,009
2	2	800	0,179	0,001	6	0,324	0,001	1026	0	1022	0	1,1	0,0	7,0	0,0	3,7	0,3	1,8	0,1	0,083	0,006	1,7	0,1	0,097	0,006
3	4	1300	0,354	0,000	6	0,331	0,001	1026	5	1016	5	1,1	0,0	7,2	0,0	4,1	0,2	1,9	0,1	0,078	0,004	1,8	0,1	0,091	0,004
4	2	1800	0,574	0,001	6	0,333	0,002	1036	0	1020	0	1,1	0,0	7,2	0,0	4,4	0,3	2,0	0,1	0,073	0,005	1,9	0,1	0,087	0,005
5	4	2300	0,845	0,002	6	0,347	0,003	1039	5	1015	5	1,2	0,0	7,5	0,0	4,6	0,2	2,0	0,1	0,072	0,003	1,9	0,1	0,085	0,003
6	4	300	0,053	0,001	10	0,621	0,006	1016	2	1013	3	2,1	0,0	13,4	0,1	3,9	0,3	1,0	0,1	0,150	0,012	1,0	0,1	0,172	0,014
7	4	800	0,183	0,004	10	0,610	0,003	1021	4	1013	3	2,0	0,0	13,2	0,0	6,3	0,4	1,6	0,1	0,093	0,005	1,5	0,1	0,107	0,006
8	4	1300	0,360	0,001	10	0,621	0,004	1029	2	1016	2	2,1	0,0	13,4	0,0	7,4	0,4	1,8	0,1	0,081	0,004	1,8	0,1	0,094	0,004
9	4	1800	0,593	0,004	10	0,623	0,002	1037	2	1016	2	2,1	0,0	13,5	0,0	8,0	0,4	2,0	0,1	0,075	0,003	1,9	0,1	0,088	0,004
10	4	2300	0,871	0,007	10	0,629	0,010	1047	2	1016	2	2,1	0,0	13,6	0,1	8,4	0,4	2,0	0,1	0,072	0,003	1,9	0,1	0,085	0,003
11	4	300	0,054	0,001	14	0,893	0,006	1013	3	1009	3	3,0	0,0	19,3	0,1	5,0	0,5	0,9	0,1	0,171	0,016	0,8	0,1	0,197	0,018
12	4	800	0,185	0,003	14	0,898	0,008	1018	3	1010	3	3,0	0,0	19,4	0,1	8,3	0,5	1,4	0,1	0,104	0,006	1,4	0,1	0,120	0,007
13	4	1300	0,364	0,002	14	0,890	0,002	1026	4	1010	4	3,0	0,0	19,2	0,0	10,1	0,6	1,7	0,1	0,085	0,004	1,7	0,1	0,099	0,005
14	4	1800	0,577	0,003	14	0,887	0,006	1035	4	1010	4	3,0	0,0	19,2	0,1	11,2	0,6	1,9	0,1	0,077	0,004	1,8	0,1	0,090	0,004
15	4	2300	0,823	0,042	14	0,898	0,003	1047	4	1012	4	3,0	0,0	19,4	0,0	12,2	0,6	2,1	0,1	0,071	0,003	1,9	0,1	0,085	0,003

Averaged values - Ethanol/n-Propanol (no packing), Sample locations S3/S4, 0.7mm jet nozzle

	no. of averaged steady states	nRot	RPB effective motor power	std RPB_Peff	Qreb	mDist	std mDist	PI01	std PI01	PI02	std PI02	F	delta F	LLeye	delta LLeye	KGa	delta KGa	NTUg	delta NTUg	ATUg	delta ATUg	Nth_oi	delta Nth_oi	HETP_oi	delta HETP_oi
Unit		RPM	kW	kW	kW	kg/min	kg/min	mbar	mbar	mbar	mbar	Pa^0.5	Pa^0.5	m3/m2/h	m3/m2/h	1/s	1/s			m2	m2			m	m
Remark / No.		of RPB		standard deviation over repeat experiments	reboiler duty	FI02	standard deviation over repeat experiments		standard deviation over repeat experiments		standard deviation over repeat experiments	at eye	uncertainty of F		uncertainty of LLeye		uncertainty of KGa									
1	4	300	0,056	0,000	6	0,332	0,002	1020	6	1019	6	1,1	0,0	7,2	0,0	1,1	0,2	0,5	0,1	0,280	0,046	0,5	0,1	0,328	0,052
2	2	800	0,179	0,001	6	0,324	0,001	1026	0	1022	0	1,1	0,0	7,0	0,0	1,8	0,3	0,9	0,1	0,171	0,026	0,8	0,1	0,210	0,030
3	4	1300	0,354	0,000	6	0,331	0,001	1026	5	1016	5	1,1	0,0	7,2	0,0	2,1	0,2	1,0	0,1	0,152	0,015	0,9	0,1	0,189	0,017
4	2	1800	0,574	0,001	6	0,333	0,002	1036	0	1020	0	1,1	0,0	7,2	0,0	2,3	0,3	1,1	0,1	0,139	0,018	0,9	0,1	0,175	0,021
5	4	2300	0,845	0,002	6	0,347	0,003	1039	5	1015	5	1,2	0,0	7,5	0,0	2,5	0,2	1,1	0,1	0,133	0,012	1,0	0,1	0,167	0,014
6	4	300	0,053	0,001	10	0,621	0,006	1016	2	1013	3	2,1	0,0	13,4	0,1	3,5	0,3	0,9	0,1	0,165	0,015	0,9	0,1	0,191	0,017
7	4	800	0,183	0,004	10	0,610	0,003	1021	4	1013	3	2,0	0,0	13,2	0,0	4,1	0,6	1,0	0,2	0,122	0,014	0,9	0,1	0,146	0,019
8	4	1300	0,360	0,001	10	0,621	0,004	1029	2	1016	2	2,1	0,0	13,4	0,0	4,5	0,4	1,1	0,1	0,130	0,011	1,0	0,1	0,160	0,014
9	4	1800	0,593	0,004	10	0,623	0,002	1037	2	1016	2	2,1	0,0	13,5	0,0	4,3	0,4	1,1	0,1	0,140	0,013	0,9	0,1	0,174	0,014
10	4	2300	0,871	0,007	10	0,629	0,010	1047	2	1016	2	2,1	0,0	13,6	0,1	4,7	0,4	1,2	0,1	0,127	0,011	1,0	0,1	0,159	0,015
11	4	300	0,054	0,001	14	0,893	0,006	1013	3	1009	3	3,0	0,0	19,3	0,1	5,2	0,5	0,9	0,1	0,162	0,014	0,9	0,1	0,187	0,016
12	4	800	0,185	0,003	14	0,898	0,008	1018	3	1010	3	3,0	0,0	19,4	0,1	7,9	0,5	1,3	0,1	0,109	0,007	1,3	0,1	0,127	0,008
13	4	1300	0,364	0,002	14	0,890	0,002	1026	4	1010	4	3,0	0,0	19,2	0,0	9,0	0,6	1,5	0,1	0,095	0,006	1,5	0,1	0,112	0,006
14	4	1800	0,577	0,003	14	0,887	0,006	1035	4	1010	4	3,0	0,0	19,2	0,1	7,9	0,6	1,4	0,1	0,107	0,007	1,3	0,1	0,128	0,009
15	4	2300	0,823	0,042	14	0,898	0,003	1047	4	1012	4	3,0	0,0	19,4	0,0	7,5	0,6	1,3	0,1	0,115	0,009	1,1	0,1	0,141	0,012

Averaged values - Ethanol/n-Propanol with packing, Sample locations S6/S4, 0.7mm jet nozzle

	no. of averaged steady states	nRot	RPB effective motor power	std RPB_Peff	Qreb	mDist	std mDist	PI01	std PI01	PI02	std PI02	F	delta F	LLeye	delta LLeye	KGa	delta KGa	NTUg	delta NTUg	ATUg	delta ATUg	Nth_oi	delta Nth_oi	HETP_oi	delta HETP_oi
Unit		RPM	kW	kW	kW	kg/min	kg/min	mbar	mbar	mbar	mbar	Pa^0.5	Pa^0.5	m3/m2/h	m3/m2/h	1/s	1/s			m2	m2			m	m
Remark / No.		of RPB		standard deviation over repeat experiments	reboiler duty	FI02	standard deviation over repeat experiments		standard deviation over repeat experiments		standard deviation over repeat experiments	at eye	uncertainty of F		uncertainty of LLeye		uncertainty of KGa								
1	2	300	0,051	0,000	6	0,328	0,002	1015	0	1014	0	1,1	0,0	7,1	0,0	5,2	0,3	2,4	0,1	0,061	0,003	2,5	0,1	0,066	0,003
2	4	800	0,161	0,000	6	0,307	0,002	1017	1	1014	1	1,1	0,0	6,6	0,0	21,1	1,4	9,5	0,6	0,015	0,001	9,5	0,5	0,017	0,001
3	4	1300	0,323	0,004	6	0,302	0,002	1020	1	1012	1	1,1	0,0	6,5	0,0	22,4	2,0	10,3	0,8	0,014	0,001	9,7	0,6	0,017	0,001
4	4	1800	0,544	0,018	6	0,310	0,002	1026	1	1010	1	1,1	0,0	6,7	0,0	16,5	0,9	7,5	0,4	0,020	0,001	6,9	0,3	0,024	0,001
5	2	2300	0,855	0,002	6	0,328	0,002	1036	0	1010	0	1,1	0,0	7,1	0,0	14,9	0,9	6,5	0,4	0,023	0,001	6,0	0,3	0,028	0,001
6	4	300	0,055	0,003	10	0,620	0,001	1017	16	1015	16	2,1	0,0	13,4	0,0	8,3	0,5	2,1	0,1	0,071	0,003	2,1	0,1	0,079	0,004
7	8	800	0,169	0,004	10	0,586	0,003	1017	10	1013	10	2,0	0,0	12,7	0,0	22,0	0,7	5,4	0,1	0,027	0,001	5,4	0,1	0,031	0,001
8	10	1300	0,345	0,007	10	0,578	0,005	1017	8	1006	8	2,0	0,0	12,5	0,0	33,7	1,3	8,2	0,3	0,018	0,001	8,0	0,2	0,020	0,001
9	6	1800	0,553	0,009	10	0,580	0,004	1019	8	1000	7	2,0	0,0	12,6	0,0	35,7	1,6	8,7	0,4	0,017	0,001	8,5	0,4	0,019	0,001
10	4	2300	0,849	0,030	10	0,591	0,003	1043	15	1016	15	2,1	0,0	12,8	0,0	29,5	1,9	7,1	0,4	0,021	0,001	6,2	0,3	0,027	0,001
11	4	300	0,050	0,002	14	0,881	0,010	1001	3	996	4	3,0	0,0	19,0	0,1	12,4	0,7	2,1	0,1	0,069	0,003	1,9	0,1	0,084	0,004
12	6	800	0,171	0,004	14	0,855	0,009	1008	9	1001	9	3,0	0,0	18,5	0,1	29,1	1,1	4,8	0,2	0,031	0,001	4,3	0,1	0,038	0,001
13	4	1300	0,336	0,010	14	0,844	0,011	1019	8	1006	7	2,9	0,0	18,3	0,1	41,5	2,5	6,9	0,4	0,021	0,001	6,0	0,3	0,028	0,001
14	6	1800	0,552	0,010	14	0,837	0,013	1021	10	1000	10	2,9	0,0	18,1	0,1	48,9	3,1	8,2	0,5	0,018	0,001	7,1	0,3	0,023	0,001
15	4	2300	0,853	0,015	14	0,851	0,007	1037	8	1005	8	3,0	0,0	18,4	0,1	45,7	3,2	7,6	0,5	0,019	0,001	6,6	0,4	0,025	0,001

Averaged values - Ethanol/n-Propanol with packing, Sample locations S3/S4, 0.7mm jet nozzle

	no. of averaged steady states	nRot	RPB effective motor power	std RPB_Peff	Qreb	mDist	std mDist	PI01	std PI01	PI02	std PI02	F	delta F	LLeye	delta LLeye	KGa	delta KGa	NTUg	delta NTUg	ATUg	delta ATUg	Nth_oi	delta Nth_oi	HETP_oi	delta HETP_oi
Unit		RPM	kW	kW	kW	kg/min	kg/min	mbar	mbar	mbar	mbar	Pa^0.5	Pa^0.5	m3/m2/h	m3/m2/h	1/s	1/s			m2	m2			m	m
Remark / No.		of RPB		standard deviation over repeat experiments	reboiler duty	FI02	standard deviation over repeat experiments		standard deviation over repeat experiments		standard deviation over repeat experiments	at eye	uncertainty of F		uncertainty of LLeye		uncertainty of KGa								
1	2	300	0,051	0,000	6	0,328	0,002	1015	0	1014	0	1,1	0,0	7,1	0,0	4,3	0,3	2,0	0,1	0,074	0,005	1,9	0,1	0,085	0,005
2	4	800	0,161	0,000	6	0,307	0,002	1017	1	1014	1	1,1	0,0	6,6	0,0	19,0	1,3	8,6	0,5	0,017	0,001	8,1	0,4	0,020	0,001
3	4	1300	0,323	0,004	6	0,302	0,002	1020	1	1012	1	1,1	0,0	6,5	0,0	20,8	1,9	9,5	0,8	0,015	0,001	8,7	0,6	0,019	0,001
4	4	1800	0,544	0,018	6	0,310	0,002	1026	1	1010	1	1,1	0,0	6,7	0,0	14,9	0,9	6,7	0,4	0,022	0,001	5,9	0,2	0,028	0,001
5	2	2300	0,855	0,002	6	0,328	0,002	1036	0	1010	0	1,1	0,0	7,1	0,0	13,1	0,9	5,7	0,3	0,026	0,002	5,0	0,3	0,033	0,002
6	4	300	0,055	0,003	10	0,620	0,001	1017	16	1015	16	2,1	0,0	13,4	0,0	7,1	0,4	1,8	0,1	0,083	0,004	1,8	0,1	0,094	0,004
7	8	800	0,169	0,004	10	0,586	0,003	1017	10	1013	10	2,0	0,0	12,7	0,0	21,5	0,7	5,3	0,1	0,027	0,001	5,2	0,1	0,032	0,001
8	10	1300	0,345	0,007	10	0,578	0,005	1017	8	1006	8	2,0	0,0	12,5	0,0	33,1	1,3	8,0	0,3	0,018	0,001	7,9	0,2	0,021	0,001
9	6	1800	0,553	0,009	10	0,580	0,004	1019	8	1000	7	2,0	0,0	12,6	0,0	34,6	1,6	8,4	0,3	0,018	0,001	8,3	0,3	0,019	0,001
10	4	2300	0,849	0,030	10	0,591	0,003	1043	15	1016	15	2,1	0,0	12,8	0,0	26,7	1,9	6,4	0,4	0,023	0,001	5,5	0,3	0,030	0,002
11	4	300	0,050	0,002	14	0,881	0,010	1001	3	996	4	3,0	0,0	19,0	0,1	14,4	0,7	2,4	0,1	0,060	0,003	2,4	0,1	0,069	0,003
12	6	800	0,171	0,004	14	0,855	0,009	1008	9	1001	9	3,0	0,0	18,5	0,1	29,3	1,1	4,9	0,2	0,030	0,001	4,4	0,1	0,037	0,001
13	4	1300	0,336	0,010	14	0,844	0,011	1019	8	1006	7	2,9	0,0	18,3	0,1	40,6	2,5	6,8	0,4	0,022	0,001	5,9	0,3	0,028	0,001
14	6	1800	0,552	0,010	14	0,837	0,013	1021	10	1000	10	2,9	0,0	18,1	0,1	48,0	3,1	8,0	0,5	0,018	0,001	6,9	0,3	0,024	0,001
15	4	2300	0,853	0,015	14	0,851	0,007	1037	8	1005	8	3,0	0,0	18,4	0,1	44,5	3,2	7,4	0,5	0,020	0,001	6,4	0,4	0,026	0,002

Averaged values - Ethanol/n-Propanol with packing, Sample locations S6/S4, 1mm jet nozzle

	no. of averaged steady states	nRot	RPB effective motor power	std RPB_Peff	Qreb	mDist	std mDist	PI01	std PI01	PI02	std PI02	F	delta F	LLeye	delta LLeye	KGa	delta KGa	NTUg	delta NTUg	ATUg	delta ATUg	Nth_oi	delta Nth_oi	HETP_oi	delta HETP_oi
Unit		RPM	kW	kW	kW	kg/min	kg/min	mbar	mbar	mbar	mbar	Pa^0.5	Pa^0.5	m3/m2/h	m3/m2/h	1/s	1/s			m2	m2			m	m
Remark / No.		of RPB		standard deviation over repeat experiments	reboiler duty	FI02	standard deviation over repeat experiments		standard deviation over repeat experiments		standard deviation over repeat experiments	at eye	uncertainty of F		uncertainty of LLeye		uncertainty of KGa								
1	2	300	0,054	0,000	14	0,889	0,008	1020	1	1014	0	3,0	0,0	19,2	0,1	10,1	0,8	1,7	0,1	0,085	0,006	1,7	0,1	0,099	0,007
2	2	800	0,167	0,001	14	0,849	0,001	1018	0	1010	0	2,9	0,0	18,4	0,0	28,3	1,8	4,8	0,3	0,031	0,002	4,2	0,3	0,039	0,002
3	2	1300	0,343	0,000	14	0,842	0,001	1027	1	1013	1	2,9	0,0	18,2	0,0	40,3	3,5	6,8	0,5	0,022	0,002	5,9	0,4	0,028	0,002
4	2	1800	0,564	0,003	14	0,850	0,004	1035	0	1013	0	3,0	0,0	18,4	0,1	44,2	4,4	7,4	0,7	0,020	0,002	6,4	0,6	0,026	0,002
5	4	2300	0,843	0,004	14	0,855	0,006	1046	0	1014	0	3,0	0,0	18,5	0,1	42,2	2,7	7,0	0,4	0,021	0,001	6,1	0,4	0,027	0,002

Averaged values - Ethanol/n-Propanol with packing, Sample locations S3/S4, 1mm jet nozzle

	no. of averaged steady states	nRot	RPB effective motor power	std RPB_Peff	Qreb	mDist	std mDist	PI01	std PI01	PI02	std PI02	F	delta F	LLeye	delta LLeye	KGa	delta KGa	NTUg	delta NTUg	ATUg	delta ATUg	Nth_oi	delta Nth_oi	HETP_oi	delta HETP_oi
Unit		RPM	kW	kW	kW	kg/min	kg/min	mbar	mbar	mbar	mbar	Pa^0.5	Pa^0.5	m3/m2/h	m3/m2/h	1/s	1/s			m2	m2			m	m
Remark / No.		of RPB		standard deviation over repeat experiments	reboiler duty	FI02	standard deviation over repeat experiments		standard deviation over repeat experiments		standard deviation over repeat experiments	at eye	uncertainty of F		uncertainty of LLeye		uncertainty of KGa								
1	2	300	0,054	0,000	14	0,889	0,008	1020	1	1014	0	3,0	0,0	19,2	0,1	11,8	0,8	2,0	0,1	0,073	0,005	1,9	0,1	0,085	0,005
2	2	800	0,167	0,001	14	0,849	0,001	1018	0	1010	0	2,9	0,0	18,4	0,0	28,6	1,8	4,8	0,3	0,031	0,002	4,3	0,3	0,038	0,002
3	2	1300	0,343	0,000	14	0,842	0,001	1027	1	1013	1	2,9	0,0	18,2	0,0	39,6	3,5	6,7	0,5	0,022	0,002	5,8	0,4	0,029	0,002
4	2	1800	0,564	0,003	14	0,850	0,004	1035	0	1013	0	3,0	0,0	18,4	0,1	43,4	4,4	7,2	0,7	0,020	0,002	6,2	0,6	0,027	0,003
5	4	2300	0,843	0,004	14	0,855	0,006	1046	0	1014	0	3,0	0,0	18,5	0,1	41,0	2,7	6,8	0,4	0,022	0,001	5,9	0,3	0,028	0,001

Averaged values - Ethanol/Water with packing, Sample locations S6/S4, 0.7mm jet nozzle

	no. of averaged steady states	nRot	RPB effective motor power	std RPB_Peff	Qreb	mDist	std mDist	PI01	std PI01	PI02	std PI02	F	delta F	LLeye	delta LLeye	KGa	delta KGa	NTUg	delta NTUg	ATUg	delta ATUg	Nth_oi	delta Nth_oi	HETP_oi	delta HETP_oi
Unit		RPM	kW	kW	kW	kg/min	kg/min	mbar	mbar	mbar	mbar	Pa^0.5	Pa^0.5	m3/m2/h	m3/m2/h	1/s	1/s			m2	m2			m	m
Remark / No.		of RPB		standard deviation over repeat experiments	reboiler duty	FI02	standard deviation over repeat experiments		standard deviation over repeat experiments		standard deviation over repeat experiments	at eye	uncertainty of F		uncertainty of LLeye		uncertainty of KGa								
1	2	300	0,049	0,000	12	0,595	0,002	1046	0	1044	0	2,3	0,0	12,4	0,0	21,4	3,0	4,3	0,7	0,034	0,005	3,1	0,6	0,054	0,009
2	4	800	0,168	0,004	12	0,634	0,004	1036	16	1032	16	2,3	0,0	13,4	0,0	35,0	5,8	6,9	1,2	0,021	0,004	5,2	1,0	0,031	0,006
3	4	1300	0,342	0,022	12	0,641	0,005	1039	15	1031	15	2,4	0,0	13,5	0,1	37,3	6,6	7,3	1,4	0,020	0,004	5,6	1,2	0,029	0,006
4	2	1800	0,553	0,040	12	0,636	0,006	1029	0	1014	0	2,4	0,0	13,4	0,1	34,3	7,8	6,7	1,6	0,022	0,005	5,0	1,3	0,033	0,009
5	2	2300	0,822	0,002	12	0,627	0,002	1067	0	1044	0	2,3	0,0	13,2	0,0	27,3	4,8	5,4	1,0	0,027	0,005	4,0	0,8	0,041	0,008
6	4	300	0,053	0,007	17	0,836	0,004	1031	11	1027	11	3,2	0,0	17,3	0,0	24,9	2,1	3,4	0,3	0,043	0,004	2,4	0,3	0,068	0,007
7	4	800	0,171	0,004	17	0,908	0,004	1035	12	1029	12	3,4	0,0	19,1	0,0	45,3	6,5	6,2	0,9	0,024	0,004	4,6	0,8	0,035	0,006
8	5	1300	0,343	0,035	17	0,919	0,006	1030	16	1019	16	3,4	0,0	19,4	0,0	51,5	7,8	6,9	1,1	0,021	0,003	5,3	0,9	0,031	0,005
9	4	1800	0,541	0,044	17	0,923	0,001	1043	14	1025	14	3,4	0,0	19,4	0,0	49,9	8,2	6,8	1,2	0,022	0,004	5,1	1,0	0,032	0,006
10	4	2300	0,802	0,046	17	0,919	0,005	1049	17	1024	17	3,4	0,0	19,3	0,0	46,8	7,3	6,4	1,1	0,023	0,004	4,8	0,9	0,034	0,006
11	4	300	0,052	0,002	25	1,197	0,006	1033	8	1021	8	4,7	0,0	24,6	0,1	30,3	2,5	2,9	0,3	0,052	0,005	1,9	0,2	0,085	0,007
12	4	800	0,191	0,010	25	1,318	0,006	1028	1	1016	1	4,9	0,0	27,7	0,1	62,0	8,7	5,7	0,9	0,026	0,004	4,2	0,7	0,039	0,006
13	6	1300	0,336	0,019	25	1,326	0,023	1031	11	1016	11	5,0	0,0	27,8	0,3	69,0	8,6	6,4	0,9	0,023	0,003	4,8	0,7	0,034	0,005
14	4	1800	0,556	0,039	25	1,342	0,010	1037	2	1014	1	5,0	0,0	28,2	0,1	71,7	11,6	6,6	1,1	0,022	0,004	5,0	0,9	0,033	0,006
15	4	2300	0,853	0,011	25	1,348	0,004	1047	1	1015	1	5,0	0,0	28,3	0,1	70,7	11,2	6,5	1,1	0,023	0,004	4,9	0,9	0,033	0,006

Averaged values - Ethanol/Water with packing, Sample locations S3/S4, 0.7mm jet nozzle

	no. of averaged steady states	nRot	RPB effective motor power	std RPB_Peff	Qreb	mDist	std mDist	PI01	std PI01	PI02	std PI02	F	delta F	LLeye	delta LLeye	KGa	delta KGa	NTUg	delta NTUg	ATUg	delta ATUg	Nth_oi	delta Nth_oi	HETP_oi	delta HETP_oi
Unit		RPM	kW	kW	kW	kg/min	kg/min	mbar	mbar	mbar	mbar	Pa^0.5	Pa^0.5	m3/m2/h	m3/m2/h	1/s	1/s			m2	m2			m	m
Remark / No.		of RPB		standard deviation over repeat experiments	reboiler duty	FI02	standard deviation over repeat experiments		standard deviation over repeat experiments		standard deviation over repeat experiments	at eye	uncertainty of F		uncertainty of LLeye		uncertainty of KGa								
1	2	300	0,049	0,000	12	0,595	0,002	1046	0	1044	0	2,3	0,0	12,4	0,0	18,5	3,2	3,7	0,7	0,040	0,007	2,7	0,5	0,062	0,012
2	4	800	0,168	0,004	12	0,634	0,004	1036	16	1032	16	2,3	0,0	13,4	0,0	32,0	6,0	6,3	1,2	0,023	0,004	4,8	1,0	0,034	0,007
3	4	1300	0,342	0,022	12	0,641	0,005	1039	15	1031	15	2,4	0,0	13,5	0,1	35,9	6,7	7,1	1,4	0,021	0,004	5,4	1,2	0,031	0,006
4	2	1800	0,553	0,040	12	0,636	0,006	1029	0	1014	0	2,4	0,0	13,4	0,1	33,0	7,9	6,4	1,6	0,023	0,006	4,8	1,4	0,034	0,009
5	2	2300	0,822	0,002	12	0,627	0,002	1067	0	1044	0	2,3	0,0	13,2	0,0	20,1	5,3	4,0	1,1	0,037	0,010	3,0	0,9	0,054	0,016
6	4	300	0,053	0,007	17	0,836	0,004	1031	11	1027	11	3,2	0,0	17,3	0,0	22,0	2,5	3,0	0,4	0,049	0,006	2,0	0,3	0,081	0,012
7	4	800	0,171	0,004	17	0,908	0,004	1035	12	1029	12	3,4	0,0	19,1	0,0	45,2	6,5	6,1	1,0	0,024	0,004	4,6	0,8	0,036	0,006
8	5	1300	0,343	0,035	17	0,919	0,006	1030	16	1019	16	3,4	0,0	19,4	0,0	49,6	7,8	6,7	1,1	0,022	0,004	5,1	0,9	0,032	0,006
9	4	1800	0,541	0,044	17	0,923	0,001	1043	14	1025	14	3,4	0,0	19,4	0,0	47,7	8,3	6,5	1,2	0,023	0,004	4,9	1,0	0,034	0,007
10	4	2300	0,802	0,046	17	0,919	0,005	1049	17	1024	17	3,4	0,0	19,3	0,0	44,4	7,4	6,1	1,1	0,024	0,004	4,6	0,9	0,036	0,007
11	4	300	0,052	0,002	25	1,197	0,006	1033	8	1021	8	4,7	0,0	24,6	0,1	29,7	2,5	2,8	0,3	0,052	0,005	1,9	0,2	0,086	0,008
12	4	800	0,191	0,010	25	1,318	0,006	1028	1	1016	1	4,9	0,0	27,7	0,1	63,6	8,6	5,9	0,9	0,025	0,004	4,4	0,7	0,037	0,006
13	6	1300	0,336	0,019	25	1,326	0,023	1031	11	1016	11	5,0	0,0	27,8	0,3	67,3	8,7	6,3	0,9	0,024	0,003	4,7	0,7	0,035	0,005
14	4	1800	0,556	0,039	25	1,342	0,010	1037	2	1014	1	5,0	0,0	28,2	0,1	68,3	11,7	6,3	1,2	0,023	0,004	4,8	1,0	0,035	0,007
15	4	2300	0,853	0,011	25	1,348	0,004	1047	1	1015	1	5,0	0,0	28,3	0,1	66,9	11,3	6,2	1,1	0,024	0,004	4,7	0,9	0,035	0,007

Averaged values - Ethanol/Water with packing, Sample locations S2/S7, 0.7mm jet nozzle

	no. of averaged steady states	nRot	RPB effective motor power	std RPB_Peff	Qreb	mDist	std mDist	PI01	std PI01	PI02	std PI02	F	delta F	LLeye	delta LLeye	KGa	delta KGa	NTUg	delta NTUg	ATUg	delta ATUg	Nth_oi	delta Nth_oi	HETP_oi	delta HETP_oi
Unit		RPM	kW	kW	kW	kg/min	kg/min	mbar	mbar	mbar	mbar	Pa^0.5	Pa^0.5	m3/m2/h	m3/m2/h	1/s	1/s			m2	m2			m	m
Remark / No.		of RPB		standard deviation over repeat experiments	reboiler duty	FI02	standard deviation over repeat experiments		standard deviation over repeat experiments		standard deviation over repeat experiments	at eye	uncertainty of F		uncertainty of LLeye		uncertainty of KGa								
6	4	300	0,053	0,007	17	0,836	0,004	1031	11	1027	11	3,2	0,0	17,3	0,0	30,9	4,7	4,3	0,7	0,034	0,006	3,1	0,6	0,053	0,010
7	4	800	0,171	0,004	17	0,908	0,004	1035	12	1029	12	3,4	0,0	19,1	0,0	46,5	12,1	6,3	1,7	0,023	0,006	4,8	1,5	0,034	0,010
8	5	1300	0,343	0,035	17	0,919	0,006	1030	16	1019	16	3,4	0,0	19,4	0,0	48,3	11,4	6,5	1,6	0,023	0,005	5,0	1,3	0,033	0,009
9	4	1800	0,541	0,044	17	0,923	0,001	1043	14	1025	14	3,4	0,0	19,4	0,0	47,5	14,6	6,4	2,1	0,023	0,007	5,0	1,7	0,033	0,011
10	4	2300	0,802	0,046	17	0,919	0,005	1049	17	1024	17	3,4	0,0	19,3	0,0	46,3	15,0	6,3	2,2	0,023	0,008	4,9	1,8	0,034	0,012
12	4	800	0,191	0,010	25	1,318	0,006	1028	1	1016	1	4,9	0,0	27,7	0,1	65,9	16,2	6,1	1,6	0,024	0,006	4,6	1,4	0,036	0,010
13	6	1300	0,336	0,019	25	1,326	0,023	1031	11	1016	11	5,0	0,0	27,8	0,3	72,1	20,1	6,8	2,0	0,022	0,006	5,2	1,7	0,031	0,010
14	4	1800	0,556	0,039	25	1,342	0,010	1037	2	1014	1	5,0	0,0	28,2	0,1	69,8	21,1	6,5	2,1	0,023	0,007	5,1	1,7	0,033	0,011
15	4	2300	0,853	0,011	25	1,348	0,004	1047	1	1015	1	5,0	0,0	28,3	0,1	67,7	20,1	6,3	2,0	0,023	0,007	4,9	1,6	0,033	0,011

Ethanol/n-Propanol (no packing), Sample locations S6/S4, 0.7mm jet nozzle

	nRot	RPB_Peff	F	Qreb	mDist	LLeye	rhoL	rhoLfeed	TLfeed	TLVfeed	PI01	PI02	TI03	TI04	TI05	TI12	wi	wo	NTUg	delta NTUg	ATUg	delta ATUg	KGa	delta KGa	Nth_oi	delta Nth_oi	HETP_oi	delta HETP_oi
Unit	RPM	kW	Pa^0.5	kW	kg/min	m3/m2/h	kg/m3	kg/m3	°C	°C	mbar	mbar	°C	°C	°C	°C	g EtOH/g Mix	g EtOH/g Mix			m2	m2	1/s	1/s			m	m
Note / Steady State No.	of RPB		at eye	reboiler duty	FI02		DI02	DI02 at TIfeed	TI08	bubble point temperature of S4 at PI02							S4 weight frac.	S6 weight frac.	NTU (overall vapor)	uncertainty of NTUg				uncertainty of Kga	oi -> calculated starting at wo until wi is reached			
178	800	0,179	2,0	10	0,607	13,1	770,8	736,8	83,0	83,2	1018	1010	89,8	90,2	86,9	87,6	0,568	0,298	1,6	0,2	0,093	0,010	6,3	0,8	1,5	0,2	0,107	0,011
179	800	0,179	2,1	10	0,612	13,2	770,9	737,0	82,9	83,2	1018	1010	89,8	90,2	86,9	87,6	0,568	0,299	1,6	0,2	0,093	0,010	6,4	0,8	1,5	0,2	0,107	0,011
180	300	0,055	2,1	10	0,625	13,5	771,1	737,1	83,9	84,4	1014	1011	90,2	90,6	88,2	87,5	0,494	0,322	1,0	0,2	0,148	0,024	4,0	0,7	1,0	0,2	0,171	0,027
181	300	0,054	2,1	10	0,624	13,5	771,2	737,1	84,0	84,5	1014	1011	90,2	90,6	88,2	87,4	0,493	0,323	1,0	0,2	0,150	0,024	3,9	0,7	1,0	0,2	0,173	0,028
182	2300	0,881	2,1	10	0,618	13,3	770,6	737,0	82,0	82,7	1048	1017	90,4	90,5	86,4	89,5	0,620	0,279	2,1	0,2	0,072	0,006	8,3	0,8	1,9	0,2	0,085	0,007
183	2300	0,872	2,1	10	0,623	13,5	770,4	736,7	82,3	82,7	1048	1018	90,5	90,6	86,4	89,5	0,619	0,279	2,1	0,2	0,072	0,006	8,3	0,8	1,9	0,2	0,085	0,007
184	1800	0,596	2,1	10	0,621	13,4	770,2	736,8	82,4	82,8	1038	1017	90,3	90,4	86,5	88,8	0,609	0,281	2,0	0,2	0,075	0,007	8,0	0,8	1,9	0,2	0,088	0,007
185	1800	0,596	2,1	10	0,624	13,5	770,4	736,9	82,3	82,8	1039	1018	90,3	90,5	86,6	88,9	0,608	0,280	2,0	0,2	0,075	0,007	8,0	0,8	1,9	0,2	0,088	0,007
186	1300	0,358	2,1	10	0,625	13,5	770,5	736,9	82,5	83,1	1031	1018	90,1	90,3	86,7	88,2	0,593	0,285	1,8	0,2	0,080	0,008	7,5	0,8	1,8	0,2	0,093	0,008
187	1300	0,361	2,1	10	0,624	13,5	770,3	736,9	82,6	83,1	1031	1017	90,1	90,3	86,7	88,2	0,592	0,285	1,8	0,2	0,081	0,008	7,4	0,8	1,8	0,2	0,094	0,008
188	800	0,186	2,1	10	0,612	13,2	770,7	737,0	82,9	83,5	1024	1016	90,0	90,4	87,2	87,8	0,562	0,294	1,6	0,2	0,093	0,010	6,3	0,7	1,5	0,2	0,107	0,011
189	800	0,187	2,0	10	0,610	13,2	770,8	737,0	83,0	83,5	1024	1016	90,1	90,4	87,2	87,9	0,563	0,293	1,6	0,2	0,093	0,010	6,3	0,7	1,5	0,2	0,107	0,011
190	300	0,052	2,0	10	0,612	13,2	771,2	737,0	84,2	84,7	1018	1016	90,4	90,8	88,4	87,4	0,489	0,319	1,0	0,2	0,150	0,024	3,9	0,7	1,0	0,2	0,172	0,028
191	300	0,052	2,1	10	0,625	13,5	771,2	737,3	83,9	84,7	1017	1015	90,4	90,8	88,4	87,4	0,487	0,319	1,0	0,2	0,152	0,025	3,9	0,7	0,9	0,2	0,174	0,028
192	1300	0,361	2,1	10	0,618	13,4	770,6	736,8	82,7	83,1	1028	1015	90,1	90,4	86,7	88,2	0,586	0,280	1,8	0,2	0,081	0,008	7,3	0,8	1,8	0,2	0,094	0,008
193	1300	0,359	2,1	10	0,619	13,4	770,7	736,8	82,8	83,1	1028	1014	90,1	90,4	86,7	88,2	0,586	0,280	1,8	0,2	0,081	0,008	7,4	0,8	1,8	0,2	0,094	0,008
194	1800	0,591	2,1	10	0,624	13,5	770,3	736,8	82,5	82,8	1036	1014	90,3	90,5	86,6	88,9	0,602	0,275	2,0	0,2	0,075	0,007	8,0	0,8	1,9	0,2	0,088	0,007
195	1800	0,588	2,1	10	0,623	13,5	770,3	736,9	82,5	82,9	1036	1014	90,3	90,5	86,6	88,9	0,599	0,274	1,9	0,2	0,076	0,007	7,9	0,8	1,9	0,2	0,088	0,007
196	2300	0,865	2,1	10	0,637	13,7	770,1	737,0	82,3	82,7	1045	1015	90,6	90,7	86,5	89,6	0,609	0,271	2,0	0,2	0,073	0,007	8,4	0,8	1,9	0,2	0,085	0,007
197	2300	0,866	2,1	10	0,637	13,8	770,1	736,9	82,3	82,7	1045	1015	90,6	90,7	86,5	89,6	0,609	0,270	2,0	0,2	0,072	0,006	8,5	0,8	1,9	0,2	0,085	0,007
202	2300	0,859	3,0	14	0,902	19,5	766,8	736,8	82,0	82,4	1050	1015	90,3	90,4	86,0	89,2	0,636	0,293	2,1	0,2	0,071	0,006	12,3	1,3	2,0	0,2	0,085	0,007
203	2300	0,859	3,0	14	0,900	19,4	766,8	736,8	82,0	82,4	1050	1015	90,3	90,5	86,0	89,2	0,636	0,293	2,1	0,2	0,071	0,006	12,2	1,3	1,9	0,2	0,085	0,007
204	1800	0,580	3,0	14	0,891	19,3	767,1	736,9	82,2	82,5	1038	1013	90,0	90,2	86,2	88,4	0,621	0,298	2,0	0,2	0,076	0,007	11,4	1,2	1,8	0,2	0,090	0,008
205	1800	0,580	3,0	14	0,887	19,2	767,2	736,9	82,2	82,6	1038	1014	90,0	90,2	86,2	88,4	0,619	0,298	1,9	0,2	0,076	0,007	11,2	1,2	1,8	0,2	0,090	0,008
206	1300	0,361	3,0	14	0,891	19,2	767,4	737,0	82,4	82,9	1029	1013	89,8	90,2	86,5	87,7	0,597	0,305	1,7	0,2	0,085	0,009	10,1	1,2	1,7	0,2	0,099	0,010
207	1300	0,364	3,0	14	0,887	19,2	767,3	737,0	82,4	82,9	1029	1013	89,8	90,2	86,5	87,8	0,597	0,305	1,7	0,2	0,085	0,009	10,1	1,2	1,7	0,2	0,099	0,010
208	800	0,187	3,0	14	0,907	19,6	767,6	737,0	83,0	83,4	1021	1012	89,8	90,3	87,1	87,4	0,559	0,317	1,4	0,2	0,104	0,012	8,4	1,1	1,4	0,2	0,120	0,014
209	800	0,188	3,0	14	0,904	19,5	767,6	737,0	83,0	83,4	1021	1012	89,8	90,3	87,1	87,4	0,560	0,317	1,4	0,2	0,103	0,012	8,4	1,1	1,4	0,2	0,120	0,014
210	300	0,053	3,0	14	0,889	19,2	768,3	737,1	84,0	84,5	1015	1011	89,9	90,3	88,2	86,8	0,491	0,341	0,9	0,2	0,170	0,031	4,9	1,0	0,8	0,2	0,197	0,036
211	300	0,053	3,0	14	0,888	19,2	768,3	737,1	84,0	84,5	1015	1012	89,9	90,3	88,2	86,8	0,491	0,341	0,9	0,2	0,170	0,031	4,9	1,0	0,8	0,2	0,197	0,036
212	300	0,055	3,0	14	0,902	19,5	768,3	737,2	84,0	84,4	1010	1007	89,8	90,2	88,1	86,7	0,488	0,339	0,9	0,2	0,172	0,032	5,0	1,0	0,8	0,2	0,198	0,036
213	300	0,055	3,0	14	0,893	19,3	768,3	737,1	84,0	84,4	1010	1007	89,8	90,2	88,1	86,6	0,488	0,338	0,9	0,2	0,171	0,031	5,0	1,0	0,8	0,2	0,197	0,036
214	800	0,182	3,0	14	0,892	19,3	767,7	737,1	83,0	83,3	1016	1007	89,8	90,2	87,0	87,3	0,555	0,314	1,4	0,2	0,104	0,013	8,2	1,1	1,4	0,2	0,120	0,015
215	800	0,181	3,0	14	0,890	19,2	767,7	737,1	83,0	83,4	1016	1007	89,8	90,2	87,0	87,3	0,555	0,313	1,4	0,2	0,104	0,013	8,2	1,1	1,4	0,2	0,120	0,015
216	1300	0,366	3,0	14	0,889	19,2	767,5	737,0	82,5	82,8	1023	1007	89,8	90,1	86,5	87,7	0,590	0,300	1,7	0,2	0,085	0,009	10,1	1,1	1,7	0,2	0,100	0,010
217	1300	0,365	3,0	14	0,892	19,3	767,4	737,0	82,5	82,8	1022	1007	89,8	90,1	86,5	87,7	0,590	0,300	1,7	0,2	0,086	0,009	10,1	1,2	1,7	0,2	0,100	0,010
218	1800	0,574	3,0	14	0,878	19,0	767,2	737,0	82,2	82,5	1030	1006	89,9	90,2	86,2	88,4	0,612	0,293	1,9	0,2	0,077	0,007	11,1	1,2	1,8	0,2	0,091	0,008
219	1800	0,574	3,0	14	0,892	19,3	767,3	737,0	82,2	82,5	1031	1007	90,0	90,2	86,2	88,4	0,610	0,292	1,9	0,2	0,077	0,007	11,2	1,2	1,8	0,2	0,091	0,008
220	2300	0,787	3,0	14	0,894	19,3	767,0	737,0	82,0	82,4	1043	1009	90,3	90,5	86,0	89,2	0,625	0,285	2,1	0,2	0,072	0,007	12,0	1,2	1,9	0,2	0,085	0,007
221	2300	0,786	3,0	14	0,898	19,4	767,0	737,0	82,0	82,4	1043	1009	90,3	90,5	86,1	89,2	0,624	0,285	2,1	0,2	0,072	0,007	12,1	1,2	1,9	0,2	0,085	0,007
222	300	0,057	1,1	6	0,334	7,2	777,2	737,0	83,5	84,2	1025	1024	90,2	90,6	87,9	87,3	0,527	0,312	1,3	0,2	0,118	0,016	2,7	0,4	1,2	0,2	0,135	0,018
223	300	0,056	1,1	6	0,332	7,2	777,2	736,9	83,6	84,2	1024	1023	90,1	90,6	87,9	87,3	0,527	0,315	1,2	0,2	0,119	0,016	2,6	0,4	1,2	0,2	0,137	0,019
224	800	0,180	1,1	6	0,323	7,0	776,7	736,5	83,0	83,2	1026	1022	89,8	90,0	86,7	87,8	0,591	0,294	1,8	0,2	0,083	0,008	3,7	0,4	1,7	0,2	0,097	0,009
225	800	0,179	1,1	6	0,324	7,0	777,0	736,6	82,9	83,2	1026	1022	89,8	90,0	86,7	87,8	0,591	0,292	1,8	0,2	0,083	0,008	3,8	0,4	1,7	0,2	0,096	0,009
226	1300	0,354	1,1	6	0,332	7,2	776,5	736,9	82,4	83,0	1031	1022	89,9	90,0	86,4	88,2	0,607	0,287	1,9	0,2	0,077	0,007	4,2	0,4	1,8	0,2	0,090	0,008
227	1300	0,353	1,1	6	0,333	7,2	776,3	736,9	82,4	82,9	1029	1020	89,8	90,0	86,3	88,2	0,605	0,286	1,9	0,2	0,077	0,007	4,1	0,4	1,8	0,2	0,090	0,008
228	1800	0,575	1,1	6	0,334	7,2	776,0	736,9	82,2	82,8	1036	1020	90,1	90,1	86,2	88,8	0,616	0,282	2,0	0,2	0,073	0,007	4,4	0,5	1,9	0,2	0,086	0,007
229	1800	0,573	1,1	6	0,331	7,2	776,2	736,9	82,2	82,8	1036	1020	90,1	90,1	86,2	88,8	0,615	0,282	2,0	0,2	0,073	0,007	4,3	0,4	1,9	0,2	0,087	0,007
230	2300	0,847	1,2	6	0,344	7,4	775,6	736,8	82,2	82,7	1044	1019	90,3	90,3	86,4	89,4	0,619	0,279	2,1	0,2	0,072	0,007	4,6	0,5	1,9	0,2	0,085	0,007
231	2300	0,842	1,2	6	0,345	7,5	775,5	736,9	82,2	82,7	1042	1018	90,3	90,3	86,3	89,4	0,618	0,278	2,1	0,2	0,072	0,007	4,6	0,5	1,9	0,2	0,085	0,007
232	300	0,056	1,1	6	0,330	7,1	777,1	736,8	83,8	84,1	1015	1015	90,0	90,4	87,7	87,3	0,523	0,311	1,2	0,2	0,119	0,016	2,6	0,4	1,2	0,2	0,136	0,019
233	300	0,056	1,1	6	0,330	7,1	776,9	736,8	83,8	84,0	1014	1013	90,0	90,4	87,7	87,3	0,523	0,311	1,2	0,2	0,120	0,016	2,6	0,4	1,2	0,2	0,137	0,019
234	1300	0,354	1,1	6	0,330	7,1	776,1	736,8	82,6	82,8	1022	1012	89,7	89,9	86,2	88,1	0,600	0,283	1,9	0,2	0,078	0,007	4,1	0,4	1,8	0,2	0,091	0,008
235	1300	0,353	1,1	6	0,330	7,1	775,9	736,8	82,6	82,8	1022	1012	89,7	89,9	86,2	88,1	0,598	0,282	1,9	0,2	0,078	0,007	4,1	0,4	1,8	0,2	0,091	0,008
236	2300	0,846	1,2	6	0,349	7,5	775,4	736,8	82,3	82,6	1035	1010	90,2	90,2	86,3	89,3	0,611	0,275	2,0	0,2	0,073	0,007	4,6	0,5	1,9	0,2	0,086	0,007
237	2300	0,845	1,2	6	0,352	7,6	775,3	736,9	82,3	82,6	1035	1011	90,2	90,2	86,3	89,3	0,612	0,274	2,0	0,2	0,073	0,007	4,7	0,5	1,9	0,2	0,085	0,007

Ethanol/n-Propanol (no packing), Sample locations S3/S4, 0.7mm jet nozzle

	nRot	RPB_Peff	F	Qreb	mDist	LLeye	rhoL	rhoLfeed	TLfeed	TLVfeed	PI01	PI02	TI03	TI04	TI05	TI12	wi	wo	NTUg	delta NTUg	ATUg	delta ATUg	KGa	delta KGa	Nth_oi	delta Nth_oi	HETP_oi	delta HETP_oi
Unit	RPM	kW	Pa^0.5	kW	kg/min	m3/m2/h	kg/m3	kg/m3	°C	°C	mbar	mbar	°C	°C	°C	°C	g EtOH/g Mix	g EtOH/g Mix			m2	m2	1/s	1/s			m	m
Note / Steady State No.	of RPB		at eye	reboiler duty	FI02		DI02	DI02 at TIfeed	TI08	bubble point temperature of S4 at PI02							S4 weight frac.	S3 weight frac.	NTU (overall vapor)	uncertainty of NTUg				uncertainty of Kga	oi -> calculated starting at wo until wi is reached			
178	800	0,179	2,0	10	0,607	13,1	770,8	736,8	83,0	83,2	1018	1010	89,8	90,2	86,9	87,6	0,568	0,360	1,2	0,2	0,120	0,017	4,9	0,8	1,2	0,2	0,142	0,022
179	800	0,179	2,1	10	0,612	13,2	770,9	737,0	82,9	83,2	1018	1010	89,8	90,2	86,9	87,6	0,568	0,341	1,3	0,2	0,110	0,014	5,4	0,8	1,3	0,2	0,129	0,017
180	300	0,055	2,1	10	0,625	13,5	771,1	737,1	83,9	84,4	1014	1011	90,2	90,6	88,2	87,5	0,494	0,333	0,9	0,2	0,159	0,027	3,7	0,7	0,9	0,2	0,184	0,031
181	300	0,054	2,1	10	0,624	13,5	771,2	737,1	84,0	84,5	1014	1011	90,2	90,6	88,2	87,4	0,493	0,331	0,9	0,2	0,158	0,027	3,8	0,7	0,9	0,2	0,182	0,031
182	2300	0,881	2,1	10	0,618	13,3	770,6	737,0	82,0	82,7	1048	1017	90,4	90,5	86,4	89,5	0,620	0,427	1,2	0,2	0,123	0,020	4,8	0,8	1,1	0,2	0,154	0,029
183	2300	0,872	2,1	10	0,623	13,5	770,4	736,7	82,3	82,7	1048	1018	90,5	90,6	86,4	89,5	0,619	0,431	1,2	0,2	0,126	0,021	4,7	0,8	1,0	0,2	0,158	0,031
184	1800	0,596	2,1	10	0,621	13,4	770,2	736,8	82,4	82,8	1038	1017	90,3	90,4	86,5	88,8	0,609	0,438	1,1	0,2	0,140	0,026	4,3	0,8	0,9	0,2	0,175	0,029
185	1800	0,596	2,1	10	0,624	13,5	770,4	736,9	82,3	82,8	1039	1018	90,3	90,5	86,6	88,9	0,608	0,438	1,0	0,2	0,141	0,026	4,3	0,8	0,9	0,2	0,176	0,029
186	1300	0,358	2,1	10	0,625	13,5	770,5	736,9	82,5	83,1	1031	1018	90,1	90,3	86,7	88,2	0,593	0,410	1,1	0,2	0,133	0,022	4,5	0,8	1,0	0,2	0,165	0,028
187	1300	0,361	2,1	10	0,624	13,5	770,3	736,9	82,6	83,1	1031	1017	90,1	90,3	86,7	88,2	0,592	0,428	1,0	0,2	0,148	0,028	4,0	0,8	0,9	0,2	0,183	0,031
188	800	0,186	2,1	10	0,612	13,2	770,7	737,0	82,9	83,5	1024	1016	90,0	90,4	87,2	87,8	0,562	0,430	0,8	0,2	0,186	0,042	3,2	0,8	0,7	0,2	0,224	0,048
189	800	0,187	2,0	10	0,610	13,2	770,8	737,0	83,0	83,5	1024	1016	90,1	90,4	87,2	87,9	0,563	0,437	0,8	0,2	0,195	0,047	3,0	0,8	0,7	0,2	0,236	0,053
190	300	0,052	2,0	10	0,612	13,2	771,2	737,0	84,2	84,7	1018	1016	90,4	90,8	88,4	87,4	0,489	0,344	0,8	0,2	0,177	0,034	3,3	0,7	0,8	0,2	0,204	0,038
191	300	0,052	2,1	10	0,625	13,5	771,2	737,3	83,9	84,7	1017	1015	90,4	90,8	88,4	87,4	0,487	0,341	0,8	0,2	0,176	0,033	3,4	0,7	0,8	0,2	0,203	0,038
192	1300	0,361	2,1	10	0,618	13,4	770,6	736,8	82,7	83,1	1028	1015	90,1	90,4	86,7	88,2	0,586	0,380	1,2	0,2	0,120	0,018	5,0	0,8	1,1	0,2	0,144	0,023
193	1300	0,359	2,1	10	0,619	13,4	770,7	736,8	82,8	83,1	1028	1014	90,1	90,4	86,7	88,2	0,586	0,399	1,1	0,2	0,131	0,021	4,5	0,8	1,0	0,2	0,161	0,030
194	1800	0,591	2,1	10	0,624	13,5	770,3	736,8	82,5	82,8	1036	1014	90,3	90,5	86,6	88,9	0,602	0,425	1,1	0,2	0,136	0,024	4,4	0,8	1,0	0,2	0,170	0,027
195	1800	0,588	2,1	10	0,623	13,5	770,3	736,9	82,5	82,9	1036	1014	90,3	90,5	86,6	88,9	0,599	0,429	1,0	0,2	0,142	0,026	4,2	0,8	0,9	0,2	0,177	0,029
196	2300	0,865	2,1	10	0,637	13,7	770,1	737,0	82,3	82,7	1045	1015	90,6	90,7	86,5	89,6	0,609	0,424	1,1	0,2	0,130	0,022	4,7	0,8	1,0	0,2	0,163	0,031
197	2300	0,866	2,1	10	0,637	13,8	770,1	736,9	82,3	82,7	1045	1015	90,6	90,7	86,5	89,6	0,609	0,425	1,1	0,2	0,131	0,022	4,7	0,8	1,0	0,2	0,164	0,030
202	2300	0,859	3,0	14	0,902	19,5	766,8	736,8	82,0	82,4	1050	1015	90,3	90,4	86,0	89,2	0,636	0,422	1,3	0,2	0,110	0,016	7,9	1,3	1,2	0,2	0,136	0,022
203	2300	0,859	3,0	14	0,900	19,4	766,8	736,8	82,0	82,4	1050	1015	90,3	90,5	86,0	89,2	0,636	0,447	1,2	0,2	0,124	0,021	7,0	1,3	1,1	0,2	0,157	0,031
204	1800	0,580	3,0	14	0,891	19,3	767,1	736,9	82,2	82,5	1038	1013	90,0	90,2	86,2	88,4	0,621	0,378	1,5	0,2	0,100	0,013	8,6	1,2	1,4	0,2	0,120	0,016
205	1800	0,580	3,0	14	0,887	19,2	767,2	736,9	82,2	82,6	1038	1014	90,0	90,2	86,2	88,4	0,619	0,380	1,5	0,2	0,101	0,013	8,5	1,2	1,4	0,2	0,122	0,016
206	1300	0,361	3,0	14	0,891	19,2	767,4	737,0	82,4	82,9	1029	1013	89,8	90,2	86,5	87,7	0,597	0,343	1,5	0,2	0,097	0,012	8,8	1,2	1,4	0,2	0,115	0,014
207	1300	0,364	3,0	14	0,887	19,2	767,3	737,0	82,4	82,9	1029	1013	89,8	90,2	86,5	87,8	0,597	0,338	1,5	0,2	0,096	0,011	9,0	1,2	1,5	0,2	0,113	0,013
208	800	0,187	3,0	14	0,907	19,6	767,6	737,0	83,0	83,4	1021	1012	89,8	90,3	87,1	87,4	0,559	0,330	1,3	0,2	0,110	0,014	7,9	1,1	1,3	0,2	0,127	0,017
209	800	0,188	3,0	14	0,904	19,5	767,6	737,0	83,0	83,4	1021	1012	89,8	90,3	87,1	87,4	0,560	0,330	1,4	0,2	0,109	0,014	7,9	1,1	1,3	0,2	0,127	0,017
210	300	0,053	3,0	14	0,889	19,2	768,3	737,1	84,0	84,5	1015	1011	89,9	90,3	88,2	86,8	0,491	0,336	0,9	0,2	0,165	0,029	5,1	1,0	0,9	0,2	0,190	0,033
211	300	0,053	3,0	14	0,888	19,2	768,3	737,1	84,0	84,5	1015	1012	89,9	90,3	88,2	86,8	0,491	0,334	0,9	0,2	0,163	0,029	5,2	1,0	0,9	0,2	0,188	0,033
212	300	0,055	3,0	14	0,902	19,5	768,3	737,2	84,0	84,4	1010	1007	89,8	90,2	88,1	86,7	0,488	0,329	0,9	0,2	0,160	0,028	5,4	1,0	0,9	0,2	0,184	0,031
213	300	0,055	3,0	14	0,893	19,3	768,3	737,1	84,0	84,4	1010	1007	89,8	90,2	88,1	86,6	0,488	0,328	0,9	0,2	0,160	0,027	5,3	1,0	0,9	0,2	0,184	0,031
214	800	0,182	3,0	14	0,892	19,3	767,7	737,1	83,0	83,3	1016	1007	89,8	90,2	87,0	87,3	0,555	0,327	1,3	0,2	0,110	0,014	7,8	1,1	1,3	0,2	0,128	0,017
215	800	0,181	3,0	14	0,890	19,2	767,7	737,1	83,0	83,4	1016	1007	89,8	90,2	87,0	87,3	0,555	0,323	1,4	0,2	0,109	0,014	7,9	1,1	1,3	0,2	0,126	0,016
216	1300	0,366	3,0	14	0,889	19,2	767,5	737,0	82,5	82,8	1023	1007	89,8	90,1	86,5	87,7	0,590	0,330	1,5	0,2	0,095	0,011	9,0	1,1	1,5	0,2	0,112	0,013
217	1300	0,365	3,0	14	0,892	19,3	767,4	737,0	82,5	82,8	1022	1007	89,8	90,1	86,5	87,7	0,590	0,324	1,6	0,2	0,093	0,011	9,3	1,2	1,5	0,2	0,109	0,012
218	1800	0,574	3,0	14	0,878	19,0	767,2	737,0	82,2	82,5	1030	1006	89,9	90,2	86,2	88,4	0,612	0,414	1,2	0,2	0,122	0,019	7,0	1,2	1,1	0,2	0,150	0,027
219	1800	0,574	3,0	14	0,892	19,3	767,3	737,0	82,2	82,5	1031	1007	90,0	90,2	86,2	88,4	0,610	0,400	1,3	0,2	0,116	0,017	7,5	1,2	1,2	0,2	0,141	0,023
220	2300	0,787	3,0	14	0,894	19,3	767,0	737,0	82,0	82,4	1043	1009	90,3	90,5	86,0	89,2	0,625	0,403	1,4	0,2	0,108	0,015	8,0	1,2	1,3	0,2	0,132	0,020
221	2300	0,786	3,0	14	0,898	19,4	767,0	737,0	82,0	82,4	1043	1009	90,3	90,5	86,1	89,2	0,624	0,436	1,2	0,2	0,126	0,021	6,9	1,2	1,0	0,2	0,158	0,031
222	300	0,057	1,1	6	0,334	7,2	777,2	737,0	83,5	84,2	1025	1024	90,2	90,6	87,9	87,3	0,527	0,436	0,5	0,2	0,275	0,089	1,1	0,4	0,5	0,2	0,323	0,100
223	300	0,056	1,1	6	0,332	7,2	777,2	736,9	83,6	84,2	1024	1023	90,1	90,6	87,9	87,3	0,527	0,445	0,5	0,2	0,303	0,110	1,0	0,4	0,5	0,2	0,355	0,122
224	800	0,180	1,1	6	0,323	7,0	776,7	736,5	83,0	83,2	1026	1022	89,8	90,0	86,7	87,8	0,591	0,449	0,9	0,2	0,169	0,037	1,8	0,4	0,8	0,2	0,208	0,041
225	800	0,179	1,1	6	0,324	7,0	777,0	736,6	82,9	83,2	1026	1022	89,8	90,0	86,7	87,8	0,591	0,452	0,9	0,2	0,173	0,038	1,8	0,4	0,8	0,2	0,212	0,043
226	1300	0,354	1,1	6	0,332	7,2	776,5	736,9	82,4	83,0	1031	1022	89,9	90,0	86,4	88,2	0,607	0,448	1,0	0,2	0,150	0,029	2,1	0,4	0,9	0,2	0,187	0,033
227	1300	0,353	1,1	6	0,333	7,2	776,3	736,9	82,4	82,9	1029	1020	89,8	90,0	86,3	88,2	0,605	0,448	1,0	0,2	0,152	0,030	2,1	0,4	0,9	0,2	0,189	0,034
228	1800	0,575	1,1	6	0,334	7,2	776,0	736,9	82,2	82,8	1036	1020	90,1	90,1	86,2	88,8	0,616	0,446	1,1	0,2	0,140	0,026	2,3	0,5	0,9	0,2	0,176	0,029
229	1800	0,573	1,1	6	0,331	7,2	776,2	736,9	82,2	82,8	1036	1020	90,1	90,1	86,2	88,8	0,615	0,444	1,1	0,2	0,139	0,026	2,3	0,4	0,9	0,2	0,175	0,029
230	2300	0,847	1,2	6	0,344	7,4	775,6	736,8	82,2	82,7	1044	1019	90,3	90,3	86,4	89,4	0,619	0,438	1,1	0,2	0,131	0,023	2,5	0,5	1,0	0,2	0,166	0,029
231	2300	0,842	1,2	6	0,345	7,5	775,5	736,9	82,2	82,7	1042	1018	90,3	90,3	86,3	89,4	0,618	0,438	1,1	0,2	0,132	0,023	2,5	0,5	1,0	0,2	0,167	0,028
232	300	0,056	1,1	6	0,330	7,1	777,1	736,8	83,8	84,1	1015	1015	90,0	90,4	87,7	87,3	0,523	0,429	0,6	0,2	0,266	0,083	1,2	0,4	0,5	0,2	0,312	0,093
233	300	0,056	1,1	6	0,330	7,1	776,9	736,8	83,8	84,0	1014	1013	90,0	90,4	87,7	87,3	0,523	0,435	0,5	0,2	0,285	0,096	1,1	0,4	0,5	0,2	0,334	0,107
234	1300	0,354	1,1	6	0,330	7,1	776,1	736,8	82,6	82,8	1022	1012	89,7	89,9	86,2	88,1	0,600	0,441	1,0	0,2	0,152	0,030	2,1	0,4	0,9	0,2	0,188	0,034
235	1300	0,353	1,1	6	0,330	7,1	775,9	736,8	82,6	82,8	1022	1012	89,7	89,9	86,2	88,1	0,598	0,442	1,0	0,2	0,155	0,031	2,1	0,4	0,9	0,2	0,191	0,035
236	2300	0,846	1,2	6	0,349	7,5	775,4	736,8	82,3	82,6	1035	1010	90,2	90,2	86,3	89,3	0,611	0,432	1,1	0,2	0,133	0,023	2,5	0,5	1,0	0,2	0,167	0,027
237	2300	0,845	1,2	6	0,352	7,6	775,3	736,9	82,3	82,6	1035	1011	90,2	90,2	86,3	89,3	0,612	0,434	1,1	0,2	0,134	0,024	2,5	0,5	1,0	0,2	0,169	0,027

Ethanol/n-Propanol with packing, Sample locations S6/S4, 0.7mm jet nozzle

	nRot	RPB_Peff	F	Qreb	mDist	LLeye	rhoL	rhoLfeed	TLfeed	TLVfeed	PI01	PI02	TI03	TI04	TI05	TI12	wi	wo	NTUg	delta NTUg	ATUg	delta ATUg	KGa	delta KGa	Nth_oi	delta Nth_oi	HETP_oi	delta HETP_oi
Unit	RPM	kW	Pa^0.5	kW	kg/min	m3/m2/h	kg/m3	kg/m3	°C	°C	mbar	mbar	°C	°C	°C	°C	g EtOH/g Mix	g EtOH/g Mix			m2	m2	1/s	1/s			m	m
Note / Steady State No.	of RPB		at eye	reboiler duty	FI02		DI02	DI02 at Tlfeed	TI08	bubble point temperature of S4 at PI02							S4 weight frac.	S6 weight frac.	NTU (overall vapor)	uncertainty of NTUg				uncertainty of Kga	oi -> calculated starting at wo until wi is reached			
066	800	0,172	2,0	10	0,587	12,7	769,7	736,7	80,0	80,4	1008	1003	95,1	95,2	85,7	93,6	0,770	0,067	5,2	0,3	0,028	0,002	21,3	1,4	5,4	0,3	0,031	0,002
067	800	0,172	2,0	10	0,585	12,6	769,3	736,6	80,0	80,3	1008	1003	95,1	95,2	85,7	93,6	0,775	0,066	5,3	0,3	0,028	0,002	21,6	1,5	5,4	0,3	0,030	0,002
068	1300	0,346	2,0	10	0,580	12,5	768,5	736,2	79,0	79,4	1015	1005	96,5	96,5	81,4	95,4	0,867	0,023	7,7	0,5	0,019	0,001	31,5	2,5	7,9	0,4	0,021	0,001
069	1300	0,347	2,0	10	0,577	12,5	768,7	736,2	79,1	79,5	1016	1005	96,5	96,5	81,4	95,4	0,860	0,023	7,6	0,5	0,019	0,001	30,9	2,4	7,9	0,4	0,021	0,001
070	1800	0,560	2,0	10	0,572	12,4	768,6	736,0	79,0	79,3	1025	1006	97,1	97,1	81,3	96,2	0,877	0,012	8,6	0,6	0,017	0,001	34,7	3,0	9,1	0,8	0,018	0,002
071	1800	0,560	2,0	10	0,581	12,6	768,6	736,1	79,0	79,3	1026	1006	97,1	97,1	81,4	96,2	0,875	0,012	8,6	0,6	0,017	0,001	35,1	3,0	9,1	0,8	0,018	0,002
072	800	0,174	2,0	10	0,586	12,7	769,2	736,1	80,6	81,0	1033	1028	95,5	95,6	86,1	93,9	0,771	0,074	5,1	0,3	0,029	0,002	20,5	1,4	5,2	0,3	0,032	0,002
073	800	0,173	2,0	10	0,585	12,6	769,2	736,0	80,6	81,0	1033	1028	95,5	95,7	86,1	93,9	0,776	0,075	5,2	0,3	0,029	0,002	20,6	1,4	5,3	0,3	0,031	0,002
074	300	0,057	2,1	10	0,620	13,4	771,3	736,7	84,4	84,9	1030	1028	93,7	93,9	88,6	91,3	0,494	0,180	1,9	0,2	0,076	0,006	7,6	0,7	2,0	0,2	0,081	0,007
075	300	0,057	2,1	10	0,620	13,4	771,4	736,6	84,4	84,9	1030	1028	93,7	93,9	88,7	91,3	0,494	0,179	1,9	0,2	0,076	0,006	7,6	0,7	2,0	0,2	0,081	0,007
076	2300	0,873	2,0	10	0,592	12,8	767,4	735,2	78,7	79,2	1056	1028	91,7	91,8	80,1	90,8	0,945	0,231	6,9	0,9	0,021	0,003	28,2	4,0	5,8	0,6	0,028	0,003
077	2300	0,874	2,1	10	0,595	12,9	767,3	735,2	78,7	79,2	1056	1028	91,7	91,9	80,1	90,8	0,945	0,227	6,9	0,9	0,021	0,003	28,5	4,1	5,9	0,6	0,028	0,003
088	800	0,173	2,9	14	0,845	18,3	765,3	736,6	79,0	79,4	1002	995	91,8	92,2	83,0	89,7	0,844	0,205	4,7	0,4	0,031	0,002	28,2	2,5	4,3	0,4	0,039	0,003
089	800	0,173	2,9	14	0,842	18,2	765,2	736,5	79,0	79,4	1002	995	91,8	92,2	83,0	89,8	0,844	0,203	4,7	0,4	0,031	0,002	28,2	2,5	4,3	0,3	0,039	0,003
090	1800	0,566	2,9	14	0,822	17,8	764,1	736,0	77,8	78,3	1017	997	92,6	92,8	79,2	91,4	0,956	0,158	7,9	1,1	0,019	0,003	46,6	7,1	6,8	0,8	0,024	0,003
091	1800	0,563	2,9	14	0,822	17,8	764,0	736,0	77,8	78,3	1018	998	92,6	92,8	79,2	91,5	0,958	0,161	8,0	1,2	0,018	0,003	47,2	7,5	6,9	0,8	0,024	0,003
092	2300	0,860	3,0	14	0,842	18,2	763,9	736,0	77,9	78,4	1030	999	92,8	93,0	79,3	91,9	0,949	0,162	7,6	1,0	0,020	0,002	45,3	6,4	6,6	0,7	0,025	0,003
093	2300	0,869	3,0	14	0,848	18,3	764,0	736,1	77,9	78,4	1029	998	92,8	93,0	79,3	91,9	0,948	0,161	7,5	0,9	0,020	0,002	45,3	6,3	6,6	0,7	0,025	0,003
094	300	0,052	3,0	14	0,875	18,9	768,0	737,2	82,1	82,4	1003	999	90,8	91,3	85,9	88,3	0,604	0,277	2,0	0,2	0,075	0,007	11,4	1,2	1,9	0,2	0,088	0,007
095	300	0,052	3,0	14	0,876	18,9	767,9	737,2	82,1	82,4	1004	1000	90,8	91,3	85,9	88,4	0,604	0,279	1,9	0,2	0,076	0,007	11,4	1,2	1,9	0,2	0,089	0,008
096	1300	0,345	3,0	14	0,845	18,3	764,7	736,1	78,2	78,7	1012	1000	92,8	93,1	81,1	91,4	0,926	0,155	6,8	0,7	0,022	0,002	41,0	4,6	6,0	0,5	0,028	0,002
097	1300	0,344	2,9	14	0,828	17,9	764,7	736,0	78,2	78,6	1012	1000	92,9	93,1	81,2	91,4	0,929	0,153	6,9	0,7	0,021	0,002	40,9	4,7	6,1	0,6	0,027	0,003
107	800	0,166	2,1	10	0,589	12,7	768,6	735,7	78,7	79,0	1014	1010	92,8	93,1	83,2	91,0	0,915	0,160	6,4	0,6	0,023	0,002	27,0	2,8	5,7	0,4	0,029	0,002
108	800	0,166	2,1	10	0,590	12,8	768,7	735,9	78,7	79,1	1014	1010	92,8	93,1	83,2	91,0	0,906	0,161	6,2	0,6	0,024	0,002	26,0	2,6	5,6	0,4	0,030	0,002
109	1300	0,357	2,0	10	0,572	12,4	768,2	735,6	77,9	78,3	1016	1006	93,6	93,8	82,2	92,4	0,979	0,120	9,8	2,5	0,015	0,004	40,8	10,8	8,5	1,8	0,019	0,004
110	1300	0,356	2,1	10	0,583	12,6	768,1	735,7	77,7	78,3	1015	1005	93,4	93,7	82,2	92,3	0,980	0,123	9,9	2,7	0,015	0,004	42,0	11,8	8,6	2,0	0,019	0,004
111	1800	0,557	2,0	10	0,583	12,6	768,3	735,7	78,1	78,5	1022	1004	93,4	93,6	79,4	92,4	0,960	0,127	8,4	1,2	0,018	0,003	35,0	5,5	7,4	1,0	0,022	0,003
112	1800	0,556	2,0	10	0,583	12,6	768,2	735,6	78,1	78,4	1021	1004	93,4	93,6	79,4	92,4	0,960	0,127	8,4	1,2	0,018	0,003	35,1	5,6	7,4	1,0	0,022	0,003
113	2300	0,834	2,1	10	0,590	12,8	768,3	736,0	78,1	78,6	1030	1003	93,4	93,5	80,1	92,6	0,936	0,135	7,3	0,8	0,020	0,002	30,6	3,7	6,5	0,6	0,025	0,002
114	2300	0,813	2,1	10	0,587	12,7	768,4	736,0	78,1	78,7	1030	1003	93,4	93,5	80,0	92,7	0,934	0,132	7,2	0,8	0,020	0,002	30,2	3,5	6,5	0,6	0,025	0,002
115	300	0,052	2,1	10	0,619	13,4	770,8	737,3	81,9	82,3	1003	1001	91,6	91,9	85,8	88,9	0,612	0,244	2,2	0,2	0,067	0,005	9,2	0,9	2,2	0,2	0,077	0,007
116	300	0,053	2,1	10	0,623	13,4	770,8	737,3	81,9	82,3	1003	1001	91,6	91,9	85,8	88,9	0,612	0,244	2,2	0,2	0,067	0,005	9,2	0,9	2,2	0,2	0,077	0,007
117	1300	0,343	2,0	10	0,583	12,6	768,1	736,0	78,0	78,3	1003	993	96,1	96,1	79,9	95,0	0,941	0,026	9,4	0,9	0,016	0,002	39,7	4,4	9,1	0,9	0,018	0,002
118	1300	0,334	2,0	10	0,582	12,6	768,1	736,0	78,0	78,3	1003	992	96,1	96,2	79,9	95,1	0,941	0,024	9,4	0,9	0,016	0,002	39,9	4,4	9,3	1,0	0,018	0,002
119	1800	0,542	2,1	10	0,584	12,6	768,0	735,9	78,0	78,2	1009	991	95,5	95,6	79,3	94,6	0,949	0,046	9,0	1,0	0,016	0,002	38,3	4,7	8,5	0,8	0,019	0,002
120	1800	0,542	2,0	10	0,579	12,5	768,0	735,8	78,0	78,2	1009	991	95,5	95,6	79,3	94,6	0,954	0,046	9,3	1,1	0,016	0,002	39,0	5,1	8,7	0,8	0,019	0,002
121	1800	0,545	3,0	14	0,841	18,2	764,4	736,1	77,6	78,1	1012	992	94,0	94,2	79,1	93,1	0,960	0,098	8,7	1,3	0,017	0,002	53,3	8,3	7,8	0,9	0,021	0,002
122	1800	0,547	2,9	14	0,834	18,0	764,4	736,2	77,5	78,1	1011	991	93,9	94,1	79,2	92,9	0,959	0,098	8,7	1,2	0,017	0,002	52,5	8,0	7,7	0,8	0,021	0,002
123	800	0,173	3,0	14	0,863	18,6	765,6	736,7	78,6	79,2	1003	995	91,9	92,3	82,8	89,9	0,854	0,195	4,9	0,4	0,030	0,002	30,3	2,7	4,5	0,3	0,037	0,003
124	800	0,172	3,0	14	0,857	18,5	765,7	736,8	78,6	79,3	1002	994	91,9	92,4	82,9	89,9	0,852	0,194	4,9	0,4	0,030	0,002	29,9	2,6	4,5	0,3	0,037	0,003
126	300	0,049	3,1	14	0,896	19,3	767,2	737,7	80,6	81,4	999	993	90,0	90,7	84,5	87,5	0,668	0,299	2,3	0,2	0,065	0,006	13,9	1,4	2,1	0,2	0,078	0,008
127	300	0,049	3,0	14	0,876	18,9	767,1	737,6	80,7	81,3	998	993	90,0	90,6	84,5	87,5	0,669	0,300	2,3	0,2	0,065	0,006	13,7	1,4	2,1	0,2	0,078	0,008
128	800	0,166	3,0	14	0,862	18,6	765,3	736,0	79,2	79,6	1020	1012	91,6	92,1	82,9	89,5	0,863	0,228	4,9	0,4	0,030	0,002	29,3	2,7	4,3	0,4	0,038	0,003
129	800	0,166	3,0	14	0,861	18,6	765,4	736,1	79,2	79,6	1020	1012	91,7	92,2	82,9	89,5	0,860	0,228	4,8	0,4	0,031	0,002	28,9	2,7	4,3	0,4	0,039	0,003
130	1300	0,328	3,0	14	0,852	18,4	764,4	735,8	78,2	78,8	1026	1012	92,1	92,5	79,8	90,6	0,942	0,197	7,0	0,9	0,021	0,003	42,2	5,7	6,0	0,6	0,028	0,003
131	1300	0,327	3,0	14	0,851	18,4	764,5	735,8	78,2	78,8	1025	1012	92,1	92,5	79,9	90,6	0,942	0,194	7,0	0,9	0,021	0,003	42,3	5,7	6,0	0,7	0,028	0,003
132	1800	0,547	3,0	14	0,850	18,4	764,1	735,5	78,2	78,7	1034	1013	93,0	93,3	79,5	91,9	0,957	0,160	7,9	1,1	0,019	0,003	47,7	7,4	6,8	0,8	0,024	0,003
133	1800	0,545	3,0	14	0,853	18,5	764,1	735,6	78,2	78,7	1034	1012	93,0	93,3	79,5	91,9	0,956	0,158	7,9	1,1	0,019	0,003	47,7	7,3	6,8	0,8	0,024	0,003
134	2300	0,845	3,0	14	0,853	18,5	764,2	735,7	78,2	78,7	1044	1012	93,1	93,3	79,6	92,2	0,951	0,161	7,6	1,0	0,019	0,002	45,9	6,6	6,7	0,7	0,025	0,003
135	2300	0,837	3,0	14	0,859	18,6	764,2	735,6	78,2	78,7	1044	1012	93,1	93,4	79,7	92,3	0,951	0,158	7,7	1,0	0,019	0,002	46,4	6,6	6,7	0,7	0,025	0,003
136	1300	0,343	2,0	10	0,571	12,3	768,1	735,6	78,1	78,7	1024	1014	93,0	93,2	81,1	91,7	0,965	0,153	8,4	1,4	0,017	0,003	34,4	6,1	7,3	1,2	0,023	0,004
137	1300	0,342	2,0	10	0,570	12,3	767,9	735,6	78,0	78,6	1024	1014	93,0	93,3	82,5	91,8	0,967	0,149	8,6	1,5	0,017	0,003	35,2	6,6	7,4	1,2	0,022	0,004
138	1300	0,342	2,0	10	0,578	12,5	767,9	735,4	78,4	78,7	1025	1014	94,0	94,2	82,5	92,8	0,957	0,113	8,4	1,1	0,018	0,002	34,6	5,2	7,5	0,9	0,022	0,003
139	1300	0,340	2,0	10	0,579	12,5	767,7	735,3	78,4	78,7	1025	1014	94,0	94,2	81,5	92,8	0,958	0,113	8,5	1,2	0,017	0,002	35,0	5,3	7,5	0,9	0,022	0,003
140	800	0,165	2,0	10	0,581	12,6	768,8	736,0	78,8	79,2	1014	1010	92,5	92,8	83,3	90,5	0,893	0,177	5,8	0,5	0,025	0,002	23,9	2,3	5,2	0,5	0,032	0,003
141	800	0,164	2,0	10	0,588	12,7	768,8	736,0	78,8	79,3	1014	1010	92,5	92,8	83,2	90,6	0,891	0,178	5,7	0,5	0,026	0,002	23,8	2,3	5,1	0,5	0,032	0,003
150	800	0,161	1,1	6	0,308	6,7	773,2	735,5	78,0	78,5	1018	1015	96,4	96,4	84,2	95,0	0,978	0,030	11,3	2,4	0,013	0,003	25,3	5,6	10,6	1,8	0,016	0,003
151	800	0,162	1,1	6	0,308	6,7	773,1	735,4	78,0	78,5	1018	1014	96,4	96,3	84,2	95,0	0,977	0,030	11,2	2,3	0,013	0,003	25,1	5,4	10,5	1,7	0,016	0,003
152	300	0,051	1,1	6	0,329	7,1	776,8	736,9	82,9	83,2	1015	1014	93,0	93,2	86,8	90,4	0,574	0,180	2,4	0,2	0,061	0,004	5,2	0,4	2,5	0,2	0,066	0,005
153	300	0,052	1,1	6	0,326	7,0	776,9	736,8	83,0	83,2	1015	1014	93,0	93,2	86,7	90,4	0,576	0,178	2,4	0,2	0,060	0,004	5,2	0,4	2,5	0,2	0,066	0,005
154	800	0,161	1,1	6	0,306	6,6	773,4	735,5	78,7	79,0	1016	1012	96,6	96,6	84,9	95,3	0,929	0,023	9,1	0,8	0,016	0,001	20,0	2,0	9,0	0,9	0,018	0,002
155	800	0,161	1,1	6	0,304	6,6	773,6	735,3	78,7	78,9	1016	1013	96,7	96,6	84,9	95,3	0,939	0,020	9,6	0,9	0,015	0,002	20,9	2,3	9,5	0,9	0,017	0,002
156	1300	0,320	1,1	6	0,304	6,6	773,7	735,7	78,0	78,6	1021	1012	96,5	96,4	80,9	95,4	0,961	0,029	10,2	1,3	0,015	0,002	22,2	3,2	9,7	1,0	0,017	0,002

Ethanol/n-Propanol with packing, Sample locations S6/S4, 0.7mm jet nozzle (contd.)

	nRot	RPB_Peff	F	Qreb	mDist	LLeye	rhoL	rhoLfeed	TLfeed	TLVfeed	PI01	PI02	TI03	TI04	TI05	TI12	wi	wo	NTUg	delta NTUg	ATUg	delta ATUg	KGa	delta KGa	Nth_oi	delta Nth_oi	HETP_oi	delta HETP_oi
Unit	RPM	kW	Pa^0.5	kW	kg/min	m3/m2/h	kg/m3	kg/m3	°C	°C	mbar	mbar	°C	°C	°C	°C	g EtOH/g Mix	g EtOH/g Mix			m2	m2	1/s	1/s			m	m
Note / Steady State No.	of RPB		at eye	reboiler duty	FI02		DI02	DI02 at TIfeed	TI08	bubble point temperature of S4 at PI02							S4 weight frac.	S6 weight frac.	NTU (overall vapor)	uncertainty of NTUg				uncertainty of Kga	oi -> calculated starting at wo until wi is reached			
157	1300	0,319	1,1	6	0,303	6,6	773,6	735,6	78,1	78,6	1019	1011	96,4	96,4	81,0	95,4	0,963	0,028	10,3	1,4	0,014	0,002	22,5	3,3	9,8	1,0	0,017	0,002
158	1300	0,327	1,1	6	0,299	6,5	774,1	735,4	78,0	78,5	1021	1012	95,1	95,1	83,5	94,0	0,980	0,073	10,6	2,7	0,014	0,003	22,9	6,1	9,4	1,9	0,018	0,003
159	1300	0,326	1,1	6	0,303	6,6	773,7	735,4	78,0	78,5	1019	1011	95,0	95,0	83,5	93,9	0,978	0,072	10,4	2,3	0,014	0,003	22,7	5,4	9,2	1,7	0,018	0,003
160	1800	0,529	1,1	6	0,308	6,7	774,1	735,8	78,4	78,9	1027	1011	94,5	94,5	80,3	93,5	0,929	0,098	7,5	0,7	0,020	0,002	16,3	1,8	6,8	0,5	0,024	0,002
161	1800	0,528	1,1	6	0,310	6,7	774,2	735,8	78,4	78,9	1027	1011	94,6	94,5	80,2	93,5	0,928	0,096	7,5	0,7	0,020	0,002	16,4	1,8	6,8	0,5	0,024	0,002
162	2300	0,853	1,1	6	0,327	7,1	773,6	736,0	78,7	79,2	1036	1010	94,4	94,3	80,9	93,6	0,895	0,109	6,5	0,5	0,023	0,002	14,8	1,3	6,0	0,4	0,028	0,002
163	2300	0,856	1,1	6	0,330	7,1	773,6	736,1	78,7	79,2	1036	1010	94,4	94,4	80,9	93,6	0,894	0,106	6,5	0,5	0,023	0,002	15,0	1,3	6,0	0,4	0,028	0,002
164	1800	0,559	1,1	6	0,311	6,7	773,8	735,7	78,5	78,9	1024	1008	94,6	94,6	80,3	93,6	0,928	0,092	7,5	0,7	0,020	0,002	16,6	1,8	6,9	0,5	0,024	0,002
165	1800	0,561	1,1	6	0,312	6,7	773,7	735,8	78,4	78,9	1025	1009	94,7	94,7	80,2	93,7	0,929	0,090	7,6	0,7	0,020	0,002	16,7	1,8	6,9	0,5	0,024	0,002

Ethanol/n-Propanol with packing, Sample locations S3/S4, 0.7mm jet nozzle

	nRot	RPB_Peff	F	Qreb	mDist	LLeye	rhoL	rhoLfeed	TLfeed	TLVfeed	PI01	PI02	TI03	TI04	TI05	TI12	wi	wo	NTUg	delta NTUg	ATUg	delta ATUg	KGa	delta KGa	Nth_oi	delta Nth_oi	HETP_oi	delta HETP_oi
Unit	RPM	kW	Pa^0.5	kW	kg/min	m3/m2/h	kg/m3	kg/m3	°C	°C	mbar	mbar	°C	°C	°C	°C	g EtOH/g Mix	g EtOH/g Mix			m2	m2	1/s	1/s			m	m
Note / Steady State No.	of RPB		at eye	reboiler duty	FI02		DI02	DI02 at Tlfeed	TI08	bubble point temperature of S4 at PI02							S4 weight frac.	S3 weight frac.	NTU (overall vapor)	uncertainty of NTUg				uncertainty of Kga	oi -> calculated starting at wo until wi is reached			
066	800	0,172	2,0	10	0,587	12,7	769,7	736,7	80,0	80,4	1008	1003	95,1	95,2	85,7	93,6	0,770	0,075	5,1	0,3	0,029	0,002	20,8	1,4	5,2	0,3	0,032	0,002
067	800	0,172	2,0	10	0,585	12,6	769,3	736,6	80,0	80,3	1008	1003	95,1	95,2	85,7	93,6	0,775	0,071	5,2	0,3	0,028	0,002	21,2	1,4	5,3	0,3	0,031	0,002
068	1300	0,346	2,0	10	0,580	12,5	768,5	736,2	79,0	79,4	1015	1005	96,5	96,5	81,4	95,4	0,867	0,026	7,5	0,5	0,020	0,001	30,9	2,4	7,8	0,4	0,021	0,001
069	1300	0,347	2,0	10	0,577	12,5	768,7	736,2	79,1	79,5	1016	1005	96,5	96,5	81,4	95,4	0,860	0,025	7,5	0,5	0,020	0,001	30,4	2,3	7,7	0,4	0,021	0,001
070	1800	0,560	2,0	10	0,572	12,4	768,6	736,0	79,0	79,3	1025	1006	97,1	97,1	81,3	96,2	0,877	0,014	8,4	0,6	0,018	0,001	33,8	2,8	8,8	0,5	0,019	0,001
071	1800	0,560	2,0	10	0,581	12,6	768,6	736,1	79,0	79,3	1026	1006	97,1	97,1	81,4	96,2	0,875	0,014	8,4	0,6	0,018	0,001	34,4	2,9	8,9	0,5	0,019	0,001
072	800	0,174	2,0	10	0,586	12,7	769,2	736,1	80,6	81,0	1033	1028	95,5	95,6	86,1	93,9	0,771	0,081	5,0	0,3	0,029	0,002	20,1	1,4	5,1	0,4	0,033	0,002
073	800	0,173	2,0	10	0,585	12,6	769,2	736,0	80,6	81,0	1033	1028	95,5	95,7	86,1	93,9	0,776	0,081	5,1	0,3	0,029	0,002	20,2	1,4	5,1	0,4	0,032	0,002
074	300	0,057	2,1	10	0,620	13,4	771,3	736,7	84,4	84,9	1030	1028	93,7	93,9	88,6	91,3	0,494	0,216	1,7	0,2	0,089	0,008	6,6	0,7	1,7	0,2	0,096	0,009
075	300	0,057	2,1	10	0,620	13,4	771,4	736,6	84,4	84,9	1030	1028	93,7	93,9	88,7	91,3	0,494	0,218	1,7	0,2	0,089	0,009	6,5	0,7	1,7	0,2	0,097	0,009
076	2300	0,873	2,0	10	0,592	12,8	767,4	735,2	78,7	79,2	1056	1028	91,7	91,8	80,1	90,8	0,945	0,310	6,4	0,9	0,023	0,003	26,2	4,0	5,3	0,8	0,031	0,005
077	2300	0,874	2,1	10	0,595	12,9	767,3	735,2	78,7	79,2	1056	1028	91,7	91,9	80,1	90,8	0,945	0,315	6,4	0,9	0,023	0,003	26,2	4,0	5,3	0,8	0,031	0,005
088	800	0,173	2,9	14	0,845	18,3	765,3	736,6	79,0	79,4	1002	995	91,8	92,2	83,0	89,7	0,844	0,205	4,7	0,4	0,031	0,002	28,2	2,5	4,2	0,4	0,039	0,003
089	800	0,173	2,9	14	0,842	18,2	765,2	736,5	79,0	79,4	1002	995	91,8	92,2	83,0	89,8	0,844	0,201	4,7	0,4	0,031	0,002	28,3	2,5	4,3	0,3	0,038	0,003
090	1800	0,566	2,9	14	0,822	17,8	764,1	736,0	77,8	78,3	1017	997	92,6	92,8	79,2	91,4	0,956	0,183	7,7	1,1	0,019	0,003	45,5	7,1	6,6	0,8	0,025	0,003
091	1800	0,563	2,9	14	0,822	17,8	764,0	736,0	77,8	78,3	1018	998	92,6	92,8	79,2	91,5	0,958	0,185	7,8	1,2	0,019	0,003	46,1	7,5	6,7	0,8	0,025	0,003
092	2300	0,860	3,0	14	0,842	18,2	763,9	736,0	77,9	78,4	1030	999	92,8	93,0	79,3	91,9	0,949	0,184	7,4	1,0	0,020	0,003	44,2	6,3	6,4	0,8	0,026	0,003
093	2300	0,869	3,0	14	0,848	18,3	764,0	736,1	77,9	78,4	1029	998	92,8	93,0	79,3	91,9	0,948	0,186	7,3	0,9	0,020	0,003	44,1	6,2	6,3	0,8	0,026	0,004
094	300	0,052	3,0	14	0,875	18,9	768,0	737,2	82,1	82,4	1003	999	90,8	91,3	85,9	88,3	0,604	0,226	2,3	0,2	0,065	0,005	13,3	1,2	2,3	0,2	0,073	0,006
095	300	0,052	3,0	14	0,876	18,9	767,9	737,2	82,1	82,4	1004	1000	90,8	91,3	85,9	88,4	0,604	0,224	2,3	0,2	0,064	0,005	13,4	1,2	2,3	0,2	0,073	0,006
096	1300	0,345	3,0	14	0,845	18,3	764,7	736,1	78,2	78,7	1012	1000	92,8	93,1	81,1	91,4	0,926	0,175	6,6	0,7	0,022	0,002	40,0	4,6	5,8	0,5	0,028	0,002
097	1300	0,344	2,9	14	0,828	17,9	764,7	736,0	78,2	78,6	1012	1000	92,9	93,1	81,2	91,4	0,929	0,171	6,7	0,7	0,022	0,002	40,0	4,7	5,9	0,5	0,028	0,002
107	800	0,166	2,1	10	0,589	12,7	768,6	735,7	78,7	79,0	1014	1010	92,8	93,1	83,2	91,0	0,915	0,179	6,3	0,6	0,024	0,002	26,3	2,8	5,5	0,5	0,030	0,003
108	800	0,166	2,1	10	0,590	12,8	768,7	735,9	78,7	79,1	1014	1010	92,8	93,1	83,2	91,0	0,906	0,168	6,2	0,6	0,024	0,002	25,8	2,6	5,5	0,5	0,030	0,003
109	1300	0,357	2,0	10	0,572	12,4	768,2	735,6	77,9	78,3	1016	1006	93,6	93,8	82,2	92,4	0,979	0,132	9,7	2,5	0,015	0,004	40,3	10,8	8,4	1,7	0,020	0,004
110	1300	0,356	2,1	10	0,583	12,6	768,1	735,7	77,7	78,3	1015	1005	93,4	93,7	82,2	92,3	0,980	0,138	9,8	2,7	0,015	0,004	41,4	11,8	8,4	1,8	0,020	0,004
111	1800	0,557	2,0	10	0,583	12,6	768,3	735,7	78,1	78,5	1022	1004	93,4	93,6	79,4	92,4	0,960	0,166	8,0	1,2	0,018	0,003	33,5	5,5	6,9	0,9	0,024	0,003
112	1800	0,556	2,0	10	0,583	12,6	768,2	735,6	78,1	78,4	1021	1004	93,4	93,6	79,4	92,4	0,960	0,167	8,0	1,2	0,018	0,003	33,6	5,5	6,9	0,9	0,024	0,003
113	2300	0,834	2,1	10	0,590	12,8	768,3	736,0	78,1	78,6	1030	1003	93,4	93,5	80,1	92,6	0,936	0,231	6,6	0,8	0,023	0,003	27,5	3,6	5,6	0,6	0,029	0,003
114	2300	0,813	2,1	10	0,587	12,7	768,4	736,0	78,1	78,7	1030	1003	93,4	93,5	80,0	92,7	0,934	0,237	6,4	0,8	0,023	0,003	26,8	3,5	5,5	0,6	0,030	0,003
115	300	0,052	2,1	10	0,619	13,4	770,8	737,3	81,9	82,3	1003	1001	91,6	91,9	85,8	88,9	0,612	0,290	1,9	0,2	0,076	0,007	8,0	0,9	1,8	0,2	0,090	0,008
116	300	0,053	2,1	10	0,623	13,4	770,8	737,3	81,9	82,3	1003	1001	91,6	91,9	85,8	88,9	0,612	0,301	1,9	0,2	0,079	0,008	7,8	0,9	1,8	0,2	0,093	0,008
117	1300	0,343	2,0	10	0,583	12,6	768,1	736,0	78,0	78,3	1003	993	96,1	96,1	79,9	95,0	0,941	0,032	9,1	0,9	0,016	0,002	38,7	4,3	8,8	0,7	0,019	0,001
118	1300	0,334	2,0	10	0,582	12,6	768,1	736,0	78,0	78,3	1003	992	96,1	96,2	79,9	95,1	0,941	0,027	9,3	0,9	0,016	0,002	39,4	4,4	9,0	0,9	0,018	0,002
119	1800	0,542	2,1	10	0,584	12,6	768,0	735,9	78,0	78,2	1009	991	95,5	95,6	79,3	94,6	0,949	0,060	8,7	1,0	0,017	0,002	37,0	4,6	8,1	0,9	0,020	0,002
120	1800	0,542	2,0	10	0,579	12,5	768,0	735,8	78,0	78,2	1009	991	95,5	95,6	79,3	94,6	0,954	0,068	8,8	1,1	0,017	0,002	37,2	5,1	8,1	1,0	0,020	0,002
121	1800	0,545	3,0	14	0,841	18,2	764,4	736,1	77,6	78,1	1012	992	94,0	94,2	79,1	93,1	0,960	0,108	8,6	1,3	0,017	0,002	52,6	8,3	7,7	0,9	0,022	0,003
122	1800	0,547	2,9	14	0,834	18,0	764,4	736,2	77,5	78,1	1011	991	93,9	94,1	79,2	92,9	0,959	0,111	8,5	1,2	0,017	0,002	51,5	8,0	7,6	0,9	0,022	0,003
123	800	0,173	3,0	14	0,863	18,6	765,6	736,7	78,6	79,2	1003	995	91,9	92,3	82,8	89,9	0,854	0,188	5,0	0,4	0,030	0,002	30,6	2,7	4,5	0,3	0,036	0,003
124	800	0,172	3,0	14	0,857	18,5	765,7	736,8	78,6	79,3	1002	994	91,9	92,4	82,9	89,9	0,852	0,188	5,0	0,4	0,030	0,002	30,2	2,6	4,5	0,3	0,037	0,003
126	300	0,049	3,1	14	0,896	19,3	767,2	737,7	80,6	81,4	999	993	90,0	90,7	84,5	87,5	0,668	0,229	2,7	0,2	0,054	0,004	16,6	1,4	2,6	0,2	0,063	0,004
127	300	0,049	3,0	14	0,876	18,9	767,1	737,6	80,7	81,3	998	993	90,0	90,6	84,5	87,5	0,669	0,270	2,5	0,2	0,060	0,005	14,7	1,4	2,3	0,2	0,071	0,006
128	800	0,166	3,0	14	0,862	18,6	765,3	736,0	79,2	79,6	1020	1012	91,6	92,1	82,9	89,5	0,863	0,220	4,9	0,4	0,030	0,002	29,7	2,7	4,4	0,4	0,038	0,003
129	800	0,166	3,0	14	0,861	18,6	765,4	736,1	79,2	79,6	1020	1012	91,7	92,2	82,9	89,5	0,860	0,219	4,9	0,4	0,030	0,002	29,3	2,7	4,3	0,4	0,038	0,003
130	1300	0,328	3,0	14	0,852	18,4	764,4	735,8	78,2	78,8	1026	1012	92,1	92,5	79,8	90,6	0,942	0,210	6,9	0,9	0,021	0,003	41,6	5,7	5,9	0,6	0,028	0,003
131	1300	0,327	3,0	14	0,851	18,4	764,5	735,8	78,2	78,8	1025	1012	92,1	92,5	79,9	90,6	0,942	0,211	6,9	0,9	0,021	0,003	41,6	5,6	5,9	0,6	0,028	0,003
132	1800	0,547	3,0	14	0,850	18,4	764,1	735,5	78,2	78,7	1034	1013	93,0	93,3	79,5	91,9	0,957	0,178	7,8	1,1	0,019	0,003	46,8	7,4	6,7	0,8	0,025	0,003
133	1800	0,545	3,0	14	0,853	18,5	764,1	735,6	78,2	78,7	1034	1012	93,0	93,3	79,5	91,9	0,956	0,176	7,8	1,1	0,019	0,003	46,8	7,3	6,7	0,8	0,025	0,003
134	2300	0,845	3,0	14	0,853	18,5	764,2	735,7	78,2	78,7	1044	1012	93,1	93,3	79,6	92,2	0,951	0,193	7,4	1,0	0,020	0,003	44,4	6,5	6,3	0,9	0,026	0,004
135	2300	0,837	3,0	14	0,859	18,6	764,2	735,6	78,2	78,7	1044	1012	93,1	93,4	79,7	92,3	0,951	0,182	7,5	1,0	0,020	0,003	45,3	6,6	6,5	0,8	0,026	0,003
136	1300	0,343	2,0	10	0,571	12,3	768,1	735,6	78,1	78,7	1024	1014	93,0	93,2	81,1	91,7	0,965	0,173	8,3	1,4	0,018	0,003	33,7	6,1	7,0	1,1	0,023	0,004
137	1300	0,342	2,0	10	0,570	12,3	767,9	735,6	78,0	78,6	1024	1014	93,0	93,3	82,5	91,8	0,967	0,172	8,4	1,5	0,018	0,003	34,4	6,5	7,2	1,2	0,023	0,004
138	1300	0,342	2,0	10	0,578	12,5	767,9	735,4	78,4	78,7	1025	1014	94,0	94,2	82,5	92,8	0,957	0,130	8,2	1,1	0,018	0,002	33,9	5,1	7,2	1,0	0,023	0,003
139	1300	0,340	2,0	10	0,579	12,5	767,7	735,3	78,4	78,7	1025	1014	94,0	94,2	81,5	92,8	0,958	0,132	8,3	1,2	0,018	0,003	34,2	5,3	7,2	1,0	0,023	0,003
140	800	0,165	2,0	10	0,581	12,6	768,8	736,0	78,8	79,2	1014	1010	92,5	92,8	83,3	90,5	0,893	0,188	5,7	0,5	0,026	0,002	23,5	2,3	5,0	0,5	0,033	0,003
141	800	0,164	2,0	10	0,588	12,7	768,8	736,0	78,8	79,3	1014	1010	92,5	92,8	83,2	90,6	0,891	0,192	5,6	0,5	0,026	0,002	23,4	2,3	5,0	0,4	0,033	0,002
150	800	0,161	1,1	6	0,308	6,7	773,2	735,5	78,0	78,5	1018	1015	96,4	96,4	84,2	95,0	0,978	0,065	10,5	2,3	0,014	0,003	23,3	5,5	9,4	1,7	0,018	0,003
151	800	0,162	1,1	6	0,308	6,7	773,1	735,4	78,0	78,5	1018	1014	96,4	96,3	84,2	95,0	0,977	0,065	10,4	2,2	0,014	0,003	23,2	5,3	9,3	1,6	0,018	0,003
152	300	0,051	1,1	6	0,329	7,1	776,8	736,9	82,9	83,2	1015	1014	93,0	93,2	86,8	90,4	0,574	0,237	2,0	0,2	0,073	0,006	4,4	0,4	2,0	0,2	0,083	0,007
153	300	0,052	1,1	6	0,326	7,0	776,9	736,8	83,0	83,2	1015	1014	93,0	93,2	86,7	90,4	0,576	0,250	1,9	0,2	0,076	0,007	4,2	0,4	1,9	0,2	0,087	0,007
154	800	0,161	1,1	6	0,306	6,6	773,4	735,5	78,7	79,0	1016	1012	96,6	96,6	84,9	95,3	0,929	0,054	8,1	0,7	0,018	0,002	17,9	1,8	7,8	0,6	0,021	0,002
155	800	0,161	1,1	6	0,304	6,6	773,6	735,3	78,7	78,9	1016	1013	96,7	96,6	84,9	95,3	0,939	0,045	8,7	0,9	0,017	0,002	19,1	2,1	8,3	0,8	0,020	0,002
156	1300	0,320	1,1	6	0,304	6,6	773,7	735,7	78,0	78,6	1021	1012	96,5	96,4	80,9	95,4	0,961	0,055	9,5	1,3	0,016	0,002	20,7	3,1	8,7	0,9	0,019	0,002

Ethanol/n-Propanol with packing, Sample locations S3/S4, 0.7mm jet nozzle (contd.)

	nRot	RPB_Peff	F	Qreb	mDist	LLeye	rhoL	rhoLfeed	TLfeed	TLVfeed	PI01	PI02	TI03	TI04	TI05	TI12	wi	wo	NTUg	delta NTUg	ATUg	delta ATUg	KGa	delta KGa	Nth_oi	delta Nth_oi	HETP_oi	delta HETP_oi
Unit	RPM	kW	Pa^0.5	kW	kg/min	m3/m2/h	kg/m3	kg/m3	°C	°C	mbar	mbar	°C	°C	°C	°C	g EtOH/g Mix	g EtOH/g Mix			m2	m2	1/s	1/s			m	m
Note / **Steady State No.**	of RPB		at eye	reboiler duty	FI02		DI02	DI02 at Tlfeed	TI08	bubble point temperature of S4 at PI02							S4 weight frac.	S3 weight frac.	NTU (overall vapor)	uncertainty of NTUg				uncertainty of Kga	oi -> calculated starting at wo until wi is reached			
157	1300	0,319	1,1	6	0,303	6,6	773,6	735,6	78,1	78,6	1019	1011	96,4	96,4	81,0	95,4	0,963	0,056	9,5	1,3	0,016	0,002	20,8	3,2	8,8	1,0	0,019	0,002
158	1300	0,327	1,1	6	0,299	6,5	774,1	735,4	78,0	78,5	1021	1012	95,1	95,1	83,5	94,0	0,980	0,124	9,9	2,7	0,015	0,004	21,5	6,0	8,6	1,9	0,019	0,004
159	1300	0,326	1,1	6	0,303	6,6	773,7	735,4	78,0	78,5	1019	1011	95,0	95,0	83,5	93,9	0,978	0,133	9,6	2,3	0,015	0,004	21,1	5,4	8,2	1,7	0,020	0,004
160	1800	0,529	1,1	6	0,308	6,7	774,1	735,8	78,4	78,9	1027	1011	94,5	94,5	80,3	93,5	0,929	0,173	6,7	0,7	0,022	0,002	14,7	1,7	5,9	0,5	0,028	0,002
161	1800	0,528	1,1	6	0,310	6,7	774,2	735,8	78,4	78,9	1027	1011	94,6	94,5	80,2	93,5	0,928	0,172	6,7	0,7	0,022	0,002	14,8	1,7	5,9	0,5	0,028	0,002
162	2300	0,853	1,1	6	0,327	7,1	773,6	736,0	78,7	79,2	1036	1010	94,4	94,3	80,9	93,6	0,895	0,191	5,7	0,5	0,026	0,002	13,1	1,3	5,0	0,5	0,033	0,003
163	2300	0,856	1,1	6	0,330	7,1	773,6	736,1	78,7	79,2	1036	1010	94,4	94,4	80,9	93,6	0,894	0,194	5,7	0,5	0,026	0,002	13,1	1,3	5,0	0,4	0,033	0,003
164	1800	0,559	1,1	6	0,311	6,7	773,8	735,7	78,5	78,9	1024	1008	94,6	94,6	80,3	93,6	0,928	0,169	6,7	0,7	0,022	0,002	14,9	1,7	5,9	0,5	0,028	0,002
165	1800	0,561	1,1	6	0,312	6,7	773,7	735,8	78,4	78,9	1025	1009	94,7	94,7	80,2	93,7	0,929	0,165	6,8	0,7	0,022	0,002	15,1	1,8	5,9	0,5	0,028	0,002

Ethanol/n-Propanol with packing, Sample locations S6/S4, 1mm jet nozzle

	nRot	RPB_Peff	F	Qreb	mDist	LLeye	rhoL	rhoLfeed	TLfeed	TLVfeed	PI01	PI02	TI03	TI04	TI05	TI12	wi	wo	NTUg	delta NTUg	ATUg	delta ATUg	KGa	delta KGa	Nth_oi	delta Nth_oi	HETP_oi	delta HETP_oi
Unit	RPM	kW	Pa^0.5	kW	kg/min	m3/m2/h	kg/m3	kg/m3	°C	°C	mbar	mbar	°C	°C	°C	°C	g EtOH/g Mix	g EtOH/g Mix			m2	m2	1/s	1/s			m	m
Note / Steady State No.	of RPB		at eye	reboiler duty	FI02		DI02	DI02 at Tlfeed	TI08	bubble point temperature of S4 at PI02							S4 weight frac.	S6 weight frac.	NTU (overall vapor)	uncertainty of NTUg				uncertainty of Kga	oi -> calculated starting at wo until wi is reached			
166	800	0,167	2,9	14	0,849	18,4	765,2	736,1	79,3	79,6	1018	1010	91,8	92,2	82,9	89,7	0,854	0,222	4,7	0,4	0,031	0,002	28,2	2,6	4,2	0,4	0,039	0,003
167	800	0,166	2,9	14	0,848	18,3	765,2	736,1	79,2	79,6	1018	1010	91,8	92,1	82,9	89,7	0,856	0,222	4,8	0,4	0,031	0,002	28,4	2,6	4,3	0,4	0,039	0,003
168	1300	0,343	2,9	14	0,842	18,2	764,5	736,0	78,2	78,9	1026	1013	92,4	92,6	80,3	90,9	0,931	0,187	6,7	0,7	0,022	0,002	39,8	4,8	5,8	0,5	0,028	0,002
169	1300	0,343	2,9	14	0,841	18,2	764,3	735,8	78,2	78,9	1027	1014	92,4	92,7	80,6	91,0	0,935	0,184	6,9	0,8	0,022	0,002	40,8	5,1	5,9	0,6	0,028	0,003
170	1800	0,566	3,0	14	0,853	18,4	764,1	735,6	78,3	78,8	1035	1013	92,5	92,7	79,8	91,3	0,948	0,180	7,4	0,9	0,020	0,003	44,3	6,3	6,4	0,8	0,026	0,003
171	1800	0,562	3,0	14	0,847	18,3	764,1	735,6	78,3	78,8	1035	1014	92,6	92,8	79,8	91,4	0,948	0,179	7,4	0,9	0,020	0,003	44,0	6,2	6,4	0,8	0,026	0,003
172	2300	0,839	2,9	14	0,846	18,3	764,1	735,8	78,3	78,9	1046	1014	92,7	92,9	80,6	91,7	0,938	0,178	7,0	0,8	0,021	0,002	41,5	5,2	6,0	0,7	0,027	0,003
173	2300	0,843	3,0	14	0,854	18,5	764,0	735,8	78,3	78,9	1046	1014	92,7	92,8	80,7	91,7	0,939	0,180	7,0	0,8	0,021	0,002	42,1	5,4	6,1	0,7	0,027	0,003
174	2300	0,841	3,0	14	0,861	18,7	764,0	733,9	80,1	78,9	1045	1013	92,8	92,9	79,8	91,8	0,940	0,177	7,1	0,8	0,021	0,002	42,8	5,5	6,1	0,7	0,027	0,003
175	2300	0,848	3,0	14	0,859	18,6	764,0	735,6	78,4	78,9	1046	1014	92,8	93,0	79,8	91,9	0,941	0,178	7,1	0,8	0,021	0,002	42,7	5,6	6,1	0,8	0,027	0,003
176	300	0,053	3,0	14	0,895	19,3	767,5	737,1	82,5	83,0	1020	1014	90,7	91,2	86,5	88,1	0,590	0,300	1,7	0,2	0,086	0,009	10,1	1,2	1,7	0,2	0,100	0,010
177	300	0,054	3,0	14	0,884	19,1	767,5	736,8	82,6	82,9	1019	1014	90,7	91,2	86,5	88,1	0,595	0,301	1,8	0,2	0,084	0,009	10,1	1,2	1,7	0,2	0,099	0,009

Ethanol/n-Propanol with packing, Sample locations S3/S4, 1mm jet nozzle

	nRot	RPB_Peff	F	Qreb	mDist	LLeye	rhoL	rhoLfeed	TLfeed	TLVfeed	PI01	PI02	TI03	TI04	TI05	TI12	wi	wo	NTUg	delta NTUg	ATUg	delta ATUg	KGa	delta KGa	Nth_oi	delta Nth_oi	HETP_oi	delta HETP_oi
Unit	RPM	kW	Pa^0.5	kW	kg/min	m3/m2/h	kg/m3	kg/m3	°C	°C	mbar	mbar	°C	°C	°C	°C	g EtOH/g Mix	g EtOH/g Mix			m2	m2	1/s	1/s			m	m
Note / Steady State No.	of RPB		at eye	reboiler duty	FI02		DI02	DI02 at Tlfeed	TI08	bubble point temperature of S4 at PI02							S4 weight frac.	S3 weight frac.	NTU (overall vapor)	uncertainty of NTUg				uncertainty of Kga	oi -> calculated starting at wo until wi is reached			
166	800	0,167	2,9	14	0,849	18,4	765,2	736,1	79,3	79,6	1018	1010	91,8	92,2	82,9	89,7	0,854	0,212	4,8	0,4	0,031	0,002	28,6	2,6	4,3	0,4	0,038	0,003
167	800	0,166	2,9	14	0,848	18,3	765,2	736,1	79,2	79,6	1018	1010	91,8	92,1	82,9	89,7	0,856	0,216	4,8	0,4	0,031	0,002	28,6	2,6	4,3	0,4	0,038	0,003
168	1300	0,343	2,9	14	0,842	18,2	764,5	736,0	78,2	78,9	1026	1013	92,4	92,6	80,3	90,9	0,931	0,201	6,6	0,7	0,022	0,002	39,2	4,8	5,7	0,5	0,029	0,003
169	1300	0,343	2,9	14	0,841	18,2	764,3	735,8	78,2	78,9	1027	1014	92,4	92,7	80,6	91,0	0,935	0,202	6,7	0,8	0,022	0,002	40,0	5,1	5,8	0,5	0,028	0,003
170	1800	0,566	3,0	14	0,853	18,4	764,1	735,6	78,3	78,8	1035	1013	92,5	92,7	79,8	91,3	0,948	0,197	7,2	0,9	0,020	0,003	43,6	6,2	6,2	0,8	0,027	0,004
171	1800	0,562	3,0	14	0,847	18,3	764,1	735,6	78,3	78,8	1035	1014	92,6	92,8	79,8	91,4	0,948	0,196	7,2	0,9	0,020	0,003	43,3	6,2	6,2	0,8	0,027	0,004
172	2300	0,839	2,9	14	0,846	18,3	764,1	735,8	78,3	78,9	1046	1014	92,7	92,9	80,6	91,7	0,938	0,213	6,7	0,8	0,022	0,003	39,9	5,2	5,8	0,5	0,029	0,003
173	2300	0,843	3,0	14	0,854	18,5	764,0	735,8	78,3	78,9	1046	1014	92,7	92,8	80,7	91,7	0,939	0,203	6,9	0,8	0,022	0,003	41,1	5,4	5,9	0,6	0,028	0,003
174	2300	0,841	3,0	14	0,861	18,7	764,0	733,9	80,1	78,9	1045	1013	92,8	92,9	79,8	91,8	0,940	0,202	6,9	0,8	0,021	0,003	41,6	5,5	5,9	0,6	0,028	0,003
175	2300	0,848	3,0	14	0,859	18,6	764,0	735,6	78,4	78,9	1046	1014	92,8	93,0	79,8	91,9	0,941	0,201	6,9	0,8	0,021	0,003	41,7	5,6	5,9	0,6	0,028	0,003
176	300	0,053	3,0	14	0,895	19,3	767,5	737,1	82,5	83,0	1020	1014	90,7	91,2	86,5	88,1	0,590	0,262	2,0	0,2	0,075	0,007	11,5	1,2	1,9	0,2	0,087	0,007
177	300	0,054	3,0	14	0,884	19,1	767,5	736,8	82,6	82,9	1019	1014	90,7	91,2	86,5	88,1	0,595	0,246	2,1	0,2	0,071	0,006	12,1	1,2	2,0	0,2	0,081	0,008

Ethanol/Water with packing, Sample locations S6/S4, 0.7mm jet nozzle

	nRot	RPB_Peff	F	Qreb	mDist	LLeye	rhoL	rhoLfeed	TLfeed	TLVfeed	PI01	PI02	TI03	TI04	TI05	TI12	wi	wo	NTUg	delta NTUg	ATUg	delta ATUg	KGa	delta KGa	Nth_oi	delta Nth_oi	HETP_oi	delta HETP_oi
Unit	RPM	kW	Pa^0.5	kW	kg/min	m3/m2/h	kg/m3	kg/m3	°C	°C	mbar	mbar	°C	°C	°C	°C	g EtOH/g Mix	g EtOH/g Mix			m2	m2	1/s	1/s			m	m
Note / Steady State No.	of RPB		at eye	reboiler duty	FI02		DI02	DI02 at Tlfeed	TI08	bubble point temperature of S4 at PI02							S4 weight frac.	S6 weight frac.	NTU (overall vapor)	uncertainty of NTUg				uncertainty of Kga	oi -> calculated starting at wo until wi is reached			
005	1300	0,323	4,9	25	1,302	27,1	782,7	764,5	70,0	78,1	1021	1007	88,7	91,0	78,9	83,5	0,908	0,325	6,3	2,0	0,023	0,007	67,7	20,0	4,8	1,7	0,034	0,012
006	1300	0,322	4,9	25	1,296	27,0	782,8	764,0	70,0	78,1	1022	1007	88,9	91,2	79,2	83,7	0,910	0,313	6,5	2,1	0,023	0,007	69,4	21,1	4,9	1,8	0,033	0,012
007	800	0,168	3,4	17	0,903	19,0	786,9	757,5	78,5	78,4	1025	1019	89,6	91,9	80,5	83,5	0,903	0,320	5,8	1,7	0,025	0,007	43,4	11,7	4,4	1,4	0,038	0,012
008	800	0,167	3,4	17	0,909	19,1	786,8	756,3	78,5	78,4	1025	1019	89,7	92,0	80,5	83,6	0,908	0,317	6,3	2,0	0,023	0,007	46,9	13,7	4,8	1,7	0,035	0,012
009	300	0,047	3,2	17	0,834	17,3	800,9	767,9	79,6	78,7	1022	1017	90,4	93,3	81,6	83,7	0,854	0,351	3,4	0,6	0,044	0,008	24,9	4,1	2,4	0,5	0,068	0,014
010	300	0,047	3,2	17	0,833	17,3	800,7	768,0	79,4	78,7	1022	1018	90,6	93,4	81,7	83,8	0,854	0,348	3,4	0,6	0,043	0,008	25,0	4,1	2,4	0,5	0,068	0,014
011	1300	0,321	3,5	17	0,925	19,5	785,1	755,8	78,0	78,1	1018	1008	87,6	89,7	80,2	83,1	0,912	0,328	6,7	2,3	0,022	0,007	50,8	16,1	5,1	1,9	0,032	0,012
012	1300	0,316	3,5	17	0,923	19,4	785,1	755,2	78,0	78,1	1018	1008	87,7	89,8	80,1	83,2	0,915	0,324	7,0	2,5	0,021	0,007	52,6	17,5	5,4	2,1	0,031	0,012
013	1300	0,316	3,4	17	0,923	19,4	784,8	756,1	77,0	78,1	1019	1008	85,2	87,1	79,0	81,6	0,915	0,463	6,8	2,5	0,022	0,008	50,4	17,7	5,1	2,1	0,032	0,013
014	2300	0,766	3,5	17	0,925	19,4	785,3	757,7	76,0	78,2	1035	1009	84,8	86,1	78,2	82,5	0,912	0,450	6,5	2,3	0,023	0,008	48,4	16,2	4,9	1,9	0,034	0,013
015	2300	0,758	3,5	17	0,921	19,3	785,4	758,6	76,0	78,2	1035	1009	84,8	86,2	78,2	82,6	0,908	0,445	6,1	2,0	0,024	0,008	45,5	14,1	4,6	1,7	0,036	0,013
016	1800	0,508	3,4	17	0,923	19,4	785,1	756,9	77,0	78,3	1030	1013	85,5	87,1	79,2	82,7	0,912	0,425	6,5	2,3	0,023	0,008	48,4	15,8	4,9	1,9	0,034	0,013
017	1800	0,499	3,4	17	0,923	19,4	785,0	756,4	77,0	78,2	1030	1013	85,5	87,2	78,6	82,8	0,914	0,419	6,8	2,4	0,022	0,008	50,1	17,0	5,1	2,0	0,032	0,012
018	1800	0,498	5,0	25	1,331	28,0	779,4	756,8	77,0	78,3	1037	1015	86,6	88,6	78,4	83,0	0,912	0,413	6,6	2,3	0,022	0,008	70,3	23,0	4,9	1,9	0,033	0,013
019	1800	0,568	5,1	25	1,355	28,5	778,9	756,8	77,0	78,3	1038	1015	86,7	88,8	78,3	83,0	0,912	0,408	6,6	2,3	0,022	0,008	71,5	23,3	4,9	1,9	0,033	0,013
020	2300	0,847	5,0	25	1,342	28,2	779,0	756,9	77,0	78,3	1047	1016	86,5	88,2	78,6	83,4	0,911	0,401	6,5	2,2	0,023	0,008	69,9	22,5	4,9	1,9	0,034	0,013
021	2300	0,845	5,0	25	1,348	28,3	779,0	756,9	77,0	78,3	1048	1016	86,6	88,4	78,6	83,5	0,912	0,392	6,6	2,2	0,023	0,007	70,6	22,7	4,9	1,9	0,034	0,012
022	800	0,200	5,0	25	1,325	27,8	781,3	758,9	77,0	78,4	1027	1016	88,5	91,1	79,0	82,2	0,903	0,415	5,7	1,7	0,026	0,008	62,1	17,5	4,2	1,4	0,039	0,013
023	800	0,201	5,0	25	1,323	27,7	781,3	759,0	77,0	78,4	1028	1016	88,7	91,2	79,1	82,2	0,902	0,405	5,7	1,7	0,026	0,008	61,6	17,1	4,2	1,4	0,039	0,013
024	1300	0,329	5,0	25	1,340	28,2	779,5	756,1	78,0	78,7	1046	1029	87,9	90,3	79,6	83,0	0,911	0,391	6,5	2,2	0,023	0,007	69,6	22,1	4,9	1,8	0,034	0,012
025	1300	0,324	4,9	25	1,325	27,9	779,5	756,5	78,1	78,7	1045	1029	88,0	90,5	80,0	83,0	0,909	0,382	6,3	2,1	0,023	0,007	67,0	20,4	4,7	1,7	0,035	0,013
026	300	0,050	4,6	25	1,196	24,6	798,9	772,5	78,0	79,1	1040	1029	88,7	92,4	79,7	82,8	0,841	0,421	2,9	0,5	0,051	0,009	30,5	5,0	2,0	0,3	0,084	0,014
027	300	0,050	4,6	25	1,189	24,5	799,0	772,9	78,0	79,1	1040	1028	88,8	92,5	79,8	82,8	0,839	0,427	2,8	0,5	0,052	0,009	29,7	4,8	1,9	0,3	0,085	0,013
028	800	0,173	2,4	12	0,639	13,5	788,0	754,4	79,0	78,4	1023	1018	86,9	89,1	80,6	82,1	0,914	0,399	6,8	2,4	0,022	0,008	35,0	11,8	5,1	2,0	0,032	0,012
029	800	0,170	2,4	12	0,635	13,4	788,0	754,5	79,0	78,4	1022	1018	87,0	89,2	80,6	82,2	0,913	0,392	6,7	2,4	0,022	0,007	34,6	11,4	5,1	2,0	0,033	0,012
030	1300	0,326	2,4	12	0,637	13,4	787,0	754,2	78,5	78,3	1026	1018	85,9	87,6	80,4	82,8	0,917	0,384	7,1	2,7	0,021	0,007	36,5	12,9	5,5	2,3	0,030	0,012
031	1300	0,321	2,4	12	0,637	13,5	786,7	754,1	78,5	78,3	1026	1017	86,0	87,7	80,3	82,9	0,917	0,379	7,2	2,8	0,020	0,007	37,1	13,3	5,6	2,3	0,030	0,012
032	1800	0,525	2,4	12	0,639	13,5	788,2	755,7	78,0	78,3	1029	1014	85,6	87,1	79,8	83,5	0,913	0,362	6,7	2,3	0,022	0,007	34,6	11,2	5,1	1,9	0,033	0,012
033	1800	0,581	2,4	12	0,632	13,3	788,3	755,8	78,0	78,3	1029	1014	85,7	87,2	80,0	83,6	0,912	0,360	6,7	2,3	0,022	0,007	34,0	10,9	5,0	1,9	0,033	0,012
034	800	0,165	2,3	12	0,633	13,4	784,8	753,8	79,5	79,0	1050	1045	88,9	91,1	81,6	83,9	0,914	0,322	7,0	2,5	0,021	0,007	35,0	11,6	5,4	2,0	0,031	0,012
035	800	0,164	2,3	12	0,629	13,3	785,0	753,6	79,5	79,0	1049	1045	88,9	91,1	81,6	84,0	0,915	0,321	7,1	2,5	0,021	0,007	35,2	11,9	5,4	2,1	0,030	0,012
036	300	0,049	2,3	12	0,596	12,5	795,4	761,4	80,5	79,2	1046	1045	92,2	93,8	82,5	84,6	0,878	0,346	4,3	0,9	0,034	0,007	21,4	4,3	3,1	0,8	0,054	0,013
037	300	0,049	2,2	12	0,594	12,4	795,4	761,5	80,5	79,2	1046	1044	92,3	93,9	82,5	84,7	0,878	0,341	4,3	0,9	0,034	0,007	21,3	4,3	3,1	0,8	0,054	0,013
038	2300	0,823	2,3	12	0,626	13,1	789,2	757,6	79,6	79,1	1067	1044	86,6	87,9	81,1	84,9	0,898	0,318	5,5	1,5	0,027	0,007	27,5	6,9	4,1	1,2	0,040	0,012
039	2300	0,820	2,3	12	0,628	13,2	789,2	758,1	79,5	79,1	1067	1044	86,7	88,0	81,1	85,0	0,896	0,317	5,4	1,4	0,027	0,007	27,1	6,6	4,0	1,2	0,042	0,012
040	1300	0,361	2,4	12	0,646	13,6	783,7	753,0	79,5	79,0	1052	1043	87,8	89,6	81,4	84,8	0,918	0,299	7,5	2,8	0,020	0,007	37,9	13,4	5,8	2,4	0,029	0,012
041	1300	0,363	2,4	12	0,644	13,6	783,7	753,0	79,5	79,0	1053	1044	87,9	89,7	81,4	84,8	0,918	0,295	7,5	2,8	0,020	0,007	37,8	13,4	5,8	2,4	0,029	0,012
042	800	0,174	3,4	17	0,909	19,1	785,0	756,0	79,0	78,9	1045	1039	89,7	92,1	81,0	83,7	0,907	0,336	6,2	1,9	0,024	0,007	45,3	13,2	4,7	1,6	0,035	0,012
043	800	0,173	3,4	17	0,911	19,2	784,8	755,7	79,0	78,9	1045	1039	89,8	92,1	81,0	83,8	0,909	0,332	6,4	2,0	0,023	0,007	46,6	13,9	4,8	1,7	0,034	0,012
044	2300	0,845	3,4	17	0,915	19,3	784,0	755,4	78,5	78,9	1064	1038	87,3	88,8	80,0	84,9	0,912	0,329	6,7	2,3	0,022	0,007	48,3	15,3	5,1	1,9	0,032	0,012
045	2300	0,840	3,4	17	0,915	19,3	784,1	756,4	78,5	78,9	1064	1038	87,4	88,9	79,6	85,0	0,908	0,315	6,3	2,0	0,023	0,007	45,8	13,4	4,8	1,7	0,034	0,012
046	1800	0,580	3,4	17	0,922	19,4	783,2	754,9	78,5	78,9	1055	1038	87,8	89,5	80,6	84,9	0,914	0,313	7,0	2,4	0,021	0,007	50,7	16,6	5,3	2,0	0,031	0,012
047	1800	0,579	3,4	17	0,922	19,4	783,3	755,0	78,5	78,9	1055	1038	87,8	89,6	80,7	85,0	0,913	0,308	6,9	2,4	0,021	0,007	50,5	16,4	5,3	2,0	0,031	0,011
048	1300	0,379	3,4	17	0,914	19,3	782,9	754,4	78,5	78,8	1047	1037	87,8	89,9	80,8	83,6	0,916	0,346	7,2	2,6	0,021	0,007	51,8	17,9	5,5	2,2	0,030	0,012
049	1300	0,384	3,4	17	0,912	19,2	782,6	754,3	78,5	78,8	1047	1036	87,9	90,0	80,8	83,7	0,916	0,341	7,2	2,7	0,021	0,007	51,9	18,0	5,5	2,3	0,030	0,012
050	300	0,058	3,2	17	0,835	17,3	798,6	767,3	79,5	79,2	1040	1036	90,2	93,2	81,7	83,7	0,857	0,379	3,4	0,7	0,043	0,008	24,8	4,3	2,5	0,5	0,067	0,015
051	300	0,059	3,2	17	0,841	17,4	798,9	767,5	79,5	79,2	1040	1036	90,3	93,3	81,7	83,7	0,856	0,375	3,4	0,6	0,043	0,008	24,8	4,2	2,4	0,5	0,068	0,015
052	800	0,183	4,9	25	1,315	27,6	778,3	758,1	78,0	78,4	1029	1018	89,1	91,6	79,6	82,5	0,902	0,389	5,7	1,7	0,026	0,008	61,6	16,9	4,2	1,4	0,039	0,013
053	800	0,181	4,9	25	1,311	27,5	778,5	757,7	78,0	78,4	1028	1017	89,1	91,7	79,7	82,5	0,904	0,386	5,8	1,8	0,025	0,007	62,8	17,7	4,4	1,5	0,038	0,013
054	300	0,053	4,7	25	1,199	24,7	795,1	773,3	77,5	78,7	1026	1014	88,5	92,1	79,5	82,4	0,840	0,427	2,8	0,5	0,052	0,009	30,4	5,0	1,9	0,3	0,085	0,013
055	300	0,053	4,7	25	1,204	24,8	795,3	773,3	77,5	78,7	1026	1014	88,6	92,2	79,5	82,5	0,840	0,422	2,9	0,5	0,052	0,009	30,7	5,0	1,9	0,3	0,085	0,013
056	2300	0,869	5,0	25	1,348	28,3	775,2	757,4	76,7	78,3	1045	1014	87,2	89,0	78,6	84,0	0,911	0,354	6,6	2,2	0,023	0,007	71,0	22,2	4,9	1,8	0,033	0,012
057	2300	0,850	5,0	25	1,352	28,4	775,0	757,4	76,7	78,3	1046	1015	87,3	89,1	78,6	84,1	0,911	0,350	6,6	2,2	0,023	0,007	71,1	22,2	4,9	1,8	0,033	0,012
058	1800	0,579	5,0	25	1,340	28,2	775,2	757,1	76,7	78,2	1035	1012	87,6	89,7	78,3	83,7	0,912	0,349	6,7	2,3	0,022	0,007	72,2	23,0	5,0	1,9	0,033	0,012
059	1800	0,579	5,0	25	1,342	28,2	774,9	757,0	76,7	78,3	1036	1013	87,7	89,8	78,6	83,8	0,913	0,344	6,8	2,3	0,022	0,007	73,0	23,5	5,1	1,9	0,032	0,012
060	1300	0,358	5,0	25	1,338	28,1	775,4	757,6	76,8	78,2	1028	1012	88,1	90,5	79,0	82,9	0,910	0,356	6,4	2,1	0,023	0,007	69,8	21,3	4,8	1,8	0,034	0,012
061	1300	0,362	5,1	25	1,356	28,5	775,2	756,9	77,5	78,2	1027	1011	88,2	90,7	79,5	83,0	0,910	0,351	6,4	2,1	0,023	0,007	71,2	21,8	4,9	1,8	0,034	0,012

Ethanol/Water with packing, Sample locations S3/S4, 0.7mm jet nozzle

	nRot	RPB_Peff	F	Qreb	mDist	LLeye	rhoL	rhoLfeed	TLfeed	TLVfeed	PI01	PI02	TI03	TI04	TI05	TI12	wi	wo	NTUg	delta NTUg	ATUg	delta ATUg	KGa	delta KGa	Nth_oi	delta Nth_oi	HETP_oi	delta HETP_oi
Unit	RPM	kW	Pa^0.5	kW	kg/min	m3/m2/h	kg/m3	kg/m3	°C	°C	mbar	mbar	°C	°C	°C	°C	g EtOH/g Mix	g EtOH/g Mix			m2	m2	1/s	1/s			m	m
Note / Steady State No.	of RPB		at eye	reboiler duty	FI02		DI02	DI02 at Tlfeed	TI08	bubble point temperature of S4 at PI02							S4 weight frac.	S3 weight frac.	NTU (overall vapor)	uncertainty of NTUg				uncertainty of Kga	oi -> calculated starting at wo until wi is reached			
005	1300	0,323	4,9	25	1,302	27,1	782,7	764,5	70,0	78,1	1021	1007	88,7	91,0	78,9	83,5	0,908	0,410	6,2	2,0	0,024	0,008	65,9	20,1	4,6	1,7	0,036	0,013
006	1300	0,322	4,9	25	1,296	27,0	782,8	764,0	70,0	78,1	1022	1007	88,9	91,2	79,2	83,7	0,910	0,389	6,4	2,1	0,023	0,007	67,9	21,2	4,8	1,8	0,034	0,013
007	800	0,168	3,4	17	0,903	19,0	786,9	757,5	78,5	78,4	1025	1019	89,6	91,9	80,5	83,5	0,903	0,312	5,9	1,7	0,025	0,007	43,5	11,6	4,4	1,4	0,037	0,012
008	800	0,167	3,4	17	0,909	19,1	786,8	756,3	78,5	78,4	1025	1019	89,7	92,0	80,5	83,6	0,908	0,401	6,2	2,0	0,024	0,008	45,7	13,8	4,6	1,7	0,036	0,013
009	300	0,047	3,2	17	0,834	17,3	800,9	767,9	79,6	78,7	1022	1017	90,4	93,3	81,6	83,7	0,854	0,504	3,0	0,6	0,049	0,010	22,4	4,3	2,1	0,5	0,079	0,020
010	300	0,047	3,2	17	0,833	17,3	800,7	768,0	79,4	78,7	1022	1018	90,6	93,4	81,7	83,8	0,854	0,519	3,0	0,6	0,049	0,010	22,2	4,3	2,1	0,5	0,080	0,020
011	1300	0,321	3,5	17	0,925	19,5	785,1	755,8	78,0	78,1	1018	1008	87,6	89,7	80,2	83,1	0,912	0,476	6,4	2,3	0,023	0,008	48,5	16,3	4,8	1,9	0,034	0,013
012	1300	0,316	3,5	17	0,923	19,4	785,1	755,2	78,0	78,1	1018	1008	87,7	89,8	80,1	83,2	0,915	0,440	6,8	2,5	0,022	0,008	50,9	17,6	5,1	2,0	0,032	0,013
013	1300	0,316	3,4	17	0,923	19,4	784,8	756,1	77,0	78,1	1019	1008	85,2	87,1	79,0	81,6	0,915	0,563	6,5	2,5	0,023	0,009	48,3	17,9	4,9	2,1	0,034	0,014
014	2300	0,766	3,5	17	0,925	19,4	785,3	757,7	76,0	78,2	1035	1009	84,8	86,1	78,2	82,5	0,912	0,581	6,1	2,3	0,024	0,009	45,6	16,4	4,7	2,0	0,035	0,015
015	2300	0,758	3,5	17	0,921	19,3	785,4	758,6	76,0	78,2	1035	1009	84,8	86,2	78,2	82,6	0,908	0,578	5,7	2,1	0,026	0,009	42,7	14,4	4,3	1,7	0,038	0,015
016	1800	0,508	3,4	17	0,923	19,4	785,1	756,9	77,0	78,3	1030	1013	85,5	87,1	79,2	82,7	0,912	0,549	6,2	2,3	0,024	0,009	45,9	16,0	4,7	1,9	0,035	0,015
017	1800	0,499	3,4	17	0,923	19,4	785,0	756,4	77,0	78,2	1030	1013	85,5	87,2	78,6	82,8	0,914	0,552	6,4	2,5	0,023	0,009	47,6	17,2	4,9	2,1	0,034	0,014
018	1800	0,498	5,0	25	1,331	28,0	779,4	756,8	77,0	78,3	1037	1015	86,6	88,6	78,4	83,0	0,912	0,543	6,2	2,3	0,024	0,009	66,7	23,3	4,7	2,0	0,035	0,014
019	1800	0,568	5,1	25	1,355	28,5	778,9	756,8	77,0	78,3	1038	1015	86,7	88,8	78,3	83,0	0,912	0,540	6,2	2,3	0,024	0,008	67,9	23,6	4,7	1,9	0,035	0,014
020	2300	0,847	5,0	25	1,342	28,2	779,0	756,9	77,0	78,3	1047	1016	86,5	88,2	78,6	83,4	0,911	0,548	6,1	2,3	0,024	0,009	65,9	22,8	4,6	1,9	0,036	0,015
021	2300	0,845	5,0	25	1,348	28,3	779,0	756,9	77,0	78,3	1048	1016	86,6	88,4	78,6	83,5	0,912	0,543	6,2	2,3	0,024	0,009	66,6	23,0	4,7	1,9	0,035	0,014
022	800	0,200	5,0	25	1,325	27,8	781,3	758,9	77,0	78,4	1027	1016	88,5	91,1	79,0	82,2	0,903	0,338	5,9	1,7	0,025	0,007	63,7	17,4	4,4	1,4	0,038	0,012
023	800	0,201	5,0	25	1,323	27,7	781,3	759,0	77,0	78,4	1028	1016	88,7	91,2	79,1	82,2	0,902	0,331	5,8	1,7	0,025	0,007	63,1	17,0	4,4	1,4	0,038	0,012
024	1300	0,329	5,0	25	1,340	28,2	779,5	756,1	78,0	78,7	1046	1029	87,9	90,3	79,6	83,0	0,911	0,469	6,3	2,2	0,023	0,008	67,7	22,2	4,8	1,9	0,035	0,013
025	1300	0,324	4,9	25	1,325	27,9	779,5	756,5	78,1	78,7	1045	1029	88,0	90,5	80,0	83,0	0,909	0,465	6,1	2,1	0,024	0,008	65,1	20,6	4,6	1,7	0,036	0,014
026	300	0,050	4,6	25	1,196	24,6	798,9	772,5	78,0	79,1	1040	1029	88,7	92,4	79,7	82,8	0,841	0,546	2,6	0,5	0,057	0,012	27,0	5,2	1,8	0,3	0,092	0,017
027	300	0,050	4,6	25	1,189	24,5	799,0	772,9	78,0	79,1	1040	1028	88,8	92,5	79,8	82,8	0,839	0,519	2,6	0,5	0,057	0,011	27,3	5,0	1,8	0,3	0,092	0,016
028	800	0,173	2,4	12	0,639	13,5	788,0	754,4	79,0	78,4	1023	1018	86,9	89,1	80,6	82,1	0,914	0,617	6,1	2,5	0,024	0,009	31,7	12,1	4,7	2,1	0,035	0,015
029	800	0,170	2,4	12	0,635	13,4	788,0	754,5	79,0	78,4	1022	1018	87,0	89,2	80,6	82,2	0,913	0,627	6,0	2,4	0,025	0,010	31,0	11,8	4,6	2,1	0,036	0,016
030	1300	0,326	2,4	12	0,637	13,4	787,0	754,2	78,5	78,3	1026	1018	85,9	87,6	80,4	82,8	0,917	0,505	6,9	2,7	0,022	0,008	35,1	13,0	5,2	2,2	0,032	0,013
031	1300	0,321	2,4	12	0,637	13,5	786,7	754,1	78,5	78,3	1026	1017	86,0	87,7	80,3	82,9	0,917	0,480	7,0	2,8	0,021	0,008	35,9	13,4	5,4	2,3	0,031	0,013
032	1800	0,525	2,4	12	0,639	13,5	788,2	755,7	78,0	78,3	1029	1014	85,6	87,1	79,8	83,5	0,913	0,484	6,4	2,3	0,023	0,008	33,2	11,3	4,8	1,9	0,034	0,013
033	1800	0,581	2,4	12	0,632	13,3	788,3	755,8	78,0	78,3	1029	1014	85,7	87,2	80,0	83,6	0,912	0,470	6,4	2,3	0,023	0,008	32,8	11,0	4,8	1,9	0,034	0,013
034	800	0,165	2,3	12	0,633	13,4	784,8	753,8	79,5	79,0	1050	1045	88,9	91,1	81,6	83,9	0,914	0,524	6,5	2,5	0,023	0,008	32,8	11,8	4,9	2,1	0,033	0,014
035	800	0,164	2,3	12	0,629	13,3	785,0	753,6	79,5	79,0	1049	1045	88,9	91,1	81,6	84,0	0,915	0,551	6,6	2,6	0,023	0,009	32,6	12,1	5,0	2,1	0,033	0,014
036	300	0,049	2,3	12	0,596	12,5	795,4	761,4	80,5	79,2	1046	1045	92,2	93,8	82,5	84,6	0,878	0,574	3,7	1,0	0,040	0,010	18,6	4,5	2,7	0,7	0,062	0,016
037	300	0,049	2,2	12	0,594	12,4	795,4	761,5	80,5	79,2	1046	1044	92,3	93,9	82,5	84,7	0,878	0,578	3,7	1,0	0,040	0,010	18,4	4,5	2,7	0,7	0,062	0,017
038	2300	0,823	2,3	12	0,626	13,1	789,2	757,6	79,6	79,1	1067	1044	86,6	87,9	81,1	84,9	0,898	0,708	4,2	1,6	0,035	0,013	21,0	7,6	3,2	1,3	0,052	0,021
039	2300	0,820	2,3	12	0,628	13,2	789,2	758,1	79,5	79,1	1067	1044	86,7	88,0	81,1	85,0	0,896	0,742	3,8	1,6	0,039	0,016	19,1	7,5	2,9	1,2	0,057	0,024
040	1300	0,361	2,4	12	0,646	13,6	783,7	753,0	79,5	79,0	1052	1043	87,8	89,6	81,4	84,8	0,918	0,435	7,2	2,8	0,020	0,008	36,6	13,5	5,5	2,4	0,030	0,013
041	1300	0,363	2,4	12	0,644	13,6	783,7	753,0	79,5	79,0	1053	1044	87,9	89,7	81,4	84,8	0,918	0,461	7,1	2,8	0,021	0,008	36,1	13,5	5,5	2,4	0,030	0,013
042	800	0,174	3,4	17	0,909	19,1	785,0	756,0	79,0	78,9	1045	1039	89,7	92,1	81,0	83,7	0,907	0,342	6,2	1,9	0,024	0,007	45,3	13,2	4,7	1,6	0,035	0,012
043	800	0,173	3,4	17	0,911	19,2	784,8	755,7	79,0	78,9	1045	1039	89,8	92,1	81,0	83,8	0,909	0,313	6,4	2,0	0,023	0,007	46,8	13,9	4,8	1,7	0,034	0,012
044	2300	0,845	3,4	17	0,915	19,3	784,0	755,4	78,5	78,9	1064	1038	87,3	88,8	80,0	84,9	0,912	0,465	6,4	2,3	0,023	0,008	46,3	15,4	4,8	1,9	0,034	0,013
045	2300	0,840	3,4	17	0,915	19,3	784,1	756,4	78,5	78,9	1064	1038	87,4	88,9	79,6	85,0	0,908	0,458	6,0	2,0	0,024	0,008	43,7	13,5	4,5	1,7	0,037	0,014
046	1800	0,580	3,4	17	0,922	19,4	783,2	754,9	78,5	78,9	1055	1038	87,8	89,5	80,6	84,9	0,914	0,452	6,7	2,5	0,022	0,008	48,7	16,8	5,0	2,0	0,033	0,013
047	1800	0,579	3,4	17	0,922	19,4	783,3	755,0	78,5	78,9	1055	1038	87,8	89,6	80,7	85,0	0,913	0,446	6,7	2,4	0,022	0,008	48,5	16,5	5,0	2,0	0,033	0,013
048	1300	0,379	3,4	17	0,914	19,3	782,9	754,4	78,5	78,8	1047	1037	87,8	89,9	80,8	83,6	0,916	0,445	7,0	2,7	0,021	0,008	50,3	18,0	5,3	2,2	0,031	0,013
049	1300	0,384	3,4	17	0,912	19,2	782,6	754,3	78,5	78,8	1047	1036	87,9	90,0	80,8	83,7	0,916	0,442	7,0	2,7	0,021	0,008	50,5	18,1	5,3	2,2	0,031	0,013
051	300	0,059	3,2	17	0,841	17,4	798,9	767,5	79,5	79,2	1040	1036	90,3	93,3	81,7	83,7	0,856	0,561	2,9	0,7	0,050	0,011	21,4	4,5	2,0	0,5	0,082	0,020
052	800	0,183	4,9	25	1,315	27,6	778,3	758,1	78,0	78,4	1029	1018	89,1	91,6	79,6	82,5	0,902	0,303	5,9	1,7	0,025	0,007	63,2	16,8	4,4	1,4	0,037	0,012
053	800	0,181	4,9	25	1,311	27,5	778,5	757,7	78,0	78,4	1028	1017	89,1	91,7	79,7	82,5	0,904	0,300	6,0	1,8	0,025	0,007	64,4	17,6	4,5	1,5	0,036	0,012
054	300	0,053	4,7	25	1,199	24,7	795,1	773,3	77,5	78,7	1026	1014	88,5	92,1	79,5	82,4	0,840	0,377	2,9	0,5	0,050	0,009	31,5	4,9	2,0	0,4	0,082	0,015
055	300	0,053	4,7	25	1,204	24,8	795,3	773,3	77,5	78,7	1026	1014	88,6	92,2	79,5	82,5	0,840	0,341	3,0	0,5	0,049	0,008	32,4	4,9	2,1	0,5	0,079	0,017
056	2300	0,869	5,0	25	1,348	28,3	775,2	757,4	76,7	78,3	1045	1014	87,2	89,0	78,6	84,0	0,911	0,494	6,3	2,2	0,024	0,008	67,7	22,5	4,7	1,9	0,035	0,014
057	2300	0,850	5,0	25	1,352	28,4	775,0	757,4	76,7	78,3	1046	1015	87,3	89,1	78,6	84,1	0,911	0,502	6,2	2,2	0,024	0,008	67,5	22,5	4,7	1,9	0,035	0,014
058	1800	0,579	5,0	25	1,340	28,2	775,2	757,1	76,7	78,2	1035	1012	87,6	89,7	78,3	83,7	0,912	0,486	6,4	2,3	0,023	0,008	69,0	23,2	4,8	1,9	0,034	0,013
059	1800	0,579	5,0	25	1,342	28,2	774,9	757,0	76,7	78,3	1036	1013	87,7	89,8	78,6	83,8	0,913	0,481	6,5	2,3	0,023	0,008	69,8	23,7	4,9	1,9	0,034	0,013
060	1300	0,358	5,0	25	1,338	28,1	775,4	757,6	76,8	78,2	1028	1012	88,1	90,5	79,0	82,9	0,910	0,427	6,3	2,1	0,024	0,008	68,3	21,4	4,7	1,8	0,035	0,013
061	1300	0,362	5,1	25	1,356	28,5	775,2	756,9	77,5	78,2	1027	1011	88,2	90,7	79,5	83,0	0,910	0,424	6,3	2,1	0,023	0,008	69,6	21,9	4,7	1,8	0,035	0,013

Ethanol/Water with packing, Sample locations S2/S7, 0.7mm jet nozzle

	nRot	RPB_Peff	F	Qreb	mDist	LLeye	rhoL	rhoLfeed	TLfeed	TLVfeed	PI01	PI02	TI03	TI04	TI05	TI12	wi	wo	NTUg	delta NTUg	ATUg	delta ATUg	KGa	delta KGa	Nth_oi	delta Nth_oi	HETP_oi	delta HETP_oi
Unit	RPM	kW	Pa^0.5	kW	kg/min	m3/m2/h	kg/m3	kg/m3	°C	°C	mbar	mbar	°C	°C	°C	°C	g EtOH/g Mix	g EtOH/g Mix			m2	m2	1/s	1/s			m	m
Note / **Steady State No.**	of RPB		at eye	reboiler duty	FI02		DI02	DI02 at TIfeed	TI08	bubble point temperature of S4 at PI02							S7 weight frac.	S2 weight frac.	NTU (overall vapor)	uncertainty of NTUg				uncertainty of Kga	oi -> calculated starting at wo until wi is reached			
005	1300	0,323	4,9	25	1,302	27,1	782,7	764,5	70,0	78,1	1021	1007	88,7	91,0	78,9	83,5	0,917	0,504	6,7	2,8	0,022	0,009	71,1	27,5	5,1	2,2	0,032	0,014
006	1300	0,322	4,9	25	1,296	27,0	782,8	764,0	70,0	78,1	1022	1007	88,9	91,2	79,2	83,7	0,919	0,564	7,0	3,0	0,021	0,009	73,2	29,4	5,4	2,5	0,031	0,014
007	800	0,168	3,4	17	0,903	19,0	786,9	757,5	78,5	78,4	1025	1019	89,6	91,9	80,5	83,5	0,914	0,565	6,3	2,5	0,023	0,009	46,2	16,9	4,8	2,1	0,034	0,015
008	800	0,167	3,4	17	0,909	19,1	786,8	756,3	78,5	78,4	1025	1019	89,7	92,0	80,5	83,6	0,914	0,574	6,3	2,5	0,023	0,009	46,8	17,2	4,8	2,1	0,034	0,014
009	300	0,047	3,2	17	0,834	17,3	800,9	767,9	79,6	78,7	1022	1017	90,4	93,3	81,6	83,7	0,885	0,572	4,6	1,1	0,032	0,007	32,6	7,1	3,4	0,9	0,049	0,014
010	300	0,047	3,2	17	0,833	17,3	800,7	768,0	79,4	78,7	1022	1018	90,6	93,4	81,7	83,8	0,878	0,357	4,1	1,0	0,036	0,008	29,5	6,2	2,9	0,7	0,056	0,013
011	1300	0,321	3,5	17	0,925	19,5	785,1	755,8	78,0	78,1	1018	1008	87,6	89,7	80,2	83,1	0,917	0,422	6,5	2,8	0,023	0,009	48,5	19,7	5,0	2,3	0,033	0,015
012	1300	0,316	3,5	17	0,923	19,4	785,1	755,2	78,0	78,1	1018	1008	87,7	89,8	80,1	83,2	0,916	0,631	6,5	2,6	0,023	0,009	48,6	18,7	4,9	2,2	0,033	0,014
013	1300	0,316	3,4	17	0,923	19,4	784,8	756,1	77,0	78,1	1019	1008	85,2	87,1	79,0	81,6	0,919	0,591	6,4	3,0	0,023	0,010	47,8	21,0	5,0	2,4	0,033	0,016
014	2300	0,766	3,5	17	0,925	19,4	785,3	757,7	76,0	78,2	1035	1009	84,8	86,1	78,2	82,5	0,919	0,678	6,3	3,0	0,024	0,011	46,1	21,1	4,9	2,5	0,034	0,017
015	2300	0,758	3,5	17	0,921	19,3	785,4	758,6	76,0	78,2	1035	1009	84,8	86,2	78,2	82,6	0,919	0,704	6,3	3,1	0,023	0,011	46,4	21,5	5,0	2,5	0,033	0,017
016	1800	0,508	3,4	17	0,923	19,4	785,1	756,9	77,0	78,3	1030	1013	85,5	87,1	79,2	82,7	0,918	0,705	6,5	3,0	0,023	0,010	47,7	20,8	5,0	2,4	0,033	0,016
017	1800	0,499	3,4	17	0,923	19,4	785,0	756,4	77,0	78,2	1030	1013	85,5	87,2	78,6	82,8	0,918	0,669	6,4	2,9	0,023	0,010	47,4	20,5	5,0	2,4	0,033	0,016
018	1800	0,498	5,0	25	1,331	28,0	779,4	756,8	77,0	78,3	1037	1015	86,6	88,6	78,4	83,0	0,917	0,670	6,4	2,8	0,023	0,010	67,5	28,3	4,9	2,3	0,034	0,016
019	1800	0,568	5,1	25	1,355	28,5	778,9	756,8	77,0	78,3	1038	1015	86,7	88,8	78,3	83,0	0,920	0,657	6,7	3,1	0,022	0,010	72,6	31,7	5,2	2,6	0,031	0,015
020	2300	0,847	5,0	25	1,342	28,2	779,0	756,9	77,0	78,3	1047	1016	86,5	88,2	78,6	83,4	0,919	0,650	6,6	3,0	0,022	0,010	69,8	30,0	5,1	2,4	0,032	0,015
021	2300	0,845	5,0	25	1,348	28,3	779,0	756,9	77,0	78,3	1048	1016	86,6	88,4	78,6	83,5	0,916	0,653	6,2	2,7	0,024	0,010	66,0	27,0	4,8	2,2	0,035	0,016
022	800	0,200	5,0	25	1,325	27,8	781,3	758,9	77,0	78,4	1027	1016	88,5	91,1	79,0	82,2	0,912	0,659	6,1	2,3	0,024	0,009	65,1	23,5	4,6	2,0	0,036	0,015
023	800	0,201	5,0	25	1,323	27,7	781,3	759,0	77,0	78,4	1028	1016	88,7	91,2	79,1	82,2	0,911	0,591	6,2	2,2	0,024	0,008	66,7	22,2	4,7	1,9	0,035	0,014

Ethanol/n-Propanol/Water with packing, 0.7mm jet nozzle

	nRot	RPB effective motor power	F	Qreb	mDist	LLeye	rhoL	rhoLfeed	TLfeed	TLVfeed	PI01	PI02	TI03	TI04	TI05	TI12
Unit	RPM	kW	Pa^0.5	kW	kg/min	m3/m2/h	kg/m3	kg/m3	°C	°C	mbar	mbar	°C	°C	°C	°C
Note	of RPB		at eye	reboiler duty	FI02		DI02	DI02 at Tlfeed	TI08	bubble point temperature of S4 at PI02						
Steady State No.																
Ethanol/Water side of ternary diagram ("Region 1")																
243	2300	0,80	3,6	18	0,933	19,3	792,8	768,8	79,3	79,6	1042	1017	86,9	87,0	81,1	85,9
244	2300	0,80	3,5	18	0,925	19,2	793,1	768,9	79,2	79,6	1041	1016	86,9	87,0	81,1	85,9
245	1800	0,54	3,6	18	0,932	19,3	793,7	769,2	79,6	79,7	1035	1017	86,7	86,8	80,7	85,7
246	1800	0,54	3,6	18	0,930	19,3	793,7	769,1	79,5	79,7	1035	1017	86,7	86,9	80,7	85,7
247	1300	0,37	3,5	18	0,919	18,9	796,5	772,2	79,5	80,1	1028	1017	86,4	86,6	81,1	85,0
248	1300	0,37	3,5	18	0,908	18,7	796,5	772,3	79,4	80,0	1027	1015	86,4	86,6	81,1	84,9
249	300	0,05	3,4	18	0,868	17,6	809,1	784,1	81,6	81,9	1025	1019	85,6	86,4	83,3	83,2
250	300	0,05	3,4	18	0,867	17,6	809,3	784,2	81,6	81,9	1025	1019	85,6	86,4	83,3	83,2
251	800	0,18	3,4	18	0,885	18,1	801,3	776,2	80,6	80,8	1027	1020	86,2	86,7	82,0	84,3
252	800	0,18	3,4	18	0,885	18,1	801,4	776,3	80,6	80,8	1027	1019	86,2	86,7	82,0	84,3
253	1300	0,34	3,5	18	0,899	18,5	797,5	773,1	79,8	80,3	1032	1020	86,6	86,8	81,4	85,1
254	1300	0,34	3,5	18	0,903	18,6	797,4	773,0	79,8	80,3	1032	1020	86,6	86,8	81,4	85,1
255	300	0,05	2,4	13	0,614	12,5	814,1	783,6	81,4	81,7	1018	1014	85,7	86,3	83,1	83,5
256	300	0,05	2,4	13	0,610	12,4	814,1	783,5	81,5	81,7	1019	1015	85,8	86,4	83,1	83,5
257	800	0,17	2,4	13	0,628	12,9	806,0	775,3	80,3	80,6	1022	1016	86,2	86,5	81,8	84,4
258	800	0,17	2,4	13	0,633	13,0	806,2	775,8	80,2	80,6	1022	1016	86,2	86,5	81,8	84,4
259	1300	0,34	2,5	13	0,643	13,3	801,9	771,8	79,7	80,0	1026	1017	86,6	86,7	81,0	85,3
260	1300	0,33	2,5	13	0,649	13,4	802,0	771,7	79,6	80,0	1028	1018	86,6	86,8	81,1	85,4
261	2300	0,79	2,5	13	0,661	13,7	799,7	769,5	79,5	79,8	1045	1022	87,2	87,2	80,8	86,2
262	2300	0,79	2,5	13	0,661	13,7	799,5	769,3	79,6	79,8	1045	1022	87,2	87,2	80,8	86,3
263	1800	0,54	2,5	13	0,654	13,5	799,8	769,2	79,5	79,8	1037	1021	87,0	87,0	80,8	86,0
264	1800	0,54	2,5	13	0,650	13,5	799,9	769,3	79,6	79,8	1037	1021	87,0	87,1	80,8	86,1
265	1300	0,34	2,5	13	0,642	13,3	801,7	771,2	79,7	80,1	1031	1022	86,7	86,9	81,7	85,4
266	1300	0,34	2,5	13	0,640	13,2	801,8	771,1	79,8	80,1	1030	1021	86,7	86,8	81,9	85,4
267	300	0,05	1,4	8	0,353	7,2	819,3	782,2	80,9	81,7	1024	1023	86,1	86,6	83,1	83,7
268	300	0,05	1,4	8	0,352	7,2	819,3	782,0	81,2	81,7	1023	1022	86,1	86,5	83,1	83,7
269	800	0,17	1,4	8	0,355	7,3	810,9	774,0	80,1	80,4	1023	1020	86,4	86,5	81,6	84,6
270	800	0,17	1,4	8	0,358	7,4	810,9	774,1	80,0	80,5	1024	1021	86,4	86,6	81,7	84,6
271	1300	0,33	1,4	8	0,366	7,6	807,1	771,0	79,4	80,0	1026	1019	86,7	86,7	82,4	85,7
272	1300	0,33	1,4	8	0,364	7,5	807,2	771,1	79,4	80,0	1025	1019	86,7	86,7	82,4	85,7
273	2300	0,80	1,4	8	0,374	7,7	809,7	773,7	80,0	80,2	1036	1016	86,6	86,5	83,0	85,7
274	2300	0,80	1,4	8	0,374	7,7	809,8	774,1	79,9	80,2	1036	1016	86,6	86,6	83,0	85,7
275	1800	0,54	1,4	8	0,372	7,7	807,1	771,6	79,3	79,9	1027	1014	86,7	86,8	82,3	85,9
276	1800	0,54	1,4	8	0,371	7,7	807,1	771,2	79,4	79,8	1026	1013	86,7	86,7	82,2	85,9
Ethanol/n-Propanol side of ternary diagram ("Region 2")																
277	800	0,17	3,4	18	0,890	18,3	800,4	775,7	80,0	80,5	1020	1012	86,0	86,3	81,8	84,1
278	800	0,17	3,5	18	0,907	18,6	800,3	775,8	80,0	80,5	1020	1012	86,0	86,3	81,8	84,1
279	300	0,05	3,4	18	0,880	17,9	806,4	781,7	81,5	82,0	1016	1010	85,5	85,9	83,4	83,4
280	300	0,05	3,5	18	0,891	18,1	806,1	781,7	81,5	82,0	1018	1011	85,6	85,9	83,5	83,4
281	1300	0,34	3,5	18	0,917	18,9	795,0	771,3	79,0	79,7	1022	1010	86,0	86,2	80,8	84,5
282	1300	0,33	3,5	18	0,919	19,0	795,0	771,1	79,0	79,7	1023	1010	86,1	86,2	80,8	84,5
283	1800	0,53	3,5	18	0,919	19,0	791,3	767,8	78,6	79,3	1027	1008	86,2	86,3	80,1	85,1

Ethanol/n-Propanol/Water with packing, Sample locations S6/S4, 0.7mm jet nozzle (contd.)

	wi EtOH	wi nPropOH	wo EtOH	wo nPropOH	Nth_oi EtOH	delta Nth_oi EtOH	HETP_oi EtOH	delta HETP_oi EtOH	Nth_oi nPrOH	delta Nth_oi nPrOH	HETP_oi nPrOH	delta HETP_oi nPrOH	Nth_oi H2O	delta Nth_oi H2O	HETP_oi H2O	delta HETP_oi H2O
Unit	g EtOH/g Mix	g nPrOH/g Mix	g EtOH/g Mix	g nPrOH/g Mix			m	m			m	m			m	m
Note / **Steady State No.**	S4 weight frac.	S4 weight frac.	S6 weight frac.	S6 weight frac.	theoretical stages based on EtOH	uncertainty of Nth_oi, EtOH	oi -> calculated starting at wo until wi is reached									
Ethanol/Water side of ternary diagram ("Region 1")																
243	0,740	0,120	0,128	0,540	5,9	0,4	0,028	0,002	5,9	0,3	0,028	0,001	5,9	0,5	0,028	0,003
244	0,741	0,119	0,124	0,543	6,0	0,5	0,028	0,002	6,0	0,4	0,027	0,002	5,9	0,6	0,028	0,003
245	0,730	0,128	0,133	0,535	5,7	0,4	0,029	0,002	5,7	0,3	0,029	0,002	5,7	0,5	0,029	0,003
246	0,731	0,127	0,134	0,535	5,7	0,4	0,029	0,002	5,7	0,3	0,029	0,002	5,7	0,5	0,029	0,003
247	0,688	0,160	0,155	0,513	4,9	0,3	0,034	0,002	4,9	0,3	0,034	0,002	4,9	0,5	0,034	0,003
248	0,689	0,159	0,155	0,514	4,9	0,3	0,034	0,002	4,9	0,3	0,034	0,002	4,9	0,5	0,034	0,003
249	0,491	0,307	0,270	0,409	1,8	0,3	0,090	0,014	1,6	0,4	0,102	0,026	2,0	0,4	0,084	0,017
250	0,490	0,308	0,268	0,409	1,8	0,3	0,090	0,013	1,6	0,3	0,101	0,022	2,0	0,4	0,083	0,017
251	0,613	0,217	0,191	0,483	3,7	0,3	0,044	0,004	3,6	0,3	0,045	0,004	3,8	0,5	0,044	0,006
252	0,612	0,217	0,189	0,483	3,7	0,3	0,044	0,004	3,7	0,3	0,045	0,004	3,8	0,5	0,044	0,006
253	0,673	0,171	0,149	0,521	4,8	0,3	0,034	0,002	4,8	0,3	0,034	0,002	4,8	0,5	0,034	0,004
254	0,672	0,171	0,149	0,520	4,8	0,3	0,034	0,002	4,8	0,3	0,034	0,002	4,9	0,5	0,034	0,004
255	0,498	0,303	0,255	0,423	2,0	0,3	0,081	0,012	1,9	0,4	0,088	0,018	2,2	0,5	0,076	0,016
256	0,498	0,303	0,256	0,423	2,0	0,3	0,082	0,012	1,9	0,4	0,089	0,018	2,2	0,5	0,076	0,016
257	0,630	0,204	0,173	0,499	4,1	0,4	0,040	0,004	4,0	0,4	0,041	0,004	4,2	0,5	0,040	0,005
258	0,627	0,206	0,171	0,501	4,1	0,4	0,041	0,004	4,0	0,4	0,041	0,004	4,1	0,5	0,040	0,005
259	0,692	0,156	0,129	0,539	5,4	0,4	0,031	0,002	5,4	0,4	0,031	0,002	5,4	0,6	0,031	0,003
260	0,693	0,156	0,129	0,538	5,4	0,4	0,031	0,002	5,4	0,4	0,031	0,002	5,4	0,6	0,031	0,003
261	0,730	0,126	0,106	0,560	6,2	0,4	0,027	0,002	6,2	0,4	0,026	0,002	6,1	0,6	0,027	0,003
262	0,733	0,124	0,105	0,560	6,2	0,4	0,026	0,002	6,3	0,4	0,026	0,002	6,2	0,6	0,027	0,003
263	0,729	0,129	0,109	0,556	6,1	0,4	0,027	0,002	6,1	0,4	0,027	0,002	6,1	0,6	0,027	0,003
264	0,728	0,129	0,108	0,557	6,1	0,4	0,027	0,002	6,1	0,4	0,027	0,002	6,1	0,6	0,027	0,003
265	0,697	0,153	0,129	0,537	5,4	0,4	0,030	0,002	5,4	0,4	0,031	0,002	5,5	0,6	0,030	0,003
266	0,698	0,152	0,129	0,538	5,4	0,4	0,030	0,002	5,4	0,4	0,030	0,002	5,5	0,6	0,030	0,003
267	0,520	0,288	0,242	0,433	2,4	0,3	0,070	0,009	2,2	0,4	0,075	0,013	2,5	0,5	0,066	0,012
268	0,519	0,289	0,241	0,433	2,3	0,3	0,070	0,009	2,2	0,4	0,075	0,013	2,5	0,5	0,066	0,012
269	0,651	0,188	0,149	0,520	4,6	0,3	0,036	0,003	4,6	0,3	0,036	0,003	4,7	0,5	0,035	0,004
270	0,651	0,189	0,148	0,521	4,6	0,3	0,036	0,003	4,6	0,3	0,036	0,003	4,7	0,5	0,035	0,004
271	0,705	0,146	0,112	0,554	5,8	0,4	0,028	0,002	5,8	0,3	0,028	0,002	5,8	0,5	0,028	0,003
272	0,705	0,146	0,111	0,555	5,8	0,4	0,028	0,002	5,8	0,3	0,028	0,002	5,8	0,5	0,028	0,003
273	0,666	0,174	0,138	0,530	4,9	0,3	0,034	0,002	4,9	0,3	0,033	0,002	4,9	0,5	0,034	0,003
274	0,662	0,177	0,136	0,531	4,9	0,3	0,034	0,002	4,9	0,3	0,034	0,002	4,9	0,5	0,034	0,004
275	0,703	0,146	0,108	0,557	5,8	0,4	0,028	0,002	5,9	0,3	0,028	0,002	5,8	0,5	0,028	0,003
276	0,707	0,144	0,108	0,557	5,9	0,4	0,028	0,002	5,9	0,3	0,028	0,002	5,8	0,5	0,028	0,003
Ethanol/n-Propanol side of ternary diagram ("Region 2")																
277	0,624	0,210	0,210	0,615	3,6	0,3	0,046	0,004	3,6	0,3	0,046	0,004	3,6	0,6	0,046	0,007
278	0,622	0,212	0,212	0,615	3,6	0,3	0,046	0,004	3,6	0,3	0,046	0,004	3,6	0,6	0,046	0,007
279	0,463	0,349	0,266	0,571	1,6	0,3	0,101	0,021	1,7	0,3	0,099	0,015	1,4	1,5	0,114	0,122
280	0,460	0,353	0,266	0,568	1,6	0,3	0,103	0,022	1,6	0,3	0,101	0,016	1,5	1,5	0,110	0,108
281	0,708	0,145	0,189	0,629	4,7	0,4	0,035	0,003	4,7	0,3	0,035	0,002	4,6	0,6	0,035	0,004
282	0,707	0,145	0,188	0,630	4,7	0,4	0,035	0,003	4,7	0,3	0,035	0,002	4,7	0,5	0,035	0,004
283	0,757	0,109	0,170	0,643	5,5	0,4	0,030	0,002	5,6	0,3	0,030	0,002	5,5	0,6	0,030	0,003

Ethanol/n-Propanol/Water with packing, Sample locations S3/S4, 0.7mm jet nozzle

	wi EtOH	wi nPropOH	wo EtOH	wo nPropOH	Nth_oi EtOH	delta Nth_oi EtOH	HETP_oi EtOH	delta HETP_oi EtOH	Nth_oi nPrOH	delta Nth_oi nPrOH	HETP_oi nPrOH	delta HETP_oi nPrOH	Nth_oi H2O	delta Nth_oi H2O	HETP_oi H2O	delta HETP_oi H2O
Unit	g EtOH/g Mix	g nPrOH/g Mix	g EtOH/g Mix	g nPrOH/g Mix			m	m			m	m			m	m
Note / **Steady State No.**	S4 weight frac.	S4 weight frac.	S3 weight frac.	S3 weight frac.	theoretical stages based on EtOH	uncertainty of Nth_oi, EtOH	oi -> calculated starting at wo until wi is reached									
Ethanol/Water side of ternary diagram ("Region 1")																
243	0,740	0,120	0,151	0,545	5,6	0,4	0,030	0,002	5,6	0,3	0,029	0,002	5,6	0,6	0,030	0,003
244	0,741	0,119	0,144	0,553	5,7	0,4	0,029	0,002	5,8	0,3	0,029	0,002	5,7	0,6	0,029	0,003
245	0,730	0,128	0,152	0,545	5,4	0,4	0,030	0,002	5,5	0,4	0,030	0,002	5,4	0,6	0,030	0,003
246	0,731	0,127	0,149	0,549	5,5	0,4	0,030	0,002	5,5	0,4	0,030	0,002	5,5	0,6	0,030	0,003
247	0,688	0,160	0,163	0,530	4,8	0,3	0,034	0,002	4,8	0,3	0,035	0,002	4,8	0,5	0,034	0,004
248	0,689	0,159	0,164	0,529	4,8	0,3	0,034	0,002	4,8	0,3	0,034	0,002	4,8	0,5	0,034	0,004
249	0,491	0,307	0,275	0,406	1,8	0,3	0,093	0,015	1,6	0,4	0,105	0,028	1,9	0,4	0,085	0,017
250	0,490	0,308	0,285	0,410	1,7	0,3	0,097	0,016	1,5	0,4	0,111	0,030	1,8	0,4	0,090	0,019
251	0,613	0,217	0,180	0,498	3,8	0,3	0,043	0,004	3,8	0,3	0,044	0,004	3,9	0,5	0,042	0,005
252	0,612	0,217	0,178	0,501	3,9	0,3	0,043	0,004	3,8	0,3	0,043	0,004	3,9	0,5	0,042	0,005
253	0,673	0,171	0,156	0,535	4,8	0,3	0,035	0,003	4,7	0,3	0,035	0,002	4,8	0,5	0,035	0,004
254	0,672	0,171	0,155	0,537	4,8	0,3	0,035	0,002	4,7	0,3	0,035	0,002	4,8	0,5	0,034	0,004
255	0,498	0,303	0,283	0,433	1,8	0,3	0,092	0,015	1,6	0,4	0,100	0,023	1,9	0,4	0,086	0,020
256	0,498	0,303	0,294	0,430	1,7	0,3	0,097	0,016	1,6	0,4	0,106	0,025	1,8	0,4	0,091	0,022
257	0,630	0,204	0,173	0,512	4,1	0,4	0,040	0,004	4,0	0,4	0,041	0,004	4,2	0,5	0,040	0,005
258	0,627	0,206	0,170	0,514	4,1	0,4	0,040	0,004	4,0	0,4	0,041	0,004	4,1	0,5	0,040	0,005
259	0,692	0,156	0,141	0,550	5,2	0,4	0,032	0,002	5,2	0,4	0,032	0,002	5,2	0,6	0,032	0,004
260	0,693	0,156	0,139	0,552	5,2	0,4	0,032	0,002	5,2	0,4	0,032	0,002	5,2	0,6	0,032	0,003
261	0,730	0,126	0,117	0,573	6,0	0,5	0,028	0,002	6,0	0,4	0,027	0,002	5,9	0,6	0,028	0,003
262	0,733	0,124	0,117	0,573	6,0	0,5	0,027	0,002	6,1	0,4	0,027	0,002	5,9	0,6	0,028	0,003
263	0,729	0,129	0,120	0,571	5,9	0,4	0,028	0,002	5,9	0,3	0,028	0,001	5,9	0,5	0,028	0,002
264	0,728	0,129	0,120	0,571	5,9	0,4	0,028	0,002	5,9	0,3	0,028	0,002	5,9	0,5	0,028	0,003
265	0,697	0,153	0,136	0,554	5,3	0,4	0,031	0,002	5,3	0,4	0,031	0,002	5,3	0,6	0,031	0,003
266	0,698	0,152	0,137	0,553	5,3	0,4	0,031	0,002	5,3	0,4	0,031	0,002	5,3	0,6	0,031	0,003
267	0,520	0,288	0,287	0,436	1,9	0,3	0,085	0,014	1,8	0,4	0,092	0,019	2,1	0,5	0,079	0,018
268	0,519	0,289	0,300	0,431	1,8	0,3	0,091	0,015	1,7	0,4	0,099	0,021	2,0	0,4	0,085	0,019
269	0,651	0,188	0,228	0,505	3,7	0,3	0,045	0,004	3,6	0,3	0,045	0,004	3,7	0,5	0,044	0,006
270	0,651	0,189	0,226	0,511	3,7	0,3	0,045	0,004	3,7	0,3	0,045	0,004	3,8	0,5	0,044	0,006
271	0,705	0,146	0,169	0,554	4,9	0,3	0,033	0,002	4,9	0,3	0,034	0,002	4,9	0,5	0,033	0,003
272	0,705	0,146	0,168	0,555	4,9	0,3	0,033	0,002	4,9	0,3	0,033	0,002	4,9	0,5	0,034	0,003
273	0,666	0,174	0,208	0,522	4,0	0,4	0,041	0,004	4,0	0,4	0,041	0,004	4,0	0,6	0,041	0,006
274	0,662	0,177	0,215	0,521	3,9	0,3	0,042	0,003	3,9	0,3	0,042	0,003	3,9	0,5	0,043	0,005
275	0,703	0,146	0,130	0,566	5,5	0,4	0,030	0,002	5,5	0,4	0,030	0,002	5,4	0,6	0,030	0,003
276	0,707	0,144	0,132	0,565	5,5	0,4	0,030	0,002	5,5	0,4	0,030	0,002	5,4	0,6	0,030	0,003
Ethanol/n-Propanol side of ternary diagram ("Region 2")																
277	0,624	0,210	0,198	0,624	3,7	0,3	0,044	0,004	3,7	0,3	0,044	0,004	3,8	0,6	0,044	0,006
278	0,622	0,212	0,198	0,628	3,7	0,3	0,044	0,004	3,7	0,3	0,045	0,004	3,7	0,6	0,044	0,007
279	0,463	0,349	0,218	0,638	2,1	0,3	0,079	0,013	2,1	0,3	0,079	0,011	2,1	0,8	0,078	0,031
280	0,460	0,353	0,218	0,640	2,1	0,3	0,080	0,013	2,1	0,3	0,080	0,012	2,1	0,9	0,079	0,033
281	0,708	0,145	0,195	0,616	4,6	0,4	0,036	0,003	4,7	0,3	0,035	0,002	4,6	0,6	0,036	0,004
282	0,707	0,145	0,194	0,617	4,6	0,4	0,036	0,003	4,7	0,3	0,035	0,002	4,6	0,5	0,036	0,004
283	0,757	0,109	0,185	0,618	5,4	0,4	0,031	0,002	5,4	0,4	0,031	0,002	5,4	0,6	0,031	0,003

Appendix G

Overview of MOSAICmodeling elements of the developed rate-based RPB model

The MOSAICmodeling software is available through https://mosaic-modeling.de/.

Tab. G.1: MOSAICmodeling IDs of the RPB mass transfer models employing literature correlations for the component system ethanol / n-propanol, discretized using 101 elements.

Reference	Correlations (cf. Tab. 7.2)	Evaluation	Equation System	Parameter Specs	Variable Specs	Notation	Parameter List
Singh (1989)[a]	$k^L a_e$	147208	147188	147207	147209	122182	122184
Kelleher and Fair (1996)	$k^V a_e$						
Reddy et al. (2006)	$k^L_{loc} a_e$	146928	146925	146896	146927	122182	122184
	$k^V_{loc} a_e$						
Chen et al. (2006)	$k^L a_e$	146931	146929	146899	146930	122182	122184
Chen (2011)	$k^V a_e$						

[a] Simulation results using correlations of Singh (1989) and Kelleher and Fair (1996) are not presented in this work, but in Hilpert et al. (2022).

Tab. G.2: MOSAICmodeling IDs of the developed RPB mass transfer models for distillation, discretized using 101 elements.

Component System	Evaluation	Equation System	Parameter Specs	Variable Specs	Notation	Parameter List
ethanol/n-propanol	146637	146631	146632	146636	122182	122184
ethanol/water	146649		146644	146648		
ethanol/n-propanol/water	146665	146656	146658	146663		

Appendix H

Simulation of distillation data from literature using the developed model

In Fig. H.2 model predictions are compared to experimental data of Kelleher and Fair (1996), Qammar et al. (2019), and Nascimento et al. (2009) for distillation of binary mixtures at infinite reflux in single-block packing RPBs. y-variables have been kept identical to the respective publications (i.e. NTU_{og}, N_{th}, ATU_{og}).

Kelleher and Fair (1996) distilled cyclohexane/n-heptane at a pressure of 1.655 bar(a) in a rotor (r_i =87.5 mm, r_o =300 mm, h_p =150 mm) packed with Sumitomo Cr-Ni foam (a_p =2500 $m^2\,m^{-3}$, ϵ =0.92). Kelleher and Fair (1996) do not clearly state whether published NTU values are calculated with respect to vapor (NTU_{og}) or liquid side (NTU_{OL}). Assuming the values were calculated with respect to vapor side, the model significantly overpredicts the data, as illustrated by Fig. H.2a. The authors stated that flooding was observed at 500 min^{-1} and all F-factors, marked as a loss in separation efficiency. Furthermore, flooding was observed at 1.2 $Pa^{0.5}$ and 750 min^{-1}. According to Wem (2012) (cf. Fig. H.1), separation efficiency deteriorates at a throughput within approximately 70 % of the flood point. This might be a possible reason for the overprediction.

Qammar et al. (2019) distilled ethanol/water in a rotor packed with Recemat NCX1116 Cr-Ni foam (a_p =1000 $m^2\,m^{-3}$, ϵ =0.92) at atmospheric pressure at an F-factor of 0.6 $Pa^{0.5}$. Compared to the present study, the rotor size is very similar (r_i =73 mm, r_o =190 mm, h_p =10 mm) and the packing material is identical. The separation efficiency obtained by Qammar et al. is much lower, as illustrated by Fig. H.2b. The maximum in separation efficiency, observed by Qammar et al. (2019) around 200 min^{-1}, was observed in this study around 1300 min^{-1}. Possibly, the differences are due to suboptimal design of the liquid distributor for the employed low liquid flowrates. A strong influence of liquid distributor placement on separation performance was observed

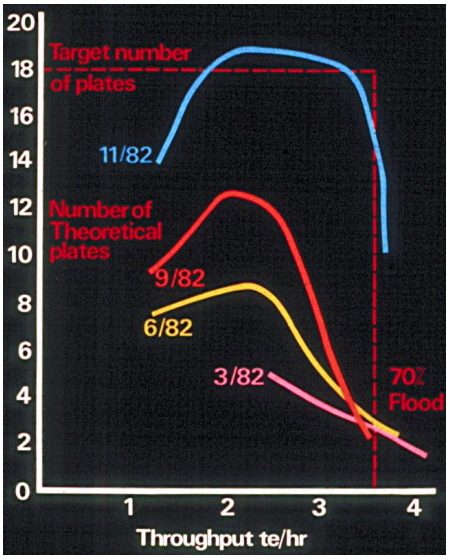
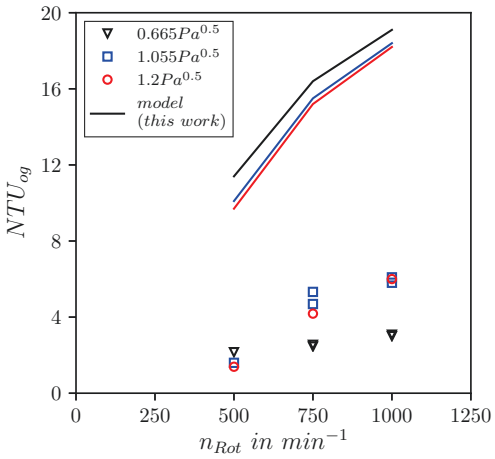


Fig. H.1: Number of theoretical stages vs. throughput for distillation of ethanol/iso-propanol at infinite reflux in one rotor of the ICI full-scale RPB (d_i =200 mm, d_o =800 mm, h_p =150 mm, rotational speed not given [5], cf. Sec. 2.5). Experiments from various dates between March and November 1982 (Wem, 2012).

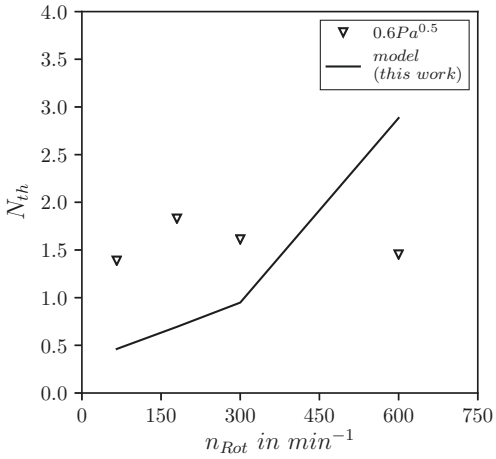
by Wem (2012). The use of flat fan nozzles for example might deteriorate separation efficiency due to liquid droplet entrainment with the vapor. However, details of the liquid distribution system of Qammar et al. are not provided.

Nascimento et al. (2009) distilled n-hexane/n-heptane in a rotor (r_i =22 mm, r_o =80 mm, h_p =40 mm) packed with structured stainless steel wire mesh sheets (a_p =2100 $m^2\,m^{-3}$, ϵ =0.74, 1 mm opening) at atmospheric pressure. Instead of the full jet distributors applied in this work, eight fins attached helicoidally to the eye of the rotor (similar to a spiral staircase) served as the liquid distributor. Possibly, the mass transfer at the eye (inner end effect) was thus less intense compared to this work, causing the significant overprediction of separation efficiency, i.e. lower ATU_{og}, shown in Fig. H.2c.

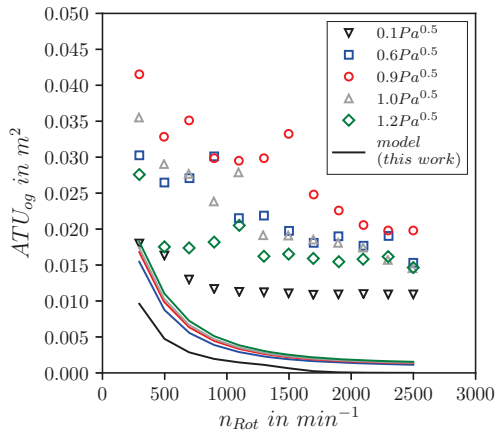
[5] Since flood point is unchanged at ≈3.5 $t\,h^{-1}$, rotational speed is constant. The increase in separation efficiency for the curves of the consecutive experiments likely resulted from optimized placement of the liquid distributor, as hinted in the abstract of Wem (2012).



(a) Kelleher and Fair (1996).



(b) Qammar et al. (2019).



(c) Nascimento et al. (2009).

Fig. H.2: Comparison of experimental data of (a) Kelleher and Fair (1996) (1.655 bar(a)), (b) Qammar et al. (2019) (packing NCX1116), and (c) Nascimento et al. (2009) (packing e01) for distillation at infinite reflux and simulated data using correlations of this study. Separation efficiency shown in dependence of n_{Rot} for various F-factors at the eye.

List of References

Agarwal, L., V. Pavani, D. P. Rao, and N. Kaistha (2010): Process Intensification in HiGee Absorption and Distillation: Design Procedure and Applications. *Industrial & Engineering Chemistry Research* 49 (20), 10046–10058. ISSN: 0888-5885. DOI: 10.1021/ie101195k (cit. on pp. 1, 2, 18–20, 29, 37, 60, 103).

Agrawal, R. and R. Tumbalam Gooty (2020): Misconceptions about efficiency and maturity of distillation. *AIChE Journal* 66 (8), 195. ISSN: 00011541. DOI: 10.1002/aic.16294 (cit. on pp. 3, 48).

Arlt, W. and U. Onken (1990): *Recommended test mixtures for distillation columns*. 2. ed. Rugby, Warwickshire: The Institution of Chemical Engineers. ISBN: 0852952481 (cit. on p. 55).

Arrhenius, S. (1887): Über die innere Reibung verdünnter wässeriger Lösungen. *Zeitschrift für Physikalische Chemie* 1U (1). ISSN: 2196-7156. DOI: 10.1515/zpch-1887-0133 (cit. on pp. 124, 125).

Aspen Plus V10 — *Aspen Plus V10 (36.0.0.249)* (2017). USA (cit. on pp. 76, 82).

Beer, M. de, A. M. Koolaard, H. Vos, G. Bargeman, and R. Schmuhl (2018): Intensified and Flexible Flash Degassing in a Rotating Packed Bed. *Industrial & Engineering Chemistry Research* 57 (42), 14261–14272. ISSN: 0888-5885. DOI: 10.1021/acs.iecr.8b03370 (cit. on pp. 83, 84, 92, 149).

Billet, R. and M. Schultes (1999): Prediction of Mass Transfer Columns with Dumped and Arranged Packings. *Chemical Engineering Research and Design* 77 (6), 498–504. ISSN: 02638762. DOI: 10.1205/026387699526520 (cit. on p. 13).

Bird, R. B., W. E. Stewart, and E. N. Lightfoot (2002): *Transport phenomena*. 2. ed., Wiley internat. ed. New York: Wiley. ISBN: 0-471-41077-2. URL: http://www.loc.gov/catdir/description/wiley036/2001023739.html (cit. on pp. 31, 95).

Blum, S. (1995): *Eignung des Stoffaustauschmodells für die Beschreibung der Vakuumrektifikation oleochemischer Grundstoffe: Zugl.: Diss*. Als Ms. gedr. Vol. Nr. 382. Fortschritt-Berichte / VDI Reihe 3, Verfahrenstechnik. Düsseldorf: VDI-Verl. ISBN: 3-18-338203-2 (cit. on pp. 12, 121).

Bravo, J. L. and J. R. Fair (1982): Generalized correlation for mass transfer in packed distillation columns. *Industrial & Engineering Chemistry Process Design and Development* 21 (1), 162–170. ISSN: 0196-4305. DOI: 10.1021/i200016a028 (cit. on p. 120).

Buckingham, E. (1914): On Physically Similar Systems; Illustrations of the Use of Dimensional Equations. *Physical Review* 4 (4), 345–376. DOI: 10.1103/PhysRev.4.345 (cit. on p. 31).

Burns, J. R., J. N. Jamil, and C. Ramshaw (2000): Process intensification: Operating characteristics of rotating packed beds — determination of liquid hold-up for a high-voidage structured packing. *Chemical Engineering Science* 55 (13), 2401–2415. ISSN: 00092509. DOI: 10.1016/S0009-2509(99)00520-5 (cit. on pp. 15, 16, 106, 107).

Burns, J. R. and C. Ramshaw (1996): Process intensification: Visual study of liquid maldistribution in rotating packed beds. *Chemical Engineering Science* 51 (8), 1347–1352. ISSN: 00092509. DOI: 10.1016/0009-2509(95)00367-3 (cit. on pp. 1, 15, 107, 115).

Byval'tsev, Y. A. and V. M. Perelygin (1970): Heat of mixing of water+propanol and ethanol+water+propanol systems (in Russian). *Izv Vyss Uchebn Zaved Pishch Tekhnol.* (5), 115 (cit. on p. 76).

Calvillo Aranda, G. U. (2020): Steady State Rate-Based Modeling of Distillation in a Rotating Packed Bed. *Master Thesis*. Berlin: Technische Universität Berlin (cit. on p. 76).

Chandra, A., P. S. Goswami, and D. P. Rao (2005): Characteristics of Flow in a Rotating Packed Bed (HIGEE) with Split Packing. *Industrial & Engineering Chemistry Research* 44 (11), 4051–4060. ISSN: 0888-5885. DOI: 10.1021/ie048815u (cit. on p. 25).

Chen, Q.-Y., G.-W. Chu, Y. Luo, L. Sang, L.-L. Zhang, H.-K. Zou, and J.-.-F. Chen (2016): Polytetrafluoroethylene Wire Mesh Packing in a Rotating Packed Bed: Mass-Transfer Studies. *Industrial & Engineering Chemistry Research* 55 (44), 11606–11613. ISSN: 0888-5885. DOI: 10.1021/acs.iecr.6b02630 (cit. on pp. 27, 31, 87, 89, 90, 106, 107, 149, 151, 154).

Chen, Y.-S. (2011): Correlations of Mass Transfer Coefficients in a Rotating Packed Bed. *Industrial & Engineering Chemistry Research* 50 (3), 1778–1785. ISSN: 0888-5885. DOI: 10.1021/ie101251z (cit. on pp. 32, 38, 49, 112, 115–117, 177).

Chen, Y.-S., C.-C. Lin, and H.-S. Liu (2005a): Mass Transfer in a Rotating Packed Bed with Various Radii of the Bed. *Industrial & Engineering Chemistry Research* 44 (20), 7868–7875. ISSN: 0888-5885. DOI: 10.1021/ie048962s (cit. on pp. 23, 32, 84, 87, 92, 93, 148, 152, 156).

Chen, Y.-S., C.-C. Lin, and H.-S. Liu (2005b): Mass Transfer in a Rotating Packed Bed with Viscous Newtonian and Non-Newtonian Fluids. *Industrial & Engineering Chemistry Research* 44 (4), 1043–1051. ISSN: 0888-5885. DOI: 10.1021/ie0499409 (cit. on pp. 32, 148, 152, 156).

Chen, Y.-S., F.-Y. Lin, C.-C. Lin, C. Y.-D. Tai, and H.-S. Liu (2006): Packing Characteristics for Mass Transfer in a Rotating Packed Bed. *Industrial & Engineering Chemistry Research* 45 (20), 6846–6853. ISSN: 0888-5885. DOI: 10.1021/ie060399l (cit. on pp. 21, 28, 32, 38, 49, 92, 93, 112, 115–117, 148, 153, 156, 177).

Chen, Y.-S. and H.-S. Liu (2002): Absorption of VOCs in a Rotating Packed Bed. *Industrial & Engineering Chemistry Research* 41 (6), 1583–1588. ISSN: 0888-5885. DOI: 10.1021/ie010752h (cit. on pp. 20, 32).

Chen, Y. H., C. Y. Chang, W. L. Su, C. C. Chen, C. Y. Chiu, Y. H. Yu, P. C. Chiang, and S. I. M. Chiang (2004): Modeling Ozone Contacting Process in a Rotating Packed Bed. *Industrial & Engineering Chemistry Research* 43 (1), 228–236. ISSN: 0888-5885. DOI: 10.1021/ie030545c (cit. on pp. 89, 148, 151, 152).

Chiang, C.-Y., Y.-S. Chen, M.-S. Liang, F.-Y. Lin, C. Y.-D. Tai, and H.-S. Liu (2009): Absorption of ethanol into water and glycerol/water solution in a rotating packed bed. *Journal of the Taiwan Institute of Chemical Engineers* 40 (4), 418–423. ISSN: 18761070. DOI: 10.1016/j.jtice.2008.11.006 (cit. on p. 32).

Chu, G.-W., X. Gao, Y. Luo, H.-K. Zou, L. Shao, and J.-.-F. Chen (2013): Distillation studies in a two-stage counter-current rotating packed bed. *Separation and Purification Technology* 102, 62–66. ISSN: 13835866. DOI: 10.1016/j.seppur.2012.09.029 (cit. on pp. 26, 37, 41, 48, 87).

Chu, G.-W., Y. Luo, Z.-Y. Xing, L. Sang, H.-K. Zou, L. Shao, and J.-.-F. Chen (2014): Mass-Transfer Studies in a Novel Multiliquid-Inlet Rotating Packed Bed. *Industrial &*

Engineering Chemistry Research 53 (48), 18580–18584. ISSN: 0888-5885. DOI: 10.1021/ie503579q (cit. on pp. 22, 26).

Chu, G.-W., L. Sang, X.-K. Du, Y. Luo, H.-K. Zou, and J.-.-F. Chen (2015): Studies of CO2 absorption and effective interfacial area in a two-stage rotating packed bed with nickel foam packing. *Chemical Engineering and Processing: Process Intensification* 90, 34–40. ISSN: 02552701. DOI: 10.1016/j.cep.2015.02.007 (cit. on pp. 22, 23).

Cooper, E. F. (1988): *Density and viscosity of n-alkane binary mixtures as a function of composition at several temperatures*. Canadian theses = Thèses canadiennes. Ottawa: National Library of Canada. ISBN: 0-315-48150-1 (cit. on p. 58).

Cortes Garcia, G. E., J. van der Schaaf, and A. A. Kiss (2017): A review on process intensification in HiGee distillation. *Journal of Chemical Technology & Biotechnology* 92 (6), 1136–1156. ISSN: 02682575. DOI: 10.1002/jctb.5206 (cit. on pp. 2, 3, 25, 30, 36, 44, 66).

Coughlin, R. W. (1969): Effect of liquid-packing surface interaction on gas absorption and flooding in a packed column. *AIChE Journal* 15 (5), 654–659. ISSN: 00011541. DOI: 10.1002/aic.690150506 (cit. on p. 11).

Counsell, J. F., J. O. Fenwick, and E. B. Lees (1970): Thermodynamic properties of organic oxygen compounds 24. Vapour heat capacities and enthalpies of vaporization of ethanol, 2-methylpropan-1-ol, and pentan-1-ol. *The Journal of Chemical Thermodynamics* 2 (3), 367–372. ISSN: 00219614. DOI: 10.1016/0021-9614(70)90007-8 (cit. on p. 76).

Cussler, E. L. (2000): *Diffusion: Mass transfer in fluid systems*. 2. ed., reprint. Cambridge series in chemical engineering. Cambridge: Cambridge Univ. Press. ISBN: 0521564778 (cit. on pp. 9, 33).

Danckwerts, P. V. (1970): *Gas-liquid reactions*. New York: McGraw-Hill Book Co. ISBN: 9780070152878 (cit. on p. 10).

Deed, D. W., P. W. Schutz, and T. B. Drew (1947): Comparison of Rectification and Desorption in Packed Columns. *Ind. Eng. Chem.* 39 (6), 766–774. DOI: 10.1021/ie50450a012 (cit. on p. 11).

Delaloye, M. M., U. von Stockar, and L. Xiao-ping (1991): The influence of viscosity on the liquid-phase mass transfer resistance in packed columns. *The Chemical*

Engineering Journal 47 (1), 51–61. ISSN: 03009467. DOI: 10.1016/0300-9467(91)85007-I (cit. on pp. 11, 33, 124).

DIN 1319-4 — DIN Deutsches Institut für Normung e.V. (1999-02): *Grundlagen der Messtechnik, Teil 4: Auswertung von Messungen - Messunsicherheiten*. Berlin (cit. on pp. 136, 137).

Dodge, B. F. and J. R. Huffman (1937): Calculation of the Number of Theoretical Plates for a Rectifying Column. *Ind. Eng. Chem.* 29 (12), 1434–1436. URL: http://pubs.acs.org/doi/abs/10.1021/ie50336a026 (last access 10/06/2017) (cit. on pp. 36, 42).

Dutra e Mello, Marcus V. and H.-M. Huang (2018): System and Methods for Deaerating Seawater using a Rotating Packed Bed Device. WO 2018/013350 (A1) (cit. on p. 89).

Edye, E. (1955): Rektifizierwirkung niedriger Füllkörperschichten. *Chemie Ingenieur Technik* 27 (11), 651–660. ISSN: 0009286X. DOI: 10.1002/cite.330271104 (cit. on pp. 12, 50, 65).

Elsenhans, A. (1906): Apparatus for purifying gas. US 820772 (cit. on p. 2).

European Chemicals Agency (2020): *Search for Chemicals*. URL: https://echa.europa.eu/de/home (last access 11/05/2020) (cit. on p. 57).

Fourer, R., D. M. Gay, and B. W. Kernighan (2009): *AMPL: A modeling language for mathematical programming*. 2. ed. Belmont, Ca.: Brooks/Cole. ISBN: 0-534-38809-4 (cit. on p. 76).

Fowler, R. (1989): Higee - a status report. *The Chemical Engineer* 456 (1), 35–37 (cit. on pp. 2, 36, 43, 47).

Gangoso Posadas, I. (2018): Espumas Metálicas de Níquel. Caracterización y Comportamiento en servicio. *Bachelor Thesis*. Valladolid: Universidad de Valladolid (cit. on p. 93).

Gao, X.-Y., G.-W. Chu, Y. Ouyang, H.-K. Zou, Y. Luo, Y. Xiang, and J.-F. Chen (2017): Gas Flow Characteristics in a Rotating Packed Bed by Particle Image Velocimetry Measurement. *Industrial & Engineering Chemistry Research* 56 (48), 14350–14361. ISSN: 0888-5885. DOI: 10.1021/acs.iecr.7b03286 (cit. on p. 18).

Garcia, H. E. and L. I. Gordon (1992): Oxygen solubility in seawater: Better fitting equations. *Limnology and Oceanography* 37 (6), 1307–1312. ISSN: 00243590. DOI: 10.4319/lo.1992.37.6.1307 (cit. on p. 84).

Gerakis, J. P. (2021): Experimental Investigation and Model Validation of Multi-Component Distillation in a Rotating Packed Bed Test Stand. *Bachelor Thesis*. Berlin: Technische Universität Berlin (cit. on pp. 118, 119).

Goedecke, R. (2006): *Fluidverfahrenstechnik*. Hoboken: Wiley-VCH. ISBN: 9783527623648. URL: http://gbv.eblib.com/patron/FullRecord.aspx?p=482022 (cit. on p. 69).

Gorak, A. and Z. Olujic (2014): *Distillation: Equipment and processes*. Burlington: Elsevier Science. ISBN: 978-0-12-386878-7. URL: http://gbv.eblib.com/patron/FullRecord.aspx?p=1719975 (cit. on p. 1).

Gorak, A. and H. Schoenmakers, eds. (2014): *Distillation: Operation and applications*. London: Academic Press. ISBN: 978-0-12-386876-3. URL: http://search.ebscohost.com/login.aspx?direct=true&scope=site&db=nlebk&db=nlabk&AN=501469 (cit. on pp. 1, 47).

Gorak, A. and A. I. Stankiewicz (2011): Intensified reaction and separation systems. *Annual review of chemical and biomolecular engineering* 2, 431–451. ISSN: 1947-5438. DOI: 10.1146/annurev-chembioeng-061010-114159 (cit. on p. 1).

Gottheil, L. (2021): Experimentelle Untersuchung der Destillation in einer rotierenden Packungskolonne (RPB). *Research Internship Report*. Berlin: Technische Universität Berlin (cit. on p. 73).

Gränicher, H. (1996): *Messung beendet - was nun? Einführung und Nachschlagewerk für die Planung und Auswertung von Messungen*. 2., überarb. Aufl. Stuttgart: Teubner. ISBN: 3-519-13659-7 (cit. on pp. 135, 137).

Groß, K., M. de Beer, S. Dohrn, and M. Skiborowski (2020): Scale-Up of the Radial Packing Length in Rotating Packed Beds for Deaeration Processes. *Industrial & Engineering Chemistry Research* 59 (23), 11042–11053. ISSN: 0888-5885. DOI: 10.1021/acs.iecr.0c00868 (cit. on pp. 91, 92, 149).

Groß, K., A. Bieberle, K. Gladyszewski, M. Schubert, U. Hampel, M. Skiborowski, and A. Gorak (2019): Analysis of Flow Patterns in High–Gravity Equipment Using Gamma–Ray Computed Tomography. *Chemie Ingenieur Technik* 91 (7), 1032–1040. ISSN: 0009286X. DOI: 10.1002/cite.201800085 (cit. on pp. 16, 76).

Gudena, K., T. H. Min, and G. P. Rangaiah (2012a): Modeling and Analysis of Novel Reactive HiGee Distillation. In: *11th International Symposium on Process Systems Engineering*. Vol. 31. Computer Aided Chemical Engineering. Elsevier, 1201–1205. ISBN: 9780444595058. DOI: 10.1016/B978-0-444-59506-5.50071-7 (cit. on pp. 29, 32, 38, 92).

Gudena, K., G. P. Rangaiah, and S. Lakshminarayanan (2012b): Modeling and analysis of solid catalyzed reactive HiGee stripping. *Chemical Engineering Science* 80, 242–252. ISSN: 00092509. DOI: 10.1016/j.ces.2012.06.008 (cit. on p. 38).

Gudena, K., G. P. Rangaiah, and S. Lakshminarayanan (2012c): Optimal Design of a Rotating Packed Bed for VOC Stripping from Contaminated Groundwater. *Industrial & Engineering Chemistry Research* 51 (2), 835–847. ISSN: 0888-5885. DOI: 10.1021/ie201218w (cit. on p. 115).

Gudena, K., G. P. Rangaiah, and L. Samavedham (2013): Modeling and Optimization of Reactive HiGee Stripper-Membrane Process for Methyl Lactate Hydrolysis. *Industrial & Engineering Chemistry Research* 52 (23), 7795–7802. ISSN: 0888-5885. DOI: 10.1021/ie303314a (cit. on pp. 29, 32, 38).

GUM 1995 — International Organization for Standardization (First edition 2008, corrected Version 2010): *Uncertainty of measurement — Part 3: Guide to the expression of uncertainty in measurement (GUM:1995)* (cit. on p. 135).

Guo, F., C. Zheng, K. Guo, Y. Feng, and N. C. Gardner (1997): Hydrodynamics and mass transfer in cross-flow rotating packed bed. *Chemical Engineering Science* 52 (21-22), 3853–3859. ISSN: 00092509. DOI: 10.1016/S0009-2509(97)00229-7 (cit. on pp. 30, 148).

Guo, J., W. Jiao, G. Qi, Z. Yuan, and Y. Liu (2019): Applications of high-gravity technologies in gas purifications: A review. *Chinese Journal of Chemical Engineering* 27 (6), 1361–1373. ISSN: 10049541. DOI: 10.1016/j.cjche.2019.01.011 (cit. on pp. 2, 44).

Guo, K., F. Guo, Y. Feng, J.-.-F. Chen, C. Zheng, and N. C. Gardner (2000): Synchronous visual and RTD study on liquid flow in rotating packed-bed contactor. *Chemical Engineering Science* 55 (9), 1699–1706. ISSN: 00092509. DOI: 10.1016/S0009-2509(99)00369-3 (cit. on pp. 1, 14, 20, 106, 107).

Guo, K., J. Wen, Y. Zhao, Y. Wang, Z. Zhang, Z. Li, and Z. Qian (2014a): Optimal packing of a rotating packed bed for H(2)S removal. *Environmental science & technology* 48 (12), 6844–6849. ISSN: 0013-936X. DOI: 10.1021/es404913e (cit. on pp. 14, 88, 103).

Guo, K., Z. Zhang, H. Luo, J. Dang, and Z. Qian (2014b): An Innovative Approach of the Effective Mass Transfer Area in the Rotating Packed Bed. *Industrial & Engineering Chemistry Research* 53 (10), 4052–4058. ISSN: 0888-5885. DOI: 10.1021/ie4029285 (cit. on pp. 17, 22).

Guo, T.-Y., K.-P. Cheng, L.-X. Wen, R. Andersson, and J.-F. Chen (2017): Three-Dimensional Simulation on Liquid Flow in a Rotating Packed Bed Reactor. *Industrial & Engineering Chemistry Research* 56 (28), 8169–8179. ISSN: 0888-5885. DOI: 10.1021/acs.iecr.7b01759 (cit. on p. 28).

Guo, T.-Y., X. Shi, G.-W. Chu, Y. Xiang, L.-X. Wen, and J.-F. Chen (2016): Computational Fluid Dynamics Analysis of the Micromixing Efficiency in a Rotating-Packed-Bed Reactor. *Industrial & Engineering Chemistry Research* 55 (17), 4856–4866. ISSN: 0888-5885. DOI: 10.1021/acs.iecr.6b00213 (cit. on p. 28).

Hampel, U., M. Schubert, A. Döß, J. Sohr, V. Vishwakarma, J.-.-U. Repke, S. J. Gerke, H. Leuner, M. Rädle, V. Kapoustina, L. Schmitt, M. Grünewald, J. H. Brinkmann, D. Plate, E. Y. Kenig, N. Lutters, L. Bolenz, F. Buckmann, D. Toye, W. Arlt, T. Linder, R. Hoffmann, H. Klein, S. Rehfeldt, T. Winkler, H.-.-J. Bart, D. Wirz, J. Schulz, S. Scholl, W. Augustin, K. Jasch, F. Schlüter, N. Schwerdtfeger, S. Jahnke, A. Jupke, C. Kabatnik, A. S. Braeuer, M. D'Auria, T. Runowski, M. F. Casal, K. Becker, A.-.-L. David, A. Górak, M. Skiborowski, K. Groß, and H. Qammar (2020): Recent Advances in Experimental Techniques for Flow and Mass Transfer Analyses in Thermal Separation Systems. *Chemie Ingenieur Technik* 92 (7), 926–948. ISSN: 0009286X. DOI: 10.1002/cite.202000076 (cit. on pp. 13, 121).

Harbold, G. and J. Park (2008): *Using the GasTran® Deaeration System to achieve low dissolved oxygen levels for superior line speed and product quality: a case study in carbonated soft drink bottling*. URL: https://www.gastransfer.com/documents/CSD_Deaeration_Tech_paper.pdf (last access 09/16/2020) (cit. on pp. 2, 44, 83).

Harriott, P. (1962): A review of mass transfer to interfaces. *The Canadian Journal of Chemical Engineering* 40 (2), 60–69. ISSN: 00084034. DOI: 10.1002/cjce.5450400205 (cit. on p. 6).

Hassan-Beck, H. M. (1997): Process Intensification: Mass Transfer and Pressure Drop for Countercurrent Rotating Packed Beds. *Dissertation*. University of Newcastle-upon-Tyne. URL: https://theses.ncl.ac.uk/dspace/bitstream/10443/665/1/Hassan-Beck97.pdf (last access 02/06/2017) (cit. on p. 127).

Hegely, L., J. Roesler, P. Alix, D. Rouzineau, and M. Meyer (2017): Absorption methods for the determination of mass transfer parameters of packing internals: A literature review. *AIChE Journal* 63 (8), 3246–3275. ISSN: 00011541. DOI: 10.1002/aic.15737 (cit. on pp. 9, 10, 89, 119).

Henley, E. J., J. D. Seader, and D. K. Roper (2011): *Separation process principles*. 3. ed., internat. student version. Hoboken, NJ: Wiley. ISBN: 978-0-470-48183-7 (cit. on pp. 3, 5–8, 82, 102).

Hilpert, M., G. U. Calvillo Aranda, and J.-U. Repke (2022): Experimental analysis and rate-based stage modeling of multicomponent distillation in a Rotating Packed Bed. *Chemical Engineering and Processing: Process Intensification* 171, 108651. ISSN: 0255-2701. DOI: 10.1016/j.cep.2021.108651 (cit. on pp. 3, 29, 35, 47, 53, 71, 75, 77, 96, 97, 101, 105, 109, 110, 120, 157, 177).

Hilpert, M. and J.-U. Repke (2020): Systematische Untersuchungen des Stofftransportes zur Modellierung der Rektifikation in Rotating Packed Beds (Presentation). *Jahrestreffen der ProcessNet-Fachgruppen Fluidverfahrenstechnik, Adsorption und Extraktion*. Feb. 26-28, Berchtesgaden (Germany) (cit. on p. 68).

Hilpert, M. and J.-U. Repke (2021): Experimental Investigation and Correlation of Liquid-Side Mass Transfer in Pilot-Scale Rotating Packed Beds. *Industrial & Engineering Chemistry Research* 60 (14), 5251–5263. ISSN: 0888-5885. DOI: 10.1021/acs.iecr.1c00440 (cit. on pp. 29, 53, 71, 83, 87, 89, 92, 95, 135, 139, 145, 147, 148, 151, 152).

Huerta-Pérez, F. and J. R. Pérez-Correa (2018): Optimizing ethanol recovery in a spinning cone column. *Journal of the Taiwan Institute of Chemical Engineers* 83, 1–9. ISSN: 18761070. DOI: 10.1016/j.jtice.2017.11.030 (cit. on p. 2).

Jiao, W. Z., Y. Z. Liu, and G. S. Qi (2010): Gas Pressure Drop and Mass Transfer Characteristics in a Cross-flow Rotating Packed Bed with Porous Plate Packing. *Industrial & Engineering Chemistry Research* 49 (8), 3732–3740. ISSN: 0888-5885. DOI: 10.1021/ie9009777 (cit. on p. 31).

Joel, A. S., M. Wang, and C. Ramshaw (2015): Modelling and simulation of intensified absorber for post-combustion CO2 capture using different mass transfer correlations. *Applied Thermal Engineering* 74, 47–53. ISSN: 13594311. DOI: 10.1016/j.applthermaleng.2014.02.064 (cit. on pp. 29, 32).

Joel, A. S., M. Wang, C. Ramshaw, and E. Oko (2014): Process analysis of intensified absorber for post-combustion CO2 capture through modelling and simulation. *International Journal of Greenhouse Gas Control* 21, 91–100. ISSN: 17505836. DOI: 10.1016/j.ijggc.2013.12.005 (cit. on p. 29).

Kapoustina, V., J. Guffart, A. Hien, J. Strischakov, I. Medina, M. Rädle, and J.-U. Repke (2019): Influence of a single microstructure on local mass transfer in liquid film flows. *Chemical Engineering Research and Design* 146, 352–362. ISSN: 02638762. DOI: 10.1016/j.cherd.2019.04.022 (cit. on p. 90).

Kelleher, T. and J. R. Fair (1996): Distillation Studies in a High-Gravity Contactor. *Industrial & Engineering Chemistry Research* 35 (12), 4646–4655. ISSN: 0888-5885. DOI: 10.1021/ie950662a (cit. on pp. 19, 21, 36, 39, 51, 68, 69, 93, 128, 177, 179, 181).

Kenig, E. Y. and S. Blagov (2014): Chapter 10 - Modeling of Distillation Processes. In: *Distillation: Fundamentals and Principles*. Ed. by A. Gorak and E. Sorensen. Elsevier, 383–436. ISBN: 9780123865472. DOI: 10.1016/B978-0-12-386547-2.00010-7 (cit. on p. 29).

Keyvani, M. and N. C. Gardner (1988): *Operating Characteristics of Rotating Beds: Technical Progress Report*. Cleveland, Ohio. URL: https://www.osti.gov/scitech/servlets/purl/7279454 (last access 02/06/2017) (cit. on p. 58).

Keyvani, M. and N. C. Gardner (1989): Operating Characteristics of Rotating Beds. *Chemical Engineering Progress* 85 (9), 48–52 (cit. on pp. 16, 18).

Khattab, I. S., F. Bandarkar, M. A. A. Fakhree, and A. Jouyban (2012): Density, viscosity, and surface tension of water+ethanol mixtures from 293 to 323K. *Korean Journal of Chemical Engineering* 29 (6), 812–817. ISSN: 0256-1115. DOI: 10.1007/s11814-011-0239-6 (cit. on p. 73).

Kiss, A. A. (2013): *Advanced distillation technologies: Design, control, and applications*. 1st ed. Chichester, West Sussex, United Kingdom: Wiley. ISBN: 9781119993612. URL: http://search.ebscohost.com/login.aspx?direct=true&scope=site&db=nlebk&db=nlabk&AN=566490 (cit. on pp. 1, 47).

Kister, H. Z. (1992): *Distillation design*. New York: McGraw Hill. ISBN: 0-07-034909-6 (cit. on p. 120).

Kletz, T. A. and P. Amyotte (1998): *Process plants: A handbook for inherently safer design*. [New ed.] Philadelphia, PA: Taylor & Francis. ISBN: 1560326190 (cit. on pp. 44, 47).

Kooijman, H. A. and R. Taylor (1991): Estimation of diffusion coefficients in multicomponent liquid systems. *Industrial & Engineering Chemistry Research* 30 (6), 1217–1222. ISSN: 0888-5885. DOI: 10.1021/ie00054a023 (cit. on p. 81).

Kraume, M. (2012): *Transportvorgänge in der Verfahrenstechnik: Grundlagen und apparative Umsetzungen*. 2., bearb. Aufl. VDI Verfahrenstechnik. Berlin: Springer Vieweg. ISBN: 978-3-642-25149-8 (cit. on p. 6).

Krink, N. (2019): Implementierung des Prozessleitsystems und Inbetriebnahme eines Rotating-Packed-Bed-Versuchsstandes. *Master Thesis*. Berlin: Technische Universität Berlin (cit. on p. 60).

Krishna, R., H. F. Martinez, R. Sreedhar, and G. L. Standart (1977): Murphree Point Efficiencies in Multicomponent Systems. *Transactions of the Institution of Chemical Engineers* 55, 178–183 (cit. on p. 102).

Krishnamurthy, R. and R. Taylor (1985): A nonequilibrium stage model of multicomponent separation processes. Part II: Comparison with experiment. *AIChE Journal* 31 (3), 456–465. ISSN: 00011541. DOI: 10.1002/aic.690310313 (cit. on p. 82).

Kumar, M. P. and D. P. Rao (1990): Studies on a high-gravity gas-liquid contactor. *Industrial & Engineering Chemistry Research* 29 (5), 917–920. ISSN: 0888-5885. DOI: 10.1021/ie00101a031 (cit. on p. 19).

Larkin, J. (1975): Thermodynamic properties of aqueous non-electrolyte mixtures I. Excess enthalpy for water + ethanol at 298.15 to 383.15 K. *The Journal of Chemical Thermodynamics* 7 (2), 137–148. ISSN: 00219614. DOI: 10.1016/0021-9614(75)90261-X (cit. on p. 76).

Leffler, J. and H. T. Cullinan (1970): Variation of Liquid Diffusion Coefficients with Composition. Binary Systems. *Industrial & Engineering Chemistry Fundamentals* 9 (1), 84–88. ISSN: 0196-4313. DOI: 10.1021/i160033a013 (cit. on pp. 124, 126).

Li, W., X. Shi, S. Zhang, and G. Qi (2020): Modelling of ammonia recovery from wastewater by air stripping in rotating packed beds. *The Science of the total environment* 702, 134971. DOI: 10.1016/j.scitotenv.2019.134971 (cit. on pp. 92, 115).

Li, W., B. Song, X. Li, and Y. Liu (2017a): Modelling of vacuum distillation in a rotating packed bed by Aspen. *Applied Thermal Engineering* 117, 322–329. ISSN: 13594311. DOI: 10.1016/j.applthermaleng.2017.01.046 (cit. on pp. 32, 36, 38, 41, 48, 49, 87, 92, 106, 115).

Li, W., W. Wu, H.-K. Zou, G. Chu, L. Shao, and J.-.-F. Chen (2010): A Mass Transfer Model for Devolatilization of Highly Viscous Media in Rotating Packed Bed. *Chinese Journal of Chemical Engineering* 18 (2), 194–201. ISSN: 10049541. DOI: 10.1016/S1004-9541(08)60342-0 (cit. on p. 30).

Li, X. and Y. Liu (2010): Characteristics of Fin Baffle Packing Used in Rotating Packed Bed. *Chinese Journal of Chemical Engineering* 18 (1), 55–60. ISSN: 10049541. DOI: 10.1016/S1004-9541(08)60323-7 (cit. on pp. 36, 40).

Li, X., Y. Liu, Z. Li, and X. Wang (2008): Continuous Distillation Experiment with Rotating Packed Bed. *Chinese Journal of Chemical Engineering* 16 (4), 656–662. ISSN: 10049541. DOI: 10.1016/S1004-9541(08)60137-8 (cit. on pp. 36, 39).

Li, Y., J. Ji, Z. Xu, G. Wang, X. Li, and X. Liu (2013a): Pressure Drop Model on Rotating Zigzag Bed as a New High-Gravity Technology. *Industrial & Engineering Chemistry Research* 52 (12), 4638–4649. ISSN: 0888-5885. DOI: 10.1021/ie301207e (cit. on p. 26).

Li, Y., X. Li, Y. Wang, Y. Chen, J. Ji, Y. Yu, and Z. Xu (2014): Distillation in a Counterflow Concentric-Ring Rotating Bed. *Industrial & Engineering Chemistry Research* 53 (12), 4821–4837. ISSN: 0888-5885. DOI: 10.1021/ie4019337 (cit. on pp. 30, 37, 41, 69).

Li, Y., Y. Lu, X. Liu, G. Wang, Y. Nie, and J. Ji (2017b): Mass-transfer characteristics in a rotating zigzag bed as a Higee device. *Separation and Purification Technology* 186, 156–165. ISSN: 13835866. DOI: 10.1016/j.seppur.2017.05.049 (cit. on p. 26).

Li, Y., Y. YuLi, Z. XuLi, X. LiLi, X. Liu, and J. Ji (2013b): Rotating zigzag bed as trayed HIGEE and its power consumption. *Asia-Pacific Journal of Chemical Engineering* 8 (4), 494–506. ISSN: 19322135. DOI: 10.1002/apj.1688 (cit. on pp. 25, 37).

Lin, C.-C. and Y.-W. Chen (2011): Performance of a cross-flow rotating packed bed in removing carbon dioxide from gaseous streams by chemical absorption. *International Journal of Greenhouse Gas Control* 5 (4), 668–675. ISSN: 17505836. DOI: 10.1016/j.ijggc.2011.02.002 (cit. on p. 127).

Lin, C.-C., T.-J. Ho, and W.-T. Liu (2002): Distillation in a Rotating Packed Bed. *JOURNAL OF CHEMICAL ENGINEERING OF JAPAN* 35 (12), 1298–1304. ISSN: 00219592. DOI: 10.1252/jcej.35.1298 (cit. on pp. 36, 39, 48, 69, 106, 127, 128).

Lin, C.-C. and G.-S. Jian (2007): Characteristics of a rotating packed bed equipped with blade packings. *Separation and Purification Technology* 54 (1), 51–60. ISSN: 13835866. DOI: 10.1016/j.seppur.2006.08.006 (cit. on pp. 31, 87, 89, 148, 153, 155).

Lin, C.-C. and W.-T. Liu (2007): Mass Transfer Characteristics of a High-voidage Rotating Packed Bed. *Journal of Industrial and Engineering Chemistry* 13 (1), 71–78 (cit. on p. 148).

Lin, C.-C., T.-Y. Wei, W.-T. Liu, and K.-P. Shen (2004): Removal of VOCs from Gaseous Streams in a High-Voidage Rotating Packed Bed. *JOURNAL OF CHEMICAL ENGINEERING OF JAPAN* 37 (12), 1471–1477. ISSN: 00219592. DOI: 10.1252/jcej.37.1471 (cit. on p. 32).

Linek, V., T. Moucha, E. Prokopová, and J. F. Rejl (2005): Simultaneous Determination of Vapour- and Liquid-Side Volumetric Mass Transfer Coefficients in Distillation Column. *Chemical Engineering Research and Design* 83 (8), 979–986. ISSN: 02638762. DOI: 10.1205/cherd.03311 (cit. on pp. 12, 50).

Liu, H.-S., C.-C. Lin, S.-C. Wu, and H.-W. Hsu (1996): Characteristics of a Rotating Packed Bed. *Industrial & Engineering Chemistry Research* 35 (10), 3590–3596. ISSN: 0888-5885. DOI: 10.1021/ie960183r (cit. on pp. 18, 32).

Liu, T., D. Wang, W. Wang, Q. Liang, and L. Shao (2019a): Study on the Efficient Production of Ozone Water by a Rotating Packed Bed. *Industrial & Engineering Chemistry Research* 58 (17), 7227–7232. ISSN: 0888-5885. DOI: 10.1021/acs.iecr.8b06486 (cit. on pp. 21, 87).

Liu, W., G.-W. Chu, Y. Luo, Y.-Z. Liu, F.-Y. Meng, B.-.-C. Sun, and J.-.-F. Chen (2019b): Mass transfer in a rotating packed bed reactor with a mesh-pin rotor: Modeling and experimental studies. *Chemical Engineering Journal* 369, 600–610. ISSN: 13858947. DOI: 10.1016/j.cej.2019.03.081 (cit. on pp. 30, 149).

Liu, W., Y. Luo, Y.-B. Li, and G.-W. Chu (2020): Scale-Up of a Rotating Packed Bed Reactor with a Mesh-Pin Rotor: (II) Mass Transfer and Application. *Industrial & Engineering Chemistry Research* 59 (11), 5124–5132. ISSN: 0888-5885. DOI: 10.1021/acs.iecr.9b06684 (cit. on pp. 27, 30, 31).

Liu, Y., Y. Luo, G.-W. Chu, J.-Z. Luo, M. Arowo, and J.-.-F. Chen (2017): 3D numerical simulation of a rotating packed bed with structured stainless steel wire mesh packing. *Chemical Engineering Science* 170, 365–377. ISSN: 00092509. DOI: 10.1016/j.ces.2017.01.033 (cit. on pp. 18, 22, 28).

Llerena-Chavez, H. and F. Larachi (2009): Analysis of flow in rotating packed beds via CFD simulations—Dry pressure drop and gas flow maldistribution. *Chemical Engineering Science* 64 (9), 2113–2126. ISSN: 00092509. DOI: 10.1016/j.ces.2009.01.019 (cit. on pp. 27, 62).

Lockett, M. J. (1995): Flooding of rotating structured packing and its application to conventional packed columns. *Chemical Engineering Research & Design* 73, 379–384 (cit. on p. 1).

Lukin, I., L. Pietzka, I. Wingartz, and G. Schembecker (2021): Aroma absorption in rapeseed oil using rotating packed bed. *Flavour and Fragrance Journal* 36 (1), 137–147. ISSN: 0882-5734. DOI: 10.1002/ffj.3623 (cit. on p. 127).

Luo, Y., G.-W. Chu, H.-K. Zou, F. Wang, Y. Xiang, L. Shao, and J.-.-F. Chen (2012a): Mass Transfer Studies in a Rotating Packed Bed with Novel Rotors: Chemisorption of CO2. *Industrial & Engineering Chemistry Research* 51 (26), 9164–9172. ISSN: 0888-5885. DOI: 10.1021/ie300466f (cit. on pp. 21, 22, 30, 58).

Luo, Y., G.-W. Chu, H.-K. Zou, Y. Xiang, L. Shao, and J.-.-F. Chen (2012b): Characteristics of a two-stage counter-current rotating packed bed for continuous distillation. *Chemical Engineering and Processing: Process Intensification* 52, 55–62. ISSN: 02552701. DOI: 10.1016/j.cep.2011.11.011 (cit. on pp. 26, 37, 40, 48, 87).

Luo, Y., G. Chu, L. Sang, H.-K. Zou, Y. Xiang, and J.-.-F. Chen (2016): A two-stage blade-packing rotating packed bed for intensification of continuous distillation. *Chinese Journal of Chemical Engineering* 24 (1), 109–115. ISSN: 10049541. DOI: 10.1016/j.cjche.2015.06.015 (cit. on pp. 37, 41, 48, 49, 87, 106).

Luo, Y., J.-Z. Luo, G.-W. Chu, Z.-Q. Zhao, M. Arowo, and J.-.-F. Chen (2017): Investigation of effective interfacial area in a rotating packed bed with structured stainless steel wire mesh packing. *Chemical Engineering Science* 170, 347–354. ISSN: 00092509. DOI: 10.1016/j.ces.2016.10.023 (cit. on pp. 23, 90, 106, 107).

Ma, C., M.-J. Su, Y. Luo, G.-W. Chu, B.-.-C. Sun, and J.-.-F. Chen (2019): Wetting Behavior of the Stainless Steel Wire Mesh with Al2O3 Coatings and Mass Transfer Intensification in a Rotating Packed Bed. *Industrial & Engineering Chemistry Re-*

search 59 (3), 1374–1382. ISSN: 0888-5885. DOI: 10.1021/acs.iecr.9b04745 (cit. on pp. 27, 31, 90, 106, 107).

MacInnes, J. M. and A. A. Ayash (2018): Mass transfer characteristics of rotating spiral gas-liquid contacting. *Chemical Engineering Science* 175, 320–334. ISSN: 00092509. DOI: 10.1016/j.ces.2017.10.005 (cit. on p. 2).

Majer, V., V. Svoboda, V. Hynek, and J. Pick (1978): A new calorimeter for determination of the temperature dependence of heat of vaporization. *Collection of Czechoslovak Chemical Communications* 43 (5), 1313–1324. ISSN: 0010-0765. DOI: 10.1135/cccc19781313 (cit. on p. 76).

Meeuwse, M., J. van der Schaaf, and J. C. Schouten (2012): Multistage rotor-stator spinning disc reactor. *AIChE Journal* 58 (1), 247–255. ISSN: 00011541. DOI: 10.1002/aic.12586 (cit. on p. 2).

Mersmann, A., H. Voit, and R. Zeppenfeld (1986): Brauchen wir Stoffaustausch-Maschinen?. *Chemie Ingenieur Technik* 58 (2), 87–96. ISSN: 0009286X. DOI: 10.1002/cite.330580202 (cit. on p. 43).

Mondal, A., A. Pramanik, A. Bhowal, and S. Datta (2012): Distillation studies in rotating packed bed with split packing. *Chemical Engineering Research and Design* 90 (4), 453–457. ISSN: 02638762. DOI: 10.1016/j.cherd.2011.08.008 (cit. on pp. 37, 40, 48, 69, 106).

Moore, S. R. (1986): Mass transfer to thin liquid films on rotating surfaces, with and without chemical reaction. *PhD Thesis*. Newcastle upon Tyne: Newcastle University. URL: http://hdl.handle.net/10443/329 (last access 10/14/2020) (cit. on p. 15).

Munjal, S., M. P. Dudukovič, and P. Ramachandran (1989a): Mass-transfer in rotating packed beds—I. Development of gas—liquid and liquid—solid mass-transfer correlations. *Chemical Engineering Science* 44 (10), 2245–2256. ISSN: 00092509. DOI: 10.1016/0009-2509(89)85159-0 (cit. on pp. 94, 118).

Munjal, S., M. P. Dudukovič, and P. Ramachandran (1989b): Mass-transfer in rotating packed beds—II. Experimental results and comparison with theory and gravity flow. *Chemical Engineering Science* 44 (10), 2257–2268. ISSN: 00092509. DOI: 10.1016/0009-2509(89)85160-7 (cit. on pp. 23, 30).

Narasimhan, S. and C. Jordache (2010): *Data reconciliation & gross error detection: An intelligent use of process data*. Houston: Gulf Pub. Co. ISBN: 9780080503714. URL: http://www.sciencedirect.com/science/book/9780884152552 (cit. on pp. 135, 136).

Nascimento, J. V. S., T. M. K. Ravagnani, and Pereira, J. A. F. R. (2009): Experimental study of a rotating packed bed distillation column. *Brazilian Journal of Chemical Engineering* 26 (1), 219–226. ISSN: 0104-6632. DOI: 10.1590/S0104-66322009000100021 (cit. on pp. 36, 40, 48, 49, 87, 106, 128, 179–181).

Neumann, K. (2018): *Operating Characteristics of Rotating Packed Beds*. Verfahrenstechnik. München: Dr. Hut. ISBN: 978-3-8439-3800-6 (cit. on pp. 21, 24, 47, 60, 68, 127).

Neumann, K., S. Hunold, M. de Beer, M. Skiborowski, and A. Gorak (2018): Mass Transfer Studies in a Pilot Scale RPB with Different Packing Diameters. *Industrial & Engineering Chemistry Research* 57 (6), 2258–2266. ISSN: 0888-5885. DOI: 10.1021/acs.iecr.7b04186 (cit. on p. 20).

Neumann, K., S. Hunold, K. Groß, and A. Gorak (2017a): Experimental investigations on the upper operating limit in rotating packed beds. *Chemical Engineering and Processing: Process Intensification* 121, 240–247. ISSN: 02552701. DOI: 10.1016/j.cep.2017.09.003 (cit. on pp. 20, 54, 56, 68, 70, 88, 101, 127).

Neumann, K., S. Hunold, M. Skiborowski, and A. Gorak (2017b): Dry Pressure Drop in Rotating Packed Beds—Systematic Experimental Studies. *Industrial & Engineering Chemistry Research*. ISSN: 0888-5885. DOI: 10.1021/acs.iecr.7b03203 (cit. on pp. 19, 79).

Oko, E., M. Wang, and C. Ramshaw (2019): Study of mass transfer correlations for rotating packed bed columns in the context of solvent-based carbon capture. *International Journal of Greenhouse Gas Control* 91, 102831. ISSN: 17505836. DOI: 10.1016/j.ijggc.2019.102831 (cit. on p. 32).

Onda, K., H. Takeuchi, and Y. Okumoto (1968): MASS TRANSFER COEFFICIENTS BETWEEN GAS AND LIQUID PHASES IN PACKED COLUMNS. *JOURNAL OF CHEMICAL ENGINEERING OF JAPAN* 1 (1), 56–62. ISSN: 00219592. DOI: 10.1252/jcej.1.56 (cit. on pp. 11–13, 31, 36, 50, 54, 95, 118).

Ovejero, G., R. van Grieken, L. Rodriguez, and J. L. Valverde (1992): The use of gas absorption correlations for mass transfer coefficients in distillation processes. *In-*

ternational Journal of Heat and Mass Transfer 35 (11), 2963–2968. ISSN: 00179310. DOI: 10.1016/0017-9310(92)90316-K (cit. on p. 11).

Papaioannou, D., T. Evangelou, and C. Panayiotou (1991): Dynamic viscosity of multicomponent liquid mixtures. *Journal of Chemical & Engineering Data* 36 (1), 43–46. ISSN: 0021-9568. DOI: 10.1021/je00001a013 (cit. on pp. 124, 125).

Pelkonen, S. (1997): *Multicomponent mass transfer in packed distillation columns: Zugl.: Dortmund, Univ., Diss., 1997*. Als Ms. gedr. Berichte aus der Verfahrenstechnik. Aachen: Shaker. ISBN: 3-8265-3164-7 (cit. on pp. 50, 54, 55).

Perry, R. H. and D. W. Green (2008): *Perry's chemical engineers' handbook*. 8. ed. New York, NY: McGraw-Hill. ISBN: 978-0-07-142294-9 (cit. on pp. 92, 145).

Poling, B. E., J. M. Prausnitz, and J. P. O'Connell (2001): *The properties of gases and liquids*. 5. ed., internat. ed. McGraw-Hill international editions Chemical engineering series. New York, NY: McGraw-Hill. ISBN: 0070116822 (cit. on pp. 81, 146).

Prada, R. J., E. L. Martínez, and M. R. Wolf Maciel (2012): Computational Study of a Rotating Packed Bed Distillation Column. In: *22nd European Symposium on Computer Aided Process Engineering*. Vol. 30. Computer Aided Chemical Engineering. Elsevier, 1113–1117. ISBN: 9780444594310. DOI: 10.1016/B978-0-444-59520-1.50081-6 (cit. on pp. 29, 37).

PubChem (2020a): *PubChem Compound Summary for CID 1031, Propanol*. Ed. by National Center for Biotechnology Information. URL: https://pubchem.ncbi.nlm.nih.gov/compound/Propanol (last access 11/05/2020) (cit. on p. 58).

PubChem (2020b): *PubChem Compound Summary for CID 6560, Isobutanol*. Ed. by National Center for Biotechnology Information. URL: https://pubchem.ncbi.nlm.nih.gov/compound/Isobutanol (last access 11/05/2020) (cit. on p. 58).

PubChem (2020c): *PubChem Compound Summary for CID 702, Ethanol*. Ed. by National Center for Biotechnology Information. URL: https://pubchem.ncbi.nlm.nih.gov/compound/Ethanol (last access 11/05/2020) (cit. on p. 58).

PubChem (2020d): *PubChem Compound Summary for CID 887, Methanol*. Ed. by National Center for Biotechnology Information. URL: https://pubchem.ncbi.nlm.nih.gov/compound/Methanol (last access 11/05/2020) (cit. on p. 58).

PubChem (2020e): *PubChem Compound Summary for CID 8900, Heptane*. Ed. by National Center for Biotechnology Information. URL: https://pubchem.ncbi.nlm.nih.gov/compound/Heptane (last access 11/05/2020) (cit. on p. 58).

PubChem (2020f): *PubChem Compound Summary for CID 962, Water*. Ed. by National Center for Biotechnology Information. URL: https://pubchem.ncbi.nlm.nih.gov/compound/Water (last access 11/05/2020) (cit. on p. 58).

Qammar, H., K. Gladyszewski, A. Gorak, and M. Skiborowski (2019): Towards the Development of Advanced Packing Design for Distillation in Rotating Packed Beds. *Chemie Ingenieur Technik* 91 (11), 1663–1673. ISSN: 0009286X. DOI: 10.1002/cite.201900053 (cit. on pp. 21, 25–27, 37, 42, 47–49, 87, 106, 116, 128, 179, 181).

Qammar, H., F. Hecht, M. Skiborowski, and A. Gorak (2018): Experimental Investigation and Design of Rotating Packed Beds for Distillation. *Chemical Engineering Transactions* 69, 655–660. DOI: 10.3303/CET1869110 (cit. on pp. 36, 42, 48, 55, 87, 108, 118).

Qi, G. S., H. Wang, Y. Z. Liu, Z. W. Zhu, J. X. Tian, and J. Fu (2016): Characteristics of gas pressure drop of a countercurrent-flow rotating packed bed. *Indian Journal of Chemical Technology* 23, 59–64. URL: http://nopr.niscair.res.in/handle/123456789/33816 (last access 02/14/2017) (cit. on p. 18).

Qian, Z., L. Xu, H. Cao, and K. Guo (2009): Modeling Study on Absorption of CO2 by Aqueous Solutions of N-Methyldiethanolamine in Rotating Packed Bed. *Industrial & Engineering Chemistry Research* 48 (20), 9261–9267. ISSN: 0888-5885. DOI: 10.1021/ie900894a (cit. on p. 30).

Rajan, S., M. Kumar, M. J. Ansari, D. P. Rao, and N. Kaistha (2011): Limiting Gas Liquid Flows and Mass Transfer in a Novel Rotating Packed Bed (HiGee). *Industrial & Engineering Chemistry Research* 50 (2), 986–997. ISSN: 0888-5885. DOI: 10.1021/ie100899r (cit. on pp. 2, 22, 26, 32, 54, 58, 87).

Ramalho, R. S. and M. Ruel (1968): Heats of mixing for binary systems: N -Alkanes + n -Alcohols and n -Alcohols. *The Canadian Journal of Chemical Engineering* 46 (6), 456–461. ISSN: 00084034. DOI: 10.1002/cjce.5450460613 (cit. on p. 76).

Ramshaw, C. (1983): HIGEE Distillation - An Example of Process Intensification. *The Chemical Engineer* 389 (2), 13–14 (cit. on pp. 35, 39, 42).

Ramshaw, C. (1987): Opportunities for Exploiting Centrifugal Fields. *The Chemical Engineer* 437, 17–21 (cit. on pp. 3, 47).

Ramshaw, C. and K. Arkley (1983): Process intensification by miniature mass transfer. *Process Engineering (London)* 64 (1), 29–31 (cit. on pp. 35, 39, 43).

Ramshaw, C. and R. H. Mallinson (1981): Mass Transfer Process. US 4283255 (A) (cit. on pp. 2, 32, 35, 39, 148).

Rangaiah, G. P., ed. (2016): *Chemical process retrofitting and revamping: Techniques and applications*. Chichester, West Sussex: Wiley. ISBN: 978-1-119-01633-5. DOI: 10.1002/9781119016311. URL: http://search.ebscohost.com/login.aspx?direct=true&scope=site&db=nlebk&AN=1160057 (cit. on p. 2).

Rao, D. P., A. Bhowal, and P. S. Goswami (2004): Process Intensification in Rotating Packed Beds (HIGEE): An Appraisal. *Industrial & Engineering Chemistry Research* 43 (4), 1150–1162. ISSN: 0888-5885. DOI: 10.1021/ie030630k (cit. on pp. 2, 15, 17–20, 86).

Rao, D. P. (2015): The Story of "HIGEE". *Indian Chemical Engineer* 57 (3-4), 282–299. ISSN: 0019-4506. DOI: 10.1080/00194506.2015.1026946 (cit. on p. 25).

Reay, D. A., C. Ramshaw, and A. Harvey (2013): A Brief History of Process Intensification. In: *Process Intensification*. Elsevier, 1–25. ISBN: 9780080983042. DOI: 10.1016/B978-0-08-098304-2.00001-8 (cit. on pp. 35, 39, 47).

RECEMAT BV, ed. (2014): *DATA SHEET NICKEL-CHROMIUM - EXTRA FOAM*. Geldermalsen, The Netherlands. URL: https://www.recemat.nl/wp-content/uploads/2020/08/Datasheet_NCX.pdf (last access 03/02/2021) (cit. on pp. 61, 63).

Reddy, K. J., A. Gupta, D. P. Rao, and O. P. Rama (2006): Process Intensification in a HIGEE with Split Packing. *Industrial & Engineering Chemistry Research* 45 (12), 4270–4277. ISSN: 0888-5885. DOI: 10.1021/ie051382q (cit. on pp. 22, 23, 25, 32, 54, 87, 92–94, 112–114, 116–118, 121–123, 148, 149, 153–155, 177).

Rejl, F., L. Valenz, J. Haidl, T. Moucha, T. Cmelikova, and R. Petricek (2018): Novel model for separation efficiency of packed distillation columns. *Chemical Engineering Transactions* (69), 67–72. DOI: 10.3303/CET1869012 (cit. on p. 13).

Rejl, F. J., J. Haidl, L. Valenz, A. Marchi, T. Moucha, R. Petříček, and E. Brunazzi (2017): Liquid-phase mass-transfer coefficients of Mellapak structured packings under

desorption of oxygen from primary alcohols. *Chemical Engineering Research and Design* 127, 1–9. ISSN: 02638762. DOI: 10.1016/j.cherd.2017.09.002 (cit. on p. 11).

Rejl, J. F., J. Haidl, L. Valenz, T. Moucha, and M. Schultes (2016): Analogy of absorption and distillation processes. Wetted-wall column study. *Chemical Engineering Science* 153, 146–154. ISSN: 00092509. DOI: 10.1016/j.ces.2016.07.021 (cit. on p. 13).

Rejl, J. F., V. Linek, T. Moucha, E. Prokopová, L. Valenz, and F. Hovorka (2006): Vapour- and liquid-side volumetric mass transfer coefficients measured in distillation column. Comparison with data calculated from absorption correlations. *Chemical Engineering Science* 61 (18), 6096–6108. ISSN: 00092509. DOI: 10.1016/j.ces.2006.06.003 (cit. on p. 12).

Rejl, J. F., L. Valenz, and V. Linek (2010): "Profile Method" for the Measurement of kLa and kVa in Distillation Columns. Validation of Rate-Based Distillation Models Using Concentration Profiles Measured along the Column. *Industrial & Engineering Chemistry Research* 49 (9), 4383–4398. ISSN: 0888-5885. DOI: 10.1021/ie901690m (cit. on p. 13).

Rocha, J. A., J. L. Bravo, and J. R. Fair (1996): Distillation Columns Containing Structured Packings: A Comprehensive Model for Their Performance. 2. Mass-Transfer Model. *Industrial & Engineering Chemistry Research* 35 (5), 1660–1667. ISSN: 0888-5885. DOI: 10.1021/ie940406i (cit. on p. 8).

Romberg, W. (1955): Vereinfachte numerische Integration. *Forh. - K. Nor. Vidensk. Selsk.* 28 (7), 30–36. ISSN: 0368-6302 (cit. on pp. 95, 102).

Saha, D. (2009): Prediction of mass transfer coefficient in rotating bed contactor (Higee) using artificial neural network. *Heat and Mass Transfer* 45 (4), 451–457. ISSN: 0947-7411. DOI: 10.1007/s00231-008-0442-0 (cit. on p. 33).

Sahoo, S. S., C. H. Lampert, and G. Martius (2018): *Learning Equations for Extrapolation and Control* (cit. on p. 34).

Sandilya, P., D. P. Rao, A. Sharma, and G. Biswas (2001): Gas-Phase Mass Transfer in a Centrifugal Contactor. *Industrial & Engineering Chemistry Research* 40 (1), 384–392. ISSN: 0888-5885. DOI: 10.1021/ie0000818 (cit. on pp. 18–20).

Sang, L., Y. Luo, G.-.-W. Chu, B.-.-C. Sun, L.-.-L. Zhang, and J.-.-F. Chen (2019): A three–zone mass transfer model for a rotating packed bed. *AIChE Journal* 65 (6), e16595. ISSN: 00011541. DOI: 10.1002/aic.16595 (cit. on pp. 14, 31).

Sang, L., Y. Luo, G.-W. Chu, Y.-Z. Liu, X.-Z. Liu, and J.-.-F. Chen (2017a): Modeling and experimental studies of mass transfer in the cavity zone of a rotating packed bed. *Chemical Engineering Science* 170, 355–364. ISSN: 00092509. DOI: 10.1016/j.ces.2016.12.041 (cit. on p. 17).

Sang, L., Y. Luo, G.-W. Chu, J.-P. Zhang, Y. Xiang, and J.-.-F. Chen (2017b): Liquid flow pattern transition, droplet diameter and size distribution in the cavity zone of a rotating packed bed: A visual study. *Chemical Engineering Science* 158, 429–438. ISSN: 00092509. DOI: 10.1016/j.ces.2016.10.044 (cit. on p. 16).

Schmidt, J., M. R. G. Marques, S. Botti, and M. A. L. Marques (2019): Recent advances and applications of machine learning in solid-state materials science. *npj Computational Materials* 5 (1), 484. ISSN: 2057-3960. DOI: 10.1038/s41524-019-0221-0 (cit. on p. 34).

Schönbucher, A. (2002): *Thermische Verfahrenstechnik: Grundlagen und Berechnungsmethoden für Ausrüstungen und Prozesse*. Berlin and Heidelberg: Springer. ISBN: 978-3-642-62637-1. DOI: 10.1007/978-3-642-56308-9. URL: http://dx.doi.org/10.1007/978-3-642-56308-9 (cit. on p. 69).

Schulz, R., E. Zich, H. Jansen, and T. E. A. Hugen (2019): Stoffaustauschmaschine. EP 3456397 (B1) (cit. on p. 27).

Seider, W. D., J. D. Seader, and D. R. Lewin (2004): *Product and process design principles: Synthesis, analysis, and evaluation*. 2nd ed. New York: Wiley. ISBN: 0-471-21663-1. URL: http://www.loc.gov/catdir/bios/wiley046/2002192252.html (cit. on p. 11).

Shi, G., G.-W. Chu, and J.-.-F. Chen (2011): A new high gravity catalytic separation process for n-butyl acetate synthesis. *Journal of Beijing University of Chemical Technology (Natural Science Edition)* 38 (1), 5–9. URL: http://www.journal.buct.edu.cn/CN/Y2011/V38/I1/5 (last access 09/27/2017) (cit. on pp. 37, 40).

Shivhare, M. K., D. P. Rao, and N. Kaistha (2013): Mass transfer studies on split-packing and single-block packing rotating packed beds. *Chemical Engineering and Processing: Process Intensification* 71, 115–124. ISSN: 02552701. DOI: 10.1016/j.cep.2013.01.009 (cit. on pp. 26, 32, 148, 153–155).

Short, H. (1983): New mass-transfer find is a matter of gravity. *Chemical Engineering - Chemical Technology for Profit-minded Engineers* 90 (Feb. 21), 23–29 (cit. on pp. 35, 39).

Singh, S. P., J. H. Wilson, R. M. Counce, A. J. Lucero, G. D. Reed, R. A. Ashworth, and M. G. Elliott (1992): Removal of volatile organic compounds from groundwater using a rotary air stripper. *Industrial & Engineering Chemistry Research* 31 (2), 574–580. ISSN: 0888-5885. DOI: 10.1021/ie00002a019 (cit. on pp. 19, 22–24, 31, 33, 36, 58).

Singh, S. P. (1989): Air Stripping of Volatile Organic Compounds from Groundwater: An Evaluation of a Centrifugal Vapor-Liquid Contactor. *Dissertation*. Knoxville, Tennessee: University of Tennessee. URL: http://trace.tennessee.edu/cgi/viewcontent.cgi?article=3046&context=utk_graddiss (last access 02/06/2017) (cit. on pp. 35, 94, 101, 118, 152, 155, 177).

Song, D., A. F. Seibert, and G. T. Rochelle (2018): Mass Transfer Parameters for Packings: Effect of Viscosity. *Industrial & Engineering Chemistry Research* 57 (2), 718–729. ISSN: 0888-5885. DOI: 10.1021/acs.iecr.7b04396 (cit. on p. 11).

Souza, W. L. R., C. S. Silva, L. A. C. Meleiro, and M. F. Mendes (2016): Ethanol dehydration in packed distillation column using glycerol as entrainer: Experiments and HETP evaluation. *Brazilian Journal of Chemical Engineering* 33 (2), 415–426. ISSN: 0104-6632. DOI: 10.1590/0104-6632.20160332s20150341 (cit. on p. 120).

Sudhoff, D. (2015): *Design, analysis and investigation of rotating packed beds for distillation: Dortmund, Techn. Univ., Diss.* Verfahrenstechnik. München: Verl. Dr. Hut. ISBN: 978-3-8439-2067-4 (cit. on pp. 19, 21, 24, 29, 103).

Sudhoff, D., M. Leimbrink, M. Schleinitz, A. Gorak, and P. Lutze (2015): Modelling, design and flexibility analysis of rotating packed beds for distillation. *Chemical Engineering Research and Design* 94, 72–89. ISSN: 02638762. DOI: 10.1016/j.cherd.2014.11.015 (cit. on pp. 20, 24, 47, 54, 113).

Sudhoff, D., K. Neumann, and P. Lutze (2014): An Integrated Design Method for Rotating Packed Beds for Distillation. In: *24th European Symposium on Computer Aided Process Engineering*. Vol. 33. Computer Aided Chemical Engineering. Elsevier, 1303–1308. ISBN: 9780444634344. DOI: 10.1016/B978-0-444-63455-9.50052-0 (cit. on pp. 37, 113).

Sulzer Chemtech, ed. (2012): *Structured Packings for Distillation, Absorption and Reactive Distillation*. URL: https://www.sulzer.com/-/media/files/products/separation-technology/liquid_liquid_extraction/brochures/structured_packings.ashx (last access 06/04/2018) (cit. on p. 71).

Sun, B.-.-C., X.-M. Wang, J.-M. Chen, G.-W. Chu, J.-.-F. Chen, and L. Shao (2009): Simultaneous Absorption of CO 2 and NH 3 into Water in a Rotating Packed Bed. *Industrial & Engineering Chemistry Research* 48 (24), 11175–11180. ISSN: 0888-5885. DOI: 10.1021/ie9001316 (cit. on p. 30).

Taylor, R. and R. Krishna (1993): *Multicomponent mass transfer*. Wiley series in chemical engineering. New York: Wiley. ISBN: 0-471-57417-1 (cit. on pp. 5–8, 29, 55, 76, 77, 80–82, 124, 126).

Teja, A. S. and P. Rice (1981): Generalized corresponding states method for the viscosities of liquid mixtures. *Industrial & Engineering Chemistry Fundamentals* 20 (1), 77–81. ISSN: 0196-4313. DOI: 10.1021/i100001a015 (cit. on pp. 81, 124, 125).

Tolksdorf, G., E. Esche, G. Wozny, and J.-U. Repke (2019): Customized code generation based on user specifications for simulation and optimization (http://mosaic-modeling.de). *Computers & Chemical Engineering* 121, 670–684. ISSN: 00981354. DOI: 10.1016/j.compchemeng.2018.12.006 (cit. on p. 76).

Towler, G. P. and R. K. Sinnott (2008): *Chemical engineering design: Principles, practice and economics of plant and process design*. Amsterdam and Boston: Elsevier/Butterworth-Heinemann. ISBN: 978-0-7506-8423-1. URL: http://search.ebscohost.com/login.aspx?direct=true&scope=site&db=nlebk&db=nlabk&AN=216942 (cit. on p. 69).

Trent, D. L. (2004): Chemical Processing in High-Gravity Fields. In: *Re-engineering the chemical processing plant*. Ed. by A. I. Stankiewicz and J. A. Moulijn. Chemical industries. New York: M. Dekker, 29–60. ISBN: 0-203-91329-9 (cit. on pp. 17, 21, 24).

Trent, D. L., D. Tirtowidjojo, and G. J. Quarderer (1999): Reactive stripping in a rotating packed bed for the production of hypochlorous acid. In: *3rd International Conference on Process Intensification for the Chemical Industry - smaller, cheaper and safer production*. Ed. by A. Green. BHR Group conference series publication. Bury St Edmunds: Professional Engineering, 99–108. ISBN: 186058215X (cit. on pp. 2, 15, 17, 44).

Tsai, C.-Y. and Y.-S. Chen (2015): Effective interfacial area and liquid-side mass transfer coefficients in a rotating bed equipped with baffles. *Separation and Purification Technology* 144, 139–145. ISSN: 13835866. DOI: 10.1016/j.seppur.2015.02.008 (cit. on p. 148).

Tung, H.-H. and R. S. H. Mah (1985): MODELING LIQUID MASS TRANSFER IN HIGEE SEPARATION PROCESS. *Chemical Engineering Communications* 39 (1-6),

147–153. ISSN: 0098-6445. DOI: 10.1080/00986448508911667 (cit. on pp. 20, 30, 149).

Turton, R. (2003): *Analysis, synthesis, and design of chemical processes*. 2. ed. Prentice Hall international series in the physical and chemical engineering sciences. Upper Saddle River, NJ: Prentice Hall PTR. ISBN: 978-0130647924 (cit. on p. 69).

van Elk, E. P., M. C. Knaap, and G. F. Versteeg (2007): Application of the Penetration Theory for Gas–Liquid Mass Transfer Without Liquid Bulk. *Chemical Engineering Research and Design* 85 (4), 516–524. ISSN: 02638762. DOI: 10.1205/cherd06066 (cit. on p. 8).

VDI 2761-2 — Verein Deutscher Ingenieure (2020): *Measurement and evaluation of fluid dynamics and mass transfer in packed columns - Absorption and desorption*. Düsseldorf (cit. on pp. 58, 85).

VDI 3679-2 — Verein Deutscher Ingenieure (2014): *Wet separators: Waste gas cleaning by adsorption (scrubbers)*. Düsseldorf (cit. on pp. 9, 35).

VDI Heat Atlas 2010 — *VDI heat atlas* (2010). 2. ed. VDI-Buch. Berlin: Springer-Verlag Berlin Heidelberg. ISBN: 978-3-540-77877-6. DOI: 10.1007/978-3-540-77877-6. URL: http://www.springerlink.com/content/978-3-540-77876-9/#section=747618&page=1 (cit. on p. 32).

VDI-Wärmeatlas 2013 — *VDI-Wärmeatlas* (2013). 11., bearb. und erw. Aufl. VDI-Buch. Berlin: Springer Vieweg. ISBN: 978-3-642-19981-3. DOI: 10.1007/978-3-642-19981-3. URL: http://dx.doi.org/10.1007/978-3-642-19981-3 (cit. on pp. 68, 92, 145, 146).

Virtanen, P., R. Gommers, T. E. Oliphant, M. Haberland, T. Reddy, D. Cournapeau, E. Burovski, P. Peterson, W. Weckesser, J. Bright, S. J. van der Walt, M. Brett, J. Wilson, K. J. Millman, N. Mayorov, A. R. J. Nelson, E. Jones, R. Kern, E. Larson, C. J. Carey, İ. Polat, Y. Feng, E. W. Moore, J. VanderPlas, D. Laxalde, J. Perktold, R. Cimrman, I. Henriksen, E. A. Quintero, C. R. Harris, A. M. Archibald, A. H. Ribeiro, F. Pedregosa, P. van Mulbregt, and SciPy 1.0 Contributors (2020): SciPy 1.0: Fundamental Algorithms for Scientific Computing in Python. *Nat. Methods* 17, 261–272. DOI: 10.1038/s41592-019-0686-2 (cit. on pp. 95, 102).

Viswanath, D. S., N. V. Dutt, T. K. Ghosh, D. H. L. Prasad, and K. Y. Rani (2007): *Viscosity of Liquids: Theory, estimation, experiment, and data*. Dordrecht: Springer.

ISBN: 978-1-4020-5482-2. DOI: 10.1007/978-1-4020-5482-2. URL: http://dx.doi.org/10.1007/978-1-4020-5482-2 (cit. on p. 81).

Vlaminck, T. (2019): Planung und Aufbau eines Rotating-Packed-Bed-Versuchsstandes zur Destillation bei erhöhter Schwerkraft. *Master Thesis*. Berlin: Technische Universität Berlin (cit. on p. 60).

Wächter, A. and L. T. Biegler (2006): On the implementation of an interior-point filter line-search algorithm for large-scale nonlinear programming. *Mathematical Programming* 106 (1), 25–57. ISSN: 0025-5610. DOI: 10.1007/s10107-004-0559-y (cit. on p. 76).

Wang, G. Q., O. G. Xu, Z. C. Xu, and J. B. Ji (2008a): New HIGEE-Rotating Zigzag Bed and Its Mass Transfer Performance. *Industrial & Engineering Chemistry Research* 47 (22), 8840–8846. ISSN: 0888-5885. DOI: 10.1021/ie801020u (cit. on pp. 2, 26, 37, 39, 47, 69).

Wang, G. Q., Z. C. Xu, and J. B. Ji (2011): Progress on Higee distillation—Introduction to a new device and its industrial applications. *Chemical Engineering Research and Design* 89 (8), 1434–1442. ISSN: 02638762. DOI: 10.1016/j.cherd.2011.02.013 (cit. on pp. 26, 44).

Wang, G. Q., Z. C. Xu, Y. L. Yu, and J. B. Ji (2008b): Performance of a rotating zigzag bed—A new HIGEE. *Chemical Engineering and Processing: Process Intensification* 47 (12), 2131–2139. ISSN: 02552701. DOI: 10.1016/j.cep.2007.11.001 (cit. on pp. 37, 39).

Wang, G. Q., C. F. Guo, Z. C. Xu, Y. M. Li, and J. B. Ji (2014a): A New Crossflow Rotating Bed, Part 1: Distillation Performance. *Industrial & Engineering Chemistry Research* 53 (10), 4030–4037. ISSN: 0888-5885. DOI: 10.1021/ie4032296 (cit. on pp. 37, 41, 69).

Wang, G. Q., C. F. Guo, Z. C. Xu, Y. L. Yu, and J. B. Ji (2014b): A New Crossflow Rotating Bed, Part 2: Structure Optimization. *Industrial & Engineering Chemistry Research* 53 (10), 4038–4045. ISSN: 0888-5885. DOI: 10.1021/ie403571u (cit. on pp. 37, 41, 69).

Wang, G. Q., Z. J. Zhou, Y. M. Li, and J. B. Ji (2019): Qualitative relationships between structure and performance of rotating zigzag bed in distillation. *Chemical Engineering and Processing: Process Intensification* 135, 141–147. ISSN: 02552701. DOI: 10.1016/j.cep.2018.11.014 (cit. on pp. 26, 42).

Wem, J. (2012): *HiGee Development at ICI*. URL: http://www.pinetwork.org/pubs/PIN20/Wem.pptx (cit. on pp. 69, 179, 180).

Wen, Z.-N., W. Wu, Y. Luo, L.-L. Zhang, B.-.-C. Sun, and G.-W. Chu (2020): Novel Wire Mesh Packing with Controllable Cross-Sectional Area in a Rotating Packed Bed: Mass Transfer Studies. *Industrial & Engineering Chemistry Research* 59 (36), 16043–16051. ISSN: 0888-5885. DOI: 10.1021/acs.iecr.0c01886 (cit. on pp. 31, 87, 89, 149, 151, 154).

Williams, G. C., E. K. Stigger, and J. H. Nichols (1950): A correlation of plate efficiencies in fractionating columns. *Chemical Engineering Progress* 46 (1), 7–16 (cit. on p. 65).

Wu, J. and A.-F. A. Asfour (1992): Viscometric properties of n-alkane liquid mixtures. *Fluid Phase Equilibria* 76, 283–294. ISSN: 03783812. DOI: 10.1016/0378-3812(92)85095-P (cit. on p. 81).

Xie, P., X. Lu, H. Ding, X. Yang, D. Ingham, L. Ma, and M. Pourkashanian (2019): A mesoscale 3D CFD analysis of the liquid flow in a rotating packed bed. *Chemical Engineering Science* 199, 528–545. ISSN: 00092509. DOI: 10.1016/j.ces.2019.01.038 (cit. on p. 27).

Xie, P., X. Lu, X. Yang, D. Ingham, L. Ma, and M. Pourkashanian (2017): Characteristics of liquid flow in a rotating packed bed for CO2 capture: A CFD analysis. *Chemical Engineering Science* 172, 216–229. ISSN: 00092509. DOI: 10.1016/j.ces.2017.06.040 (cit. on p. 28).

Xing, Z.-Y., Y. Luo, G.-W. Chu, H.-K. Zou, Y. Xiang, and J.-F. Chen (2014): Study on gas pressure drop in a novel multi-liquid-inlet rotating packed bed. *Gao Xiao Hua Xue Gong Cheng Xue Bao/Journal of Chemical Engineering of Chinese Universities* 28, 234–239. DOI: 10.3969/j.issn.1003-9015.2014.02.006 (cit. on p. 26).

Xu, Y.-.-C., Y.-.-B. Li, Y.-Z. Liu, Y. Luo, G.-.-W. Chu, L.-.-L. Zhang, and J.-.-F. Chen (2019): Liquid jet impaction on the single–layer stainless steel wire mesh in a rotating packed bed reactor. *AIChE Journal* 65 (6), e16597. ISSN: 00011541. DOI: 10.1002/aic.16597 (cit. on pp. 14, 28).

Yan, Z.-y., C. Lin, and Q. Ruan (2012): Hydrodynamics in a Rotating Packed Bed. I. A Novel Experimental Method. *Industrial & Engineering Chemistry Research* 51 (31), 10472–10481. ISSN: 0888-5885. DOI: 10.1021/ie202257t (cit. on p. 15).

Yan, Z.-y., C. Lin, and Q. Ruan (2014): Dynamics of droplets and mass transfer in a rotating packed bed. *AIChE Journal* 60 (7), 2705–2723. ISSN: 00011541. DOI: 10.1002/aic.14449 (cit. on p. 15).

Yang, Y.-C., Y. Ouyang, N. Zhang, Q.-J. Yu, and M. Arowo (2019): A review on computational fluid dynamic simulation for rotating packed beds. *Journal of Chemical Technology & Biotechnology* 94 (4), 1017–1031. ISSN: 02682575. DOI: 10.1002/jctb.5880 (cit. on p. 27).

Yang, K., G. Chu, H.-K. Zou, B. Sun, L. Shao, and J.-.-F. Chen (2011): Determination of the effective interfacial area in rotating packed bed. *Chemical Engineering Journal* 168 (3), 1377–1382. ISSN: 13858947. DOI: 10.1016/j.cej.2011.01.100 (cit. on pp. 23, 89, 106, 107).

Yang, Y., Y. Xiang, G. Chu, H.-K. Zou, Y. Luo, M. Arowo, and J.-.-F. Chen (2015a): A noninvasive X-ray technique for determination of liquid holdup in a rotating packed bed. *Chemical Engineering Science* 138, 244–255. ISSN: 00092509. DOI: 10.1016/j.ces.2015.07.044 (cit. on pp. 16, 88, 107).

Yang, Y., Y. Xiang, G. Chu, H.-K. Zou, B. Sun, M. Arowo, and J.-.-F. Chen (2016): CFD modeling of gas–liquid mass transfer process in a rotating packed bed. *Chemical Engineering Journal* 294, 111–121. ISSN: 13858947. DOI: 10.1016/j.cej.2016.02.054 (cit. on pp. 28, 149).

Yang, Y., Y. Xiang, Y. Li, G. Chu, H.-K. Zou, M. Arowo, and J.-.-F. Chen (2015b): 3D CFD modelling and optimization of single-phase flow in rotating packed beds. *The Canadian Journal of Chemical Engineering* 93 (6), 1138–1148. ISSN: 00084034. DOI: 10.1002/cjce.22183 (cit. on p. 28).

Yi, F., H.-K. Zou, G.-W. Chu, L. Shao, and J.-.-F. Chen (2009): Modeling and experimental studies on absorption of CO2 by Benfield solution in rotating packed bed. *Chemical Engineering Journal* 145 (3), 377–384. ISSN: 13858947. DOI: 10.1016/j.cej.2008.08.004 (cit. on pp. 29, 30).

Yoshida, F. and T. Koyanagi (1962): Mass transfer and effective interfacial areas in packed columns. *AIChE Journal* 8 (3), 309–316. ISSN: 00011541. DOI: 10.1002/aic.690080310 (cit. on p. 11).

Zhang, L.-L., J.-X. Wang, Y. Xiang, X.-F. Zeng, and J.-.-F. Chen (2011): Absorption of Carbon Dioxide with Ionic Liquid in a Rotating Packed Bed Contactor: Mass Transfer

Study. *Industrial & Engineering Chemistry Research* 50 (11), 6957–6964. ISSN: 0888-5885. DOI: 10.1021/ie1025979 (cit. on pp. 30, 31).

Zhang, W., P. Xie, Y. Li, and J. Zhu (2021): A machine learning model for predicting the mass transfer performance of rotating packed beds based on a least squares support vector machine approach. *Chemical Engineering and Processing: Process Intensification* 165 (10), 108432. ISSN: 02552701. DOI: 10.1016/j.cep.2021.108432 (cit. on p. 34).

Zhao, B., Y. Su, and W. Tao (2014): Mass transfer performance of CO2 capture in rotating packed bed: Dimensionless modeling and intelligent prediction. *Applied Energy* 136, 132–142. ISSN: 03062619. DOI: 10.1016/j.apenergy.2014.08.108 (cit. on p. 33).

Zhao, B., W. Tao, M. Zhong, Y. Su, and G. Cui (2016): Process, performance and modeling of CO2 capture by chemical absorption using high gravity: A review. *Renewable and Sustainable Energy Reviews* 65, 44–56. ISSN: 13640321. DOI: 10.1016/j.rser.2016.06.059 (cit. on pp. 30, 34).

Zhao, Z., J. Wang, B. Sun, M. Arowo, and L. Shao (2018): Mass transfer study of water deoxygenation in a rotor–stator reactor based on principal component regression method. *Chemical Engineering Research and Design* 132, 677–685. ISSN: 02638762. DOI: 10.1016/j.cherd.2018.02.007 (cit. on pp. 149, 151, 154).

Zhao, Z., X. Zhang, G. Li, G. Chu, B. Sun, H.-K. Zou, M. Arowo, and L. Shao (2017): Mass Transfer Characteristics in a Rotor-Stator Reactor. *Chemical Engineering & Technology* 40 (6), 1078–1083. ISSN: 09307516. DOI: 10.1002/ceat.201600396 (cit. on pp. 30, 149, 154).

Zheng, C., K. Guo, Y. Song, X. Zhou, D. Ai, Z. Xin, and N. C. Gardner (1997): Industrial practice of HIGRAVITEC in water deaeration. In: *2nd International Conference on Process Intensification in Practice*. Ed. by J. Semel. BHR Group conference series publication. Bury St Edmunds: Mechanical Engineering Publications, 273–288. ISBN: 1860580939 (cit. on pp. 2, 44, 47, 83, 148).

Zheng, C., K. Guo, Y. Feng, C. Yang, and N. C. Gardner (2000): Pressure Drop of Centripetal Gas Flow through Rotating Beds †. *Industrial & Engineering Chemistry Research* 39 (3), 829–834. ISSN: 0888-5885. DOI: 10.1021/ie980703d (cit. on p. 18).

Zheng, X.-H., G.-W. Chu, D.-J. Kong, Y. Luo, J.-P. Zhang, H.-K. Zou, L.-L. Zhang, and J.-.-F. Chen (2016): Mass transfer intensification in a rotating packed bed with

surface-modified nickel foam packing. *Chemical Engineering Journal* 285, 236–242. ISSN: 13858947. DOI: 10.1016/j.cej.2015.09.083 (cit. on p. 27).